Growth and Characterisation of Indium Nitride

A thesis submitted to Cardiff University
In Candidate for the degree of

Doctor of Philosophy

By

Hassan Ali Hirshy

Division of Electrical and Electronic Engineering
School of Engineering
Cardiff University
United Kingdom

December 2007

UMI Number: U585560

All rights reserved

INFORMATION TO ALL USERS
The quality of this reproduction is dependent upon the quality of the copy submitted.

In the unlikely event that the author did not send a complete manuscript
and there are missing pages, these will be noted. Also, if material had to be removed,
a note will indicate the deletion.

UMI U585560
Published by ProQuest LLC 2013. Copyright in the Dissertation held by the Author.
Microform Edition © ProQuest LLC.
All rights reserved. This work is protected against
unauthorized copying under Title 17, United States Code.

ProQuest LLC
789 East Eisenhower Parkway
P.O. Box 1346
Ann Arbor, MI 48106-1346

Acknowledgements

I would like to express my sincere gratitude to my supervisor Dr. Richard Perks for his support, and guidance throughout this project. His support has been tremendous, since the day I joined Cardiff University. I'm truly impressed by his "always ready to help" attitude. Working with him has been a great experience.

I would like to thank Dr. Scott Butcher and Dr. Marie WintreBert-Fouquet of Macquarie University – Sydney for their invitation to their research facility where I spent four incredible months of my life. My visit to Sydney and the collaboration between us made the first miles in the journey of my PhD. I greatly appreciate their collaboration and friendship. Not to forget, many thanks to Mr. Patrick Chen for providing some information on indium nitride grown by RF sputtering and Remote Plasma Enhanced Chemical Vapour Deposition.

I would like to acknowledge the support of the Australian Institute of Nuclear Science and Engineering for the SIMS measurements, the University of Technology –Sydney and the support of the Australian Research Council.

I would like also to acknowledge the support of Dr. Oliver Briot of the University of Montpellier for providing indium nitride film grown by Metal Organic Vapour Phase Epitaxy.

I wish to offer my sincere thanks and gratitude to Mr. Mahdi Al-Tajir, the Founder of the Al-Tajir Trust, for his generous financial support. I'm overwhelmed by this support which opened the gates of knowledge into my life and gave me a clear vision of the path that I should follow in my life.

My deep thanks and prayers for the religious authority Sayyed Muhammed Hussein Fadlullah for his spiritual guidance and support, and for his personal recommendation for the scholarship.

I would like to take this opportunity to thank all the school administrative staff, in particular, "research office girls" for their support during my years of study at Cardiff University. I would like also to add all the technician of the school of Engineering who showed great attitude and it was a pleasure to work with them in particular Mr. Rolfe Wheeler-Jones.

Special thanks to a very experienced person who became a very close friend and always enlightened me with his knowledge and his genuine attitude or just for being there for just a cup of coffee, Mr. Tyrone Jones.

Last, but not least, sincere thanks for the people who without them I would be what I am now, my family. Sincere gratitude to my Dad, Mum, brothers and sister, and of course, my beautiful wife, Nour, who showed me the true meaning of happiness. I would like to thank her for her support and understanding. One last thing to say to my Mum, that whatever I achieve in my life, no matter the success I get, I can never pay you back your prayers for me.

Summary

Indium nitride (InN) was grown on both c-plane sapphire and borosilicate glass substrates by reactive evaporation. The reactive evaporation growth technique proved to be simple, cost-effective and offered the advantage of low growth temperature with consistency in growing good quality material with high mobilities and relatively low carrier concentrations. The carrier concentration ranged between 1.59×10^{17} cm^{-3} to 4.31×10^{19} cm^{-3} which is in the same range of the reported value for InN grown by MBE and MOVPE. Furthermore, a mobility as high as 2285 $cm^2V^{-1}s^{-1}$ was achieved with the elevation of the substrate temperature to 210 °C. The crystalline structure showed a strong correlation with the growth temperature. The films were of polycrystalline nature with hexagonal structure and had a tendency to orientate along the vertical c-axis with the increase in the substrate temperature. The distributed values obtained for lattice parameters were attributed to the nitrogen content in the films and the non-stoichiometry of the material. Compositional and chemical analysis by both x-ray photoelectron spectroscopy (XPS) and secondary ion mass spectroscopy (SIMS) confirmed that the material was In-rich material. The role of oxygen was also investigated with SIMS analysis, and estimated a presence of oxygen of ~ 20 at.%. Despite the presence of oxygen level, no evidence of its effect on the band gap was found. Furthermore, the controversy surrounding the band gap was reviewed and investigations on the suggested theories for the discrepancy in the reported values were carried out.

List of Publications:

1. ***"The Nature of Nitrogen Related Point Defects in Common Forms of InN."*** *K. S. A. Butcher, A.J. Fernandes, P. P-T. Chen, M. Wintrebert-Fouquet, H. Timmers, S. Shrestha, H. Hirshy, R. M. Perks, and B. F Usher, J. Appl. Phys. 101, 123702, (2007)*

2. ***"Stoichiometry effects and the Moss–Burstein effect for InN"*** *K. S. A. Butcher, H. Hirshy, R. M. Perks, M. Wintrebert-Fouquet, and P. P-T. Chen, phys. stat. sol. (a) 203, No.1 (2006).*

3. ***"Low carrier concentration indium nitride grown by reactive",*** *Wocsdice, Sweden, (2006), H. Hirshy, K.S.A. Butcher, R.M. Perks, M. Wintrebert-Fouquet, P. P-T Chen and K.E. Prince.*

4. ***"Realisation of a Novel GaN/InN Hetrostructure FET Device"*** *D. Alexandrov, R. Perks, S. Butcher, H. Hirshy, and M Wintrebert- Fouquet, LEC2006, P.95-96, Cornell University conference, USA, (2006).*

5. ***"Variations in the observed band gap of Indium Nitride"*** *R.M. Perks, H. Hirshy. Wocsdice, Cardiff (2005).*

Table of Contents

Chapter 1

Introduction

There has been remarkable interest in III-V semiconductor materials over the last decade. The developments in the field of III-nitride (InN, GaN and AlN) semiconductors have been spectacular due to their highly attractive inherent properties [1]. Transistors based on the group III nitrides should operate at higher temperatures and under more adverse conditions than similar devices based on silicon, II-VI materials, or other III-V materials, due to the wide band gap, strong chemical bonds, and the relative chemical inertness of the nitrides [2].

In recent years, indium nitride (InN), in particular, has been the subject of intense research. The significance of InN is reflected in the success of gallium nitride (GaN); with its unique properties as wide band gap material, GaN today is been used in a wide range of applications such as light emitting diodes, laser diodes, ultraviolet detectors and emitters, and high power microwave transmission devices [3,4]. For InN there was much early anticipation of its potential for optoelectronic and microelectronic device applications. This potential paved the way for intensive interest in the material; however the inability to reproduce early reports of a high mobility, low carrier concentration material with an apparent band-gap of 1.89 eV [5], has constrained this possibility.

InN was the least studied material of the III-V semiconductor family due to the difficulty in the synthesis of good quality single crystal films. Because of the low InN dissociation temperature and the high equilibrium N_2 vapour pressure over the InN film [6], the preparation of InN favours a low growth temperature. This is contrasted by the low decomposition rate of N_2 and NH_3 (the main nitrogen source used in most growth methods). In addition, the lack of a suitable lattice-matched substrate leads to material growth that is impaired by defects, stress and vacancies; which affects significantly the physical properties of the grown InN films.

In recent years, developments in the growth techniques have lead to an extensive and more focused research effort on InN. This recent interest in this material resulted in controversy over some of the material basic parameters such as the band gap, the electron effective mass, and the lattice constants. The value of 1.89eV reported by Tansley and Foley [5] was long held. However, the observation of strong photoluminescence (PL) near the band edge suggests InN has a band gap between 0.65 and 0.9 eV [7-9]. Those arguing a wide band-gap explain the observation of low band-gap as an effect of defects, non-stoichiometry, non-uniformity, and Mie resonances. On the other hand, those arguing a narrow band-gap interpret the existence of a wide band gap in terms of the Moss-Burstein effect, oxygen incorporation, quantum size effect, and stoichiometry changes. To add more variation to the discussions, a band gap of 1.1-1.5 eV has been proposed in the last year. No single solution has been successful in describing the range of observed values, and this may hinge on structural features dependent on the growth method.

InN has been shown to have the lowest effective mass among the III-nitride semiconductors [10]. This low effective mass value would result in a high mobility and high saturation velocity of the electrons [1] and hence a potential in high speed devices. Both theoretical and experimental studies of InN confirmed this potential of InN for device applications. Foutz et al. [11] have carried out device modelling calculations that show InN based HFET devices can potentially operate at higher microwave frequencies than GaN based devices; while O'leary et al. [12] have studied the electron transport in InN using an ensemble Monte-Carlo approach. They found that the transport characteristics of InN were superior to those of GaN as well as GaAs over a wide range of temperatures (150-500 K) and doping concentrations up to 10^{19} cm^{-3}. InN was found to have an extraordinary high peak drift velocity at room temperature (4.3×10^7 cms^{-1}) at a doping of 1.0×10^{17} cm^{-3}, and a large saturation drift velocity of 2.5×10^7 cms^{-1}. In a recent publication, O'leary et al. used a revised set of parameters to report an electron drift velocity that reached a maximum of 6.0×10^7 cms^{-1} and saturated at about 1.4×10^7 cms^{-1} [13]. They suggested that there might be distinct advantages in using InN for high frequency centimetre and millimetre wave devices. Furthermore, Polyakov et al. calculated a peak velocity of ~ 5×10^7 cms^{-1} and considered InN as a very promising material for high-speed electronic devices [14]. This potential is confirmed with the predicted high mobility assigned for InN. Chin, Tansley and Osotchan predicted a theoretical maximum mobility for InN to be 4400 $cm^2V^{-1}s^{-1}$ at room temperature, while at 77K the limits were beyond 33000 $cm^2V^{-1}s^{-1}$ [15]. Ng et al. carried out a study on the mobility of InN [16]. He reported a maximum mobility of 4000 $cm^2V^{-1}s^{-1}$ at room temperature while Fareed at al. predicted a value for the room temperature mobility as high as 5000 $cm^2V^{-1}s^{-1}$ [17]. Variable magnetic field analysis of thick InN films suggested maximum mobilities greater than 4000 $cm^2V^{-1}s^{-1}$ in "bulk" InN [18]. Experimentally, on the other hand, Tansley and Foley reported a maximum room temperature electron mobility of 2700 $cm^2V^{-1}s^{-1}$ associated with a carrier concentration of 5.3×10^{16} cm^{-3} for polycrystalline InN [5]. Furthermore, Xu et al. the highest mobility achieved for MBE grown InN with a mobility reaching a maximum of 2370 $cm^2V^{-1}s^{-1}$ and corresponding bulk carrier concentration of 2.8×10^{17} cm^{-3} [19]. These results act as a clear indication for the potential of indium nitride in high-speed device application.

InN is also a potential material for low-cost high-efficiency solar cells. Based on a band gap value of 1.89 eV, Yamamoto et al. used InN as a transparent conducting window material for heterojunction solar cells [20]. They assumed that a combination of a band gap of 1.89 eV for InN and 1.1 eV for silicon would result in a conversion efficiency of over 30%. However, with the emergence of recent reports suggesting a small band gap InN of 0.7-0.9 eV [7-9], this fact would significantly affect the applications of InN. The newly reported small band gap values are compatible with the wavelength of optical fibres [1]. Therefore, InN can be used in the fabrication of high-speed laser diodes (LDs) and photodiodes in optical communication systems.

The use of InN and its alloys with GaN and AlN allows tuning of the band gaps and emission wavelengths from the deep ultraviolet to the near infrared, which may be useful for a variety of applications [1]. Wu et al. showed that the band gap of the ternary alloys $In_{1-x}Ga_xN$ ($0\leq x\leq1$) can be continuously varied from 0.7 to 3.4 eV, providing a full-solar-spectrum material for multi-junction solar cells [21]. They assumed that InN offers great potential for radiation-hard high-efficiency solar cells for space applications. However, the realisation of such applications may still be sometime off in the future because of valence band alignment problems for graded heterojunctions and because of difficulties with p-type doping [22]. Because of the higher mobility and high drift velocity of InN over the other III-V material, the use of high In-fractions in the $In_{1-x}Ga_xN$ alloy system would result in much faster electronic devices [23].

In addition, there have been an increasing number of reports on the wide range of applications where InN can be used. Yoshimoto et al. used InN in the fabrication of InN/Si heterojunctions which showed good rectification characteristics [24]. McIntosh et al. considered that InN can be used as a low resistivity layer for ohmic contact formation to other wider band gap nitrides, or as an active layer in red or orange LEDs [25]. Other reports have demonstrated too the use of InN as an ohmic contact for wider band gap semiconductors [26-29]. InN and indium sub-nitride films have been tried as anodes for Li-ion thin film batteries [30]. Ascazubi et al. suggested that InN makes an interesting candidate for terahertz applications [31, 32], while Lu et al. revealed the possible potential of InN for fluid and gas monitoring applications [33].

To understand the potential application of a material, one must determine with certainty, the fundamental properties of that material. With that, the aim of this work is to take part in the debate concerning indium nitride, by attempting to clarify the controversy surrounding this material and to expand the limited knowledge on indium nitride properties. One basic property of particular interest is the band gap of InN. It is crucial to determine the correct value of the band gap of InN as the usefulness of the material for a particular application depends greatly upon it. For example, if the band gap is around 2 eV, the material may find applications in high frequency devices. Alternatively, a low band gap around 0.7 eV may be useful for full spectrum photovoltaic cells based on $In_{1-x}Ga_xN$ alloys. This work will investigate the suggested theories behind the huge discrepancy in the band gap value such as Mie-resonance, Moss-Burstein effect, inhomogeneity, stoichiometry, quantum size effect and oxygen alloying. This work also aims to resolve the growth of unintentionally doped n-type with high background electron concentration and investigate the reasons given for this as-grown unintentional doping.

One of the main limitations in understanding the properties of InN is that material grown by different techniques often showed different characteristics; thus adding more uncertainty to the basic material parameters. Other reasons behind the complications in understanding InN would be the limitations of the measurements techniques and the interpretation of the results. Therefore, in order to overcome these problems, a simple and cost-effective growth technique has been introduced, and InN was grown under controlled conditions and characterised and investigated under similar testing conditions.

1.1. Thesis outline

The second chapter of this thesis is an extensive literature review on the history and published properties of indium nitride. This chapter will be used as a reference source and will also provide a contextual platform for work detailed in this thesis. The second chapter is split into a number of sections; highlighting how the material is grown and the basic properties of indium nitride. The first few sections give a brief description of the growth of InN by different growth techniques such as reactive sputtering, molecular beam epitaxy (MBE), metalorganic chemical vapour deposition (MOCVD), pulsed laser deposition (PLD) plus other techniques used in the growth of InN, and the effect of the growth parameters on the fundamental properties of the material. The rest of the chapter covers the structural, optical and electrical properties of InN.

The third chapter in thesis discusses the difficulties governing the growth of InN by many of the growth techniques which lead to the introduction of the reactive evaporation technique to resolve some of these problems. This chapter reveals the reactive evaporation growth system used and the choice of both the substrate and the plasma gas. The sample preparation and the growth procedure are described in detail in chapter three.

The structural and compositional properties of InN are investigated in chapter four. This chapter includes a brief description of the characterisation techniques that have been used in the investigation. Scanning electron microscopy (SEM) is used to study the surface morphology of the grown films, x-ray diffraction (XRD) to investigate the crystalline structure, grain size and lattice-parameters, and x-ray photoelectron spectroscopy (XPS) to study the chemical composition, the nature of nitrogen related point defects and the surface charge accumulation. Secondary ion mass spectroscopy (SIMS) has been used to investigate the composition of InN and study the role of oxygen and hydrogen and their effect on the optical and electrical properties of the material, while the surface roughness of the material is investigated using the atomic force microscopy (AFM) technique.

In chapter five the optical and electrical properties are investigated. This chapter is also divided into many sections. In the first part, the optical characteristics of indium nitride are revealed with the transmission measurements, determination of the refractive index, optical density and the band gap determination. Some of the theories given behind the discrepancies in the band gap value such as Mie-resonance, quantum size effect and inhomogeneity are investigated here. In the second part of chapter five, the electrical properties are studied by applying the Van der Pauw technique for the Hall Effect measurement. The last part of chapter five describes the correlation between the electrical and optical properties of InN and the investigation on the Moss-Burstein effect.

References

[1] A.G. Bhuiyan, A.Hashimoto and A. Yamamoto, J. Appl. Phys. 94 (2003), 2779 and references within.

[2] D. Feiler, R. Stanley Williams, A. Alec Talin, H. Yoon and M.S. Goorsky, J. Cryst. Growth 171 (1997), 12-20.

[3] K.S.A. Butcher, InN, a Historic review- from obscurity to controversy, in: Q. Guo (Ed), Advanced Material in Electronics, Research Signpost, 2004, p.1, and references within.

[4] K.S.A. Butcher and T.L. Tansley, Superlattices Microstrcut. 38, 1, (2005) and reference within.

[5] T. L. Tansley and C. P. Foley, Electron. Lett. 20, 1066 (1984).

[6] J. B. McChesney, P. M. Bridenbaugh, and P. B. O'Connor, Mater. Res.Bull. 5, 783, (1970).

[7] J. Wu, W. Walukeiwicz, K.M. Yu, J.W. Ager III, E.E. Haller, H. Lu, W.J. Schaff, Y. Saito and Y. Nanishi, Appl. Phys. Lett. Vol.80, No.21, (2002) 3867.

[8] T. Matsouka, H. Okamoto, M. Nakao, H. Harima and E. Kurimoto, Appl. Phys. Lett. Vol.81, No.7, (2002) 1246.

[9] V.Yu. DAvydov, A.A. Klochikhin, R.P. Seisyan, V.V. Emtsev, S.V. Ivanov, F. Bechstedt, J. Furthmüller, H. Harima, A.V. Mudryi, J. Aderhold, O. Semchinova and J. Graul, Phys. Stat. Sol. (b) 229, No.3, R1-R3 (2002).

[10] S. N. Mohammad and H. Morkoc, Prog. Quantum Electron. 20, 361, (1996).

[11] B.E. Foutz, S.K. O'leary, M.S. Shur, and L.F. Eastman, J. Appl. Phys., 85, 7727, (1999).

[12] S.K. O'leary, B.E. Foutz, M.S. Shur, U.V. Bhapkar, and L.F. Eastman, J. Appl. Phys., 83, 826, (1998).

[13] S.K. O'leary, B.E. Foutz, M.S. Shur, and L.F. Eastman, Appl. Phys. Lett., 87, 222103, (2005).

[14] V.M. Polyakov and F. Schwierz, J. Appl. Phys., 99, 113705 (2006).

[15] V.W. Chin, T.L. Tansley, and T. Osotchan J. Appl. Phys. 75 (11) (1994) 7365.

[16] B.R. Ng, J. Cryst. Growth 269 (2004) 35-40.

[17] R.S.Q. Fareed, R. Jain, R. Gaska, M.S. Shur, J. Wu, W. Walukiewicz and M. Asif Khan, Appl. Phys. Lett. Vol.84, No.11, (2004), 1892.

[18] C.H. Swartz, R.P. Tompkins, N.C. Giles, T.H. Myers, H. Lu, W.J. Schaff, and L.E. Eastman, J. Cryst. Growth 269 (2004) 29-34.

[19] K. Xu, W. Terashima, T. Hata, N. Hasimoto, M. Yoshitani, B. Cao, Y. Ishitani and Y. Yoshikawa, Phys. Stat. Sol. (c) 0, No.7, 2814-2817 (2003).

[20] A. Yamamoto, M. Tsujino, M. Ohkubo, A. Hashimoto, Sol. Energy Mater. Sol. Cells 35 (1994) 53.

[21] J. Wu, W. Walukeiwicz, K.M. Yu, W. Shan, J.W. Ager III, E.E. Haller, H. Lu, W.J. Schaff, W.K. Metzger, and S. Kurtz, J. Appl. Phys., Vol.94, No.10, (2003) 6477.

[22] W. A. Doolittle, E. Trybus, G. Namkoong and W. Henderson, *Indium Nitride: A material with Photovoltaic Promise and Challenges,* presentation of the EMRS 2005 Spring Meeting, Warsaw 5-9 September 2005.

[23] A.F.M. Anwar, S. Wu, R.T. Webster, IEEE Trans. Electron. Dev., 48, 567, (2001).

[24] M. Yoshimoto, Y. Yamamoto, and J. Saraie, Phys. Stat. Sol. (c) 0, No.7, 2794-2797 (2003).

[25] F.G. McIntosh, E.L. Piner, J.C. Roberts, M.K. Behbehani, M.E. Aumer, N.A. El-Masry and S.M. Bedair, Appl. Surf. Sci. 112 (1997), 98-101.

[26] Y. Saito, N. Teraguchi, A. Suzuki, T. Araki and Y. Nanishi, Jpn. J. App. Phys. Vol.40 (2001), Pt.2, No.2A, L91-L93.

[27] M.E. Lin, F.Y. Huang, H. Morkoc, Appl. Phys. Lett. 64 (1994) 2557.

[28] F. Ren, C.R. Abernathy, S.N.G. Chu, J.R. Lothain, S.J. Pearton, Appl. Phys. Lett. 66 (1995) 1503.

[29] S.M. Donovan, J.D. MacKenzie, C.R. Abernathy, S.J. Pearton, F. Ren, K. Jones, M. Cole, Appl. Phys. Lett. 70 (1997) 2592.

[30] B.J. Neudecker, R.A. Zuhr, Electrochem. Soc. Proc. 99–24 (2000) 295.

[31] R. Ascázubi, I. Wilke, K. Denniston, H. Lu and W.J. Schaff, Appl. Phys. Lett., Vol. 84, No. 23, (2004), 4810.

[32] R. Ascázubi, I. Wilke, S. Cho, H. Lu and W.J. Schaff, Appl. Phys. Lett., 88, 112111, (2006).

[33] H. Lu, W.J. Schaff, and L.F Eastman, J. Appl. Phys., Vol. 96, No. 6, (2004), 3577.

Chapter 2

Literature review on indium nitride

The first reported study on indium nitride (InN) was by Fischer and Schröter in 1910 [1]. They had reacted indium metal with nitrogen in a cathodic discharge. In 1938 Juza and Hahn [2] obtained InN from $InF_6(NH_4)_3$ and reported the crystal structure of InN to be wurtzite. Several attempts followed to synthesize InN by Juza and Rabenua in 1956 [3], Renner in 1958 [4], Pastrnak and Souckova in 1963 [5], Samsonov in 1969 [6], MacChesney et al. in 1970 [7], Vorob'ev et al. in 1971 [8,9], Gorienko and Fenochka in 1977 [10], Sheleg and Savastenko in 1978 [11]. Gorjunova et al. in 1964 pointed out that direct interaction of metallic indium and nitrogen in an inactivated form does not take place even at rather high temperatures [12]. In 1970, MacChesney et al. [7] reported on the thermal stability of InN formed using the same procedure of Juza and Hahn reported in 1938. They concluded that the dissociation pressure of InN is extremely high and that InN is not formed by direct reaction of N_2 molecules and indium. In all of the above reported material, InN was in the form of powder or small crystals.

It was not until 1972 when some good electrical properties were reported by Hovel and Cuomo [13]. They succeeded in growing polycrystalline InN films with highly preferred orientation on sapphire and silicon substrates at a range of temperatures (25-600 °C) by reactive sputtering. The grown films appeared dark red with n-type carrier concentration of $5\text{-}8\times10^{18}\text{cm}^{-3}$, hall mobility of $250\pm50\ \text{cm}^2\text{V}^{-1}\text{s}^{-1}$ and resistivity in the range of $3\text{-}5\times10^{-3}\ \Omega$ cm. The high carrier concentration was attributed to a high density of native defects. Osamura et al. used an electron beam technique to synthesize $Ga_xIn_{(1-x)}N$ alloys [14]. They measured the direct energy gap of InN to be 1.95 eV at room temperature and to be 2.11 eV at 78 K. In a follow up in 1975 [15], they further confirmed the stability of these alloys by detailed X-ray scattering and infrared spectroscopic techniques. Trainer and Rose, in 1974, produced InN films on sapphire using reactive evaporation. The films were n-type with carrier concentration of $10^{20}\ \text{cm}^{-3}$ and hall mobility of $20\ \text{cm}^2\text{V}^{-1}\text{s}^{-1}$ [16]. In 1976, using reactive cathodic sputtering, Puychevrier and Menoret grew InN films on glass with a direct band gap of 2.07 eV at room temperature and of 2.21 eV at 77K. The reported film was n-type with a carrier concentration of $3\text{-}10\times10^{18}\text{cm}^{-3}$ and mobility of 20-50 $\text{cm}^2\text{V}^{-1}\text{s}^{-1}$ [17]. In the 1980s, many properties of the grown InN films were studied, where the work of Tansley and Foley [18-20] formed the basis of the long held band gap of 1.89 eV. Using radio frequency (RF) sputter growth, they achieved the highest electron mobility ever reported for InN with a room temperature value of 2700 $\text{cm}^2\text{V}^{-1}\text{s}^{-1}$ at 5.3×10^{16} cm^{-3}, increasing to a value of 5000 $\text{cm}^2\text{V}^{-1}\text{s}^{-1}$ at 150 K with a fall in carrier concentration to 3×10^{16} cm^{-3} for the same sample. There were several sputtering attempts to reproduce similar electrical properties of the InN obtained by Tansley & Foley but with less success despite the improvements in the crystalline structure [21-37].

The growth of InN by metal organic vapour phase epitaxy (MOVPE) was adopted by Matsouka et al. [38] and Wakahara et al. in 1989 [39]. A remarkable improvement in the growth of InN films has been achieved with the employment of MOVPE growth technique as well as MBE. Single crystal material was reported for InN. The quality of the InN film improved significantly under optimum growth conditions. The pre-growth treatments, such as buffer layer growth, nitridation temperature and nitridation duration have dramatic effects on the growth of the InN film [40]. The quality of the films was improved by nitridation of the substrate surface before growth [41, 42]. The quality of films also has been improved with various approaches such as the use of AlN [43, 44], InN [45] and GaN [46] buffer layers between film and substrate. However, with the success in producing high quality InN material, the material became surrounded by controversy in terms of its basic parameters such as the band gap, effective mass, lattice constants, the defect properties, the role of oxygen, and the decomposition temperature [47].

Owing to a low InN dissociation temperature (~ 500 °C) and high equilibrium N_2 vapour pressure over the InN film [16], the growth should proceed at a low growth temperature in order to prevent the escape of N atoms from the surface which degrades the film quality; this has made InN a difficult material to grow. However, there have been several attempts to produce InN material using different growth techniques under different growth conditions. Sputtering was extensively used in the early works on InN, but more improvement in the material quality was achieved in using MOVPE and MBE following the great success of these techniques in the GaN growth. Other methods including electron beam plasma techniques [14, 15], reactive evaporation [16, 48-51], RF ion plating [52-53], atomic layer epitaxy (ALE) [54, 55], ion-beam-assisted filtered cathodic vacuum arc [56], pulse laser deposition [57-59], have been also employed in the growth of indium nitride.

Since bulk InN substrates are not available, InN films must be grown on a foreign substrate [29]. One particular difficulty in the growth of thin films is the unavailability of sufficiently large single crystals for use as substrates for homoepitaxial growth. Thus up to now, heteroepitaxial growth is a practical necessity and the choice of substrate is critical [60, 61]. Several problems in the epitaxial growth of InN originate from the non-availability of single crystalline InN substrates or other high quality single crystalline substrates with the same lattice parameters as InN. For this reason, most of the epitaxial growth of nitrides has been performed on other substrates. Problems due to lattice mismatch between InN epitaxial layer and substrate have to be overcome. One of the major breakthroughs in the growth of device quality group III-nitride materials was the implementation of nucleation layers [62].

The choice of the substrate, pre-growth treatment of the substrate, growth conditions and the choice of the growth techniques all play a critical role on the quality of the material obtained.

2.1 Growth techniques and the influence of growth parameters

2.1.1 Reactive sputtering

Sputtering was one of the earliest and most widely deployed growth technique to produce indium nitride material [13, 17-37, 63-69]. Reactive sputtering has the advantage of being a simple, cost-effective approach; furthermore the films can be grown at low temperatures. Greater success has been achieved by the RF sputtering of indium nitride films presumably as a result of the lower energy of the ions produced by the applied electric field. Low energy ions are an advantage since they are less capable of damaging the film by ion bombardment [47]. The control of the growth parameters and finding the optimum growth conditions is a crucial step in the growth of InN. Few studies have been reported on the influence of growth parameters on the quality of the grown material. Growth temperature, growth pressure, sputtering gas, input power and other parameters had significant impact on the grown sputtered InN.

In 1972, Hovel and Cuomo were the first to report on InN grown by RF sputtering technique [13]. They succeeded in growing polycrystalline InN films with highly preferred orientation on sapphire and silicon substrates at a range of temperatures. Most of the films were grown at a range of temperature of 25-400 °C. However, several InN layers were also grown at 500 and 600 °C, even though the equilibrium dissociation pressure at 500 °C was almost 1 atm, and at 600 °C exceeds 20 atm [7]. It was assumed that the growth of the material, under thermodynamically unstable conditions, was most likely due to the very active nitrogen species (N and N^+) in the plasma above the InN surface, rather than the N_2 which would result from composition under equilibrium conditions. Those grown films were dark red and had n-type carrier concentration of $5\text{-}8\times10^{18}\text{cm}^{-3}$ associated with Hall mobility of 250 ± 50 $\text{cm}^2\text{V}^{-1}\text{s}^{-1}$ and resistivity in the range of $3\text{-}5\times10^{-3}$ Ω cm. Westra, Lawason and Brett pointed that the low base pressure achieved by Hovel and Cuomo and their pre-growth sputter clean, may have been significant in lowering the oxygen incorporation during growth resulting in films with good electrical properties [63].

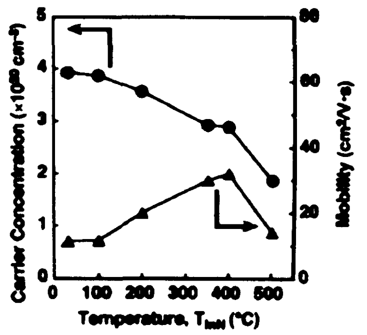

Figure 2.1: Hall mobilities and carrier concentrations of InN films deposited on bare α-Al_2O_3 at various growth temperatures. From [25].

Ikuta et al. established an optimum growth temperature of 400 °C from electrical properties, to study the influence of the insertion of ZnO buffer for InN growth [25]. Hall mobilities and carrier concentrations of InN films deposited on bare α-Al_2O_3 showed clear dependence on the growth temperature as shown in Figure 2.1. With the insertion of a ZnO buffer layer, significant improvement in the electrical and structural quality of InN films was observed. The Hall mobility increased with temperature up to 400 °C, which was considered as an indication for a decrease in scattered carriers at crystalline boundaries. However, at 500 °C, the mobility was reported to decrease to less than half of that that at 400 °C. It was considered that the reason why the quality becomes poor at 500 °C was due to the onset of thermal dissociation. Ikuta et al. explained the change in the carrier concentration over the range of temperatures (100-400 °C) was due to the decrease in defects promoted by more complete nitridation. On the other hand, the low carrier density at 500 °C was caused by insufficient nitride formation due to thermal decomposition; highlighted by the rapid decrease in the Hall mobility at that temperature. It was concluded that 400 °C was the best temperature to grow InN films.

Edgar et al., on the other hand, found that the optimum deposition temperature for the best epitaxial quality was in the range (325-375 °C) [64]. The best films showed the highest hardness characteristics (11.2 GPa). The best epitaxial film quality was produced at 350 °C confirmed by XRD analysis which was revealed by the minimum c-lattice constant (and thus minimum normal) and narrowest rocking curve full width half maximum (FWHM). Edgar et al. observed a decrease in the c-lattice parameter with increasing deposition temperature, where it reached a minimum at 350 °C, beyond that it increased slightly at 400 °C. The FWHMs of the (002) and (004) peaks followed the same trend. They explained the drastic increase in the FWHM with the increase in temperature from 350 °C to 400 °C to be due to low nitrogen incorporation leading to increases in the crystal defect concentration (Figure 2.2). On the other hand, the hardness showed an approximately inverse relationship to the c-lattice strain, and the hardest film had the least strain (Figure 2.3). Moving away from a deposition temperature of 350 °C, changes in the composition, microstructure or residual stress causing the films to become more plastic, were observed.

Gou et al. investigated the dependence of growth rate, crystallization, carrier concentration and mobility for the InN films on substrate temperature [26]. The deposition rate was found to be independent of the substrate temperature in the range below 400 °C; however, it rapidly increased as the temperature was further increased (Figure 2.4 (a)). This tendency has also been reported by Kistenmacher et al. [65], suggesting that the growth characteristics were almost independent of the crystal structure of the substrate in RF magnetron sputtering. A similar observation was reported by Cao et al. [66]. It was found that the substrate temperature had no significant influence on the growth rate of the film when varied between 100 and

500 °C. Guo et al. observed that the FWHM of the (0002) diffraction peak decreased with increasing the temperature (Figure 2.4 (b)) [26]. It was indicated that the grain size became larger with increasing of the growth temperature. The electrical properties were also found to be dependent on the substrate temperature. The Hall mobility increased with increasing temperature, however, the carrier concentration was found to be almost independent of the growth temperature (Figure 2.4 (c)). Increasing the substrate temperature improved the crystallinity of the InN films by providing activation energy for adatoms to occupy the positions of potential minima and enhancing re-crystallization due to the coalescence of islands by increasing the surface and volume diffusion, resulting in the improvement of the electrical properties with increasing substrate temperature.

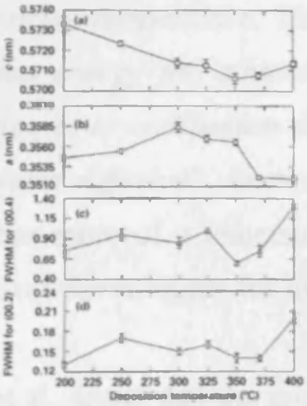

Figure 2.2: X-ray results of (a) *c*-lattice parameter, (b) *a*-lattice parameter, (c) FWHM for the (0 0. 4) peak and (d) FWHM for the (0 0.2) peak for the InN films deposited at different substrate temperatures. From [64]

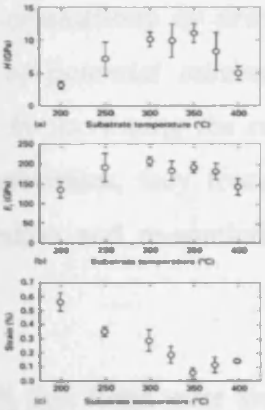

Figure 2.3: (a) Hardness H, (b) indentation modulus E_i (c) normal lattice strain vs. substrate temperature. From [64]

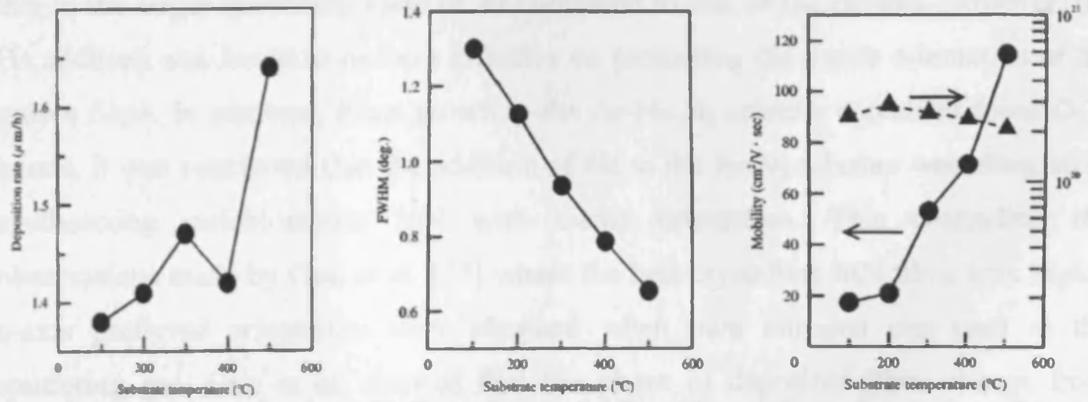

(a) Dependence of the deposition rate on substrate temperature for InN films.

(b) Dependence of full-width at half-maximum (FWHM) of InN(002) diffraction peaks on the substrate temperature.

(c) Dependence of mobility and carrier concentration on the substrate temperature for InN films.

Figure 2.4 From [26]

On the other hand, a low substrate temperature was found suitable for obtaining highly oriented InN crystalline films on (111) GaAs substrates [29]. The crystal quality degraded as the substrate temperature was increased. Such behaviour completely contradicts the observations made on sputtered InN films on sapphire and glass substrate, where crystallinity of the InN films improves with increasing the substrate temperature [26, 65]. The surface conditions of the substrate was been given as the reason for such behaviour. Guo et al. reported that growth of the film at the substrate is limited by the arrival rate of the reactive-gas atoms and the rate of reaction when reactive sputtering is used. They quoted that "*increasing the substrate temperature makes the re-evaporation and re-sputtering of atoms from the substrate more easily which results in decrease of the arrival rate of degradation of the crystal quality. At the same time, however, the rate of the reaction increases with increasing the substrate temperature. This leads to improvement of crystallinity by providing activation energy for adatoms to occupy the positions of potential minima and enhancing re-crystallization due to coalescence of islands by increasing the surface and volume diffusion*". Compared to sapphire and glass substrates, they found that GaAs has more of a temperature effect on the re-evaporation and re-sputtering of atoms from the substrate for InN growth.

Takai et al. found that the growth and nanostructure of InN thin films were strongly affected by the addition of helium (He) to the Ar-N_2 sputtering gas mixture [68]. They observed that the deposition rate of the InN thin films dropped from 2.2 nm/min in the Ar-N_2 mixture to 1.7 nm/min when helium was added to the mixture. They attributed this to the larger sputtering yield of Ar compared to that of the He-gas. However, the He addition was found to be very effective on promoting the c-axis orientation of the grown films. In addition, films grown in the Ar-He-N_2 mixture contained fewer O-In bonds. It was concluded that the addition of He to the Ar-N_2 mixture was effective in synthesizing stoichiometric InN with c-axis orientation. This contradicts the observations made by Guo et al. [27] where the best crystalline InN films with highly c-axis preferred orientation were obtained when pure nitrogen was used as the sputtering gas. Guo et al. showed that the phase of deposited films change from polycrystalline metallic In, to In + InN and to InN with wurtzite structure as nitrogen content in the sputtering gas was increased.

With reports showing that a base pressure in the deposition chamber was related to the oxygen contamination in InN thin films [63], Shinoda et al. (2002) examined the influence of base pressure by XPS measurements [69]. Figure 2.5 shows their XPS spectra for InN films deposited at different growth parametrs. The O1s signal showed a decrease in intensity as the base pressure decreased due to the reduction of residual oxygen and water vapour in the deposition chamber while the peak intensity of the O-In bond signal became much weaker when the source N_2 gas was purified by a liquid N_2 trap. Shinoda et al. indicated that the oxygen contamination in the InN thin film could be effectively reduced by both a decrease of base pressure and additional source N_2 gas purification where they found that the N-In bonding density in the films obtained was increased with both the decrease in N_2^+ ion energy and the increase in molecular N_2 pressure, and was decreased with the increase in N_2^+ ion flux density at the In-target surface as shown in figure 2.5. They also suggested that atomic N and/or N^+ ion plays a major role in the formation of In-N bonds.

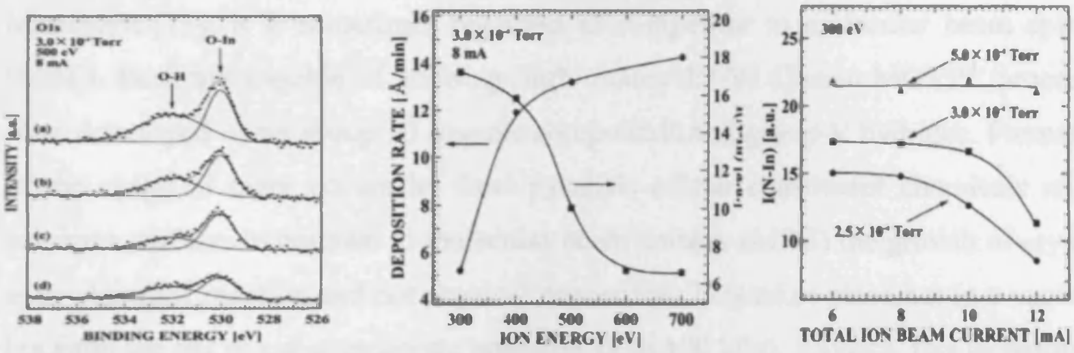

(a) XPS O1s spectra of InN thin films, together with the Gaussian fitting. The deposition chamber was evacuated to (a) 1×10^{-6} (b) 5.0×10^{-7} (c, d) 1.0×10^{-7} Torr. The film was carried out (d) with and (a-c) without liquid N_2 trap for the purification of the source of N_2 gas.

(b) XPS signal intensity of a N–In bond and film deposition rate in InN.

(c) XPS signal intensity of a N–In bond in InN thin films, as a function of total ion-beam current and gas pressure.

Figure 2.5 XPS analysis of indium nitride. From [69]

The sputtering technique allows low-temperature growth, and with precise control on the growth parameters the quality of the grown InN films can be improved. However, significant oxygen content and non-stoichiometric films are always a concern with films produced by sputtering. The structural properties of InN grown by sputtering at low temperatures are mostly polycrystalline despite many reports of single-crystal

InN, but these films showed poor electrical properties compared to the high quality InN grown by other methods such as MOVPE and MBE. This polycrystalline structure would limit the application of InN especially for electronic devices, hence the need of employing other techniques in the growth of high quality InN materials.

2.1.2 Metal organic vapour phase epitaxy (MOVPE)

Metal organic vapour phase epitaxy (MOVPE) is a chemical vapour deposition method of epitaxial growth of materials, especially compound semiconductors from the surface reaction of organic compounds or metalorganics and metal hydrides containing the required chemical elements. Alternative names for this process include organometallic vapour phase epitaxy (OMVPE), metal organic chemical vapour deposition (MOCVD) and organo-metallic chemical vapour deposition (OMCVD) [70]. MOVPE began in the late 1960s with the research of Manasevit [71]. It is sometimes regarded as competitor to molecular beam epitaxy (MBE). Both are capable of growing high quality III-V. Classic MOVPE processes were developed using group-III organic compounds and group-V hydrides. Formation of the epitaxial layer occurs by final pyrolisis of the constituent chemicals at the substrate surface. In contrast to molecular beam epitaxy (MBE) the growth of crystals is by chemical reaction and not physical deposition. This takes place not in a vacuum, but from the gas phase at moderate pressures (2 to 100 kPa). As such, this technique is preferred for the formation of devices incorporating thermodynamically metastable alloys. It has become the dominant process for the manufacture of laser diodes, solar cells, and LEDs [70]. The source materials generally used for the MOVPE growth of InN are trimethylindium (TMIn) as indium source and ammonia (NH_3) as a nitrogen source. Nitrogen (N_2) is being used as a carrier gas.

Besides a conventional MOVPE system, researchers have employed modified MOVPE systems to overcome the problems and limitations of the conventional MOVPE system in an attempt to achieve high quality III-nitrides. However, compared with the conventional MOVPE, more work for the improvement of the film quality has yet to be done. Plasma-assisted MOVPE employs reactive nitrogen radicals by plasma dissociation, which is independent of the growth temperature [72]. It has the advantages of low plasma damage in the grown films and no contamination from the electrodes. Laser-assisted MOVPE is also a potential growth technique, which can provide reactive N and In radicals by photolysis of their precursors independent of the growth temperature, therefore, the film can be grown at a low temperature [73]. It is also thought to be advantageous in reducing the nitrogen vacancies in InN film due to the temperature independence of the partial pressure of nitrogen over the InN film. Migration enhanced metal organic chemical vapour deposition (MEMOCVD) is an improved version of pulsed atomic layer epitaxy (PALE) [74], which deposits quaternary $Al_xIn_yGa_{1-x-y}N$ layers by repeats of a unit cell grown by sequential metal organic precursor pulses of Al, In, Ga, and NH_3. In PALE, the duration of each pulse in the unit cell is fixed, and the NH_3 pulse always followed each metal organic pulse. In MEMOCVD, the duration and wave forms of precursor pulses are optimized, and the pulses might overlap allowing for a continuum of growth techniques ranging from PALE to conventional MOCVD. MEMOCVD combines a fairly high growth rate for buffer layers with reduced growth temperature (by more than 150 °C) and improved quality for active layers. MEMOCVD has proved to be superior to the MOCVD and PALE techniques [75]. The epitaxial growth of InN under low-pressure conditions such as MOCVD or MBE is problematic due to large thermal decomposition pressure at the optimum, creating conflicting material properties due to point defect chemistry in InN [76, 77]. Surface stabilization data have shown that InN can be grown at much higher temperatures if stabilized at high nitrogen pressures [7] evoking the use of a novel high-pressure chemical vapour deposition (HPCVD) technique [78]. HPCVD extends processing parameters beyond those accessible by MBE and MOCVD, enabling the growth of epitaxial InN layers at temperatures as high as 1150 K for reactor pressures around 15 bars.

A narrow growth temperature window governs the growth of high quality InN. The low dissociation temperature and thermal stability limits the growth temperature from above while from below the growth temperature would cause the lack of reactive nitrogen that would react with indium to form indium nitride. Thus with a narrow temperature window, the growth of indium nitride has usually been done at rather low temperatures with extremely high V/III ratios [79, 80]. The growth is further complicated as the InN surface, unlike most III-Vs, cannot be stabilized under excess group-V flux, and is etched in ammonia ambient [81]. The limitation of the growth temperature forces the growth to be performed below 500 °C; this will lead to material with high defect densities as a result of nitrogen shortage. The decomposition efficiency of ammonia gas, which is widely used as a nitrogen source for the epitaxial growth of III-nitride compounds, is very low in this temperature region and a large amount of ammonia gas would be needed during the growth [82].

The growth temperature is a critical parameter in the MOVPE growth of InN and is strongly correlated with the V/III molar ratio [83, 84]. It is a predominating factor for surface morphology, growth rate and electrical properties of MOVPE InN [85].

Koukito et al. carried out thermodynamic studies on the MOVPE growth of III-nitrides, the role of hydrogen during the MOVPE growth, and the use of hydrazine (N_2H_4) as precursor for the MOVPE growth of III-nitrides [86-88]. They pointed out that a high input V/III ratio, the use of inert carrier gas, and a low mole fraction of the decomposed NH_3 are required for the growth of InN [86]. They also showed that the increase of hydrogen in the growth system results in a decrease of the InN deposition rate, which they suggested was due to the decrease of driving force for the deposition. Koukito et al. reported that at low temperature the driving force for the deposition is almost independent of the increase of hydrogen partial pressure while at high growth temperature it significantly decreases with increasing hydrogen pressure and even reaches a negative value; this is called etching [87]. It was concluded that the increase of H_2 would prevent the reaction depositing InN, but this reaction would proceed more effectively in the inert gas system. Hence, the necessity to use inert gas in the growth of InN. Compared with the NH_3 system, they predicted that the growth of nitride occurs rapidly using hydrazine (N_2H_4) as nitrogen source, especially for the indium containing nitrides, without the deposition of In-droplets [88].

Matsouka et al. established a phase diagram of the InN growth conditions to grow high quality InN using metal organic vapour phase epitaxy (MOVPE) [89]. This phase diagram is shown in figure 2.6. Growth under region (B) conditions could result in material with presence of metal-like indium, while under region (A) single-crystal material could be grown. However, no InN could be grown under region (C) conditions.

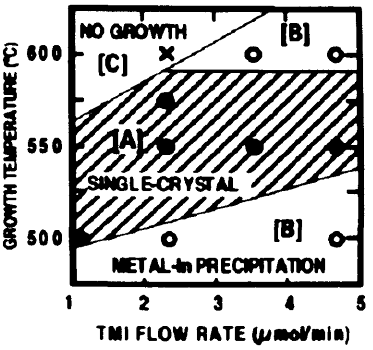

Figure 2.6 Phase diagram of InN. From [89]

Wakahara and Yoshida carried out epitaxial growth in the temperature range of 400 to 600 °C [39]. They obtained InN fibre structures with indium droplets when a high substrate temperature (~ 600 °C) was used. However, a specular surface InN film was obtained when a low substrate temperature (< 500 °C) with relatively high microwave power (>100 W) was used. When a low microwave power (< 70 W) at the same temperature, InN whiskers were observed on the InN layer.

Similar result was reported by Sato on the growth of InN epitaxial layers on (0001) sapphire by plasma-assisted MOCVD, where no InN was grown and In-droplets were deposited at temperatures higher than 650 °C because of the thermal instability of InN at high temperatures [90]. The InN layers grown at 620 °C had slightly milky surfaces with In-droplets, suggesting that 620 °C was close to the critical temperature of InN decomposition. The temperature dependence below 600 °C was not large, suggesting that the growth rate was mainly determined by tri-ethyl-indium (TEIn) supply. The electrical properties were found to be drastically affected by the growth temperature where the low carrier density of 6×10^{19} cm^{-3} was achieved at the growth temperature of 600 °C while it decreased drastically with the increase of the growth temperature to 620 °C a small number of In-droplets were observed on the surface. Sato concluded that it was more appropriate to lower the growth rate than to increase the N-radical flux to achieve low carrier density films. (Figure 2.7).

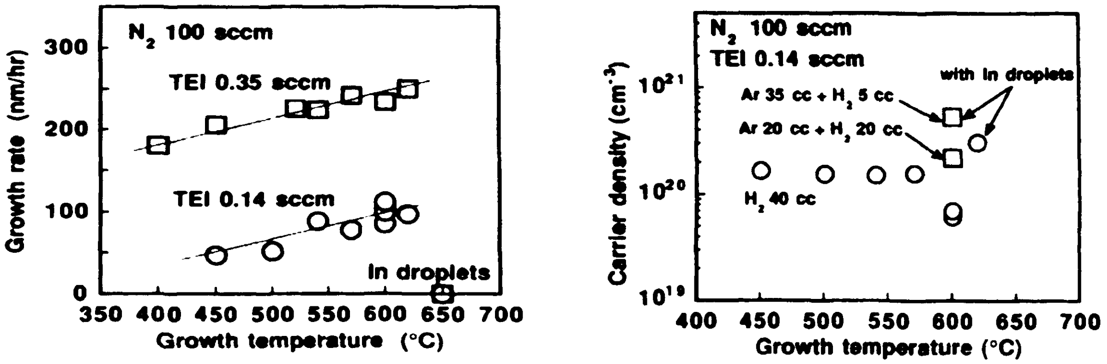

(a) Temperature dependence of the InN growth rates on (0001) sapphire with 100 sccm of N_2. In droplets with no InN were deposited above 650 °C.

(b) Carrier densities of InN as a function of the growth temperature.

Figure 2.7 From [90]

Chen et al. reported high quality InN films grown at low temperatures which were about 50 to 100 °C lower than the reported values [91]. It can be seen, from their corresponding (0002) XRC reflection spectra (Figure 2.8(a)), that the InN film grown at 600 °C exhibited quite a broad rocking curve spectrum. It was not until the temperature decreased to 450 °C when the rocking curve spectra showed some changes and sharp components started to appear. Further decrease of the growth temperature below 450 °C lead to the increase in the ratio of the sharp peak to the broad band continues to increase and the sharp XRC eventually dominates for samples prepared at temperatures below 400 °C. Chen et al. explained this phenomenon that the growth of InN conducted at a temperature below 400 °C, to some extent, experienced a much higher effective V/III ratio due to the incomplete decomposition of TMIn, which was responsible for the improved quality of the InN thin film when grown at low temperature.

The growth temperature dependence of MOVPE InN on sapphire was studied by Yamamoto et al. [85]. They produced epitaxial films of InN were grown on sapphire (0001) substrates at 500-650 °C. When the growth was done at a temperature less than 550 °C, the film had a surface with many small grains, as shown in figure 2.9, and the growth was found to be columnar due to three-dimensional growth. As the temperature increased, 600-650 °C, a continuous film with enhanced two-dimensional growth was obtained (see figure 2.9). However, when the film was grown at 650 °C, many pits were formed on the enlarged grain growth surface, and assumed to be due to the decomposition or thermal etching of the grown InN film at such high temperature. Yamamoto et al. concluded that high temperature growth was very effective to enhance grain growth and/or two-dimensional growth of InN. Furthermore, they found that the growth rate showed dependence on the growth temperature. In the temperature range 500-630 °C, the growth rate was found to be increased with increasing growth temperature and showed saturation against the increase in TMIn supply. At 630-650 °C, such saturation was not found and a growth rate as high as 0.8 μm/hr was obtained by increasing TMIn supply. The electrical properties were also found to be dependent on the growth temperature as Hall mobility was found to increase while carrier concentration decreased with increasing the growth temperature.

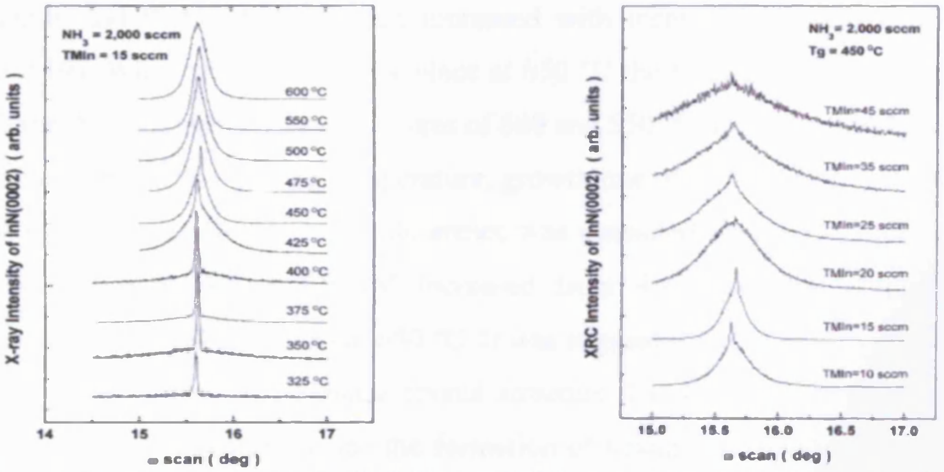

(a) X-Ray rocking curve spectra for InN films grown at temperatures ranging from 325 to 600 °C.

(b) X-Ray rocking curve spectra for InN films grown at different TMIn flow rates.

Figure 2.8: XRD diffraction peaks at different growth conditions. From [91]

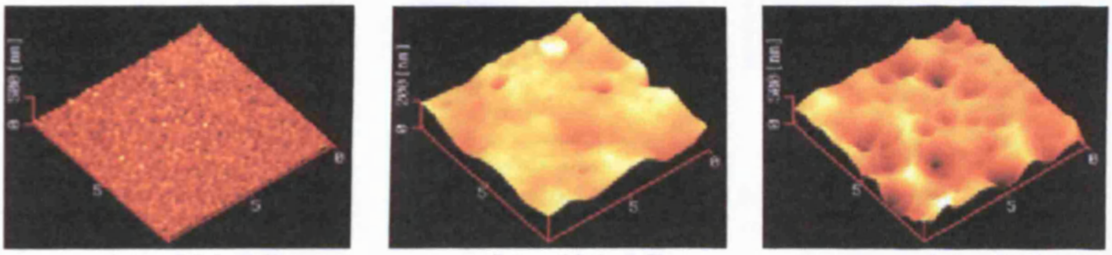

(a) 500 °C (b) 600 °C (c) 650 °C

Figure 2.9: Surface morphology (AFM image) for InN films grown at a different temperature, with growth pressure of 0.1 atm. From [85]

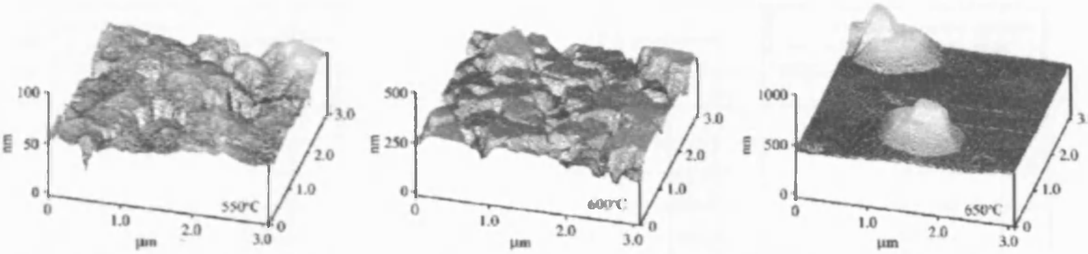

Figure 2.10 Surface morphology (AFM image) for InN films grown at a different temperature 550, 600 and 650 °C. From [92]

Suihkonen et al. suggested that the formation of metallic indium was caused by the desorption of nitrogen at high temperatures, rather than by the shortage of reactive nitrogen during growth [92]. In their AFM scans of InN surface grown at temperatures of 550, 600 and 650 °C they showed that the film surface consisted of 3D islands and that the island size increased with increasing growth temperature (figure 2.10). When the growth took place at 650 °C the islands had clear hexagonal base shape, but with growth temperatures of 600 and 550 °C the shape was less clear. They observed that the growth temperature, growth rate or V/III did not affect the ω-2θ FWHM values, as a value of 1700 arcsec was measured from all samples (Figure 2.11(a)). However, the ω FWHM increased from 4000 to 6700 arcsec as the temperature increased from 550 to 650 °C. It was suggested that the films consisted of domains of hexagonal single-phase crystal structure that were tilted with respect to each other. These domains caused the formation of hexagonal islands on the sample surface. Furthermore, increasing growth temperature resulted in larger domains that were more tilted with respect with each other.

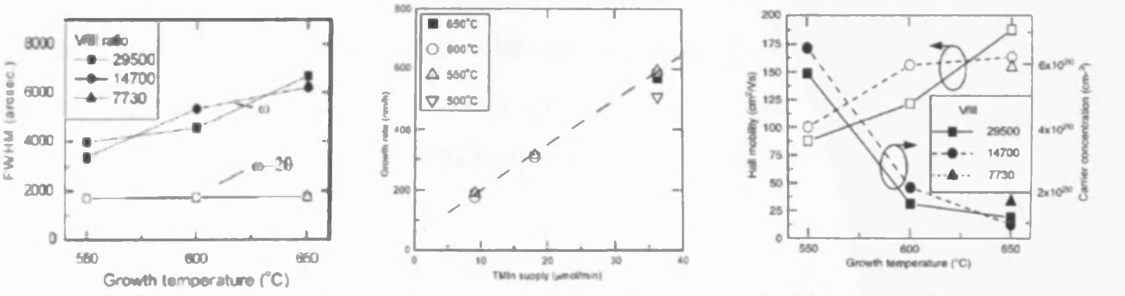

(a) FWHM values of InN (0002) reflection as a function of growth temperature with different V/III ratios.

(b) Growth rate of InN as a function of TMIn supply at different growth temperatures.

(c) Hall mobility and carrier concentration of the InN samples as a function of growth temperature with various V/III ratios.

Figure 2.11 From [92]

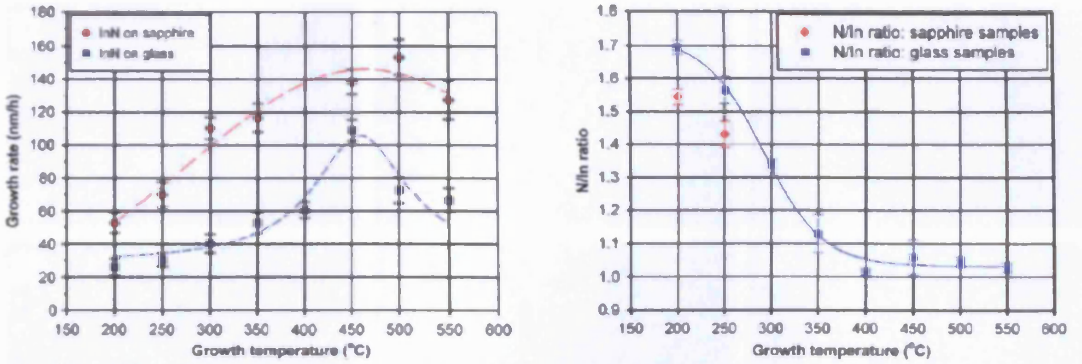

(a) Growth rate as a function of growth temperature.

(b) N/In ratio as a function of growth temperature in the bulk InN films.

Figure 2.12 From [93]

The properties of InN grown at various temperatures on c-plane sapphire and glass substrates, using remote plasma-enhanced chemical vapour deposition, have been investigated by Chen et al. [93]. They found that the growth rate of the InN grown on glass increased gradually with the growth temperature until reaching a peak at approximately 450 °C (Figure 2.12). They explained the dependence to be due to the number of available indium precursors species, decomposed from TMIn on the substrate surface, waiting to chemically interact with nitrogen radicals. When the substrate temperature was set above 400 °C the pyrolysis of TMIn would be mostly complete on the substrate surface, and the amount of desorbed indium would remain approximately the same from that point to higher growth temperatures. With further increases in the growth temperature above approximately 500 °C, the growth rate dropped significantly. The drop in the growth rate was related to the thermal decomposition of InN, which should become more prominent at the higher growth temperatures. A similar growth rate trend compared with the glass films was observed for InN on c-plane sapphire but with greater rates possibly benefiting from the availability of the preferable c-axis oriented hexagonal template. Chen et al. concluded that the required growth temperature to achieve the maximum growth rate of InN was approximately 470 °C.

The crystalline properties of their InN were also found to be affected by the growth temperature. When the growth temperature was 300 °C the InN films on both the sapphire and glass substrate showed a fine-grained highly c-axis oriented polycrystalline structure. As the growth temperature increased to approximately 450 °C the grain size increased dramatically, producing crystallites up to about 200 nm in

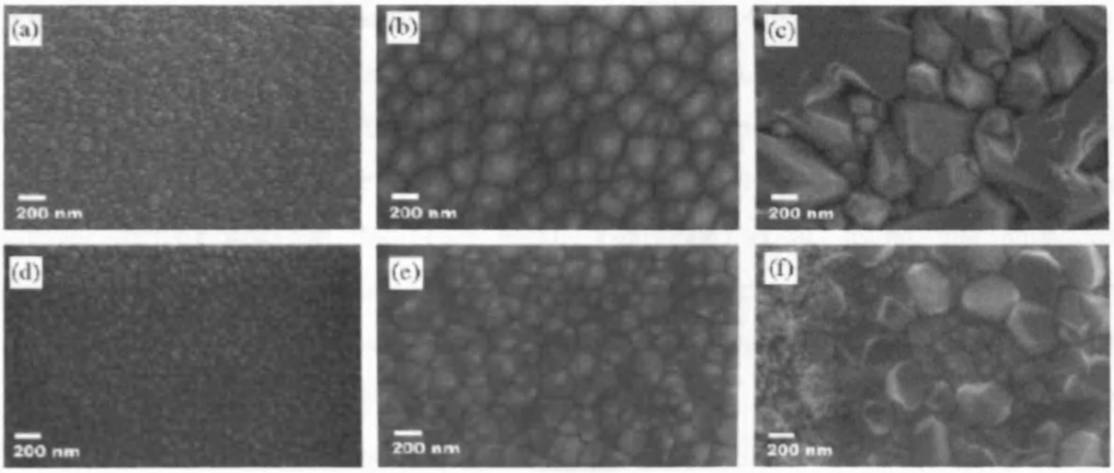

Figure 2.13 SEM surface images of the InN films grown on sapphire (a–c) and glass (d–f) at 300, 450 and 550 °C. From [93]

diameter. At the highest growth temperature of approximately 550 °C the InN film surface on sapphire showed further improvement in crystallinity. The hexagonal shape was more strongly apparent, and some of these have merged with surrounding crystals so that the onset of coalescence was evident. In contrast, for the InN grown at 550 °C on glass, there were fewer distinct hexagonal-shaped columns and coalescence was not evident. Moreover, the film has experienced severe decomposition (Figure 2.13).

Furthermore, Chen et al. investigated the compositional material of the RPE-CVD grown InN. All the InN films analysed were found to be nitrogen rich, and the degree of excess nitrogen incorporation showed a strong correlation with the growth temperature. As the growth temperature increased, the films became more stoichiometric. The films grown below 400 °C had a high degree of excess nitrogen incorporation. Those films grown between 400 and 550 °C were slightly nitrogen rich. The degree of O, H and C incorporation did not correlate to the growth rate and the surface morphology alone, but was also influenced by the degree of excess N incorporation, which was found to be the dominant impurity species.

With a growth rate showing a linear dependence on the TMIn flow in the temperature range between 550 and 650 °C, Suihkonen et al. [92] indicated that the growth rate is limited by the amount of reactive indium, and not by the NH_3 decomposition rate as has been reported by Yamamoto et al. [85]. Suihkonen et al. observed that a change in the growth rate or V/III ratio did not affect the ω-FHWM. (Figure 2.11(b)). However, an increase in the growth temperature resulted in an improvement in the electrical properties and optical properties of the grown films, while V/III did not show any clear effect on either the electrical or optical properties. So they concluded that the temperature dependence of the electrical properties did not result from more efficient cracking of NH_3 but rather from better material quality resulting from the higher growth temperature. On the other hand, Yamamoto et al. found that enhanced decomposition of NH_3 improved Hall mobility and decreased carrier concentration [94]. The blue-shift of the PL peak energy observed with decreasing growth temperature was thought to result from the increase of carrier concentration in material grown at low temperature [92]. Figure 2.11(c) shows V/III ratio dependence of carrier concentration for InN films grown at different temperatures. Yamamoto et al. reported a marked V/III dependence of carrier concentration when InN was grown at temperature lower than 600 °C [85]. That seemed to show that the increase in V/III ratio brings about the reduction of nitrogen vacancies in the InN by increasing active nitrogen in the growth atmosphere, which resulted in the improvement in the electrical properties. When InN was grown at temperature around 650 °C, the carrier concentration was found to be independent of V/III ratio, so Yamamoto et al. suggested that another mechanism governs the electrical properties of InN grown at such a high temperature (Figure 2.14). They concluded that growth reaction was limited by NH_3 decomposition at a temperature lower than 600 °C, where electrical properties of the grown InN were governed by active nitrogen concentration in the growth atmosphere. At a temperature higher than 630 °C, on the other hand, the growth was limited by TMIn supply, where active nitrogen concentration in the growth atmosphere was not a critical factor. At such high temperature, however, thermal decomposition of the grown InN could govern the electrical properties of InN, showing no V/III ratio dependence of the carrier concentration.

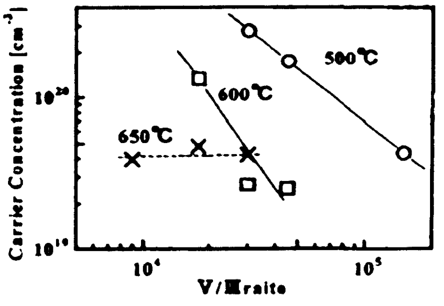

Figure 2.14 Carrier concentration of InN grown at different temperatures as a function of V/III ratio. From [85]

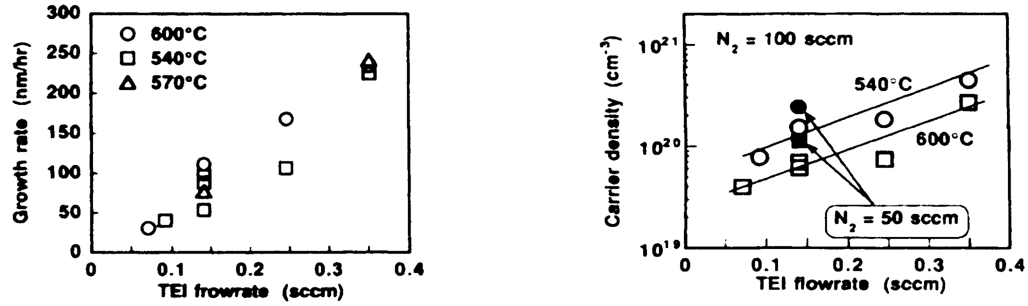

(a) InN growth rate as a function of TEIn flow rates.

(b) Carrier densities of InN epilayers as a function of TEIn flow rates. The growth temperatures were 540 °C (circles) and 600 °C (squares). The N_2 flow rates were 100 sccm (open symbols) and 50 sccm (solid symbols).

Figure 2.15 From [90]

With a growth rate that is almost linear to the tri-ethyl-indium (TEIn) supply, Sato indicated that a lot of TEIn supplied to the surface did not contribute to the growth [90]. It was suggested that the TEIn does not efficiently adsorb on the surface of InN. It was also found that lower carrier concentration can be achieved at low TEIn flow rates, and thus at low growth rates. By investigating the effect of the V/III ratio, Sato found that the low carrier densities at low growth rates were not mainly attributed to the high V/III. Therefore, he concluded that increasing N-radical flux was preferable but lowering the growth rate was essential for achieving low carrier density.

Chen at al. carried out a study of the influence of the V/III ratio and the growth temperature on InN grown by MOVPE [91]. They observed that the InN film quality grown at 450 °C deteriorated sharply as the TMIn flow rate increased over 20 sccm. Indium droplets were noticeably distributed on the surface for samples grown at high flow rates ((Figure 2.18(b)). The influence of the transitional TMIn flow rate in both the formation of In droplets and the degradation of the InN film led them to suggest that the formation of In droplets on the surface of was likely to be the major reason for the film degradation and therefore should be avoided during InN growth.

Malyere et al determined the dependence of growth rate versus V/III molar ratio was determined from the initial slope of the reflectivity oscillation [95]. They assumed that the slope of the reflectivity at the beginning would give sufficient information (Figure 2.16), since it is linearly correlated with the oscillation period (corresponding to the layer thickness). A clear decrease of the growth rate with increasing V/III molar (increasing NH_3 flow) was observed due to the hydrogen arising from the NH_3

decomposition. They thought that the effective nitrogen source permitting the growth of InN was provided directly by ammonia and not through its' decomposition into nitrogen. So it was concluded that there should a compromise in obtaining the optimum V/III molar ratio, since the injected ammonia must be large enough to permit the InN growth, but must not result in an excess amount of H_2, which would "etch" the layer, a result that agrees with the reports of Kukito et al. [87].

Kadir et al. found that the material quality was relatively poor at very low and at very high values of V/III where a higher V/III ratio increased the presence of hydrogen which reduced the forward reaction and hence impeded the formation of InN [96]. On the other hand, a lower V/III ratio resulted in poor crystallinity as indicated by the large width of the $(10\bar{1}1)$ reflection (Figure 2.17), which was attributed to the combined effects of weak In-N bond and high vapour pressure of N_2 over InN. Their best material was obtained at a moderate value of V/III ratio ~18,700.

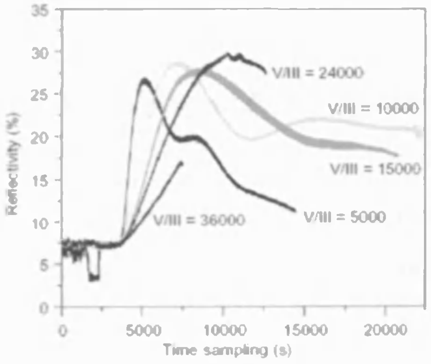

Figure 2.16 In situ reflectivity performed during InN growth. The dependence of the growth rate versus V/III molar ratio is determined from the initial slope of the oscillations, and the oscillation period. From [95]

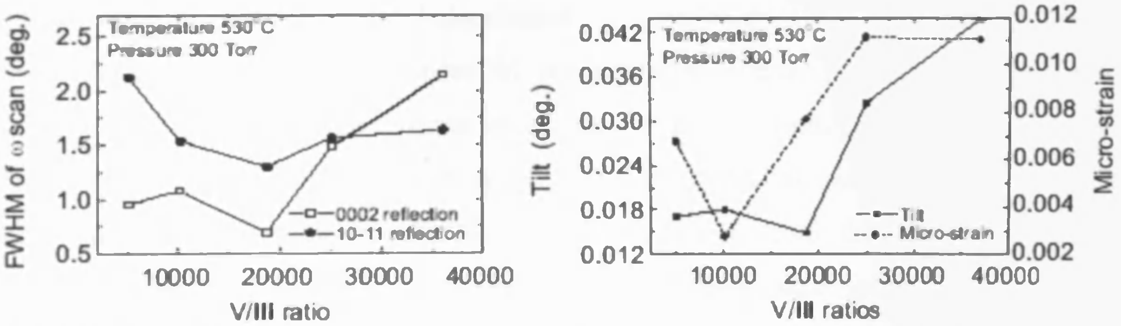

(a) FWHM vs V/III **(b) Tilt and micro-strain Vs V/III**

Figure 2.17 From [96]

Pelli et al. noted that indium vacancy concentration was almost independent of the V/III molar ratio at 4800-24000 [97]. They observed that at a V/III ratio lower than 4000 the In-droplet formation was accompanied by the formation of vacancy clusters. They assumed that due to limited sticking of In on the growth surface close to the decomposition temperature, the elevation of growth temperature enhanced the In-vacancy formation.

A high input V/III ratio is required for the growth at low temperature while a low input V/III ratio is essential for the high temperature growth. The deposition reaction of InN proceeds more effectively in the inert gas system or N_2 carrier gas and is prevented with increase of H_2 either as a reaction product or carrier gas. Despite the difficulty in controlling the growth parameters and the very narrow window of allowed growth temperature, MOVPE, as well as MBE, are considered one of the most popular growth techniques for III-nitrides, and researchers succeeded in producing good quality material using these techniques.

2.1.3 Molecular beam epitaxy (MBE)

Molecular beam epitaxy (MBE) was developed in the early 1970s as a means of growing high-purity epitaxial layers of compound semiconductors [98]. Since that time it has evolved into a popular technique for growing III-V compound semiconductors as well as several other materials. MBE can produce high-quality layers with very abrupt interfaces and good control of thickness, doping, and composition. Because of the high degree of control possible with MBE, it is a valuable tool in the development of sophisticated electronic and optoelectronic devices. In MBE, the constituent elements of a semiconductor, in the form of 'molecular beams', are deposited onto a heated crystalline substrate to form thin epitaxial layers. The 'molecular beams' are typically from thermally evaporated elemental sources, but other sources include metal-organic group III precursors (MOMBE), gaseous group V hydride or organic precursors (gas-source MBE), or some combination (chemical beam epitaxy or CBE). To obtain high-purity layers, it is critical that the material sources be extremely pure and that the entire process be done in an ultra-high vacuum environment. Another important feature is that growth rates are typically of the order of a few Å/s and the beams can be shuttered in a fraction of a second, allowing for nearly atomically abrupt transitions from one material to another.

An InN epitaxial film with sufficient quality for application to practical devices has not been obtained due to difficulties in epitaxial growth, such as a dissociation temperature as low as 600 °C [99]. Higashiwaki and Matsui assumed that conventional metal-organic chemical vapour deposition (MOCVD) and ammonia molecular beam epitaxy (MBE) techniques are not suitable for growing high quality InN films with a low defect density when epitaxial growth of InN has thus conventionally been performed below 500 °C due to the low decomposition efficiency of ammonia [46]. So they proposed a better technique for InN epitaxial growth and that would be plasma-assisted molecular beam epitaxy (PAMBE), which uses nitrogen radicals produced by an RF-plasma cell and only a small amount of N_2 gas. Another alternative for obtaining atomic nitrogen is that of the electron-cyclotron resonance (ECR) [100-103], metal organic molecular beam epitaxy (MOMBE) [106]. MOMBE is one of the potential growth techniques where the advantages of both MOVPE and MBE can be utilized [72]. Films can be grown relatively at low temperatures by MOMBE and premature reaction of the precursors, a serious problem in MOVPE, is minimized due to the large mean free path of gaseous molecules. Compared with the MBE technique, MOMBE has several advantages, such as no downtime for source replacement and has the potential for scale-up.

There are few parameters that will govern the quality of the grown material. The growth temperature is a very critical parameter for obtaining high quality InN material. Growth mode, two-dimensional (2D) or three-dimensional (3D), would play an important role in defining the crystalline quality of the grown film and the application of the material. Also the In/N ratio and the polarity of the grown film would have an impact on the structural, electrical and even optical quality of the grown epitaxial layer. One can not ignore the importance and influence of the substrate and the buffer layer used.

Koukitu et al. carried out thermodynamic analysis on molecular beam epitaxy of III-nitrides [105]. They calculated the equilibrium partial pressure, the normalized growth rate and the phase diagram of the deposition for GaN, InN and AlN. In the growth of InN, they concluded that three deposition modes, i.e., growth, droplet and etching regions, appear in the temperature range 500-900 °C. They predicted that a suitable growth temperature for InN would be 600-700 °C with V/III ≥ 1. Koukitu et al. noticed that there was a difference between the atomic nitrogen and NH_3 source where the etching region appeared (see Figure 2.18).

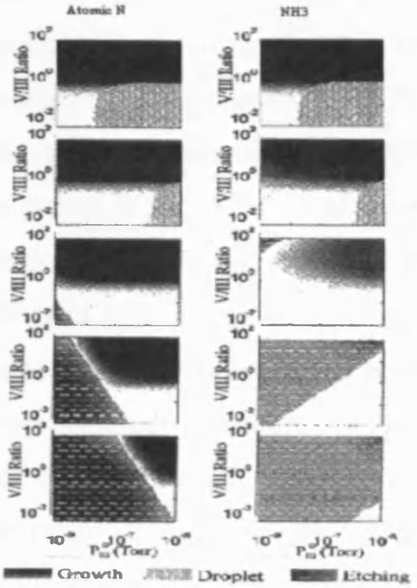

Figure 2.18: The calculated phase diagram for the deposition of InN. From [105]

In the case of the atomic nitrogen, they found that the etching region appeared constantly at the region where the input V/III ratio and the input P^{0}_{III} were low values. On the other hand, in the case of the NH_3 source, it appeared at the region where the input V/III was high and the input P^{0}_{III} was a low value. They explained this to be due to the increase in H_2 produced from the decomposition of NH_3.

Experimental growth temperatures at which high quality InN films were successfully grown, however, differed from the predicted theoretical ones. The experimental growth temperatures were found to be in the range of 450 to 550 °C. Mamutin et al. deposited InN on sapphire at various temperatures (300 to 500 °C) and studied the initial growth stages of InN by plasma-assisted MBE [43]. They showed that high temperature annealing of low temperature grown InN buffer layer, followed by the main InN layer growth at maximal T_s (~ 470 °C) promoting stoichiometric conditions at given activated nitrogen flux, provided high quality uniformly strained films with flat surface and featureless interface with the sapphire substrate. The improvement of the structural quality with variations in the initial growth stage was highlighted by a significant improvement in the electrical properties.

A series of InN samples were grown with different substrate temperatures ranging from 360 °C to 590 °C by migration-enhanced epitaxy (MEE) [44]. Lu et al. found that the FWHM of the InN(0002) peak in the XRD θ-2θ scan and ω scan nearly continuously decreased with increasing growth temperatures which implied that the best crystalline quality could be obtained at the highest growth temperature of 590 °C. However, in AFM measurements, while most of the samples grown below 550 °C exhibited acceptable surface morphology, InN films grown at 590 °C showed a very rough surface. Their combined XRD and AFM results were explained such that the rough surface should result from the dissociation effect of InN at high temperatures, while the improved crystal quality was due to the annealing process occurring at the same time. The influence of substrate temperature on electrical properties was also investigated. Lu et al. found that the improvement of the electrical properties of InN films with increasing substrate temperature in the range of 350 to 500 °C was associated with better crystalline quality at higher growth temperature, which has been reflected in the XRD measurements. Meanwhile, the degradation of electrical properties in the temperature range of 500 to 600 °C was a result of the dissociation effect of InN at high temperature, which has also been revealed from the poor surface morphology of the AFM measurements. They concluded that a substrate temperature of 500 °C was their optimum temperature for high quality InN.

From Raman analysis of indium nitride thin films grown by MBE on (111) silicon substrates at temperatures between 450 °C and 550°C (Figure 2.19), Agulló-Rueda showed that the phonon wave-numbers decreased slightly with growth temperature [106]. They attributed that dependence to thermal stress. The tensile stress, which was produced due to the mismatch in the thermal expansion between the substrate and the grown InN, would reduce the phonon frequencies and, as observed, the frequencies would decrease with growth temperature. Saito et al. studied the growth temperature dependence of InN crystalline quality using various evaluation techniques [107]. InN films were grown by RF-MBE with film thickness of 300 nm at various temperatures in the range of 460 to 550 °C on (0001) sapphire substrates after the nitridation process. Their results suggested that a higher growth temperature (550 °C) within the dissociation limit of InN is preferable to grow high quality InN films. Wang et al. carried out a study on the effect of growth temperature on InN

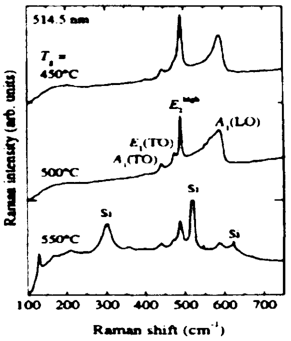

Figure 2.19: Raman Spectra for InN grown at different temperatures. From [106]

layers grown by MBE on GaN template in a temperature range of 440 to 620 °C [108]. They reported that the surface morphology was greatly influenced by the growth temperature with the observation of dentritic morphologies together with some compact hexagonal grains, observed when TG $\leq$ 540 °C; while a step-flow-like morphologies and spiral growth were clearly observed when TG $\geq$ 540 °C. Crystalline quality was improved with increasing growth up to 540 °C and was almost saturated at higher temperatures. They indicated that the epitaxial temperatures of 540 to 600 °C were best to achieve high quality InN films with a smooth surface.

Grandal et al. pointed out that the growth temperature is the most critical parameter during the growth of InN layers [109]. Growths performed at substrate temperatures above 500 °C lead to the dissociation of the InN layer and the formation of metallic In-droplets on the surface (Figure 2.20(a)). Once they set the growth temperature below 500 °C, they found out that the molecular indium flux to active nitrogen ratio (i.e. III/V ratio) was the fundamental parameter controlling the morphology of the films. N-rich conditions led to columnar InN samples (Figure 2.20(b)) with very intense low-temperature photoluminescence at 0.74 eV, while compact layers were obtained when using growth conditions towards In-rich (Figure 2.20(c)). They noted that the effective III/V ratio was strongly affected by the substrate temperature. A slight change in the growth temperature was found to have a direct effect on the morphology of the layers since the III/V ratio was also modified.

Saito et al. have demonstrated the growth of single-crystal InN with excellent surface morphology and electrical properties, using an InN buffer layer grown at a low-temperature of 300 °C by RF-MBE [45]. By keeping all the growth parameters constant throughout the experiment but varying the RF plasma power to change the effective V/III ratio, they confirmed by optical emission spectroscopy that the concentration of atomic nitrogen increased as the plasma power increased. They found that the best quality InN with excellent surface morphology and electrical properties could be obtained using a growth temperature and plasma power of 550 °C and 240W, respectively.

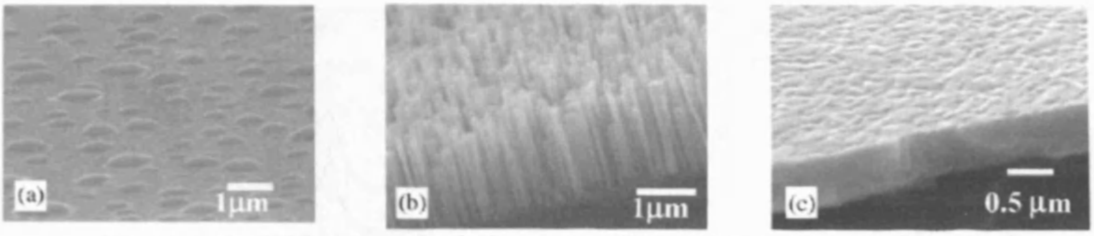

Figure 2.20: SEM pictures for InN grown at different temperatures. From [109]

Ive et al. studied the InN quality grown under In-rich conditions with variable growth temperature (420-540 °C) [110]. They observed that the samples grown under In-rich conditions had better electrical (μ = 819 cm^{2}V^{-1}s^{-1}, n = 1.6×10^{19} cm^{-3}) and optical (E_g = 0.78 eV) properties than those grown under N-rich conditions (μ = 375-441 cm^{2}V^{-1}s^{-1}, n = 5.6-6.8×10^{19} cm^{-3}, E_g = 1.1-1.2 eV). It was also found, by XRD, that crystalline In-inclusion tends to get incorporated in layers grown under In-rich conditions.

Gallinat et al. identified a temperature window necessary for growth of In-polar InN (see Figure 2.21) [111]. It was observed that at temperatures above 500°C there was no InN growth and only In-metal was deposited on the substrate, regardless of the In flux/active nitrogen ratio. Growth of In-polar InN should be possible beyond 500 °C, however, with an appropriate increase in active nitrogen to offset InN dissociation. At growth temperatures between 420 and 490 °C fully coalesced InN layers were realized. Based on that growth temperature window, two growth regimes were identified: the N-rich regime and the In-droplet regime. This observation is different from GaN where three growth regimes were identified for the PA-MBE growth in the metal-polar orientation [112, 113]. On the other hand, Losurdo et al. defined three growth regimes: In-rich, intermediate and N-rich [114]. They concluded that quality, morphology, and optical properties of InN improved for growth in the In-rich regime without In cluster segregation into the films.

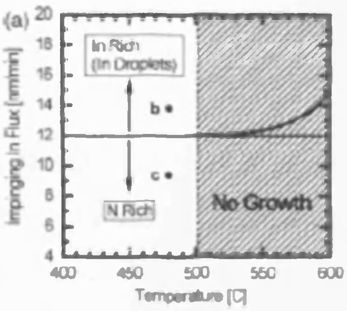

Figure 2.21: In-polar InN PA-MBE growth diagram. From [111]

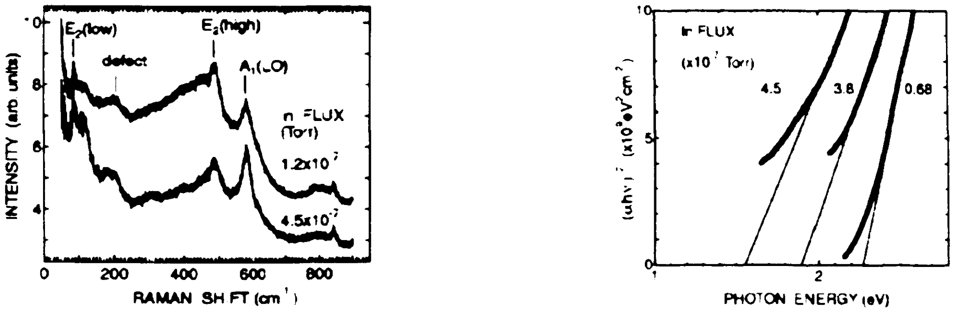

(a) Raman spectra of InN grown on quartz

(b) Determination of optical band gap for InN grown on quartz using optical absorption.

Figure 2.22 From [115]

Yoshimoto et al. investigated polycrystalline InN layers, grown on quartz and glassy carbon at a substrate temperature of 500 °C under a range of In-metal flux by MBE [115]. Careful comparison of the Raman spectra showed that the sample with higher In flux gives slightly sharper A_1(LO) and E_2(high) phonon peaks, which indicates that the increase of the In flux causes a slight improvement of crystallinity. Furthermore, the optical band gap decreased from 2.27 eV to 1.55 eV with increasing In-flux. (Figure 2.22).

Jmerik et al. investigated the growth of InN under both N-rich and In-rich growth conditions. They found that N-rich growth conditions (In/N < 1) resulted in growth of rough surface (nano-columnar) films, whereas at the In-rich ones (In/N > 1) indium micro-droplets inevitably formed on the InN surface, since indium evaporation from the liquid droplets was rather slow at typical substrate temperature used [116]. They noted precise control of the stoichiometric conditions is a crucial point in achieving a smooth surface where they found that the transition from N-rich to In-rich conditions lead to and an improvement of the structural quality in the PA-MBE films. On the other hand, InN films grown under N-rich conditions were less compressively strained than those grown under In-rich and stoichiometric conditions.

2.1.4 Pulsed laser deposition (PLD)

The PLD technique offers an alternative growth method radically different to MOCVD and MBE for the growth of indium nitride. The advantage that PLD brings to the growth process lies in the lower growth temperature that can be used to achieve good quality material. Another advantage over low-energy ion beams is less damage of the film during growth [58]. Surprisingly, only a few reports on the growth of InN using PLD have been published. Feiler et al. used PLD to deposit InN films on sapphire (0001) substrates [57]. The films were not single-crystal, but instead were found to have preferred orientation along the c-plane. The films were p-type with carrier concentration of 6.5×10^{20} and 4.7×10^{19} cm^{-3}, and mobilities of 30 and 240 $cm^2V^{-1}s^{-1}$ respectively. The c-lattice constant was found to be 5.72±0.05 Å. It is worth noting here that this is the only p-type reported for unintentionally doped InN grown by any method. Fernandez et al. successfully produced good quality InN films from metallic In targets using the PLD technique [58]. Films were grown on sapphire, silicon and glass substrates at range of temperature from ambient to 400 °C. Their films showed almost near stoichiometric growth; 50.8±0.8 at.% In and 49.2±0.8 at.% N as confirmed by the Rutherford backscattering spectroscopy analysis and had hexagonal structure with optical band gap of 1.9 eV. InN thin films were grown on (0001) sapphire substrates at 400 °C by N_2 glow discharge plasma-assisted pulsed laser deposition using elemental In as a target by Bhattacharya et al. [59]. XRD showed that the InN films were predominantly of a zinc-blend (ZB) structure along with a low intensity hexagonal wurtzite (WZ) peak. The presence of both ZB and WZ phases were also confirmed by Raman spectra. The films had band gap of 1.9 eV.

2.1.5 Other Methods

A number of methods have been used to grow InN in recent years. These methods include electron beam plasma techniques [14, 15], reactive evaporation [16, 48-51], RF ion plating [52, 53], atomic layer epitaxy (ALE) [54, 55], and ion-beam-assisted filtered cathodic vacuum arc [56].

Takai et al. grew InN with very low carrier concentration 6×10^{16} cm^{-3} but with very low mobility of 2 $cm^2V^{-1}s^{-1}$ using the RF reactive ion plating technique [52]. Using the same technique to deposit InN, Asai et al. studied the electrochromic (EC) behaviour of polycrystalline InN [53]. McIntosh et al. reported that the deposition temperatures for the ALE process is generally much lower than that for MOCVD growth [54]. In addition, ALE growth offers much better control of the growth parameters than a typical MOCVD technique. This control may be critical to the development of very good quality materials with band gaps covering the visible spectrum. McIntosh et al. have deposited single crystalline InN deposited at 480°C using the ALE approach. Hall measurements indicated that the films were n-type with carrier concentrations of $\sim 10^{19}$ cm^{-3} and mobilities of $\sim$ 10 cm^{2}V^{-1}s^{-1}. Inushima at al. used UV-assisted atomic layer epitaxy under atmospheric pressure to prepare single crystal InN [55]. Their InN was a degenerate n-type semiconductor with a carrier concentration of $\sim 3\times10^{20}$ cm^{-3} and mobility of 60 cm^{2}V^{-1}s^{-1}. They observed a reflection peak at 1.9 eV which coincided well with the absorption measurements, so they related it to the band gap. Another peak below 0.6 eV was also observed but was explained to be due to the plasma oscillation of the free carriers. Ji et al. grew InN films using an ion-beam-assisted filtered cathodic vacuum arc (I-FCVA) technique [56, 117]. FCVA has proven its merit in preparing high quality nitride and oxide films. They showed that this technique allows InN films to be grown at relatively low temperatures because of the high reactivity of nitrogen ions (generated by a radio frequency ion beam source) with an energetic indium plasma, which overcomes the difficulties in normal growth of InN films caused by the high vapour pressure of nitrogen and low decomposition temperature of InN. Their films were grown on Si(111) and exhibited a polycrystalline structure with Hall mobility and electron concentration as high as 297 cm^{2}V^{-1}s^{-1} and 2.37×10^{19} cm^{-3} respectively. At, 475 °C, InN films showed highly (0001) preferred orientation and textured surface. They also found that the oxygen incorporated in the InN film was segregated in the form of amorphous indium oxide or oxynitride phase at the grain boundaries. The band gap of the InN with $\sim$ 1.6 at.% oxygen was found to be $\sim$ 1.15 eV by PL measurement [117].

2.2 Structural Properties of indium nitride

There are three common crystal structures shared by group III-nitrides: the wurtzite, zinc-blende, and rock-salt structures [118]. Tampert et al. noted that at ambient conditions, the thermodynamically stable phase is the wurtzite structure. A phase transition to the rock-salt structure takes place at high pressure while the zinc-blende structure, on the other hand, is metastable and may be stabilized only by heteroepitaxial growth on substrate reflecting topological compatibility [119]. Indium nitride normally crystallizes in the wurtzite (hexagonal) structure. On the other hand, only few reports have been on InN in the zinc-blende (cubic) form.

Theoretical studies on the structure of InN films predicted values for *a*- and *c*-lattice parameters scattered in the range of a=3.501-3.536 Å and c=5.69-5.705 Å for the wurtzite hexagonal structure [120]. Other values were also predicted for the zinc-blend structure to be scattered in the range of a=4.92-4.98 Å.

The first reports on the crystalline structural properties were by Juza & Hahn on powder InN [2]. They obtained a wurtzite InN with lattice parameters of a=3.53 Å and c=5.69 Å. The most recent accepted values of lattice parameters were the ones reported by Paszkowicz et al. [121]. They reported a=3.5377 Å and c=5.7037 Å. The lattice parameter in the RF sputtered InN film measured by Tansley & Foley [20], a=3.548 Å and c=5.760 Å, show a *c*-lattice parameter much larger than the other measured values [123] and the reported theoretical values [44, 121, 132]. Tansley and Foley considered their material to be with low nitrogen vacancies. Since N atoms are close packed in (0001) planes and high vacancy densities would preferentially shrink the lattice in the perpendicular direction parallel to c_0.

It can be noticed from table 2.1 that there exists some variation in both lattice parameters. This can be due to the fact that different growth techniques have been employed for the growth of InN, which resulted in different crystalline quality under different growth conditions. Yamamoto et al. considered that the oxygen is a probable reason for the variation in the lattice parameter [122]. This was also suggested by Ji et al. [117]. Their *c*-lattice parameter was estimated to be 5.752-5.711 Å, which was in good agreement with the reported values of hexagonal InN. The lattice constant estimated for films deposited at 475 °C (c=5.711 Å) was very close to that of high quality InN reported by Davydov et al. [123], so they suggested that the film was not oxidized in the form of indium oxide. Indium nitride powders with their large available surface area are expected to be heavily contaminated with surface oxynitride and hydroxide species. Bulk incorporation of oxygen might also be expected for powder samples [47]. However, despite the fact that most of the early reports were in the powder form, it can be noticed from the table below that the results of the early powder samples are in excellent agreement with the recent high quality bulk material despite the high oxygen contamination in the powder samples. Butcher indicated that oxygen is mainly present as a surface species, and that the InN crystals though oxidised in various forms at the surface do not incorporate significant amounts of oxygen in the bulk crystal [47].

Butcher and co-workers excluded the oxygen role in the lattice parameter shift [34, 35, 47, 77, 93, 124]. However, they explained the variation in the lattice parameters to be due to the large amount of excess nitrogen in the grown InN films. This is to be expected when oxygen is resident at grain boundaries and excess nitrogen is embedded in the lattice as a point defect. Butcher et al. [35] observed a strong increase in the lattice parameters and attributed this to the self-interstitials in nitrogen-rich material based on similar observations made by Lagerstedt and Monemar for GaN [125]. They assumed that the observation of a large c-axis lattice parameter for nitrogen rich material provides an explanation of the anomalous value reported by Tansley and Foley [20] since, in that case, a nitrogen rich sample was probably reported [47]. Chen et al. reported that the changes in the lattice parameter observed were strongly correlated to the excess nitrogen content of the films and that both the biaxial strain and the large excess N incorporation creating either hydrostatic or linear stress were responsible for the observed lattice constants in the films [93]. Feiler et al. [57] considered their film to be under tensile stress in the surface plane when they determined a *c*-lattice constant which was slightly smaller than the reported value by Tansley & Foley [20]. Dimakis et al. observed that the continuous films exhibited smaller *c* and larger *a* lattice constants compared to columnar layers [143]. They considered the differences were consistent with the presence of tensile residual stress in the continuous films and thus it was reasonable to expect that the values of the columnar layers to be close to the ones of relaxed InN lattice constants reported by Davydov et al. 2002 [123]. Wang et al. [126] indicated that compressive residual strain existed in their InN films. They found that the lattice constant *c* increased with increasing growth temperature up to 540 °C and seemed to saturate with further increase in temperature. That indicated that the in-plane residual compressive strain was increased with temperatures up to 540 °C and began to saturate with further increases in temperature.

a [Å]	c [Å]	Reference
Theory		
3.5378	5.7033	[44]
3.5377	5.7037	[121]
3.544	5.718	[132]
Sputtering		
3.53	5.69	[2]
3.5533	5.963	[133]
3.54	5.71	[7]
3.544	5.718	[15]
3.548	5.76	[20]
3.54	5.705	[147]
3.54-3.585	5.705-5.735	[64]
	5.76	[26,27]
	5.6994	[34]
	5.772-5.792	[35]
	5.7	[36]
MOVPE		
3.5446	5.7034	[135]
	5.69	[39]
	5.7	[136]
	5.68-5.73	[90]
	5.702	[137]
	5.7	[138]
	5.73	[31]
	5.708-5.738	[124, 139]
	5.702	[95]
MBE		
3.6	5.74	[137]
	5.7012-5.7037	[43]
3.5365	5.7039	[123]
	5.705	[107]
3.532	5.704	[140]
3.486-3.536	5.7-5.742	[144]
	5.74	[141]
3.533-3.545	5.679-5.702	[143]
	5.7	[142]
3.5328-3.5259	5.7057-5.7111	[126]
Other methods		
	5.72	[57]
3.542	5.716	[145]
	5.711-5.752	[117]

Table 2.1: Reported lattice constants for InN

Zinc-blende InN was also grown by different techniques on different substrates [59, 120,127-130]. The films grown by Strite et al. were zinc-blende with a lattice constant of 4.98 Å measured by XRD [127]. Lima et al. obtained the same results using XRD measurements but they obtained a value of 5.04 Å for the lattice constant when measured by the reflection high energy electron diffraction (RHEED) pattern [128]. Bhattacharya et al. reported InN films with both wurtzite (WZ) and zinc-blende (ZB) phase structures [59]. The ZB phase oriented along the (002) plane was more predominant. The lattice constant of cubic InN was found to be 5.09±0.04 Å. Similar observations on cubic InN were made by Schörmann et al. [129]. The cubic InN layers, grown by plasma-assisted MBE on 3C-SiC (001) substrates, had zinc-blende structure with only a small fraction of wurtzite phase inclusion on the (111) facets of the cubic layer. The measured lattice constant was 5.01±0.01 Å. Lozano et al. measured the lattice parameter of c-InN grown on buffer layers of indium oxide prepared onto sapphire to be 4.9 Å [130]. All these measurements were in good agreement with the theoretical reported values scattered in the range of 4.92-4.98 Å [120].

The mismatches in lattice constant and thermal expansion coefficient between InN and the substrate are expected to generate high densities of threading edge, screw, and mixed dislocations. Specht et al. defined three types of strains for InN: hydrostatic stresses, biaxial stresses along the basal plane and linear stresses along the c-axis of the InN crystal [146]. Hydrostatic stress may result from the homogenous incorporation of point defects. Biaxial stresses are often the result of a lattice mismatch to the substrate and linear stresses in *c*-lattice direction are known to occur if point defects are incorporated preferentially along the basal line. Yamaguchi et al. observed that the residual strain in InN films grown by MOVPE gradually released above a thickness of 1200 Å [137]. Lee et al. investigated the evolution of surface morphology and lattice relaxation in InN epitaxial layers grown by dc sputtering [147, 149]. They suggested that the films thinner than ~ 170 Å should be highly strained, and be grown as two-dimensional epitaxial layers in spite of the large lattice mismatch of 29%. They observed that the strain was relieved as the film thickness increased, while columnar seeds started to nucleate on the parts of the film. Lu et al. found that most of the strain was released as the film thickness reached an *effective* critical thickness of ~ 450 Å. However, Cimalla et al. observed that a complete relaxation of the biaxial strain induced by the lattice mismatch and by the different thermal expansion coefficients between the substrate and InN layers did not occur for a thickness up to 1 μm [144]. It was also observed that InN layers relax faster on AlN buffers than on GaN. Cimalla et al. observed an enhanced relaxation in the case of 3D growth, which occurred on AlN due to the larger lattice mismatch while Ng et al. observed a gradual relaxation of the strain in InN films, grown on GaN buffer layer by plasma-assisted MBE, which commenced upon the initiation (within the first BL) of film deposition and was almost completed after 2-4 BLs growth.

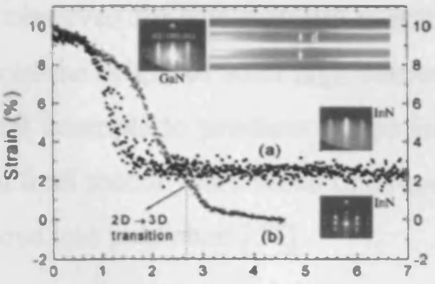

Figure 2.23 Evolution of stain as a function of film thickness. From [144]

Dimakis et al. presented a systematic study of the in-plane *a*- and out-of-plane *c*-lattice parameters of high quality InN grown by MBE on GaN/sapphire substrates [148]. They defined two types of stress: intrinsic and extrinsic. Biaxial (intrinsic) stresses were imposed in the epilayer, by the substrate, during or after the growth.The final strain state was dictated by their superposition. It was found that during the growth, the major biaxial strain component present in the epilayer was the misfit one, which was due to the different in-plane lattice parameters of substrate and epilayer. The misfit strain component was found to be compressive. Apart from the intrinsic stresses which developed during the nucleation and growth, an extrinsic thermal stress developed after growth, during cool down to room temperature. The origin of the thermal component of the biaxial strain was due to the differences in the in-plane thermal expansion coefficient between the epilayer and the substrate. It was concluded that films grown in a two-dimensional mode were found to be under biaxial compressive stress, while films for which growth proceeded through nucleation and subsequent coalescence of islands were found to be under biaxial tensile stress. Strite et al. showed in their TEM analysis that the InN film grown on GaAs substrates was highly defective with both zincblende and wurtzite domains being present and a high density of stacking fault defects was observed from the wurtzite domains of InN were nucleated [127].

2.3 Electrical properties of indium nitride

There have been several reports (theoretical and experimental) on the electrical properties of InN. As-grown InN is always n-type with a very high background carrier concentration [72]. The source of the high density of back ground n-type carriers commonly observed for this material is still not confirmed. There has been much speculation about the origin of such high carrier concentration which will be discussed below. Several attempts to produce p-type InN have been reported but with no success. It was not until recent years when one report on unintentional grown p-type InN by PLD technique was published [57].

Theoretically, the predicted values for the mobility of InN were far from close compared to the wide range of values obtained experimentally. Chin, Tansley and Osotchan predicted a theoretical maximum mobility for InN about 4400 $cm^2V^{-1}s^{-1}$ at room temperature, while at 77K the limits were beyond 33000 $cm^2V^{-1}s^{-1}$ [150]. Ng carried out a study on the mobility of InN [151]. He reported a maximum mobility of 4000 $cm^2V^{-1}s^{-1}$ at room temperature while Fareed at al. predicted a value of room temperature mobility as high as 5000 $cm^2V^{-1}s^{-1}$ [75]. Variable magnetic field analysis of thick InN films suggested maximum mobilities greater than 4000 $cm^2V^{-1}s^{-1}$ in "bulk" InN [152]. The quantitative mobility spectrum analysis technique indicated a continuous and significant spread in mobility for the bulk electron.

Despite the high predicted value of the mobility, similar values or even close values have never been achieved experimentally. The first report on the electrical properties of InN was in 1972. Hovel & Cuomo reported n-type polycrystalline InN with resistivity of $3\text{-}5\times10^{-3}$ Ω-cm, Hall mobility of 250±50 $cm^2V^{-1}s^{-1}$ and carrier concentration of $5\text{-}8\times10^{18}$ cm^{-3} [13]. They attributed the high carrier concentration to the high density of native defects. Trainor and Rose produced n-type InN films using reactive evaporation [16]. Their films had a carrier concentration of 10^{20} cm^{-3} that corresponded to a Hall mobility of 20 $cm^2V^{-1}s^{-1}$. Using reactive cathodic sputtering, Puchevrier and Menoret produced InN with relatively low carrier concentrations of $3\text{-}10\times10^{18}$ cm^{-3} and mobility of 20-50 $cm^2V^{-1}s^{-1}$ [17]. Tansley and Foley reported the best electrical properties ever achieved for InN [18]. Using RF sputter growth, they achieved the highest mobility of 2700 $cm^2V^{-1}s^{-1}$ for a carrier concentration of 5.3×10^{16} cm^{-3} at room temperature, increasing to a value of 5000 $cm^2V^{-1}s^{-1}$ at 150 K with a fall in carrier concentration to 3×10^{16} cm^{-3} for the same sample.

Ikuta et al. obtained a maximum Hall mobility of the InN thin film on the ZnO/α-Al_2O_3 substrate (60 $cm^2V^{-1}s^{-1}$) which was two times higher than that of the InN film grown on bare α-Al_2O_3 substrates (30 $cm^2V^{-1}s^{-1}$) at the same growth temperature according to the high-grade crystallinity [25]. The minimum carrier concentration they reported for the InN grown on ZnO/α-Al_2O_3 substrate was 2×10^{20} cm^{-3} which was lower than that of the InN thin film on bare α-Al_2O_3 substrate at the same growth temperature. In an attempt to reproduce the material grown by Tansley and Foley, that achieved the highest mobility and lowest carrier concentration ever reported for InN, Motlan, Goldys and Tansley using the same system that produced the material reported in 1984, they only managed to achieve a Hall mobility of 306 $cm^2V^{-1}s^{-1}$ and a carrier concentration of $1\times10^{18}cm^{-3}$ [33]. Another attempt was taken also using the same system by Butcher et al. [153]; they produced low carrier concentration material of $< 10^{17}$ cm^{-3}, but only with a maximum mobility of 25 $cm^2V^{-1}s^{-1}$. The growth of InN on sapphire by HVPE resulted in films with a carrier concentration of 3×10^{19} cm^{-3} and Hall mobility of 890 $cm^2V^{-1}s^{-1}$ [154].

Significant improvement was achieved with the development of the growth techniques (MOVPE, MBE) and precise control of the growth conditions. Sato found that to lower the carrier density it was essential to lower the growth rate than to increase the N-radical flux [90]. That yielded an epitaxial layer with a low carrier density of only 4×10^{19} cm^{-3}. Yamaguchi et al. showed that selection of GaN for the underlying layer and increased InN film thickness significantly improved the Hall mobility [137]. An electron Hall mobility of InN grown on a GaN buffer layer by MOVPE has been observed of 700 $cm^2V^{-1}s^{-1}$ at an electron concentration of 5×10^{19} cm^{-3}. Pan et al. found that the Hall behaviour of InN layer was dependent not only on the nitridation duration, but also was affected strongly by the nitridation temperature [40]. Hall mobility of 270 $cm^2V^{-1}s^{-1}$ and a carrier concentration of 5×10^{19} cm^{-3} were reported for InN grown on nitrided sapphire by MOVPE.

Yamamoto et al. showed that the reduction of nitrogen vacancies was essential to achieve a high quality films [155]. By employing atmospheric pressure growth with an V/III ratio of ~ 10^5, Yamamoto et al. reproducibly obtained InN films with a carrier concentration of ~ 5×10^{19} cm^{-3} and a Hall mobility of ~ 300 $cm^2V^{-1}s^{-1}$ on α-Al_2O_3 (0001) substrate. And with a reduced gas speed due to the atmospheric pressure and a reduced dilution N_2 gas flow rate, they attained a carrier density in the order of 10^{18} cm^{-3} with a high electron mobility of 730 $cm^2V^{-1}s^{-1}$ [94]. Yamamoto at al. concluded that improvement of morphology was needed to attain high electron mobility in InN films. They obtained a carrier concentration of 1.1×10^{19} cm^{-3} and a Hall mobility of 870 $cm^2V^{-1}s^{-1}$ by inserting a GaN buffer in the MOVPE growth of InN films [156]. Such a high mobility was due to the improved uniformity of nucleation and morphology of InN.

Matsouka et al. reported carrier concentrations of 10^{18}-10^{19} cm^{-3} and Hall mobility of 100-200 $cm^2V^{-1}s^{-1}$ [89] while Maleyre et al. succeeded in reducing the source of contamination, by using less ammonia and low pressure (200 mbar), to obtain high mobility of 800 $cm^2V^{-1}s^{-1}$ and low carrier concentrations of $6\text{-}9\times10^{18}$ cm^{-3} [89, 157]. Despite their high predicted theoretical mobility (5000 $cm^2V^{-1}s^{-1}$), experimentally, Fareed et al. only managed to achieve a mobility of 850 $cm^2V^{-1}s^{-1}$ for InN samples, grown by migration enhanced MOCVD, with an electron concentration of 4×10^{18} cm^{-3} [75]. Fu et al. investigated the influence of hydrogenation on electrical properties of InN epifilms [170]. They found that the free electron concentration was affected by the duration of the hydrogenation. Free electron concentrations ranging from 5.3×10^{18} to 2×10^{19} cm^{-3}, and mobilities ranging from 630-1110 $cm^2V^{-1}s^{-1}$ have been reported, which represent the highest mobilities reported for MOVPE grown InN.

On the other hand, MBE growth showed better electrical properties than any other growth technique. Room temperature Hall mobility up to 600 $cm^2V^{-1}s^{-1}$ has been demonstrated by Mamutin et al. [43] in spite of the high electron carrier concentration of the order of 10^{20} cm^{-3} for pure hexagonal InN films deposited on sapphire by plasma-assisted MBE. However, InN films grown by Aderhold et al. on sapphire using metalorganic MBE (MOMBE) had an electron concentration of 8.8×10^{18} cm^{-3} and Hall mobility of 500 $cm^2V^{-1}s^{-1}$ [106]. Inushima et al. reported InN grown on sapphire by MBE with carrier concentration 5×10^{19} cm^{-3} and Hall mobility as high as 1700 $cm^2V^{-1}s^{-1}$ [100]. Using low temperature intermediate layers in the growth of InN film by RF-MBE, Saito et al. obtained an electron mobility of 830 $cm^2V^{-1}s^{-1}$ and a corresponding carrier density of 1×10^{19} cm^{-3} at room temperature [107]. They attributed improvement in the electrical properties to the improvement of surface flatness.

Higashiwaki and Matsui showed that the insertion of a LT-GaN intermediate layer between the sapphire and the LT-InN buffer layer greatly improved the crystal quality and electrical properties of the main InN film grown on the buffer layer by PAMBE [46, 159]. Their reported Hall mobility of the grown InN was 1500 $cm^2V^{-1}s^{-1}$ and the residual electron concentration was 2×10^{18} cm^{-3}. Lu et al. reported epitaxial growth of InN on sapphire with AlN buffer layer by MEE [44]. Hall mobility as high as 542 $cm^2V^{-1}s^{-1}$ and an electron concentration of 3×10^{18} cm^{-3} was achieved. They demonstrated that using an AlN buffer layer significantly improved the electrical properties of InN [160]. A Hall mobility of more than 1150 $cm^2V^{-1}s^{-1}$ with electron density of 2×10^{18} cm^{-3} was obtained. They also noticed that increasing the film thickness would lead to increase in Hall mobility. In contrast to c-plane InN grown on c-plane sapphire, no apparent improvement of electrical properties was observed for a-plane InN by growing thicker layers [161]. Lu et al. concluded that impurities from the growth environment were not responsible for the high background doping of InN. Instead, they assumed that structural defects or substrate/buffer impurities were the major source for the unintentional doping, which could be reduced by growing thicker layers. Similar thickness effects were observed by Cimalla et al. [144] where they reported that the average electron density decreased monotonically with increasing layer thickness. The electrical properties were found to be affected by both the interface and the surface [142]. By using a commensurately matched AlN buffer layer, electrical properties of InN epitaxial films grown on Si substrates by PA-MBE, were significantly improved such that the grown films showed higher Hall mobility (690 $cm^2V^{-1}s^{-1}$) and lower n-type carrier concentration (6.81×10^{18} cm^{-3}). They noted that the Hall mobility increased with the AlN buffer thickness, whereas the carrier concentration decreased with AlN buffer thickness.

InN layers grown by MBE with thickness between 200 nm to 7.5 μm were unintentional doped with carrier concentrations ranging from 3.5×10^{17} to 5.5×10^{18} cm^{-3} and Hall mobilities ranging from several hundreds up to 2050 $cm^2V^{-1}s^{-1}$ [162]. Davydov et al. measured the Hall concentration of electron, for InN epilayers with oxygen concentration 0.1% to range from 9×10^{18} to 1.2×10^{19} cm^{-3} and reported a Hall mobility as high as ~ 1900 $cm^2V^{-1}s^{-1}$ [123, 163]. Thick InN films with high quality and good uniformity were demonstrated on 2-inch sapphire substrate by Xu et al. [166]. The room temperature Hall mobility of those InN films ranged from 900 to 1100 $cm^2V^{-1}s^{-1}$, with an electron concentration of the order of $(5\text{-}9)\times10^{18}$ cm^{-3}.

Room-temperature Hall measurements of N-polar InN films gave mobilities ranging from 500-1200 $cm^2V^{-1}s^{-1}$, and electron concentrations of $(1\text{-}5)\times10^{18}$ cm^{-3}; while for In-polar films, the mobility ranged from 300-900 $cm^2V^{-1}s^{-1}$ with carrier concentrations of $(4\text{-}10)\times10^{18}$ cm^{-3} [164]. Xu et al. thought that the differences in electrical properties for films grown with different polarity were mainly due to the differences in crystal quality. On the other hand, Koblmüller et al. conducted systematic growth kinetics studies to optimize the surface and structural properties of N-face InN grown on freestanding GaN [165]. High quality InN was achieved in a rather low-temperature region of 500-540 °C under In-rich conditions. They observed that the Hall mobility increased continually with increasing layer thickness, reaching a maximum mobility of 2370 $cm^2V^{-1}s^{-1}$ for a layer thickness of 4.4 μm. The electron mobilities were almost a factor of 2 higher, and the corresponding bulk carrier concentration of 2.8×10^{17} cm^{-3} was nearly one order of magnitude lower than those reported for the best MBE grown N-face InN [164]. The use of buffer layers of AlN, GaN or InN seems to contribute to the improved structural and electrical properties of MBE grown InN. The better electrical properties in the MBE InN film compared with the MOVPE are believed to be due to the fact that active nitrogen can be supplied independent of the growth temperature and therefore reduce impurity incorporation in the MBE growth [72].

One of the main challenges ahead is the growth of *p*-type InN. As-grown InN generally exhibits n-type characteristics. There have been several attempts to *p*-dope InN with very little success. Feiler et al. reported p-type InN grown by PLD [57]. The p-type conductivity was attributed to the impurities in the starting InN powder. The films obtained had carrier concentrations of 4.7×10^{19} and 6.5×10^{20} cm^{-3}, and mobilities of 240 and 30 $cm^2V^{-1}s^{-1}$, respectively. Mamutin et al. attempted Mg doping of hexagonal InN film grown on sapphire by plasma-assisted MBE [43]. P-type InN was not obtained. The heavy Mg doping resulted in an order of magnitude reduction of electron concentration in InN, but complete compensation was not achieved. Lu et al. [160] and Blant et al. [168] also attempted Mg doping but were not successful. Recently, Anderson et al. [169] revealed evidence of a buried p-type layer beneath a surface electron accumulation layer in heavily Mg-doped samples while Jones et al.

presented the first evidence of successful p-type doping of InN [170]. Anderson et al. suggested that the Mg acceptor level in InN lies near the 100 meV above the valance band maximum [169]. Jones et al. showed that InN:Mg films consisted of a p-type bulk region with a thin n-type inversion layer at the surface that would prevent electrical contact to the bulk [170].

Various studies, both theoretical and experimental, suggested that the high electron concentration originates from the following: oxygen atoms on nitrogen sites [171], silicon atoms on indium atom sites [171], hydrogen incorporation [172], or nitrogen vacancies [173, 174]. More recently, surface electron accumulation has emerged as another factor contributing to the n-type conductivity in InN [175, 176].

Jenkins and Dow have carried out an extensive study on the native defects (i.e. vacancies and antisite defects) and impurities in InN [163]. They showed that the native defect responsible for naturally occurring n-type InN is a nitrogen vacancy, not the antisite defect N_{In}. Tansley & Egan have also speculated that the N-vacancies might be the defect responsible for the natural n-type character of InN [174]. While Sato and Sato found that by decreasing the growth rate, in reactive evaporation growth of InN, and consequently the nitrogen vacancy concentration, the carrier concentration decreased significantly from 10^{20} to 10^{18} cm^{-3} [50]. Yamamoto et al. showed that the reduction of nitrogen vacancies was essential to achieve a high quality film [155].

There exists contrasting views on the possibility that N-vacancy is the main source of the n-type character of InN. Stampfl et al. investigated the electronic and atomic structure and formation energies of native defects and selected impurities [171]. The formation energies of all native defects were found to be high, excluding them as a source of n-type conductivity in as-grown material. Stampfl et al. found that O_N and Si_{In} have lower formation energies than those of any of the native donor-type defects in n-type InN and so oxygen and silicon were found to act as donors. Lu et al. argued against the common view that nitrogen vacancies are responsible for the high background n-type conductivity of InN [44]. They suggested that other defects were responsible for the high background n-type doping. Butcher at al. showed that excess nitrogen, and not the N-vacancies as it is believed, acts as a donor for InN and accounts for the high charge carrier concentrations [35, 93, 177]. Saito et al. [45] supported the finding of Stampfl et al. [171] as they too suspected that the high carrier density of InN films was due to impurities such as oxygen because of the very low growth temperatures. On the other hand, Specht et al. concluded that oxygen concentration does not explain the n-type conductivity of the InN film [146]. However, it was assumed that native defects were the origin of the n-type conductivity. Look et al. presented a formalism to determine the donor and acceptor concentrations in wutzitic InN characterized by degenerate carrier concentration and mobility [160]. Coupled with the high formation energies for the native donor defects, it was suggested that the most likely candidate for the dominant donor is hydrogen (H). Gallinat et al. measured values amongst the highest room temperature electron mobility for In-polar InN (2250 $cm^2V^{-1}s^{-1}$) and found a direct correlation between the free electron concentration in InN and the incorporation of hydrogen and oxygen [111]. They suggested that hydrogen was the dominant unintentional impurity in the films.

Motlan et al. attributed the observed low mobilities to inhomogeneous impurity distributions, particularly at crystallite interfaces, where space charges might additionally degrade the mobility [33]. Laakso et al. identified the dominant defects in InN layers grown by MBE to be indium vacancies [178] while Ho et al. reported that the In-vacancy correlated with the free electron concentration and decreased with increasing electron Hall mobility [179]. They showed that the incorporation of excess indium increases the free-electron concentration and decreases the electron mobility in InN. Mixed conduction effects were expected due to the multiple conducting layers of bulk, surface and interface.

Lu et al. revealed the existence of surface charge accumulation on InN films [158]. Mahboob et al. explained this surface charge accumulation in terms of a particularly low Γ-point conduction band minimum in wurtzite InN [176]. As a result, surface Fermi level pinning high in the conduction band in the vicinity of the Γ point, but near the average mid-gap energy, produces charged donor-type surface states with associated downward band bending.

Recently, Cimalla et al. proposed a model for the influence of different contributions to the high electron concentration in dependence on the film thickness of state-of-the-art InN layers grown by MBE [180]. They suggested that three major mechanisms determine the apparent electron concentration on different thickness scales. First, the accumulation of electrons at the surface and the interface clearly dominates the electron properties of InN for thin layers with thickness < 300 nm. For non-degenerate InN, an electron concentration below 10^{17} cm^{-3} would be necessary and already the accumulation layers would prevent this being achieved for InN films of up to ~ 5 μm thick. Secondly, layers in the micron range are strongly affected by threading dislocations. Finally, the background concentration of InN is already well controlled and would influence the apparent carrier concentration only for films with thickness > 10 μm. However, the influence of such point defects might have substantial influence on the mobility.

The variation of the Hall-measured electron concentration with increasing InN film thickness has been modelled by a constant background electron density (due to donor impurities), a fixed surface sheet density and the free electron from V_N^+ along the dislocations [181]. Piper et al. found that impurities, native defects, and electron accumulation all play a significant role in producing the n-type conductivity of the as-grown InN. They considered the existence of V_N^+, donor impurities, and surface electron accumulation in n-type InN was considered to be due to the conduction band minimum (CBM) lying far below E_B, thus they concluded that the band structure is the main reason for the n-type conductivity.

2.4 Optical properties of indium nitride

When it comes to optical properties, the band gap in particular, InN is considered one of the most debatable semiconductor materials. The material has been the focus of huge debate due to the diverse reports about the band gap of the material. As mentioned previously in the chapter, the sputtering growth technique was widely used to produce InN films in the early days. Most of the films were of polycrystalline structure. The early reports on the band gap revealed a large band gap compared to the most recently accepted value for InN. However, most of the early materials were of polycrystalline form with high oxygen concentrations compared to the high quality single crystal grown InN in recent years. The long accepted value of the band gap was the one reported by Tansley & Foley for polycrystalline InN. They reported a value of 1.89 eV [20]. The development in the growth techniques lead to the growth of high quality single crystal InN material, in which a controversy about the value of the true band gap of the material emerged. A value of 0.7 eV [100], which is much lower than the previous reported value, was introduced. The evidence for this low band gap was largely based on photoluminescence and optical absorption data. Many reasons were given to explain the difference in the band gap value. Burstein-Moss effect, oxygen incorporation, quantum effects were assumed as main reason behind a large shift to high values in the band gap. On the other hand, Mie resonance, deep level effects, stoichiometry were used as an explanation for the low observation of the lower values. To add some flavour to the debate, a new value of 1.0-1.5 eV has been introduced recently.

Hovel and Cuomo reported a band gap value of 1.9 eV for InN grown by RF sputtering with an electron concentration of 7×10^{18} cm^{-3} [13]. Osamura et al. measured the direct band gap of InN to be 1.95 eV at room temperature and to be 2.11 at 78 K [14]. In 1976, using reactive cathodic sputtering, Puychevrier and Menoret grew InN films on glass with a direct band gap of 2.07 eV at room temperature and of 2.21 eV at 77K [17]. The reported film was n-type with a carrier concentration of 3-10×10^{18} cm^{-3} and mobility of 20-50 $cm^2V^{-1}s^{-1}$. The work of Tansley and Foley formed the basis of the long held band gap of 1.89±0.01 eV, for material with an electron concentration in the order of 10^{16} cm^{-3} [20]. Most of the mentioned reports were on polycrystalline InN, but the wide band gap value was also supported by some other reports on highly oriented single crystal InN. A band gap of 1.8 eV was reported for epitaxial InN grown on ZnO/sapphire by RF reactive magnetron sputtering [25]. Hwang et al. [138] observed a strong PL peak at 1.8 eV for InN grown on sapphire substrates using a simple resistively heated MOCVD system while Yang et al. obtained the direct band gap of around 1.92-1.98 eV for highly oriented c-axis InN films with hexagonal wurtzite structure grown by reactive magnetron sputtering [31]. Yodo et al. [103-105] observed a strong band-edge photoluminescence at 1.814 eV, and two stronger emissions at 1.880 and 2.081 eV at 8.5 K from thick InN grown by

ECR-assisted MBE [101, 102]. The fundamental band gap energy of the α-InN crystal was estimated to be 1.5 eV at 6K from absorption spectra, which seemed to coincide well with that estimated from band-tails in the lower energy side of visible PL emissions based on the Burstein-Moss shift [103]. Recently, Alexandrov et al. developed theoretical *ab-initio* calculations of the energy band gaps of complex non-stoichiometric compound semiconductors, with the aim of addressing optical transitions in InN in which antisite defects occur in sufficient density. When applied to stoichiometric InN, a band gap of 2.06 eV was calculated [182].

It was not until 2001 when the large band gap value became doubtful, and the existence of a narrow band gap was favoured. Inushima et al. argued that the band gap of InN must be below 1.1 eV which is much smaller than the accepted value of 1.89 eV at that time [100]. Davydov et al. reported a band gap value of 0.9 eV for high quality MBE grown InN, studied by means of optical absorption, photoluminescence excitation spectroscopy, as well as by ab-initio calculations [123]. Their further studies lead to the calculation of a true band gap of ~ 0.7 eV for InN [163, 183]. This result was supported by many other researchers. Matsouka et al. observed, at room temperature, strong photoluminescence (PL) at 0.76 eV as well as a clear absorption edge at 0.7-1.0 eV [89, 184]. It was suggested that a wurtzite InN single crystal has a true band gap of 0.7-1.0 eV, and the discrepancy in the value of band gap from previous data was attributed to the difference in crystallinity. Optical absorption, photoluminescence, and photomodulated reflectance techniques showed an energy gap of InN grown by MBE between 0.7 and 0.8 eV, much lower than, at that time, the commonly accepted value of 1.9 eV [162]. The photoluminescence was found to be sensitive to the free-electron concentration of the sample. The measured optical properties of $In_xGa_{1-x}N$ over the entire alloy composition range showed that the band gap of InN was less than 1 eV [185]. Rickert et al. studied the effects of surface chemical treatments and metal deposition on the InN surface via synchrotron-based photoemission spectroscopy [186]. They argued that, if the InN band gap was 1.89 eV, the E_F would lead to a barrier height of 0.7±0.1 eV. Alternatively, if the band gap value of ~ 0.7 eV was employed, then E_F would be at or in the conduction band. That Fermi level position would be consistent with the observed ease of ohmic contact formation and would be consistent with the presence of an electron accumulation layer [158]. Drago et al. applied spectroscopic ellipsometry to analyse the optical properties of InN films grown by MOVPE [187]. They determined a band gap energy of 1.0 eV at room temperature. The MEMOCVD-grown material exhibited stronger photoluminescence (PL) compared to InN deposited using conventional MOCVD [75]. Room temperature PL spectra were found to be similar InN grown by MBE with peak emission at 0.8 eV. Liang et al. studied non-equilibrium optical phonons in a high quality single crystal InN with pico-second Raman spectroscopy [188]. Their experimental results not only supported a band gap of 0.8 eV but also disapproved the idea that the 0.8 eV luminescence was due to deep level radiative emission in InN. Kumagai et al. observed at room temperature a strong CL emission at 0.75 eV originating from the band gap of InN grown by HVPE on sapphire [154].

There is a clear discrepancy in the values of the band gap of InN as evident from the many reports. This is already interesting without adding some flavour to the debate by reporting band gap values that range between 1.0-1.5 eV. Briot et al. reported transition energy of 1.25 eV for thin films InN [189]. The transition was attributed to the direct band gap while the 800 meV photoluminescence signal was attributed to extrinsic recombination. Strong photoluminescence (PL) at 1.87 eV, together with a clear absorption edge at 1.97 eV, was observed at room temperature [36, 37]. That was considered to be clear evidence that the previous assignment of ~0.7 eV fundamental band gap for intrinsic InN simply from the PL and absorption data was not reliable. After a careful consideration of the Burstein-Moss shift, band gap renormalization effect, and the Urbach band tail effect, it was suggested that a room temperature band gap for InN was 1.21-1.22 eV which was in good agreement with the strongly recommended value of ~ 1.2 eV for intrinsic InN [190]. The optical properties in the visible and near IR spectral ranges were analysed by transmission spectroscopy, showing an absorption edge around 1.5 eV [191]. It was observed that the absorption edge shift did not follow the Moss-Burstein effect but was extremely sensitive to small deviations in the InN stoichiometry.

There were many explanations given for the difference in the reported values for the band gap. Suggestions for observations of a higher band gap have included a strong Moss-Burstein effect, oxygen inclusion, quantum size effects and more recently stoichiometry changes. On the other hand, explanations for lower band gap observations have included defects, non-stoichiometry, film non-uniformity and Mie resonances. However, no single solution can explain the large discrepancy in the band gap.

Davydov et al. suggested that quantum size effect might be a possible reason for the shift of the band gap to higher values for polycrystalline InN [123]. However, Anderson et al. observed strong PL for polycrystalline InN at ~ 0.8 eV [192]. Cimalla et al. have calculated only a 0.03 eV shift for a 20nm InN film [144], which would exclude the presence of a strong quantum size effect for almost all thick sputtered films, since grains tend to be larger than 20 nm, and in thin epitaxial layers [77]. The high band gap values ~ 2 eV mainly for polycrystalline material are assumed to be due to the presence of oxygen in this type of material [123, 193]. This finding was supported by Yoshimoto et al. [115] and Ji et al. [117]. The higher the oxygen concentration, the more shift of band edge emission to higher energy regions. It was suggested that a band gap of high quality InN with low oxygen content should be less than 1.15 eV [117]. Ji et al. reported a band gap of InN with ~ 16 at.-% oxygen to be ~ 1.15 eV by PL measurements. Yashimoto et al. indicated that polycrystalline InN with an optical band gap of 1.9 eV, which was reported in the early years, has been always reported, contained oxygen at the molar fraction of 3% [115]. InN-In_2O_3 alloy formation has been suggested as a possible explanation for the higher band gap [123]. Butcher et al. investigated the role of oxygen in InN [47, 77]. They assumed two ways in which sufficient quantities of oxygen in InN may affect the band gap. The first requires oxygen to form optically active centres, which, in high densities, modify a notional oxygen-free band gap by the band filling (Moss-Burstein) effect or by impurity banding within the forbidden band. These effects will increase or decrease the apparent band gap respectively. The second requires the formation of a semiconducting pseudo-binary alloy phase, InN_xO_y, with a band gap different form InN. Chen et al. presented results for InN grown by RPE-CVD with a variation in apparent band gap from 1.8 to 1.2 eV; with no change in oxygen content as observed by SIMS analysis [93]. Figure 2.31 shows Vegard's diagram for the InN-In_2O_3 alloys system [47]. It can be seen that there was insufficient oxygen in the RF sputtered samples to explain the difference in the band gap between 0.7 eV InN and 1.9 eV InN.

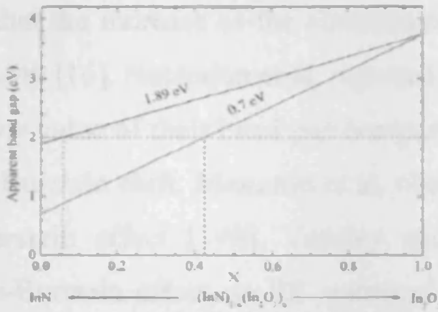

Figure 2.24: Vegard's diagram for the InN-In_2O_3 alloys system. From [47]

It is evident from Figure 2.24 that an alloy with ~ 37 at.% oxygen (44% In_2O_3) would be required to provide a band gap of 2.0 eV if the band gap of pure InN is 0.7, yet for a sample with 10 at.% oxygen the band gap would only be increased to 2.2 eV if the band gap of the pure InN is 1.9 eV., though this is based on the presumption that an alloy species can exist, for which there is no physical evidence.

A number of recent publications have assumed that Moss-Burstein effect explains all the past variations in apparent band gap for InN measured by absorption methods [72, 123, 194-196]. This effect occurs when the carrier concentration exceeds the conduction band edge and the Fermi level lies within the conduction band. Electrons fill the bottom of the conduction band and the band gap measured by optical absorption is increased [77]. With increasing carrier concentration, the Fermi level moves deeper into the conduction band and shifts the absorption edge towards higher energies, resulting in overestimation of the band gap energy. Figure 2.25 illustrate how the Moss-Burstein effect operates.

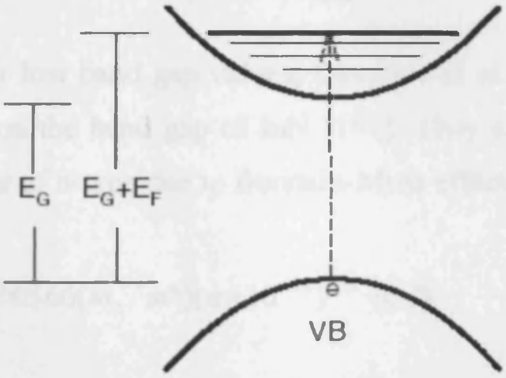

Figure 2.25: Band diagram demonstrating the Moss-Burstein effect [197]

Trainor and Rose found that the increase of the absorption edge was associated with the increase in carrier density [16]. Natarajan et al. reported a band gap of 1.7 eV [67]. They suggested that the low value of their band gap compared to previous reports may have resulted from Moss-Burstein shift. Mamutin et al. observed a blue shift of about 0.1 eV due to Moss-Burstein effect [198]. Tansley and Foley reported detailed investigation of the Moss-Burstein effect on RF sputtered InN [20]. They described the increase in the absorption edge with the carrier concentration according to the following relationship:

$$E_g = 1.89 + 2.1\times10^{-8} n^{1/3} \text{ (eV)} \qquad \textit{(Equation 2.1)}$$

for carrier concentration in the range of 10^{16}-10^{20} cm^{-3}, where E_g is the measured apparent band gap and n is the carrier concentration in cm^{-3}, assuming a band gap of 1.89 eV for InN. (Figure 2.26(a)).

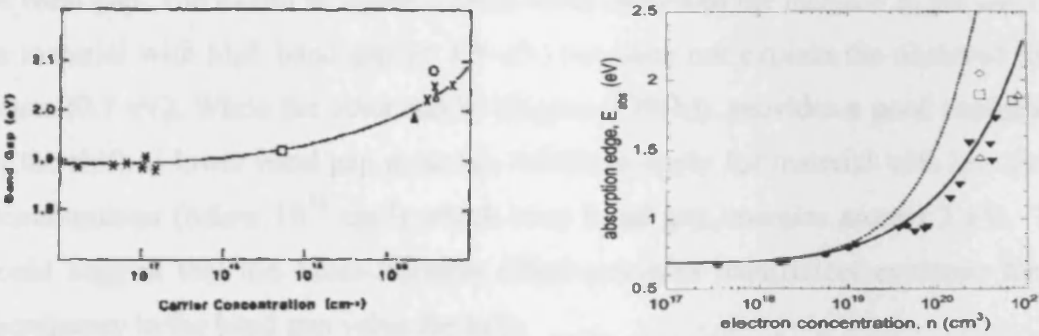

(a) Burstein-Moss shift the absorption edge with increasing carrier concentration. From [20]

(b) Burstein-Moss shift the absorption edge with increasing carrier concentration. From [199]

Figure 2.26: Moss-Burstein shift of the absorption edge with the increase in the carrier concentration

On the other hand, for low band gap values, Davydov et al. studied the influence of carrier concentration on the band gap of InN [163]. They calculated the shift of the optical absorption edge of n-type due to Burstein-Moss effect by:

$$E_g = 0.65 + 0.00166(m_0 / m^*)(n\times10^{-19})^{2/3} \text{ (eV)} \qquad \textit{(Equation 2.2)}$$

Figure 2.27 shows the (a) semilog PL spectra of InN layer with different carrier concentrations and (b) calculated shift of optical absorption edge due to the Burstein-Moss effect.

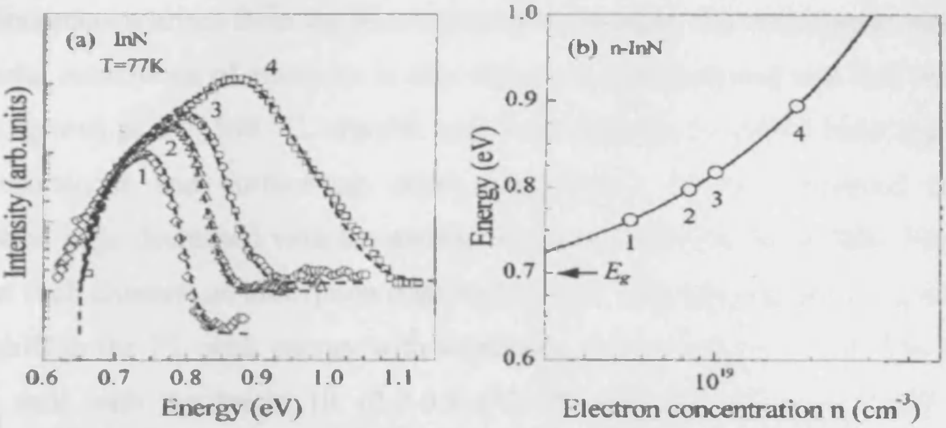

Figure 2.27 (a) Semilog PL spectra of InN layer with different carrier concentration and (b) calculated shift of optical absorption edge due to the Burstein-Moss effect. From [163]

However, Wu et al. suggested an alternative model to describe the shift in the measured band gap for InN [199]. They observed a strong Burstein-Moss shift of the absorption edge with increasing carrier concentration which is very clear in Figure 2.26(b). As can be noticed from Figure 2.28, both models partially explain the shift in the band gap. The model in figure 2.26(a) fairly describes the increase in the band gap for material with high band gap (> 1.9 eV) but does not explain the observed lower values (0.7 eV). While the other model (Figure 2.26(b)), provides a good explanation for the shift of lower band gap material, it fails to apply for material with low carrier concentrations (below 10^{19} cm^{-3}) which have band gap energies around 2 eV. This would suggest that the Moss-Burstein effect provides insufficient evidence for the discrepancy in the band gap value for InN.

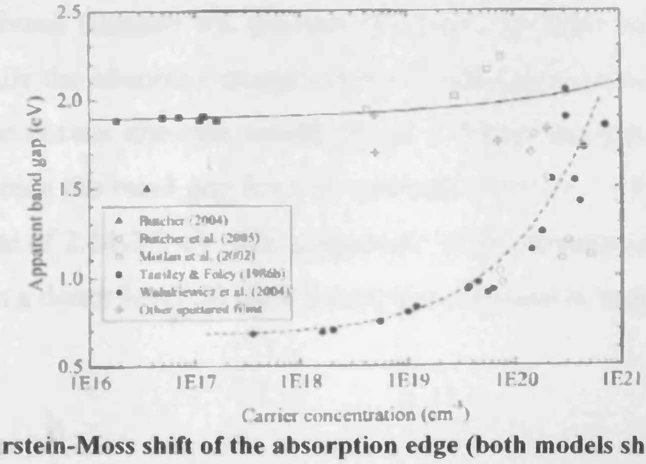

Figure 2.28: Burstein-Moss shift of the absorption edge (both models shown). From [203]

Shubina et al. investigated the effect of Mie resonance of the band gap of InN [200]. The phenomenon arises from the interaction of an incident electromagnetic wave with multipolar excitations of electrons in the clusters. It was proposed that InN with high quality, grown at T > 500 °C, absorbs and emits light far below its band gap due to Mie resonances and surface/gap states respectively. It was observed that the absorption edge decreased with the amount of indium clusters in the film. For a film without such clusters, an absorption edge near 1.4 eV was reported. Ho et al. observed a red-shift in the PL peak energy with increasing excess indium [179]. This finding agrees well with the bright IR (0.7-0.8 eV) PL emission associated with the In aggregates in InN epilayers reported by Shubina et al. The observations of Shubina et al. [200] provide a possible source for a 0.7 eV deep level trap. Briot et al. have plotted deep level PL bands observed for several group III compounds as a function of the free exciton energy and found that InN aligned perfectly (figure 2.29); the 0.7 eV emission is consistent with a 1.25-1.30 eV band gap and represents a deep level trap [189].

Butcher at al. carried out a detailed analysis of absorption data for indium nitride [201]. It was shown that the 0.7 eV band gap was actually due to a sub band deep level trap with |s> like symmetry. This level had been known in the literature, but was previously misinterpreted as a deep level trap with |p> like symmetry by Tansley and Foley [19]. It was also shown that proper interpretation of the absorption data for InN requires that the energy dependence of the refractive index to be taken into account. Consequently the assignment of non-parabolic bands to InN was unfounded [202]. A correlation was found between the amount of excess nitrogen and the magnitude of the band gap, while the observed charge carrier concentration was large [176]. It was suggested that the excess nitrogen would act as a donor and that the Moss-Burstein effect would increase the band gap from its nominal value of 1.89 eV to the observed values in the range of 2.14-2.3 eV. The magnitude of the nitrogen excess was found to be consistent with a donor level 50 meV below the conduction band.

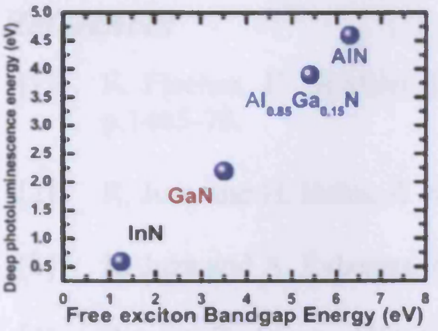

Figure 2.29 The plot of the deep level photoluminescence energy versus free exciton band gap. From [189]

It appears that no single reason can explain the variation in the band gap, but a large number of factors must be considered. Proper analysis of the optical properties should be done to realise the "true" value of the InN band gap.

References

[1] F. Fischer, F. Schröter [Ber. Dtsch. Chem. Ges. (germany) vol.43 (1910) p.1465-79.

[2] R. Juza and H. Hahn, Z. Anorg. Allg. Chem. 239, 282 (1938).

[3] R. Juza and A. Rabenau, Z. Anorg. Allg. Chem. 285, 212 (1956).

[4] Renner, Z. Anorg. Allg. Chem. 298, 28 (1958).

[5] J. Pastrnak and L. Souckova, Phys. Status Solidi 3, K71 (1963).

[6] G. V. Samsonov, Nitridy Kiev, 1969.

[7] MacChesney, J.B, Bridenbaugh, P.M., and O'Connor, P.B. 1970, Mat.Res.Bull., 5, 783.

[8] Vorob'ev et al., Russian Journal of Physical Chemistry, 45 (1971) 1501.

[9] Vorob'ev et al., Russian Journal of Physical Chemistry, 47 (1973) 1616.

[10] Gorienko, S.P., and Fenochka, B.V., 1977, Russian Journal of Physical Chemistry, 51, 315.

[11] Sheleg, A.U., and Savastenko, V.A., 1978, Neorganickeskie Materialy, 14, 1289.

[12] N. A. Gorjunova, Slosnye Almazopodobnye Poluprovodniki, Moscow, 1964.

[13] J. Hovel and J. J. Cuomo, Appl. Phys. Lett. 20, 71 (1972).

[14] K. Osamura, K. Nakajima, Y. Murakami, H. P. Shingu, and A. Ohtsuki, Solid State Commun. 11, 617 (1972).

[15] K. Osamura, S. Naka, Y. Murakami, J. Appl. Phys. Vol.46 (1975) p.3432-7.

[16] J. W. Trainor and K. Rose, J. Electron. Mater. 3, 821 (1974).

[17] N. Puychevrier and M. Menoret, Thin Solid Films vol.36, 141 (1976) p.141.

[18] T. L. Tansley and C. P. Foley, Electron. Lett. 20, 1066 (1984).

[19] T. L. Tansley and C. P. Foley, J. Appl. Phys. 60, 2092 (1986).

[20] T. L. Tansley and C. P. Foley, J. Appl. Phys., 59, 3241, (1986).

[21] B.T. Sullivan, R.R. Parsons, K.L. Westra and M.J. Brett, J. Appl. Phys. 64 (8), (1988) 4144.

[22] T.J. Kistenmacher and W.A. Bryden, Appl. Phys. Lett. 59 (15), (1991) 1844.

[23] T.J. Kistenmacher and W.A. Bryden, Appl. Phys. Lett. 62 (11), (1993) 1221.

[24] W.A. Bryden, S.A. Ecelberger and T.J. Kistenmacher, Appl. Phys. Lett. 64 (21), (1994) 1844.

[25] K. Ikuta, Y. Inoue, O. Takai, Thin Solid Films 334 (1998) 49-53.

[26] Q. Guo, N. Shingai, M. Nishio, H. Ogawa, J. Cryst. Growth 189/190 (1998) 466-470.

[27] Q. Guo, M. Nishio, H. Ogawa and A. Yoshida, Jpn J. Appl. Phys. Vol.38 (1999) Pt.2, No. 5A, L490.

[28] N. Saito and Y. Igasaki, Appl. Surf. Sci. 169-170 (2001) 349-352.

[29] Q. Guo, K. Murata, M. Nishio and H. Ogawa, Appl. Surf. Sci. 169-170 (2001) 340-344.

[30] Q. Guo, A. Okada, M. Nishio and H. Ogawa, Appl. Surf. Sci. 169-170 (2001) 345-348.

[31] H.F. Yang, W.Z. Shen, Z.G. Qian, Q.J. Pang, H. Ogawa and Q.X. Guo, J. Appl. Phys. Vol.91, No.12, (2002), 9803.

[32] Q. Guo, A. Okada, H. Kidera, T. Tanaka, M. Nishio, and H. Ogawa, J. Cryst. Growth, 237-239 (2002), 1032-1036.

[33] Motlan, E.M. Goldys and T.L. Tansley, J. Cryst. Growth, 241 (2002), 165-170.

[34] M. Wintrebert-Fouquet, K.S.A. Butcher and Motlan, Phys. Stat. Sol. (c) 0, N0.7, 2785-2789 (2003).

[35] K.S.A. Butcher, M. Wintrebert-Fouquet, P.P-T Chen, T.L. Tansley, H. Dou, S.K. Shrestha, H. Timmers, M. Kuball, K.E. Prince and J.E. Bradby, J. Appl. Phys. Vol.95, No.11 (2004) 6124.

[36] Q.X. Guo, T. Tanaka, M. Nishio, H. Ogawa, X.D. Pu and W.Z. Shen, Appl. Phys. Lett. 86, 231913 (2005).

[37] X.D. Pu, W.Z. Shen, Z.Q. Zhang, H. Ogawa and Q.X. Guo, Appl. Phys. Lett. 88, 151904 (2006).

[38] T. Matsuoka, H. Tanaka, T. Sasaki, and A. Katsui, *Proceedings of the Sixteenth International symposium on GaAs and related compounds, Karuizawa, Japan*, September 25-29, 1989 (Institute of Physics, Bristol, 1990), p.141.

[39] A. Wakahara and A. Yoshida, Appl. Phys. Lett. 54, 709 (1989).

[40] Y.C. Pan, W.H. Lee, C.K. Shu, H.C.Lin, C.I. Chiang, H. Chang, D.S. Lin, M.C. Lee and W.K. Chen, Jpn. J. Appl. Phys. Vol.38. (1999) Pt.1, No.2A, 645-648.

[41] A. Yamamoto, M. Tsujino, M. Ohkubo and A. Hashimoto, J. Cryst. Growth 137 (1994), 415-420.

[42] T. Tshuchiya, H. Yamano, O. Miki, A. Wakahara and A. Yoshida, Jpn, J. Appl. Phys. Vol.38 (1999), Pt.1, No.4A 1884-1887.

[43] V.V. Mamutin, V.A. Veshin, V.Yu. Davydov, V.V. Rantikov, T.V. Shubina, S.V. Ivanov, P.S. Kopev, M. Karlsteen, U. Söderwall and M. Willander, Phys. Stat. Sol. (a) 176, 247 (1999).

[44] H. Lu, W.J. Schaff, J. Hwang, H. Wu, W. Yeo, A. Pharkya and L.F. Eastman, Appl. Phys. Lett. Vol.77, No.16, (2000), 2548.

[45] Y. Saito, N. Teraguchi, A. Suzuki, T. Araki and Y. Nanishi, Jpn. J. App. Phys. Vol.40 (2001), Pt.2, No.2A, L91-L93.

[46] M. Higashiwaki and T. Matsui, Jpn. J. Appl. Phys. Vol.41 (2002), Pt.2, No.5B, L540-542.

[47] K.S.A. Butcher, InN, a Historic review- from obscurity to controversy, in: Q. Guo (Ed), Advanced Material in Electronics, Research Signpost, 2004, p.1 , and references within.

[48] Y. Sato and S. Sato, Jpn. J. Appl. Phys. Vol.28, No.9 (1989), L1641-L1643.

[49] Y. Sato, S. Kakinuma and S. Sato, Jpn. J. Appl. Phys. Vol.33, (1994), Pt.1, No.7B, 4377-4380.

[50] Y. Sato and S. Sato, J. Cryst. Growth 146 (1995), 262-265.

[51] S.J. Patil, D.S. Bodas, A.B. Mandale and S.A. Gangal, Thin Solid films 444 (2003), 52-57.

[52] O. Takai, J. Tomizawa and Y. Hisamatsu, Proc. of the 7th International Conference on Vacuum Metallurgy, the Iron and Steel Institute of Japan, Tokyo, 981, (1983).

[53] N. Asai, Y. Inoue, H. Sugimura and O. Takai, Thin Solid Films 332 (1998), 267-271.

[54] F.G. McIntosh, E.L. Piner, J.C. Roberts, M.K. Behbehani, M.E. Aumer, N.A. El-Masry and S.M. Bedair, Appl. Surf. Sci. 112 (1997), 98-101.

[55] T. Inushima, T. Shiraishi and V.Yu. Davydov, Solid State Comm. 110 (1999),

491-495.

[56] X.H. Ji and S.P. Lau, J. Cryst. Growth 282 (2005), 271-278.

[57] D. Feiler, R. Stanley Williams, A. Alec Talin, H. Yoon and M.S. Goorsky, J. Cryst. Growth 171 (1997), 12-20.

[58] F.E. Fernández, E. Rodrígez, M. Pumarol, T. Guzmán, W. Jia and A. Martínez, Thin Solid Films 377-378 (2000), 781-787.

[59] P. Bhattacharya, T. K. Sharma, S. Singh, A. Ingale, and L. M. Kukreja, J. Cryst. Growth 236 (2002), 5-9

[60] W.A Bryden, T.J. Kistenmacher in Gallium Nitride (GaN I) p 39 edited by J.I Pankove, T.D. Moustakas, (1998)

[61] O. Ambacher J. Phys. D Appl. Phys. 31 (1998) 2653–2710

[62] S.P DenBaars, S. Keller in Gallium Nitride (GaN I) p 20 edited by J.I Pankove, T.D. Moustakas, (1998)

[63] K.L. Westra, R.P.W. Lawson and M.J. Brett, J. Vac. Sci. Technol. A, 6, (1988), 1730.

[64] J.H. Edgar, C.H. Wei, D.T. Smith, T.J. Kistenmacher and W.A. Bryden, J. Mat. Sci.: Materials in Electronics 8 (1997) 307-312.

[65] T.J. Kistenmacher, W.A. Bryden, J.S. Morgan, T.O. Poehler, J.Appl. Phys. 68 (1990) 1541.

[66] C.B. Cao, H.L.W. Chan and C.L. Choy, Thin Solid Films 441 (2003), 287-291.

[67] B.R. Natarajan, A.H. Eltouky, J.E. Greene, Thin Soilid Films, 69, (1980), 201

[68] O. Takai, K. Ikuta and Y. Inoue, Thin Solid Films 318 (1998), 148-150.

[69] H. Shinoda and N. Matsukura, Diamond and related Materials 11 (2002), 896-900.

[70] http://en.wikipedia.org/wiki/MOVPE

[71] S.A. Campbell : The Science and Engineering of Microelectronic Fabrication p60, Oxford University Press 1996.

[72] A.G. Bhuiyan, A.Hashimoto and A. Yamamoto, J. Appl. Phys. 94 (2003), 2779 and references within.

[73] A.G. Bhuiyan, T. Tanaka, A. Yamamoto, and A. Hashimoto, Phys. Status Solidi A 194, 502 (2002)

[74] J.P. Zhang, E. Koukstis, Q. Fareed, H.M. Wang, J.W. Yang, G. Simin, M. Asif Khan, G. Tamulaitis, G. Kurilcik, S. Jursenas, A. Zukauskas, R. Gaska, and M. Shur, Phys. Status. Solidi A, 188, 95, (2001)

[75] R.S.Q. Fareed, R. Jain, R. Gaska, M.S. Shur, J. Wu, W. Walukiewicz and M. Asif Khan, Appl. Phys. Lett. Vol.84, No.11, (2004), 1892.

[76] V. Yu. Davydov and A.A. Klochikhin, Semiconductors 38, 861 (2004)

[77] K.S.A. Butcher and T.L. Tansley, Superlattices Microstrcut. 38, 1, (2005) and reference within.

[78] M. Alveli, G. Durkaya, A. Weerasekara, A.G.U. Perera, N. Dietz, W. Fenwick, V. Woods and I. ferguson, Appl. Phys. Lett. 89, 112119 (2006) and references within.

[79] A.G. Bhuiyan, A.Hashimoto and A. Yamamoto, J. Appl. Phys. 94 (2003), 2779 and references within.

[80] T. Matsuoka, H. Okamoto, H. Takahata, T. Mitate, S. Mizuno, Y. Uchiyama, T. Makimoto, J. Crystal Growth 269 (2004) 139.

[81] M. Drago, P. Vogt, W. Richter, Phys. Stat. Sol. A 203 (2006) 116.

[82] M. Higashiwaki and T. Matsui, Phys. Stat. Sol. (c) 0, No.1, 360-363 (2002).

[83] O. Briot, B. Maleyre and S. Ruffenach, Appl. Phys. Lett. Vol.83, No.14, (2003), 2919.

[84] O. Briot, B. Maleyre, S. Ruffenach, C. Pinquire, F. Demangeot and Jean Frandon, Phys. Stat. Sol. (c) 0, 7, 2851-2854 (2003).

[85] A. Yamamoto, Y. Murakami, K. Koide, M. Adachi and A. Hashimoto, Phys. Stat. Sol. (b) 228, No.1, 5-8 (2001).

[86] A. Koukitu, N. Takahashi, and H. Seki, Jpn. J. Appl. Phys. Part 2 36, L1136 (1997).

[87] A. Koukitu, T. Taki, N. Takahashi, and H. Seki, J. Cryst. Growth 197, 99 (1999).

[88] A. Koukitu, Y. Kumagai, N. Kubota, and H. Seki, Phys. Status Solidi B 216, 707 (1999)

[89] T. Matsouka, H. Okamoto and M. Nakao, Phys. Stat. Sol. (c) 0, No.7, 2806-2809 (2003).

[90] M. Sato, Jpn. J. Appl. Phys. Vol. 36 (1997), Pt.2, No.6A, L658-L660.

[91] W-K. Chen, Y-C. Pan, H-C. Lin, J. Ou, W-H. Chen and M-C. Lee, Jpn J.

Appl. Phys. Vol.36 (1997), Pt.2, No.12B, L1625-L1627.

[92] S. Suihkonen, J. Sormunen, V.T. Rangel-Kuoppa, H. Koskenvaara and M. Sopanen, J. Cryst. Growth 291 (2006), 8-11, and references within.

[93] P.P-T. Chen, K.S.A. Butcher, M. Wintrebert-Fouquet, R. Wuhrer, M. R. Phillips, K.E. Prince, H. Timmers, S.K. Shrestha and B.F. Usher, J. Cryst. Growth 288 (2006) 241-246.

[94] A. Yamamoto, T. Tanaka, K. Koide and A. Hashimoto, Phys. Stat. Sol. (b) 194, No.2, 510-514 (2002).

[95] B. Maleyre, O. Briot and S. Ruffenach, J. Cryst. Growth 269 (2004) 15-21.

[96] A. Kadir, T. Ganguli, M.R. Gokhale, A.P. Shah, S.S. Chandvankar, B.M. Arora and A. Bhattacharya, J. Cryst. Growth 298 (2007) 403-408.

[97] A. Pelli, K. Saarinen, F. Tuomisto, S. Ruffenach and O. Briot, Appl. Phys. Lett. 89, 011911 (2006).

[98] http://projects.ece.utexas.edu/ece/mrc/groups/street_mbe/mbechapter.html

[99] O. Ambacher, M.S. Brandt, R. Dimitrov, T. Metzger, M. Stutzmann, R.A. Fischer, A. Miehr, A. Bergmaier and G. Dollinger, J. Vac. Sci. Technol. B 14, (1996) 3532.

[100] T. Inushima, V.V. Mamutin, V.A. Vekshin, S.V. Ivanov, T. Sakon, M. Motokawa and S. Ohoya, J. Cryst. Growth 227-228 (2001) 481-485.

[101] T. Yodo, H. Ando, D. Nosei and Y. Harada, Phys. Stat. Sol. (b) 228, No.1, 21-26 (2001).

[102] T. Yodo, H. Yona, H. Ando, D. Nosei, and Y. Harada, Appl. Phys. Lett. V80, No.6, (2000) 968.

[103] T. Yodo, H. Yona, Y. Harada, A. Sasaki and M. Yoshimoto, Phys Stat. Sol. (c) 0, No.7, 2802-2805, (2003).

[104] J. Aderhild, V.Yu. Davydov, F. Fedler, H. Klausing, D. Mistele, t. Rotter, O. Semchinova, J. Stemmer and J. Graul, J. Cryst. Growth 222 (2001) 701-705.

[105] A. Koukitu and H. Seki, Jpn. J. Appl. Phys. Vol.36 (1997), Pt.2, No.6B, L750-L753.

[106] F. Agulló-Rueda, E.E. Mendez, B. Bojarczuk and S. Guha, Solid Stat. Comm. 115 (2000) 19-21.

[107] Y. Saito, T. Yamaguchi, H. Kanazawa, K. KAno, T. Araki, Y. Nanishi, N. Teraguchi and A. Suzaki, J. Cryst. Growth 237-239 (2002) 1017-1021.

[108] X. Wang, S-B. Che, Y. Ishitani and A. Yoshikawa, J. Appl. Phys. 99, 073512 (2006).

[109] J. Grandal and M.A. Sánchez-García, J. Cryst. Growth 278 (2005) 373-377.

[110] T. Ive, O. Brandt, M. Ramsteiner, M. Giehler, H. Kostial, and K.H. Ploog, Appl. Phys. Lett. Vol.84, No.10, (2004) 1671, and references within

[111] C.S. Gallinat, G. Koblmüller, J.S. Brown, S. Bernardis, J.S. Speck, G.D. Chern, E.D. Readinger, H. Shen and M. Wraback, Appl. Phys. Lett 89, 032109 (2006).

[112] B. Heying, I. Smorchkova, C. Poblenz, C. Elsass, P. Fini, S.D. Baars, U. Mishra, and J.S. Speck, Appl. Phys. Lett. 77, 2885 (2000)

[113] B. Heying, R. Averbeck, L.F. Chen, E. Haus, H. Riechert, and J.S. Speck, J. Appl. Phys. 88, 1855 (2000)

[114] M. Losurdo, M.M. Giangregorio, G. Bruno, T-H. Kim, P.Wu, S. Choi, A. Brown, F. Masia, M. Capizzi, and A. Polimeni, Appl. Phys. Lett. 90, 011910 (2007).

[115] M. Yoshimoto, Y. Yamamoto, and J. Saraie, Phys. Stat. Sol. (c) 0, No.7, 2794-2797 (2003).

[116] V.N. Jmerik, V.A. Vekshin, T.V. Shubina, V.V. Ratnikov, S.V. Ivanov, and B. Monemar, Phys. Stat. Sol. (c) 0, No.7, 2846-2850 (2003).

[117] X.H. Ji, S.P. Lau, H.Y. Yang, and Q.Y. Zhang, Thin Solid Films 515 (2007) 4619-4623.

[118] J.H. Edgar (Ed.), Properties of Group III Nitrides, in: EMIS Data Reviews, Publ. Inspec., London, 1994, p.3.

[119] A. Trampert, O. Brandt, K.H. Ploog in Gallium Nitride (GaN I) p 167 edited by J.I Pankove, T.D. Moustakas, 1998.

[120] K. Kim, W.R.L. Lambrecht, and B. Segall, Phys. Rev. B, Vol.53, No.24, (1996) 16310 and references within.

[121] W. Paszkowicz, R. Cerny and S. Krukowski, Powder Diffraction, 18 (2003), 114.

[122] A. Yamamoto, T. Tanaka, A. G. Bhuiyan, K. Sugita, K. Kasashima, Y. Kimura, A. Hashimoto, and V. Yu. Davydov, 5th International Conference on Nitride Semiconductors (ICNS-5), Nara, Japan, May 25–30, 2003.

[123] V.Yu. DAvydov, A.A. Klochikhin, R.P. Seisyan, V.V. Emtsev, S.V. Ivanov, F. Bechstedt, J. Furthmüller, H. Harima, A.V. Mudryi, J. Aderhold, O. Semchinova and J. Graul, Phys. Stat. Sol. (b) 229, No.3, R1-R3 (2002).

[124] K.S.A. Butcher, M. Wintrebert-Fouquet, P.P-T. Chen, K.E. Prince, H. Timmers, S.K. Shrestha, T.V. Shubina, S.V. Ivanov, R. Wuhrer, M.R.

Phillips, and B. Monemar, Phys. Stat. Sol. (c) 2, No.7, 2263-2266 (2005).

[125] O. Lagerstedt and B. Monemar, Phys. Rev. B 19, 3064 (1979).

[126] X. Wang, S-B. Che, Y. Ishitani, and A. Yoshikawa, J. Appl. Phys. 99, 073512 (2006).

[127] S. Strite, D. Chandrasekhar, D. J. Smith, J. Sariel, H. Chen, N. Teraguchi,and H. Morkoc, J. Cryst. Growth 127, 204 (1993)

[128] A. P. Lima, A. Tabata, J. R. Leite, S. Kaiser, D. Schikora, B. Schottker, T.Frey, D. J. As, and K. Lischka, J. Cryst. Growth 201-202, 396 (1999)

[129] J. Schörmann, D.J. As, K. Lischka, P. Schley, R. Goldhahn, S.F. Li, W. Löffler, M. Hetterich and H. Kalt, Appl. Phys. Lett. 89, 261903 (2006).

[130] J.G. Lozano, F.M. Morales, R. García, D. González, V. Lebedev, Ch.Y. Wang, V. Cimalla, and O. Ambacher, Appl. Phys. Lett. 90, 091901 (2007).

[131] W. Paskzkowicz, Powder Diffraction 14 (4) (1999) 258.

[132] P. Carrier and S.-H. Wei, J. Appl. Phys. 97, 033707 (2005).

[133] G. Gieseke, Semicond. Semimet. Vol.2 91966) p.63.

[134] K. Kubota, Y. Kobayashi, and K. Fujimoto, J. Appl. Phys. Vol.66 (1989) 2984-7.

[135] L.A. Marasina, I.G. Pichugin and M. Tlaczala, Kirst.Tech. (Germany) Vol.12 (1977) 541-5.

[136] Q. Guo, H. Ogawa, H. Yamano, and A. Yoshida, Appl. Phys. Lett. 66, (6), (1995) 715.

[137] S. Yamaguchi, M. Kariya, S. Nitta, T. Takeuchi, C. Wetzel, H. Amano and I. Akasaki, J. Appl. Phys. Vol.85, No.11, (1999) 7682.

[138] J.-S. Hwang, C.-H. Lee, F.-H. Yang, K.-H. Chen, L.-G. Hwa, Y.-J. Yang, and L.-C. Chen, Mat. Chem. Phys. 72 (2001) 290-295.

[139] M. Wintrebert-Fouquet, K.S.A. Butcher, and P.P-T. Chen, J. Cryst. Growth. 269 (2004) 134-138.

[140] T. Inushima, M. Higashiwaki, T. Matsui, T. Takenobu, and M. Mtokawa, Phys. Stat. Sol (c) 0, No.7, 2922-2825 (2003).

[141] H. Xiao, X. Wang, J. Wang, N. Zhang, H. Liu, Y. Zeng, J. Li, and Z. Wang, J. Cryst. Growth, 276 (2005) 401-406.

[142] C.-L. Wu, C.-H. Shen, H.-Y. Chen, S.-J. Tsai, H.-W. Lin, H.-M. Lee, S. Gwo,

T.-F. Chuang, H.-S. Chang and T.M. Hsu, J. Cryst. Growth 288 (2006) 247-253.

[143] E. Dimakis, K. Tsagaraki, E. Iliopoulos, Ph. Komninou, Th. Kehagias, A. Delmitis, and A. Georgakilas, J. Cryst. Growth 278 (2005) 367-372.

[144] V. Cimalla, Ch. Förster, G. Kittler, I. Cimalla, R. Kosiba, G. Ecke, O. Ambacher, R. Goldhahn, S. Shokhovets, A. Georgakilas, H. Lu, and W. Schaff, Phys. Stat. Sol. (c) 0, No.7, 2818-2821 (2003).

[145] D.Y. Song, V. Kuratkov, M. Basavaraj, D. Rosenbladt, S.A. Nikishin, M. Holtz, A.L. Syrkin, A.S. Usikov, V.A. Ivantsov and V.A. Dmitriev, J. Appl. Phys. 99, 116103 (2006).

[146] P. Specht, R. Armitage, J. Ho, E. Gunawan, Q. Yang, X. Xu, C. Kisielowski, E.R. Weber, J. Cryst. Growth 269 (2004) 111-118.

[147] I.J. Lee, J.W. Kim, T.-B. Hur, Y.-H. Hwang, and H.-K. Kim, Appl. Phys. Lett. Vol.81, No.3, (2002) 475.

[148] E. Dimakis, E. Iliopoulos, K. Tsagaraki, A. Adikimenakis, and A. Georgakilas, Appl. Phys. Lett. 88, 191918 (2006).

[149] I.J. Lee, J.W. Kim, T.-B. Hur, Y.-H. Hwang, and H.-K. Kim, Appl. Phys. Lett. Vol.92, No.10, (2002) 5814.

[150] V.W. Chin, T.L. Tansley, and T. Osotchan J. Appl. Phys. 75 (11) (1994) 7365.

[151] B.R. Ng, J. Cryst. Growth 269 (2004) 35-40.

[152] C.H. Swartz, R.P. Tompkins, N.C. Giles, T.H. Myers, H. Lu, W.J. Schaff, and L.E. Eastman, J. Cryst. Growth 269 (2004) 29-34.

[153] K.S.A. Butcher, M. Wintrebert-Fouquet, Motlan, S.K. Shrestha, H. Timmers, K.E. Prince, and T.L. Tansley, Mat. Res. Soc. Symp. Proc. 743, 707 (2003)

[154] Y. Kumagai, J. Kikuchi, Y. Nishizawa, H. Murakami, and A. Koukitu, J. Cryst. Growth 300 (2007) 57-61.

[155] A. Yamamoto, T. Shin-ya, t. Sugiura and A. Hashimoto, J. Cryst. Growth 189/190 (1998) 461-465.

[156] A. Yamamoto, N. Imai, A. Hashimoto, J. Cryst. Growth 261 (2004) 271-274.

[157] R. Inatrtaglia, B. Maleyre, S. Ruffenach, O. Briot, T. Taliercio and B. Gil. Appl. Phys. Lett. 86, 124104 (2005).

[158] S.P. Fu, T.J. Lin, W.S. Su, C.Y. Shieh, Y.F. Chen, C.A. Chang, N.C. Chen and P.H. Chang, J. Appl. Phys. 99, 126102 (2006).

[159] M. Higashiwaki and T. Matsui, Phys. Stat. Sol. (c) 0, No.1, 360-363 (2002).

[160] H. Lu, W.J. Schaff, J. Hwang, H. Wu, G. Koley and L. Eastman, Appl. Phys. Lett. Vol.79, No.10, (2001) 1489.

[161] H. Lu, W.J. Schaff. L.F. Eastman, J. Wu, W. Walukeiwicz, V. Cimalla and O. Ambacher, Appl. Phys. Lett. Vol.83, No.6, (2003) 1136.

[162] J. Wu, W. Walukeiwicz, K.M. Yu, J.W. Ager III, E.E. Haller, H. Lu, W.J. Schaff, Y. Saito and Y. Nanishi, Appl. Phys. Lett. Vol.80, No.21, (2002) 3867.

[163] V.Yu. DAvydov, A.A. Klochikhin, V.V. Emtsev, S.V. Ivanov, V.V. Vekshin, F. Bechstedt, J. Furthmüller, H. Harima, A. Hashimoto, A. Yamamoto, A.V. Mudryi, J. Aderhold, J. Graul, and E.E. Haller, Phys. Stat. Sol. (b) 230, No.2, R4-R6 (2002).

[164] K. Xu, W. Terashima, T. Hata, N. Hasimoto, M. Yoshitani, B. Cao, Y. Ishitani and Y. Yoshikawa, Phys. Stat. Sol. (c) 0, No.7, 2814-2817 (2003).

[165] G. Koblmüller, C.S. Gallinat, S. Bernardis, J.S. Speck, G.D. Chern, E.D. Readinger, H. Shen and M. Wraback, Appl. Phys. Lett. 89, 071902 (2006).

[166] K. Xu, N. Hashimoto, B. Cao, T. Hata, W. Terashima, M. Yoshitani, Y. Ishitani, and A. Yoshikawa, Phys. Stat. Sol. (c) 0, No.7, 2790-2793 (2003).

[167] H. Lu, W.J. Schaff, J. Hwang, and L.F. Eastman, Mater. Res. Soc. Symp. Proc. 680E, E3.2 (2001).

[168] A.V. Blant, T.S. Cheng, N.J. Jeffs, L.B. Flannery, I. Harrison, J.F.W. Mosselmans, A.D. Smith, and C.T. Foxon, Mat. Sci. Eng. B59 (1999) 218-221.

[169] P. A. Anderson, C.H. Swartz, D. Carder, R.J. Reeves, S.M. Durbin, S. Chandrill and T.H. Myres, Appl. Phys. Lett. 89, 184104 (2006).

[170] R.E. Jones, K.M. Yu, S.X. Li, W. Walukiewicz, J.W. Ager, E.E. Haller, H. Lu, and W.J. Schaff, Phys. Rev. Lett. 96, 125505 (2006).

[171] C. Stampfl, C.G. Van de Walle, D. Vogel, P. Krüger, and J. Pollmann, Phys. Rev. B, Vol.61, No.12, (2000) R7846.

[172] S. Limpijumnong, and C.G. Van de Walle, Phys. Stat. Stat B 228, 303 (2001).

[173] D.W. Jenkins and J.D. Dow, Phys. Rev. B, Vol.39, No.5, (1989) 3317.

[174] T.L. Tansley and R.J. Egan, Phys. Rev. B, Vol.45, No.19, (1992) 10942.

[175] H. Lu, W.J. Schaff, L.F. Eastman, and C.E. Stutz, Appl. Phys. Lett. Vol.82, No.11, (2003) 1736.

[176] I. Mahboob, T.D. Veal, C.F. McConville, H. Lu, and W.J. Schaff, Phys. Rev. Lett., Vol.92, No.3, (2004) 036804.

[177] S.K. Shrestha, H. Timmers, K.S.A. Butcher and M. Wintrebert-Fouquet, Current Appl. Phys. 4 (2004) 237-240.

[178] A. Laakso, J. Oila, A. Kemppinen, K. Saarinen, W. Egger, L. Liszkay, P. Sperr, H. Lu, and W.J. Schaff, J. Cryst. Growth 269 (2004) 41-49.

[179] J.C. Ho, P. Specht, Q. Yang, X. Xu, D. Hao, and E.R. Weber, J. Appl. Phys. 98, 093712 (2005).

[180] V. Cimalla, V. Lebedev, F.M. Morales, R. Goldhahn, and O. Ambacher, Appl. Phys. Lett. 89, 172109 (2006).

[181] L.F.J. Piper, T.D. Veal, C.F. McConville, H. Lu, and W.J. Schaff, Appl. Phys. Lett. 88, 252109 (2006).

[182] D. Alexandrov, K.S.A. Butcher, and T.L. Tansley, J. Cyst. Growth 288 (2006) 261-267.

[183] V.Yu. DAvydov, A.A. Klochikhin, V.V. Emtsev, D.A. Kurdyukov, S.V. Ivanov, V.V. Vekshin, F. Bechstedt, J. Furthmüller, H. Harima, A. Hashimoto, A. Yamamoto, A.V. Mudryi, J. Aderhold, J. Graul, and E.E. Haller, Phys. Stat. Sol. (b) 234, No.3, 787-795 (2002).

[184] T. Matsouka, H. Okamoto, M. Nakao, H. Harima and E. Kurimoto, Appl. Phys. Lett. Vol.81, No.7, (2002) 1246.

[185] M. Hori, K. Kano, T. Yamaguchi, Y. Saito, T. Araki, Y. Nanishi, N. Teraguchi, and A. Suzuki, Phys. Stat. Sol. (b) 234, No.3, 750-754 (2002).

[186] K.A. Rickert, A.B. Ellis, F.J. Himpsel, H. Lu, W. Schaff, J.M. Redwing, F. Dwikusuma and T.F. Kuech, Appl. Phys. Lett. Vol.82, No.19, (2003) 3254.

[187] M. Drago, T. Schumidtling, U.W. Pohl, S. Peters, and W. Richter, Phys. Stat. Sol. (c) 0, No.7, 2842-2845 (2003).

[188] W. Liang, K.T. Tsen, D.K. Ferry, H. Lu, and W.J. Schaff, Appl. Phys. Lett. Vol.84, No.19, (2004) 3849.

[189] O. Briot, B. Maleyre, S. Clur-Ruffenach, B. Gil, C. Pinquier, F. Demangeot, and J. Frandon, Phys. Stat. Sol. (c) 1, No.6, 1425-1428 (2004).

[190] K.S.A. Butcher, *Preface for the Proceedings of the First International Indium Nitride Workshop*, Fremantle, Australia, 16-20 November 2003 [J. Cryst. Growth 269, vii (2004)].

[191] M. Alveli, G. Durkaya, A. Weerasekara, A.G.U. Perera, N. Dietz, W. Fenwick, V. Woods, and I. Ferguson, Appl. Phys. Lett. 89, 112119 (2006).

[192] P.A. Anderson, T.E. Lee, C.E. Kendrick, W. Diehl, R.J. Kinsey, V.J. Kennedy, A. Markwitz, R.J. Reeves, S.M. Durbin, Proc. SPIE 5277 (2004) 90

[193] F. Chen, A.N. Cartwright, H. Lu, and W.J. Schaff, J. Cryst. Growth 269, (2004) 10-14

[194] D.B. Haddad, H. Dai, R. Naik, C. Morgan, V.M. Naik, J.S. Thakur, G.W. Auner, L.E. Wenger, H. Lu, and W.J. Schaff, Mat. Res. Soc. Symp. Proc. V798, (2004), Y12.7.1.

[195] J. Wu, W. Walukeiwicz, , W. Shan, K.M. Yu, J.W. Ager III, S.X. Li, E.E. Haller, H. Lu, and W.J. Schaff, J. Appl. Phys. V94, No 7, 4457, (2003).

[196] J. Wu, W. Walukeiwicz, , W. Shan, K.M. Yu, J.W. Ager III, E.E. Haller, H. Lu, and W.J. Schaff, Phys. Rev. B, 66, 201403, (2002).

[197] K. S. A. Butcher, H. Hirshy, R. M. Perks, M. Wintrebert-Fouquet, and P. P-T. Chen, Phys. Stat. Sol. (a) 203, 66 (2006).

[198] V.V. Mamutin, T.V. Shubina, V.A. Veshin, V.V. Rantikov, A.A. Toropov, S.V. Ivanov, M. Karlsteen, U. Söderwall and M. Willander, Appl. Surf. Sci. 166, (2000) 87-91.

[199] J. Wu, W. Walukiewicz, S.X. Li, R. Armitage, J.C. Ho, E.R. Weber, E.E. Haller, H. Lu, W.J. Schaff, A. BArcz, and R. Jakiela, Appl. Phys. Lett. Vol.84, No.15, (2004) 2805.

[200] T.V. Shubina, S.V. Ivanov, V.N. Jmerik, D.D. Solnyshkov, V.A. Vekshin, P.S. Kop'ev, A. Vasson, J. Leymarie, A. Kavokin, H. Amano, K. Shimono, A. Kasic, and B. Monemar, Phys. Rev. Lett. Vol.92, No.11, (2004) 117407.

[201] K.S.A. Butcher, M. Wintrebert-Fouquet, P.P-T. Chen, H. Timmers, S.K. Shrestha, Mat. Sci. Semicon. Proc. 6 (2003) 351-354.

[202] F. Bechstedt and J. Furthmuller, J. Cryst. Growth 246 (2002) 315-319.

[203] S.K. Shrestha, Characterisation of indium nitride films with swift ions and radioisotope probes, University of New South Wales, 2005 (PhD thesis).

Chapter 3

Growth of indium nitride: Reactive evaporation

3.1. Introduction

The difficulty in achieving homogenous InN layers with good crystal and surface quality (in comparison with other nitrides) plays a major role in the determination of the basic properties of InN [1]. InN did not receive the same attention as GaN and AlN due to the difficulty in growing high-quality indium nitride and its preparation in stoihiometric form. The thermodynamics properties of the In+N_2 system made InN a difficult material to synthesize [2]. MacChesney et al. [3] investigated the thermal stability of indium nitride and concluded that the dissociation pressure of indium nitride is extremely high and that indium nitride cannot be formed by direct reaction of N_2 molecules and indium atoms. So, owing to the low InN dissociation temperature (> 500 °C) and high equilibrium N_2 vapour pressure over the InN film [4], the growth should proceed at a low growth temperature in order to prevent the escape of N-atoms from the surface which degrades the film quality, this made InN a difficult material to grow. However, there have been several attempts to produce InN material using different growth techniques under different growth conditions. Sputtering was extensively used in the early work on InN, but more improvement in the material quality achieved in using MOVPE and MBE following the great success of these techniques in the GaN growth. Other methods including electron beam plasma techniques [5, 6], RF ion plating [7,8], atomic layer epitaxy (ALE) [9, 10], ion-beam-assisted filtered cathodic vacuum arc [11], pulse laser deposition [12-14], have been also employed in the growth of indium nitride.

3.2. Reactive evaporation

A narrow growth temperature window governs the growth of high quality InN. The low dissociation temperature and thermal stability limits the growth temperature from above while from below the growth temperature would cause the lack of reactive nitrogen that would react with indium to form indium nitride. Thus with a narrow temperature window, the growth of indium nitride has usually been done at rather low temperatures with extremely high V/III ratios [15, 16]. The growth is further complicated as the InN surface, unlike most III-Vs, cannot be stabilized under excess group-V flux, and is etched in ammonia ambient [17]. The limitation of the growth temperature forces the growth to be performed below 500 °C; this will lead to material with high defect densities as a result of nitrogen shortage. The decomposition efficiency of ammonia gas, which is widely used as a nitrogen source for the epitaxial growth of III-nitride compounds, is very low in this temperature region and a large amount of ammonia gas would be needed during the growth [18]. Another drawback would be the limitation to temperature resistant substrates including sapphire and silicon carbide. Temperature resistant substrates are much more expensive than alternatives such as silicon and glass. Another disadvantage associated with the high temperature growth method is the high cost of deploying and operating a vacuum growth system capable of operating in a high temperature environment.

So the need for an alternative method that would overcome the above mentioned problems has become an essential issue for the development of "epitaxial quality" of indium nitride films. Reactive evaporation has the advantage of being cost-effective and simple, also the films can be grown at low temperatures. The control of the growth parameters and finding the optimum conditions is a crucial step in the production of InN. This method also offers the advantage of high deposition rates. Moreover, it is expected to offer many of the advantages of MOCVD/MBE deposited InN films and eliminate the problems due to the high deposition temperature. A reduction of the growth temperature is compensated by the adding of energy to the nitrogen gas surrounding the substrate through the generation of DC active plasma, making deposition possible without reaching the very high temperatures necessary in other growth techniques. The plasma has a direct influence on the film quality. It increases adhesion and the deposition rate. The main purpose of the plasma is to enhance the reaction between the reactants and cause ionization of both coating metal and gas atoms in the vapour phase. Reactive evaporation can supply excited nitrogen effectively even at low growth temperatures. This technique is expected to be an effective growth technique at low temperature because of the strong reactivity between indium and nitrogen active atoms in the plasma.

Thus up to now, heteroepitaxial growth is a practical necessity and the choice of substrate is critical [20, 21]. Several problems in the epitaxial growth of InN originate from the non-availability of single crystalline InN substrates or other high quality single crystalline substrates with the same lattice parameters as InN. For this reason, most of the epitaxial growth of nitrides has been performed on other substrates. Problems due to lattice mismatch between the InN epitaxial layer and substrate have to be overcome. One of the major breakthroughs in the growth of device quality group III-nitride materials was the implementation of nucleation layers [22]. In this work, no nucleation layer is used, but the substrates were exposed to the nitrogen plasma, as a cleaning process, for about ten minutes before the start of any deposition. Both c-plane sapphire and borosilicate glass were used as substrates for the deposition of indium nitride despite the large lattice mismatch (28.8%) between the sapphire substrate and indium nitride. Silicon would make a good choice for device applications; however, films grown directly on Si substrates were poorly oriented [23]. The poor quality material was explained to be due to the formation of the SiN amorphous layer during the initial stages of the growth [23,24]. So the choice of silicon as substrate for reactively evaporated InN was not considered.

The choice of nitrogen source is very critical to obtain high quality indium nitride within the limitation proposed by the growth temperature. Sato & Sato [25] showed that it is necessary to use gases which can cause an effective reaction between indium and nitrogen at relatively low temperatures. The nitrogen source material generally used for the conventional MOVPE and MBE is ammonia (NH_3) [15]. However, the low growth temperature (~ 500 °C) will result in low decomposition rate of NH_3. This will result in low nitrogen radicals available for the growth of indium and consequently high defect density material will result. Koukitu et al. [26] pointed out that a high input V/III ratio is needed for the growth of InN. The decomposition rate of NH_3 favours high temperatures, and at relatively high temperature (~ 650 °C) a low V/III ratio is needed for the growth. However, with the enhancement in the decomposition rate an increase in the H_2 partial pressure will result which will prevent the growth of indium nitride, hence, a low V/III is required [27]. Sato & Sato [25] investigated the dependence of film qualities on the kind of reactive gas used. The radio frequency (RF) plasma of N_2, NH_3 and N_2-He mixtures were used for the preparation of InN thin films by reactive evaporation, and the applicability of the plasma was investigated. The best quality material was obtained when pure N_2 gas was used. The use of NH_3 leads to the formation of indium droplets on the surface, but the quality of the material deteriorated when an N_2-He mixture was used. Contrary to this observation, Takai et al. [28] found that the addition of small amount of Helium to the Ar-N_2 mixture is effective in synthesizing stoichiometric InN and promotes the c-axis orientation. Recent progress in epitaxial techniques (most notably MBE and MOVPE) using highly active nitrogen plasma [29-32] has led to significantly improved InN samples. Hence the choice to use pure nitrogen for this work as a source of active nitrogen is trivial choice, especially when it is cost-effective and easily obtainable.

3.3. Substrate preparation

In this work, only two types of substrate were used: c-plane sapphire and borosilicate micro-glass slides. Before any deposition of indium nitride, the substrates were treated to ensure clean surface which would enhance the adhesion of the film to the substrate and better structural quality. For the sapphire, a quick cleaning process was introduced. First the sapphire was soaked in acetone for five minutes and placed in an ultrasonic bath. Then the substrates were soaked in methanol and placed in an ultrasonic bath also for five minutes. After that the substrates were rinsed in deionised (DI) water (resistivity of 18 MΩ-cm) and dried with N_2 or air and then placed in the chamber for film deposition.

For the borosilicate glass substrate, a more complex procedure [19] was adopted. The glass slides were soaked in ethanol for ten minutes then dried with N_2 or air. Following this, the slides were heated in a hydrogen peroxide (H_2O_2)/ammonium hydroxide (NH_4OH)/ deionised water (using a water bath) at 45 degrees Celsius for ten minutes. The ratio of the H_2O_2:NH_4OH:DI water was 2 parts:1 part: 10 parts. After that, the slides were rinsed with lots of DI water. Following this, they were boiled in DI water for one hour followed by another rinse in DI water then dried by N_2 or air. The glass slides were then placed in the chamber and ready for the evaporation of InN.

3.4. The reactive evaporation growth system

An Edwards 308 thermal evaporation system fitted with two rings (used as DC plasma electrodes) has been used for the growth of indium nitride in this work. This system can be illustrated in Figure 3.1. The pumping system comprises of a rotary-backed diffusion pump having a liquid nitrogen trap between the diffusion pump and the chamber. In order to make sure that a suitable vacuum (10^{-7} mbar) is achieved and for better vacuum results, a liquid nitrogen trap is used throughout the deposition. This nitrogen trap is placed between the chamber and the diffusion pump and helps to avoid backstreaming of the diffusion pump oil into the growth chamber and any cross contamination between them and also help in reducing air vapour in the chamber and consequently the amount of oxygen present which would affect the film quality. The chamber is covered by a glass bell jar which allows a clear view of the evaporation process. Pure indium (99.999%) is placed in a tungsten crucible while the plasma is created by passing a high voltage through two electrodes in the middle of the chamber. The crucible is heated by an external current source while the electrodes voltage, creating the plasma, is controlled by switching to the high tension mode (HT) on the system. In standard operation, the system does not allow the use of both the low tension (LT) and the high tension (HT) modes, hence there was a need for some modification to the system so that precise control of both the plasma and the heating of the crucible are achieved at the same time. The nitrogen gas is fed into the chamber through a mass flow controller with the flow kept constant to ensure stable plasma conditions. The substrate is placed on a substrate holder which can be changed to the desired position above the indium source in or above the plasma. When more indium incorporation in the material grown is needed, the sample is moved closer to the source, but with keeping the substrate in the plasma. If the sample is placed above the plasma region, the growth was found to be very slow, and excess oxygen is easily incorporated and would result in material with very high band gap value (above 2.4 eV). On the other hand, if it is placed below the plasma region, very close to the indium source, only indium metal is produced on the substrates. Therefore, the sample must be placed in the plasma region to allow the growth of indium nitride, though

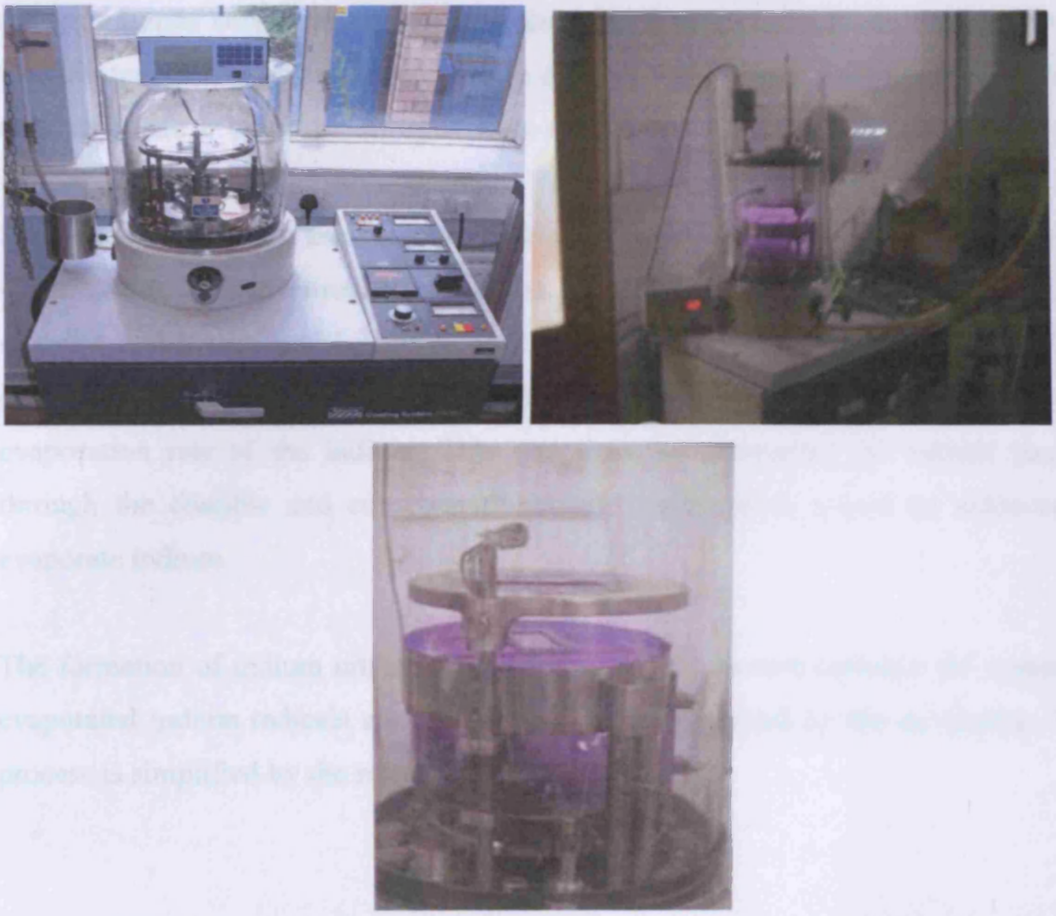

Figure 3.1: Pictures of the reactive evaporation system used for the growth of indium nitride

oxygen will be still incorporated in the growth in this region it will be shown in later chapters that it does not have significant impact on the physical properties of the material grown.

3.5. Growth procedure

The technique of reactive evaporation has been used for the deposition of InN films on a c-plane sapphire and glass. Pure indium wire (99.999%) was used as indium source and ultra high pure grade nitrogen gas (99.999%) as a plasma gas. Before the deposition, the system was evacuated to a pressure of 3×10^{-7} mbar by an oil diffusion pump with a liquid nitrogen trap. The system was flushed with nitrogen gas three times, for about three minutes each, to reduce the residual gas content in the chamber. The nitrogen gas was fed through a coil held in liquid nitrogen to help in purifying the incoming gas of any impurities. A mass flow controller connected the coil to the chamber. The substrates were treated by nitrogen plasma as a cleaning step for ten minutes before the film growth and kept at room temperature during growth. The nitrogen plasma was excited using a dc high voltage source through two circular rods to create a cloud of nitrogen ions. After achieving stable plasma conditions, indium was evaporated at a pressure of 200-300 mTorr (0.0026-0.0039 mbar). Resistive heaters were used to evaporate the indium. The evaporated indium atoms reacted with ionised nitrogen species on the substrate surface that was kept at a distance of 6-8 cm from the source, to form the indium nitride film. Keeping a fixed distance from the indium source, the deposition rate was changed by changing the evaporation rate of the indium. This was done by increasing the current passing through the crucible and consequently higher temperatures would be achieved to evaporate indium.

The formation of indium nitride occurs during the interaction between the thermally evaporated indium radicals and the nitrogen radicals excited by the dc plasma. This process is simplified by the reaction:

$$In + N \rightarrow InN \qquad \textit{(Equation 3.1)}$$

Other residual impurities such as carbon, oxygen and hydrogen are expected to be incorporated in the deposition due to air vapour present in the chamber despite the low background achieved before any deposition process. High growth rates were achieved (> 5 μm/hr) with reactive evaporation. All the films grown were of polycrystalline nature with hexagonal structure, and no preferred orientation. The film thickness ranged from 0.19 μm to 1.43 as measured by the Dectak thickness profiler. The films grown at room temperatures should low mobilities (< 60 $cm^2V^{-1}s^{-1}$). This can be attributed to the poor crystalline structure. Since the growth temperature can be considered a critical growth parameter, a resistive heater was fitted in the system to control the substrate temperature. It was found that the quality of the films improved significantly with the increase of temperature from room temperature up to 240 °C. Only few reports has been published on the reactive evaporation of indium nitride [25, 4, 33-35], but radio frequency plasma was used instead of dc plasma. Trainor & Rose [4] reported Hall mobility of 20 $cm^2V^{-1}s^{-1}$ corresponding to carrier concentration of

10^{20} cm^{-3}, while the electrical properties obtained by Sato & Sato was not much better despite the preparation of a single crystal indium nitride at 450 °C [25, 33, 34]. The Hall mobilities were below 35 cm^{2}V^{-1}s^{-1} and the carrier concentration ranged between 4.3×10^{18} and 3.2×10^{20} cm^{-3}. Patil et al. [35] produced indium nitride film at room temperature. The films were polycrystalline and of poor quality.

3.6. Conclusion

In this chapter, the system design and operating procedure for the reactive evaporation using a DC plasma system used for the growth of indium nitride for this work was briefly described. Indium metal was used as the source of indium while high purity nitrogen was used to create the plasma and provide the nitrogen radicals for the indium nitride film growth. Both c-plane sapphire and borosilicate glass micro-slides were used as substrates, and the substrate temperature ranged from room temperature to 240 °C.

References

[1] M. Drago, T. Schumidtling, U.W. Pohl, S. Peters, and W. Richter, Phys. Stat. Sol. (c) 0, No.7, 2842-2845 (2003).

[2] A.K. Murali, A.D. Barve, and S.H. Risbud, Mat. Sci. Eng. B96 (2002) 111-114.

[3] MacChesney, J.B, Bridenbaugh, P.M., and O'Connor, P.B. 1970, Mat. Res. Bull., 5, 783.

[4] J. W. Trainor and K. Rose, J. Electron. Mater. 3, 821 (1974).

[5] K. Osamura, K. Nakajima, Y. Murakami, H. P. Shingu, and A. Ohtsuki, Solid State Commun. 11, 617 (1972).

[6] K. Osamura, S. Naka, Y. Murakami, J. Appl. Phys. Vol.46 (1975) p.3432-7.

[7] O. Takai, J. Tomizawa and Y. Hisamatsu, Proc. of the 7th International Conference on Vacuum Metallurgy, the Iron and Steel Institute of Japan, Tokyo, 981, (1983).

[8] N. Asai, Y. Inoue, H. Sugimura and O. Takai, Thin Solid Films 332 (1998), 267-271.

[9] F.G. McIntosh, E.L. Piner, J.C. Roberts, M.K. Behbehani, M.E. Aumer, N.A. El-Masry and S.M. Bedair, Appl. Surf. Sci. 112 (1997), 98-101.

[10] T. Inushima, T. Shiraishi and V.Yu. Davydov, Solid State Comm. 110 (1999), 491-495.

[11] X.H. Ji and S.P. Lau, J. Cryst. Growth 282 (2005), 271-278.

[12] D. Feiler, R. Stanley Williams, A. Alec Talin, H. Yoon and M.S. Goorsky, J. Cryst. Growth 171 (1997), 12-20.

[13] F.E. Fernández, E. Rodrígez, M. Pumarol, T. Guzmán, W. Jia and A. Martínez, Thin Solid Films 377-378 (2000), 781-787.

[14] P. Bhattacharya, T. K. Sharma, S. Singh, A. Ingale, and L. M. Kukreja, J. Cryst. Growth 236 (2002), 5-9.

[15] A.G. Bhuiyan, A.Hashimoto and A. Yamamoto, J. Appl. Phys. 94 (2003), 2779 and references within.

[16] T. Matsuoka, H. Okamoto, H. Takahata, T. Mitate, S. Mizuno, Y. Uchiyama, T. Makimoto, J. Crystal Growth 269 (2004) 139.

[17] M. Drago, P. Vogt, W. Richter, Phys. Stat. Sol. A 203 (2006) 116.

[18] M. Higashiwaki and T. Matsui, Phys. Stat. Sol. (c) 0, No.1, 360-363 (2002).

[19] Q. Guo, K. Murata, M. Nishio and H. Ogawa, Appl. Surf. Sci. 169-170 (2001) 340-344.

[20] W.A Bryden, T.J. Kistenmacher in Gallium Nitride (GaN I) p 39 edited by J.I Pankove, T.D. Moustakas, (1998).

[21] O. Ambacher J. Phys. D Appl. Phys. 31 (1998) 2653–2710.

[22] S.P DenBaars, S. Keller in Gallium Nitride (GaN I) p 20 edited by J.I Pankove, T.D. Moustakas, (1998).

[23] A. Yamamoto, M. Tsujino, M. Ohkubo and A. Hashimoto, J. Cryst. Growth 137 (1994), 415-420.

[24] I. Bello, W.M. Lau, R.P.W. Lawson, K.K. Foo, J. Vac. Sci. Technol. 10 (1992) 1642.

[25] Y. Sato, S. Kakinuma and S. Sato, Jpn. J. Appl. Phys. Vol.33, (1994), Pt.1, No.7B, 4377-4380.

[26] A. Koukitu, N. Takahashi, and H. Seki, Jpn. J. Appl. Phys. Part 2 36, L1136 (1997).

[27] A. Koukitu, T. Taki, N. Takahashi, and H. Seki, J. Cryst. Growth 197, 99 (1999).

[28] O. Takai, K. Ikuta and Y. Inoue, Thin Solid Films 318 (1998), 148-150.

[29] V.Yu. Davydov, A.A. Klochikhin, R.P. Seisyan, V.V. Emtsev, S.V. Ivanov, F. Bechstedt, J. Furthmüller, H. Harima, A.V. Mudryi, J. Aderhold, O. Semchinova and J. Graul, Phys. Stat. Sol. (b) 229, No.3, R1-R3 (2002).

[30] J. Wu, W. Walukiewicz, W. Shan, K. M. Yu, J. W. Ager III, S. X. Li, E. E. Haller, H. Lu, and W. J. Schaff, J. Appl. Phys. 94, 4457 (2003).

[31] T. Matsuoka, H. Okamoto, M. Nakao, H. Harima, and E. Kurimoto, Appl. Phys. Lett. 81, 1246 (2002).

[32] K. Xu and A. Yoshikawa, Appl. Phys. Lett. 83, 251 (2003).

[33] Y. Sato and S. Sato, Jpn. J. Appl. Phys. Vol.28, No.9 (1989), L1641-L1643.

[34] Y. Sato and S. Sato, J. Cryst. Growth 146 (1995), 262-265.

[35] S.J. Patil, D.S. Bodas, A.B. Mandale and S.A. Gangal, Thin Solid Films 444 (2003), 52-57.

Chapter 4

Structural and compositional properties of indium nitride

4.1. Scanning electron microscopy (SEM)

Scanning electron microscopy (SEM) is a method for high-resolution imaging of surfaces. The SEM uses electrons for imaging, much as a light microscope uses visible light [1]. This will result in much larger magnifications since electron wavelengths are much smaller than photon wavelengths with a greater depth of field.

The image in an SEM is produced by scanning the sample with a focused electron beam and detecting the secondary and/or backscattered electrons. The incident beam electrons dissipate their kinetic energy into other forms in a large dissipation (generation or cascade) volume (figure 4.1 (a)). Any one of the six types of resultant energy may be detected, i.e. transduced into electrical signals. These signals are: (1) X-rays, (2) emitted electrons (secondary electrons), (3) charge collection (CC) or conductive mode signal, (4) cathodoluminescence (CL) light, (5) transmitted electron and (6) acoustic (ultrasonic) waves. These form the basis of the modes of operation generally known, respectively, as (1) electron probe microanalysis (EPMA) or the X-ray mode, (2) the emissive mode (conventional SEM image mode), (3) the CC mode, (4) the CL mode, (5) scanning transmission electron microscopy (STEM) and (6) the electro-acoustic mode [2]. Imaging is typically obtained using secondary electrons for the best resolution of fine surface topographical features. Figure 4.1 (b) shows a simplified schematic of the scanning electron microscope.

The SEM system was used for the characterization of the surface morphology of indium nitride grown by reactive evaporation. The presence of indium metal particles (clusters) was detected on the surface by SEM imaging. Also, the images showed the columnar structure of the material grown. The grain size was also determined from the surface morphology and was found to be larger than 30 nm in size. All the SEM pictures taken will be revealed throughout the thesis to help in the relevant discussions.

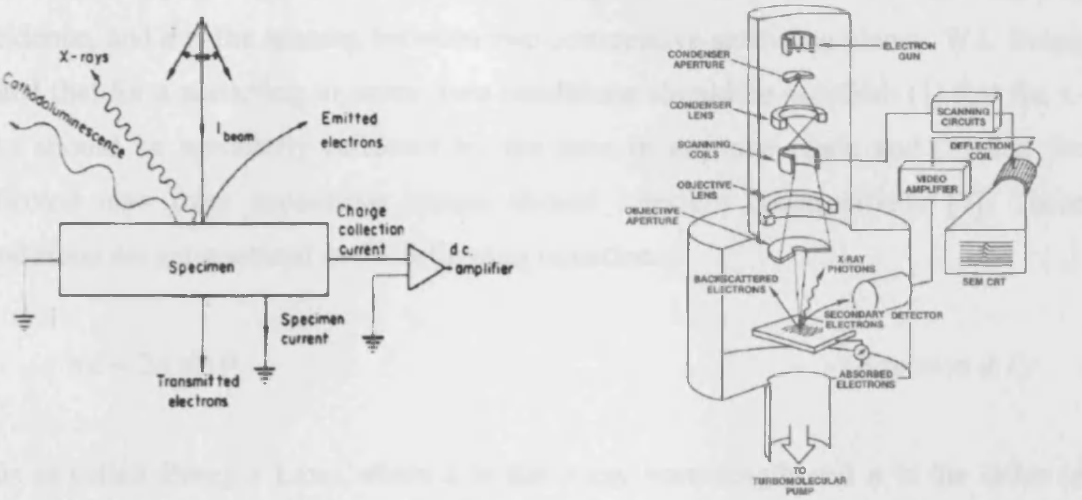

(a) The signal used in six mode of scanning electron microscope. From [3]

(b) Schematic of scanning electron microscope. From [4]

Figure 4.1: Scanning electron microscope

4.2. X-Ray diffraction (XRD)

4.2.1. Theory

X-Ray diffraction (XRD) is a non-destructive technique for the investigation of the crystalline structure of solid material. X-ray crystallography is one of the most useful methods for exploring the nature of matter and is used by researchers in many disciplines. It is used for phase identification, structure determination, as an adjunct to chemical analysis in the identification of the constituents of mixtures of crystalline phases, for measurements of the lattice parameters, and determination of the crystal perfection [5].

The phenomenon of x-ray diffraction by crystals results from a scattering process in which x-rays are scattered by the electrons of the atoms and ions without change in wavelength (coherent or Bragg scattering) [6]. This can be illustrated in figure 4.2 (a). A diffracted beam is produced by such scattering only when geometrical conditions are satisfied (can be expressed in the form of Bragg's Law). The resulting diffraction pattern of a crystal, comprising both the positions and intensities of the diffraction effects, is a fundamental physical property of the substance. Analysis of the positions of the diffraction effect leads to a knowledge of the size, shape, and orientation of the unit cell. The path difference between two rays is *2dsinθ*, where *θ* is the angle of incidence, and *d* is the spacing between two consecutive scattering planes. W.L Bragg stated that for a scattering to occur, two conditions should be satisfied: (1) that the x-rays should be specularly reflected by the ions in any one plane and (2) that the reflected rays from successive planes should interfere constructively [7]. These conditions are summarized in the following equation:

$$n\lambda = 2d\sin\theta \qquad \textit{(Equation 4.1)}$$

This is called Bragg's Law, where λ is the x-ray wavelength and *n* is the order of reflection; it may take on any integral value consistent with *sinθ* not exceeding unity and is equal to the number of wavelengths in the path difference between rays scattered by adjacent planes.

4.2.2. Experiment

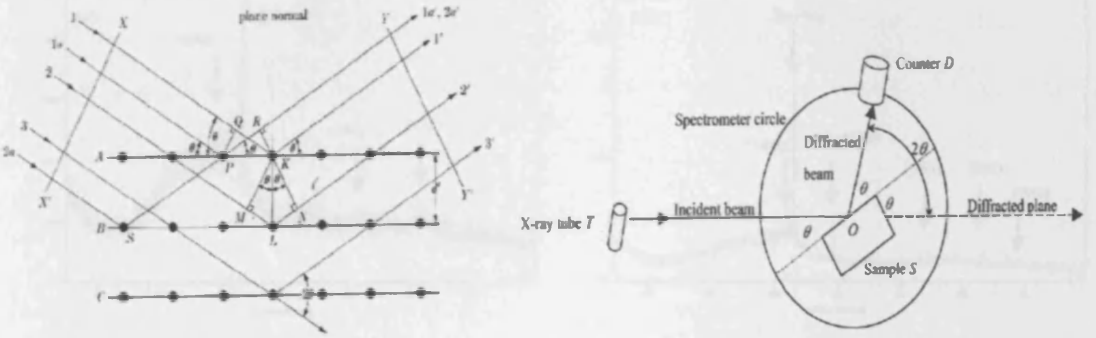

(a) Diffraction of x-rays by a crystal. From [8]

(b) Simplified schematic of the XRD system From [9]

Figure 4.2

The x-ray diffraction (XRD) measurements have been carried out in a θ-2θ coupled geometry Philips PW1710 diffractometer system using Cu*Kα* x-rays (λ = 1.54060 Å) to investigate the crystalline structure of the indium nitride grown by reactive evaporation. A 1° slit was used on the incident beam optics while a 0.5° slit was used on the diffracted beam optics for XRD. The measurements were done with angle 2θ ranging from 5° to 80°. A simplified schematic of the system is described in figure 4.2 (b).

4.2.3. Results and discussion

The intensity of the diffracted beam is plotted as a function of the angle 2θ in Figure 4.3. The peak positions in the spectrum enable to extract the crystalline structure of the material. Figure 4.3 shows diffraction peaks obtained for typical InN grown at room temperature. The braod peak observed is due to the amorphous borosilcate substrate.

The inspection of the XRD pattern shown in the Figure 4.3 shows the presence of many different diffraction peaks. This indicates that the films are of random orientation polycrystalline nature with many small grains. The grain size as confirmed by the SEM pictures shown in Figure 4.4 (b) was relatively large (≥ 50 nm). This excludes the presence of any quantum size effect on the properties of the InN films. Besides the observation of the InN (002) diffraction peak, other peaks such as (100),

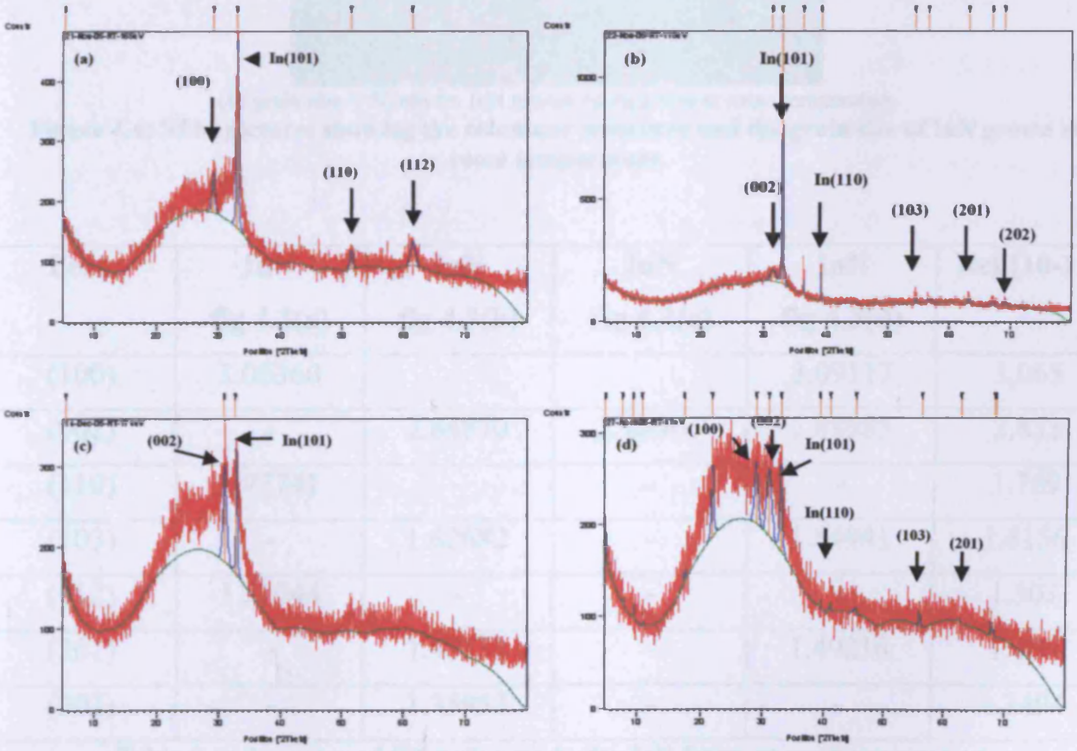

Figure 4.3: XRD patterns for reactively evaporated InN grown at room temperature

(110), (112), (103), (201), (202), and (102) were also observed. The d-spacing for these planes coincides with the peaks positions observed for wurtzite hexagonal polycrystalline InN [10, 11]. Table 4.1 shows the value for the observed d-sapcings.

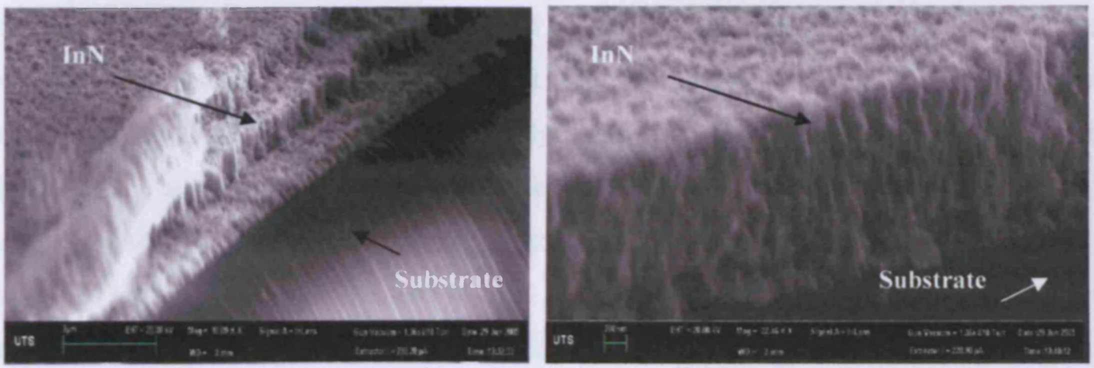

(a) columnar structure of InN

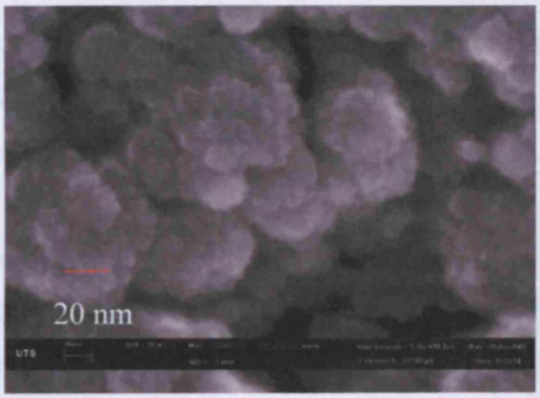

(b) grain size > 50 nm fro InN grown on sapphire at room temperature

Figure 4.4: SEM pictures showing the columnar structure and the grain size of InN grown at room temperature

Peak	InN fig 4.3(a)	InN fig 4.3(b)	InN fig 4.3(c)	InN fig 4.3(d)	Ref [10-11]
(100)	3.06360			3.09117	3.065
(002)	-	2.84870	2.88407	2.88585	2.853
(110)	1.77741	-	-	-	1.769
(103)	-	1.62682	-	1.64941	1.6156
(112)	1.51044	-	-	-	1.503
(201)	-	1.47132	-	1.49216	1.480
(202)	-	1.35957	-	-	1.3494

Table 4..1: d-sapcing of diffraction peaks for InN frown at room temperature

The polycrystalline structure or columnar structure is also observed in the SEM imaging of the samples under investigation. Figure 4.4 (a) shows this columnar structure. A similar columnar polycrystalline structure was reported by Motlan et al. [12] for indium nitride grown by RF sputtering on glass. Their material showed In-rich stoichiometry, a result which is consistent with the stoichiometry observed for reactively evaporated InN by the XPS and SIMS analysis discussed in section 4.3 and 4.4 of this work. Using the activated reactive evaporation "ARE" deposition technique, Patil et al. [13] obtained polycrystalline InN where they observed the (101), (112) and (202) indium nitride diffraction planes. Furthermore, Asai et al. [14] also obtained polycrystalline indium nitride with the observation of the (100), (001) and (101) diffraction peaks related to InN. In fact, most of the earlier literature on InN reported polycrystalline material [15-20] including the report by Tansley and Foley in which they noted the best electrical properties for indium ever reported. The observation of different diffraction peaks between reports can be explained to be due to the different growth methods, growth conditions and growth parameters and the use of different substrates.

XRD analysis showed the presence of metallic indium in the films. This was confirmed in the SEM pictures shown in figure 4.5. The presence of metallic indium was associated with the observation of the In(101) peak and in some samples the (110), (002) and (112) diffraction peaks were also observed. The intensity level of the indium peaks (which can be related to the amount indium in the film) differed from one sample to another and seemed to be affecting both the optical and electrical properties of the reactive evaporated indium nitride. As discussed in detail in chapter 5, the apparent band gap observed from the absorption edge was found to be red-shifted due to the presence of the In-clusters. This phenomenon is known as Mie-resonance. Furthermore, the low Hall mobility and high carrier concentration measured could be attributed to the presence of indium segregates in the films.

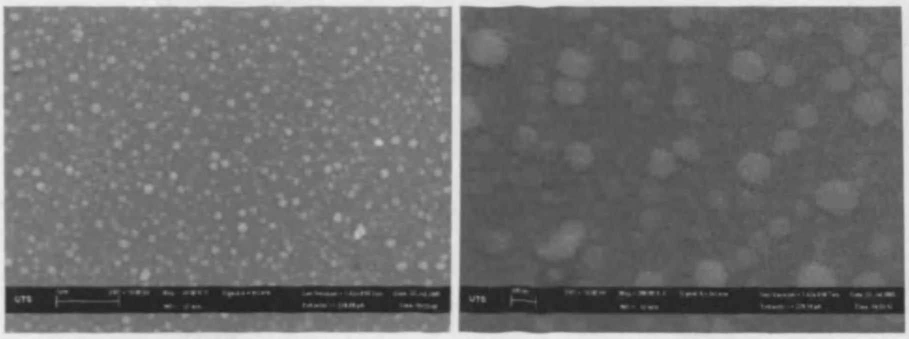

Figure 4.5: SEM pictures showing the presence of In-clusters on the surface of InN

The value of the full width half maximum (FWHM) of the (002) InN diffraction peak can be regarded as an important indicator for crystallinity quality. The smaller the FWHM the better the quality of the crystal. For the sample grown at room temperature, the FWHM ranged from 0.4723 ° to 0.9446°. This indicates a poor quality of the films when grown at room temperature. Low quality is associated with the poor electron transport properties of the film under examination. The growth temperature has proven to be a critical factor in achieving high quality InN. Many reports have supported this observation where high quality crystalline structure and improved electrical properties have been reported [21-23]. Lu et al. [21] concluded that the best crystalline quality can be obtained at the highest growth temperature (550-590 °C) and the improved crystal quality can be due to the annealing process while Hwang et al. [22] achieved an improved epitaxy in films grown at high temperatures (540 °C). The improvement in the crystalline quality with the increase in the growth temperature was attributed to the enhanced surface migration of In-adatoms [23].

In an attempt to improve the quality of the grown films by reactive evaporation, a group of samples were grown on glass at different substrate temperatures ranging from 50 °C to 240 °C. The maximum was set only to 240 °C due to limitation on the resistive heater used in the system. The crystalline structure was examined by XRD analysis. The XRD spectra of the samples grown a range of different temperature between 50 °C and 240 °C are shown in figure 4.6.

The XRD measurements showed that the films were still of polycrystalline nature, however, with more preferred orientation in the c-axis direction with the increase in

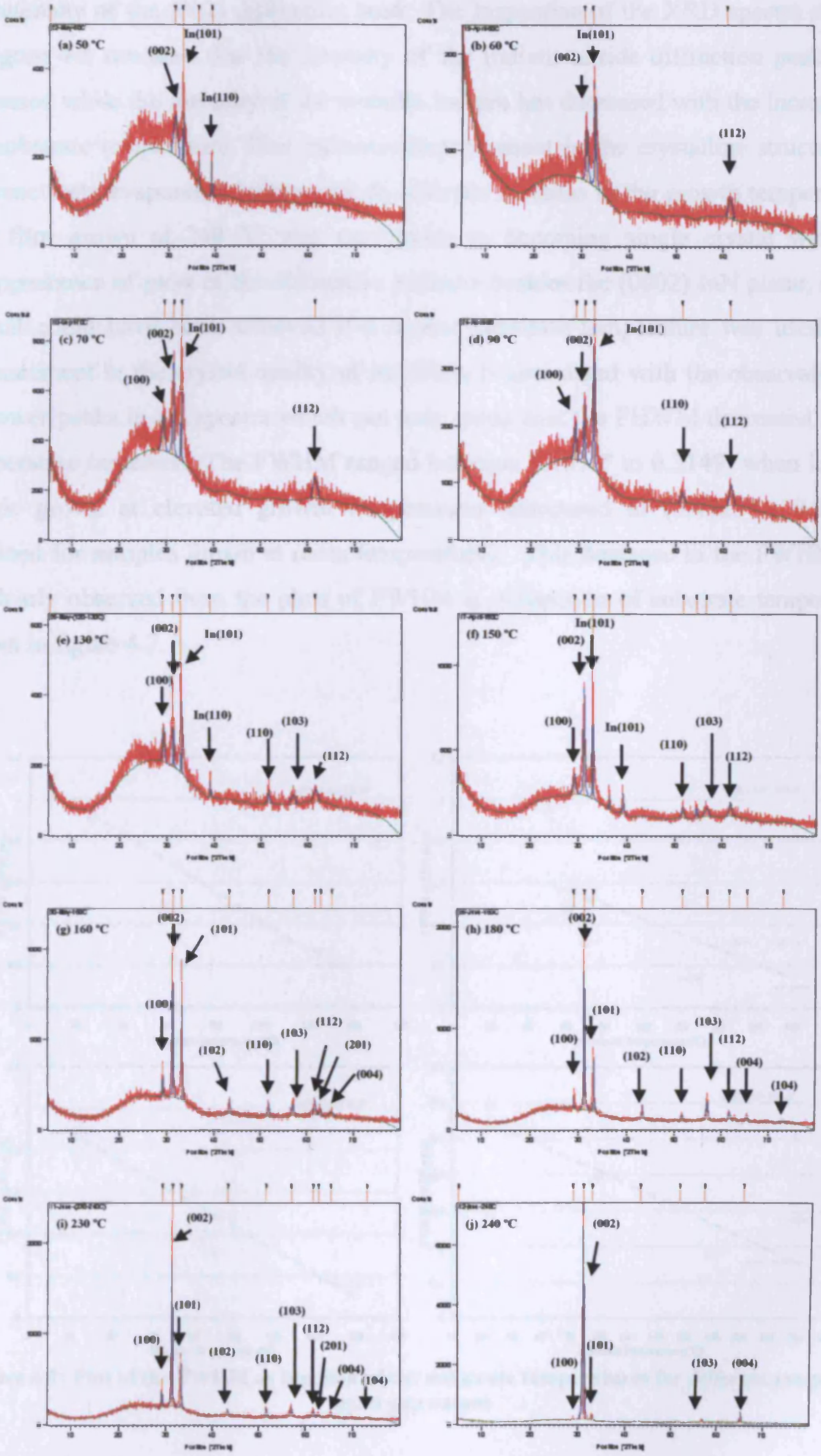

Figure 4.6: XRD patterns for reactively evaporated InN grown at different temperatures

the intensity of the (002) diffraction peak. The inspection of the XRD spectra shown in figure 4.6 revealed that the intensity of the indium nitride diffraction peaks has increased while the intensity of the metallic indium has decreased with the increase in the substrate temperature. This indicates improvement in the crystalline structure of the reactively evaporated indium nitride with the increase in the growth temperature. The film grown at 240 °C was very close to becoming single crystal with the disappearance of most of the diffraction patterns besides the (0002) InN plane; single crystal could have been achieved if a higher substrate temperature was used. The enhancement in the crystal quality of the films is associated with the observation of narrower peaks in the spectra which can only mean that the FHWM decreased as the temperature increased. The FWHM ranged between 0.1378° to 0.3149° when indium nitride grown at elevated growth temperatures compared to (0.4723° - 0.9446°) obtained for samples grown at room temperatures. This decrease in the FWHM can be clearly observed from the plots of FWHM as a function of substrate temperature shown in figure 4.7.

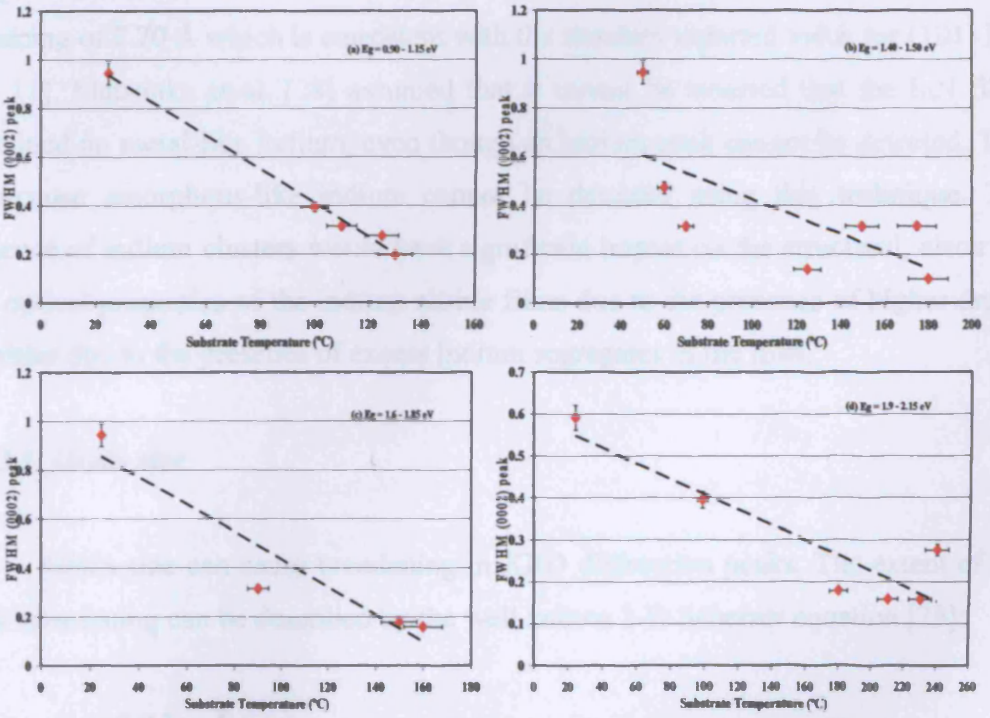

Figure 4.7: Plot of the FWHM as function of the substrate temperatures for different ranges of band gap values

These four plots were taken for different samples showing different apparent band gaps ranging from 0.95 eV to 2.15 eV. The enhancement in the FWHM value is consistent with other reports in the literature. Lu et al. [21] reported a continuous decrease in the FWHM with the increase in the growth temperature for migration-enhanced epitaxy (MEE) grown indium nitride. Similarly, Guo et al. [24] reported similar behaviour for the RF sputtered InN on glass. However, when InN was deposited on (111) GaAs substrates, the FWHM showed the opposite behaviour with the change in growth temperature [25]. The FWHM seemed to increase with the increase in the growth temperature, which lead to the conclusion that low substrate temperatures are suitable for obtaining highly oriented InN crystalline films on (111) GaAs substrate.

Further inspection of the XRD spectra and the peak positions revealed that the amount of indium in the film has decreased with the increase of the substrate temperature. No presence could be detected for metallic indium In(101) with d-spacing equal to 2.72 Å [26, 27] for samples of band gap higher than 1.6 eV and grown at substrate temperatures above 150 °C. Instead, the InN(101) diffraction peak was observed at a d-spacing of 2.70 Å which is consistent with the standard reported value for (101) InN [10, 11]. Matsouka et al. [28] assumed that it cannot be asserted that the InN films contained no metal-like indium, even though an indium peak cannot be detected. This is because amorphous-like indium cannot be detected using this technique. The presence of indium clusters would have significant impact on the structural, electrical and optical properties of the indium nitride films due to the presence of higher defect densities due to the presence of excess indium segregates in the film.

4.2.3.1. Grain size

Grain size can cause broadening in XRD diffraction peaks. The extent of the peak broadening can be described by the well known 2-D Scherrer equation [29]:

$$B = \frac{0.9\lambda}{t\cos\theta} \qquad \textit{(Equation 4.2)}$$

where B is the FWHM, t is the diameter of crystal particle, λ is the wavelength of the x-ray radiation and θ is the peak position. Hence, from equation (4.2) it can be noticed that the FWHM is inversely proportional to the grain size. The XRD analysis and the SEM pictures shown in figure 4.8 for two InN samples grown at room temperature and 150 °C confirms that as the FWHM decreased with the increase in the substrate temperature, an increase in the grain size was observed. The grain size in the sample grown at 150 °C exceeds 250 nm while the InN grown at room temperature was made of grains having size in the range 50-100 nm. Guo et al. [24] noted that the grain sizes of the RF sputtered InN on glass gets larger with the increase of the substrate temperature. A similar observation was made by Chen et al. [30] where they reported a dramatic increase in the grain size producing crystallites up to 200 nm in diameter for RPE-CVD InN.

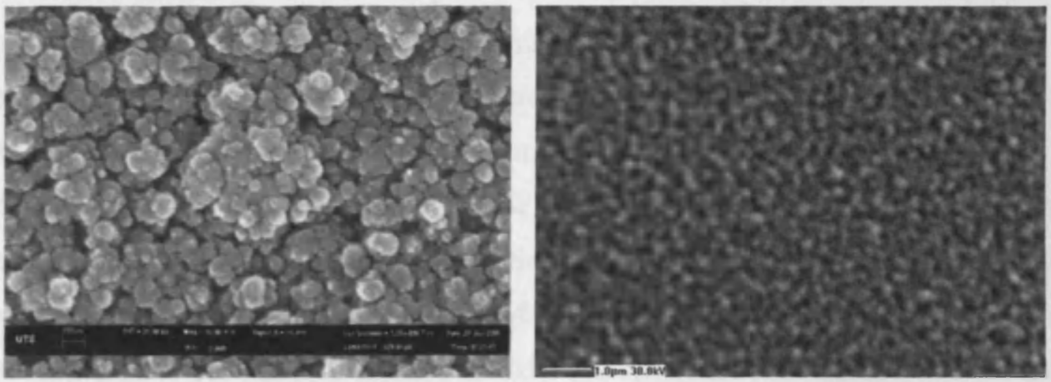
(a) InN grown at room temperature (b) InN grown at 150 °C

Figure 4.8: SEM pictures showing the grain size of reactively evaporated InN grown at room temperature and at 150 °C

4.2.3.2. Lattice parameters

The observation of different diffraction peaks in the XRD spectra makes it easy to calculate the lattice constants of the reactively grown InN films. The value of the d-spacing for the hexagonal crystalline structure, which is the distance between two adjacent planes in the set (hkl), can be expressed as follows [31]:

$$\frac{1}{d^2} = \frac{4}{3}\left(\frac{h^2 + hk + k^2}{a^2}\right) + \frac{l^2}{c^2} \qquad \textit{(Equation 4.3)}$$

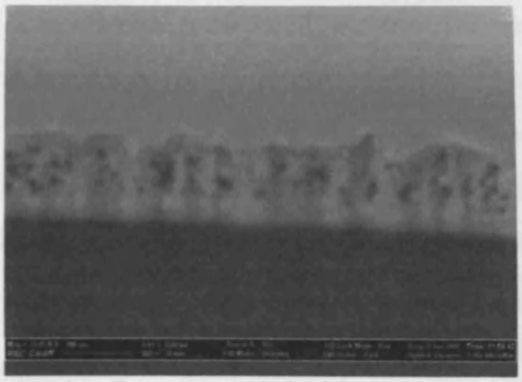

Figure 4.9: SEM picture showing the some voids in the structure of reactively evaporated InN

where *a* and *c* are the lattice constants, (*hkl*) represents the planes detected in the spectra. The values obtained for the indium nitride grown by reactive evaporation ranged between 3.5025 Å to 3.6121 Å for the *a*-lattice and from 5.7122 Å to 5.8054 Å for the *c*-lattice compared to the most recent accepted values of lattice parameters (a = 3.5377 Å and c = 5.7037 Å) [10, 11]. It can bee seen that there is an obvious scatter around the accepted values and this can be attributed to various reasons. In fact, this variation in the lattice parameter values has been the cause of dispute between researchers. Oxygen was considered as a probable reason for the change in lattice parameters [32, 33]. However, the XRD measurements did not detect any presence of oxide in the reactive evaporation InN films despite the presence of large amount of oxygen confirmed by the SIMS analysis. This presence of oxygen was associated with the observation of voids observed by SEM imaging as shown in figure 4.9. These voids would act as sites for oxygen adsorption during the exposure of the films to atmospheric oxygen and water vapour. Similar void microstructure observations were made by Kumar et al. [34] and were associated to the presence of oxygen in the films. They considered that the grain boundaries in polycrystalline indium nitride would act as a site for the incorporation of oxygen in the material.

Kurimoto et al. [35] observed a broad peak at $2\theta=30.4°$ with a longer tail to the higher angle side and they assigned this peak to (222) In_2O_3 signal in cubic phase. However, no diffraction peak at this position was observed for the reactively evaporated InN. This would exclude any significant oxygen alloying for this material. In addition, Motlan et al. [36] considered the reappearance of the (100) diffraction peak coinciding with the presence of oxygen, while Yoshimoto et al. [37] assumed that a shift by 0.2° to a lower angle in the (0002) plane was due to the incorporation of 6% oxygen.

However, a (100) peak was not observed for all examined samples and the shift of the (0002) plane position was always found to be less than 0.1° despite the presence of oxygen up to ~ 20% at. in the indium nitride grown by reactive evaporation as confirmed by the SIMS analysis (refer to section 4.4). Hence, it can be concluded that the oxygen presence likely does not have significant impact on the lattice parameters or affect the nature of the crystalline structure. This conclusion would agree with the observations made by Butcher and co-worker [30, 38-42] where they excluded the role of oxygen in the lattice parameter shift. However, they explained the variations in the lattice parameters to be due to a large amount of excess nitrogen in the grown InN films. Certainly, it can be concluded that for In-rich (non-stoichiometric) reactively evaporated indium nitride, the XRD diffraction peaks and consequently the lattice parameters are highly dependent on the nitrogen content.

Figure 4.10 shows a plot of both lattice constants *a* and *c* obtained for the reactive evaporated indium nitride. Tthe samples were grown at different temperatures ranging from room temperature (RT) to 240 °C resulting in films with different band gap values. The mismatch in lattice constant and thermal expansion coefficient between InN and the substrate are expected to generate high densities of defects and threading dislocations. As mentioned earlier in chapter 2, three types of stresses exist for InN: hydrostatic stresses, biaxial stresses along the basal plane and linear (uniaxial) stresses along the c-axis of the InN crystal. Hydrostatic strain in InN may result from N_{In} and In_N substitutional point defects, V_N and V_{In} vacancies and from N_i and In_i interstitial native point defects. Given the large covalent radius of In compared to N, the point defects In_N, N_i, and In_i are expected to result in lattice expansion, whereas the other point defects should lead to lattice compression [44]. Biaxial stresses are often the result of a lattice mismatch to the substrate while linear stresses in *c*-lattice direction are known to occur if point defects are incorporated preferentially along the basal line. The hydrostatic stress is represented by the red doted line in figure 4.10, biaxial stress is represented by the green doted line and the black doted one is for the linear stress. The lattice parameters of the unstrained InN from reference [10, 11] also shown in the plot. A clear indication of the presence of stresses is observed in the plot. It is shown that the samples were under a combination of strains maybe due to the non-stoichiometry and inhomogeneity of the material

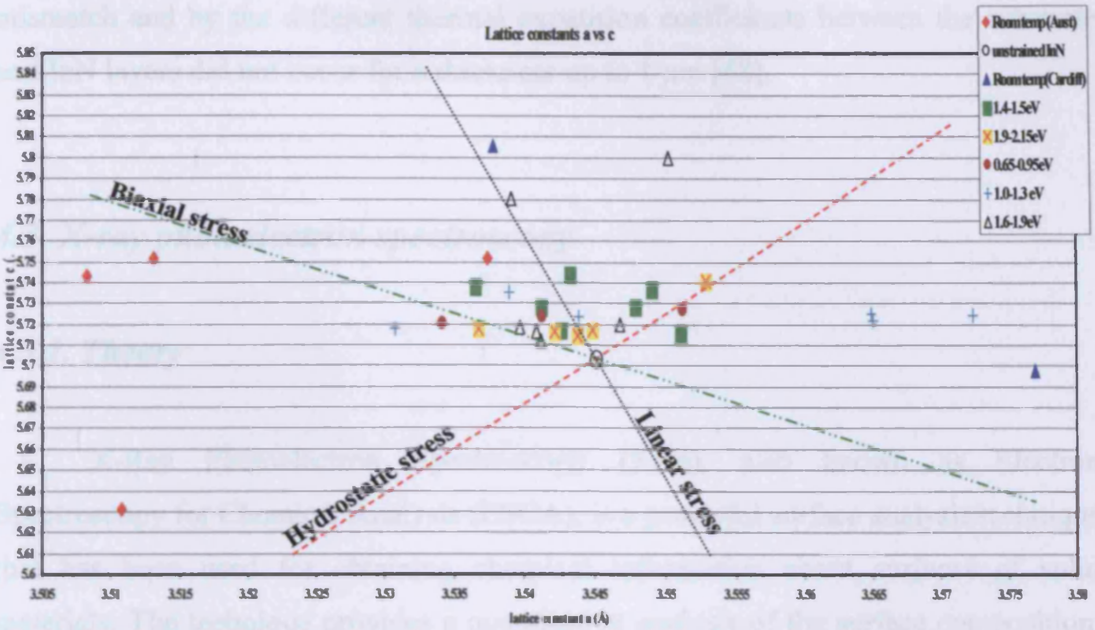

Figure 4.10: Plot of the lattice constants of reactively evaporated InN

grown. The presence of a high density of defects has significant impact on both the electrical and optical properties of the material. This is discussed in detail in the next chapter. Further investigation on the lattice constants showed that the c-lattice value decreased with the increase of the substrate temperature. This indicates that the films grow more relaxed at higher temperatures. A similar observation was reported by Chen et al. [30] in their study on the effect of the growth temperature of InN. They found that the film grown at 550 °C had the smallest lattice distortion compared to the unstrained values. In this work, the lowest distortion was also found for the InN grown at the highest temperatures (210 °C – 240 °C). These samples are represented with the yellow boxes with red-cross in figure 4.10. As the material thickness increased, the defect density was reduced with increasing distance from the nucleation layer and the substrate-film interface which resulted in a reduced carrier concentration and consequently better electrical properties (the electrical properties are shown in detail in chapter 5 of this work). However, no complete release of the strain in the InN films was achieved and this may be due to the polycrystalline nature of the reactive evaporated grown indium nitride. Yamaguchi et al. observed that the residual strain in InN films grown by MOVPE gradually released above a thickness of 1200 Å [45] while Lee et al. [46, 47] observed that most of the strain was released as the film thickness reached an *effective* critical thickness of ~ 450 Å. However, Cimalla et al. observed that a complete relaxation of the biaxial strain induced by the lattice

CARDIFF UNIVERSITY
PRIFYSGOL CAERDYDD

mismatch and by the different thermal expansion coefficients between the substrate and InN layers did not occur for a thickness up to 1 μm [48].

4.3. X-ray photoelectron spectroscopy

4.3.1. Theory

X-Ray Photoelectron Spectroscopy (XPS), also known as Electron Spectroscopy for Chemical Analysis (ESCA), is a powerful surface analysis technique that has been used for obtaining chemical information about surfaces of solid materials. The technique provides a quantitative analysis of the surface composition. XPS utilizes an x-ray beam to irradiate a solid sample which will result in the emission of photoelectrons (figure 4.11). The energy of these electrons is characteristic of the element from which they are emitted. By counting the number of electrons as a function of energy, a spectrum representative of the surface composition is obtained. The presence of peaks at particular energies therefore indicates the presence of a specific element in the sample under study; furthermore, the intensity of the peaks is related to the concentration of the element within the sampled region.

XPS is a surface-sensitive method because the emitted photoelectrons originate from the upper 5-50 Å of the sample despite deep penetration of the primary X-rays. The depth is governed by the electron escape depth or the related electron mean free path. Those electrons excited deeper within the sample are unable to exit the surface. The XPS sensitivity is around 0.1 atomic percentages [50].

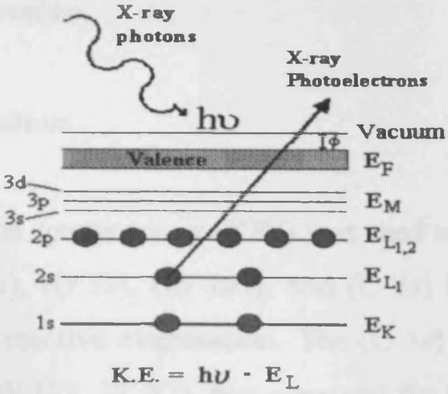

Figure 4.11: Illustration of photoelectron emission in XPS. From [49]

The exact binding energy of an electron depends not only upon the level from which photoemission is occurring, but also upon the formal oxidation state of the atom and the local chemical and physical environment. Any change in these factors will lead to the so-called chemical shift, and gives rise to small shifts in peak positions. Atoms of a higher positive oxidation state exhibit a higher binding energy due to the extra columbic interaction between the photo-emitted electron and the ion core. This ability to discriminate between different oxidation states and chemical environments is one of the major strengths of the XPS technique [51].

4.3.2. Experiment

An ESCALAB 220i-XL high-sensitivity, high-resolution XPS system manufactured by VG Scientific was used for determining the chemical composition of the InN film surfaces. The standard peak quantification software provided with the VG-XPS system was used for the quantification of the peak observed for the core level spectra of the elements analysed. In addition, XPS analysis was used to investigate the nature of nitrogen related point defects in common forms in InN grown by RF sputtering, reactive evaporation, chemical vapour deposition (CVD) and molecular beam epitaxy (MBE). Furthermore, an investigation on the surface charge accumulation in InN was conducted using the results obtained from XPS measurements.

4.3.3. Results and discussion

4.3.3.1. Chemical composition

X-ray photoelectron spectroscopy (XPS) was used to identify core level peaks associated with the (N *1s*), (O *1s*), (In *3d5*), and (C *1s*) bonding at the surface of indium nitride grown by reactive evaporation. The (C *1s*) binding energy, which is normally found at 284.8 eV [13, 38, 52], was observed for the samples examined and has been used for the calibration of all the other spectra observed to eliminate any errors arising from charging effects. The presence of a moderate level of carbon in the bulk of the film is attributed to the atmospheric contamination, which probably occurs due to diffusion of carbon species (such as CO and CO_2) through voids [34].

Curve-fitting analysis indicates three (N *1s*) components are present at the binding energy values of ~ 396.1 eV, ~397.5 eV, and 399.40 eV. The peak at ~ 396.1 eV is attributed to N-In bonds in InN and this result is consistent with observations in other reports [13, 38, 53, 54, 55]. The peak at approximately 397.47 eV is attributed to atomic nitrogen. A similar peak observation was made by Schreifels et al. [56] and Kumar et al. [34] at approximately 398.2 eV and 397.4 eV, respectively. Both reports assigned this peak to atomic nitrogen. Hence, the presence of the atomic nitrogen (interstitial) in the reactive evaporated indium nitride could be identified from a contribution seen at ~ 397.47 eV. The peak at ~ 399.40 eV may be attributed to N-H species as observed during the NH_3 dosing of metals [56]. N-H species may be expected as a hydrolysis product of InN following exposure to the water in air, via the reaction [44]:

$$InN + 3H_2O \rightarrow NH_3 + In(OH)_3 \qquad \textit{(Equation 4.4)}$$

Partial hydrolysis of InN would of course result in the presence of chemisorbed NH and NH_2 species. However, other reports assumed this peak to be associated with the N-O bond formation [13, 55]. The observation of the other product ($In(OH)_3$)in the above chemical equation (observation of peak 531.26 eV which is associated to O-H bond formation) confirms the hydrolysis process and supports the presence of the N-H bonding. The identification and positions of the (N *1s*) photoelectron peaks are provided in table 4.1.

Sample	(N *1s*) Core level assignment (eV)		
	InN	Atomic N	N-H
Sample A (InN/glass 24-Jan-06)	396.07	397.50	399.04
Sample B (InN/glass 25-Jan-06)	395.88	397.38	-
Sample C (InN/glass 30-Jan-06)	396.11	397.48	399.29

Table 4.1: Peak binding energy positions and relative atomic percentage for N 1s core level species

Figure 4.12 shows the set of typical (N *1s*) core level surface spectra obtained for the reactively evaporated InN.

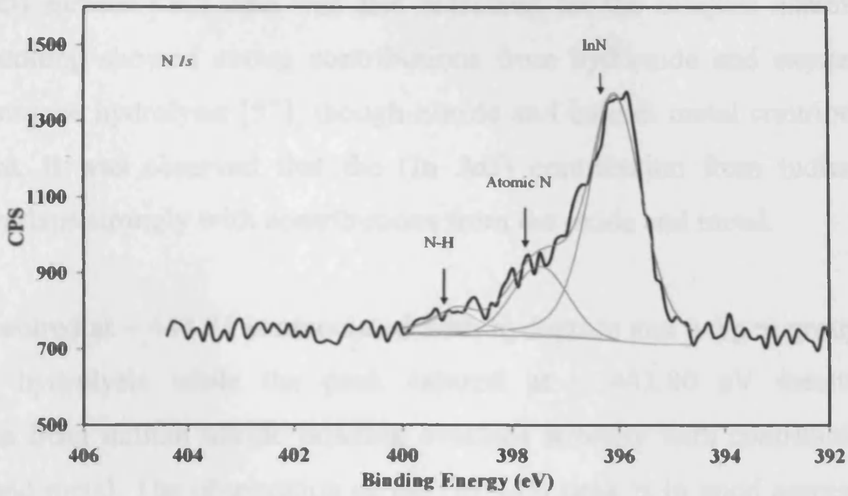

(a) N *1s* core level spectra for reactively evaporated InN (sample A)

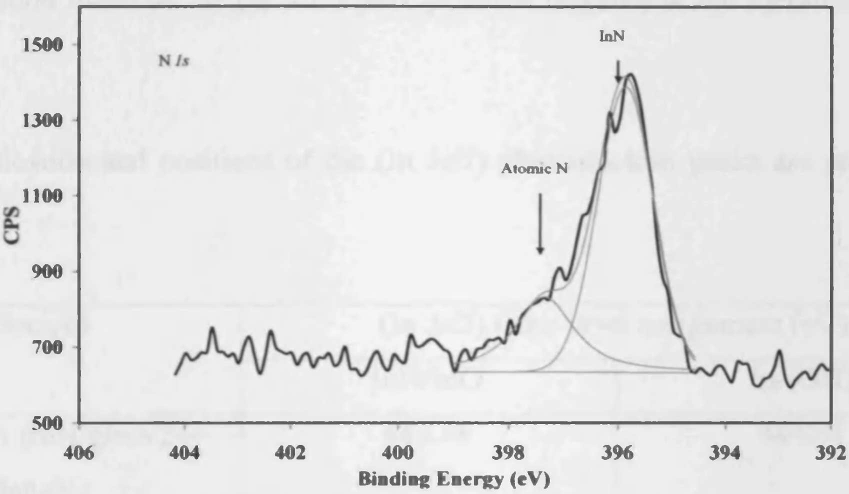

(b) N *1s* core level spectra for reactively evaporated InN (sample B)

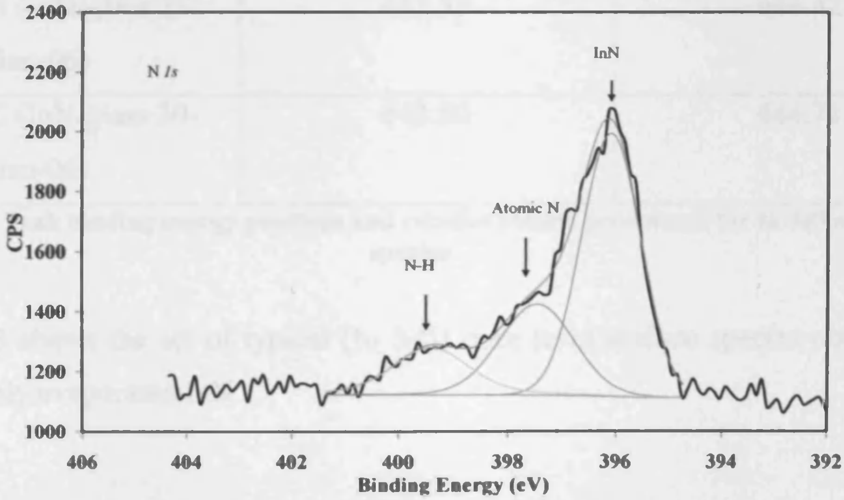

(c) N *1s* core level spectra for reactively evaporated InN (sample C)

Figure 4.12: N *1s* core level spectra for reactively evaporated InN

The (In *3d5*) surface peak data was also measured for the samples examined. The (In *3d5*) bonding showed strong contributions from hydroxide and oxygen groups related to surface hydrolysis [57], though nitride and indium metal contributions are also present. It was observed that the (In *3d5*) contribution from indium nitride bonding overlaps strongly with contributions from the oxide and metal.

The peak centred at ~ 444.71 is associated with hydroxide and oxygen groups related to surface hydrolysis while the peak centred at ~ 443.80 eV resulting from contribution from indium nitride bonding overlaps strongly with contributions from the oxide and metal. The observation of the (In *3d5*) peak is in good agreement with the observation made on the (In *3d5*) peak position reported in the literature [13, 37, 38, 53, 54].

The identification and positions of the (In *3d5*) photoelectron peaks are provided in table 4.2.

Sample	(In *3d5*) Core level assignment (eV)	
	InN/InO	In-(OH)
Sample A (InN/glass 24-Jan-06)	443.78	444.64
Sample B (InN/glass 25-Jan-06)	443.55	444.42
Sample C (InN/glass 30-Jan-06)	443.80	444.71

Table 4.2: Peak binding energy positions and relative atomic percentage for In *3d5* core level species

Figure 4.13 shows the set of typical (In *3d5*) core level surface spectra obtained for the reactively evaporated InN.

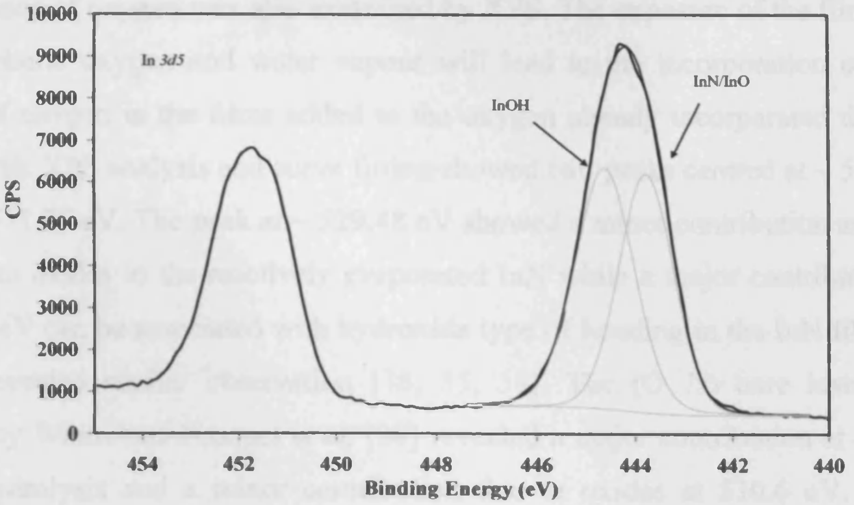

(a) In *3d5* core level spectra for reactively evaporated InN (sample A)

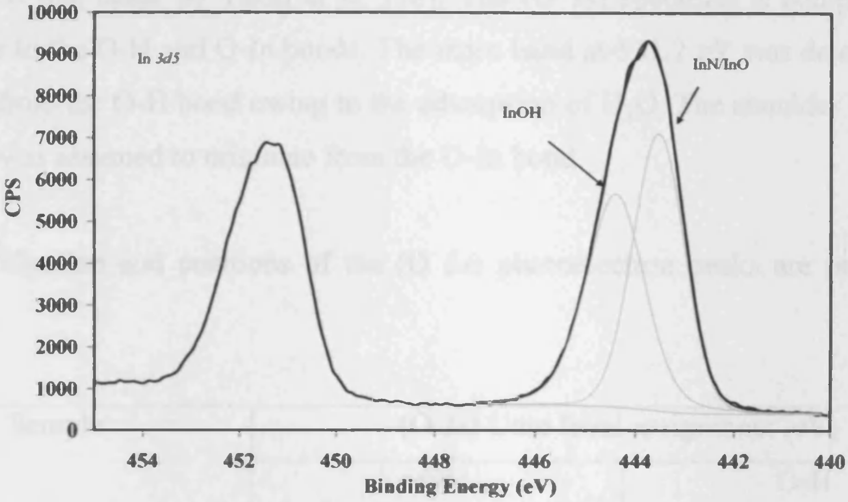

(b) In *3d5* core level spectra for reactively evaporated InN (sample B)

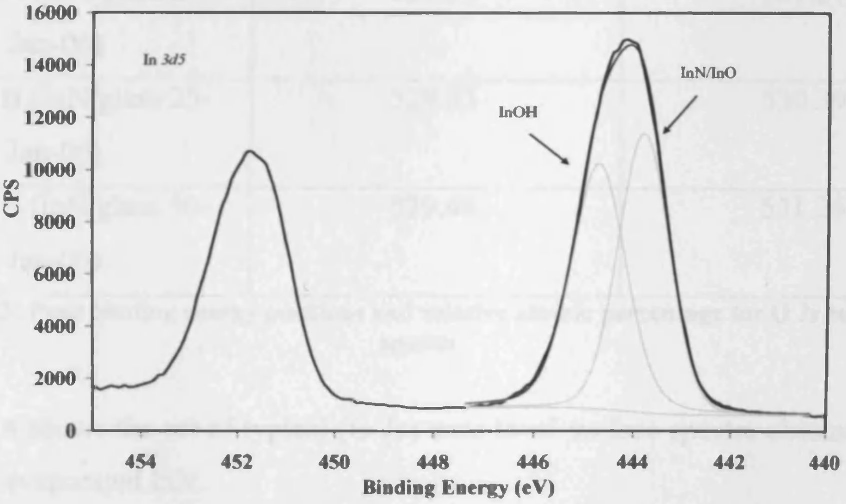

(c) In *3d5* core level spectra for reactively evaporated InN (sample C)

Figure 4.13: In *3d5* core level spectra for reactively evaporated InN

The presence of oxygen was also examined by XPS. The exposure of the film surface to atmospheric oxygen and water vapour will lead to the incorporation of a large amount of oxygen in the films added to the oxygen already incorporated during the film growth. XPS analysis and curve fitting showed two peaks centred at ~ 529.48 eV and at ~ 531.26 eV. The peak at ~ 529.48 eV showed a minor contribution and can be assigned to oxides in the reactively evaporated InN while a major contribution peak ~ 531.26 eV can be associated with hydroxide type of bonding in the InN film. Other reports revealed similar observation [38, 55, 58]. The (O *1s*) core level spectra reported by Wintrebert-Fouquet et al. [38] revealed a major contribution at 532.5 eV due to hydrolysis and a minor contribution due to oxides at 530.6 eV. Similar observation was made by Takai et al. [58]. The (O *1s*) spectrum is composed of 2 bonds due to the O-H and O-In bonds. The main band at 531.2 eV was determined to originate from the O-H bond owing to the adsorption of H_2O. The shoulder bond near 529.2 eV was assumed to originate from the O-In bond.

The identification and positions of the (O *1s*) photoelectron peaks are provided in table 4.3.

Sample	(O *1s*) Core level assignment (eV)	
	oxide	O-H
Sample A (InN/glass 24-Jan-06)	529.59	531.31
Sample B (InN/glass 25-Jan-06)	529.33	530.39
Sample C (InN/glass 30-Jan-06)	529.48	531.26

Table 4.3: Peak binding energy positions and relative atomic percentage for O *1s* core level species

Figure 4.14 shows the set of typical (O *1s*) core level surface spectra obtained for the reactively evaporated InN.

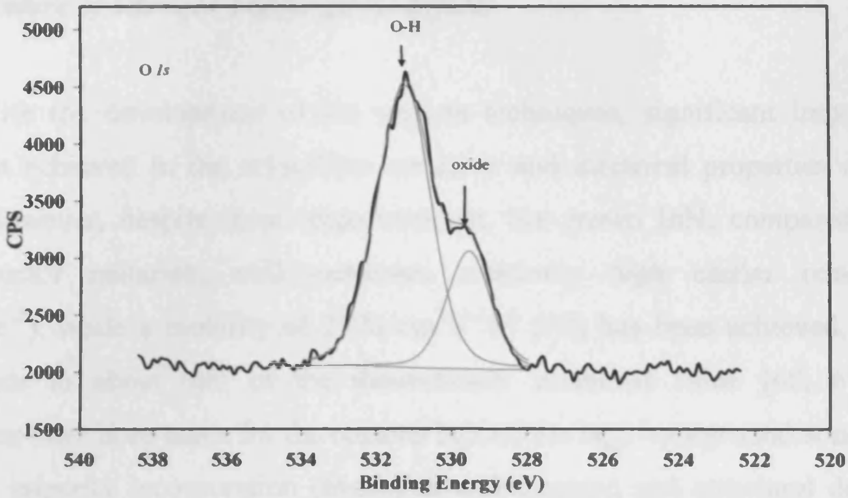

(a) O *ls* core level spectra for reactively evaporated InN (sample A)

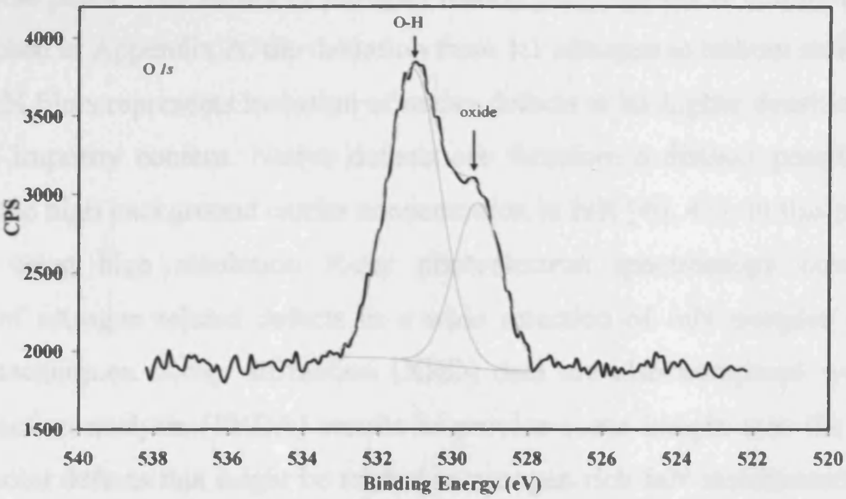

(b) O *ls* core level spectra for reactively evaporated InN (sample B)

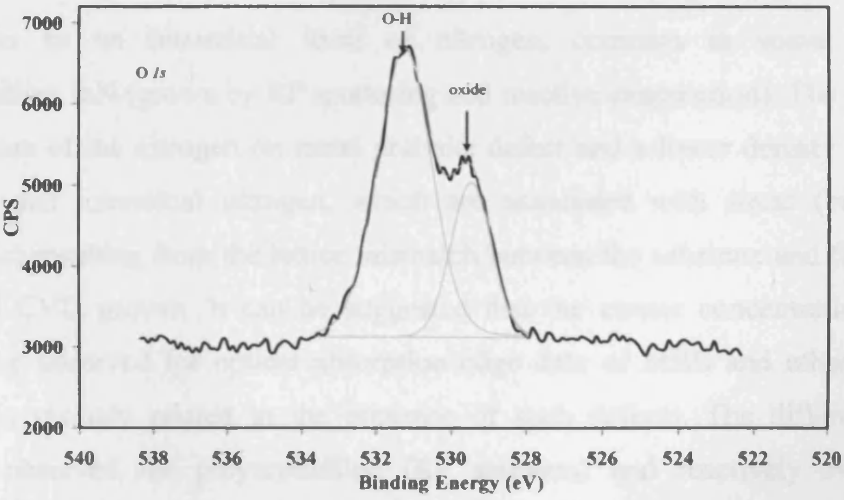

(c) O *ls* core level spectra for reactively evaporated InN (sample C)

Figure 4.14: O *ls* core level spectra for reactively evaporated InN

4.3.3.2. Nature of nitrogen related point defects

With the development of the growth techniques, significant improvements have been achieved in the crystalline structure and electrical properties of indium nitride. However, despite these improvements, the grown InN, compared to other semiconductor materials, still possesses relatively high carrier concentration ($>10^{17}$ cm^{-3}), while a mobility of 2370 $cm^2V^{-1}s^{-1}$ [59] has been achieved, this only corresponds to about half of the theoretically predicted value [60, 61]. Many suggestions have been made for the reasons behind the high background concentration including impurity incorporation (hydrogen and oxygen) and structural defects. As shown in the paper "The nature of nitrogen related point defects in common forms of InN" attached in Appendix A, the deviation from 1:1 nitrogen to indium stoichiometry in most InN films represents inclusion of native defects at far higher densities than the combined impurity content. Native defects are therefore a distinct possibility as a source of the high background carrier concentration in InN [40, 43]. In this paper, data collected using high resolution X-ray photoelectron spectroscopy confirms the presence of nitrogen related defects in a wide selection of InN samples grown by different techniques. X-ray diffraction (XRD) data are also compared with elastic recoil detection analysis (ERDA) results to provide some insight into the origin of possible point defects that might be related to nitrogen rich InN stoichiometry. It was shown that two distinct forms of point defects can be distinguished; one of these appears to be an interstitial form of nitrogen, common in some forms of polycrystalline InN (grown by RF sputtering and reactive evaporation). The other may be a mixture of the nitrogen on metal anti-site defect and a lower density of indium vacancies and interstitial nitrogen, which are associated with stress (biaxial and hydrostatic) resulting from the lattice mismatch between the substrate and film during MBE and CVD growth. It can be suggested that the carrier concentration related dependence observed for optical absorption edge data of MBE and other epitaxial material is strongly related to the presence of such defects. The different defect structure observed for polycrystalline (RF sputtered and reactively evaporated) material may be related to the different optical absorption edge and electrical properties seen for that material.

4.3.3.3. Surface charge accumulation

Few recent reports have noted the existence of a surface electron accumulation layer in MBE grown InN [62-66]. These reports investigated the presence of such high accumulation of electron carriers at the surface, and the impact of the physical properties of the grown indium nitride. Many theories have been given to explain the presence of this accumulated charge layer. Mahboob et al. [63] concluded that the surface oxide was not responsible for surface accumulation, but that the low band-gap and low position of the conduction band minima relative to the vacuum level ensured that native defect levels for InN lay predominantly in the conduction band. On the other hand, a contradictory theory was proposed by Cimalla et al. [65, 66] when they suggested that oxygen was likely to be responsible for the formation of the surface accumulation layer. It is clear that more investigation is needed to fully understand the existence of the surface charge accumulation. The high resolution X-ray photoelectron spectroscopy analysis discussed above and in the paper with title "The nature of nitrogen related point defects in common forms of InN" attached in Appendix A is used to identify a suitable explanation for the surface charge accumulation.

Hall Effect measurements (discussed in full detail in the next chapter) showed that the resistivity of the reactive evaporation samples were more than three orders of magnitude higher than any other InN samples grown by other techniques (RF sputtering, RPE-CVD, and MBE). Given that these reactive evaporation polycrystalline samples have a large available surface area at the grain boundaries, if surface accumulation had been evident in these samples then high carrier concentrations and relatively low film resistivity would be present. It is significant that the carrier concentration of the reactively evaporated material are orders of magnitude less than recently grown RF sputtered InN, which has similar oxygen levels (confirmed by SIMS analysis) present and can also be polycrystalline. From these results it is evident that the effects of electron surface accumulation are absent for this form of InN. This explains why this polycrystalline material is able to have electron carrier concentrations in the same range as MBE material. For MBE material electron surface accumulation is a significant problem. The presence of large amounts of oxygen, which resides at the surface and grain boundaries [34, 41] in the reactively evaporated material, further discounts oxygen as a source of the surface accumulation effect for InN, since surface accumulation is not observed for the reactively evaporated material.

SIMS qualitative analysis (details in section 4.4) has shown that the reactively evaporated indium nitride has indium rich stoichiometry. This can be confirmed by the XPS measurements. The stoichiometry can actually be concluded from indium to nitrogen ratio obtained as the (In *3d5*)/(N *1s*) ratios for each of the samples studied. For these ratios the (N *1s*) contributions for the N-H bonding energy at ~ 399.5 eV was not included as these contributions were for surface absorbate species unrelated to the indium nitride matrix. The (In *3d5*) peak related to In-OH bonding was also not included since it was a surface hydrolysis product unrelated to the underlying InN crystal, and because it could be clearly resolved from the indium peak due to indium nitride bonding. However, the (In *3d5*) peak used included unresolved contributions from oxygen and indium metal contributions, as well as the contribution related to indium nitride. The (In *3d5*)/(N *1s*) ratios are shown in Table 4.4.

The presence of interstitial nitrogen as defect structure in indium nitride grown by different techniques as confirmed by high resolution XPS analysis (as mentioned above), lead to the assumption that these nitrogen interstitial species observed in samples grown by the RF sputtering, reactive evaporation, MBE and CVD techniques might be responsible for the surface accumulation effect observed for epitaxial InN. Table 4.4 shows the (In *3d*)/(N *1s*) ratios for samples that were examined.

It can be clearly seen that the highest indium to nitrogen ratio is obtained for the reactively evaporated indium nitride, while MBE and RPE-CVD samples showed the lowest ratios. This means the absence of surface charge accumulation is correlated with the presence of excess indium at the sample surface of reactively evaporated samples. Additionally, it can be assumed that the nitrogen defects, observed in all the InN samples, can be assumed as potential reason for the presence of surface charge accumulation, however, with some sort of compensation in the presence of large amounts of indium at the sample surface.

Sample	(In *3d*)/(N *1s*) Ratio	Sample	(In *3d*)/(N *1s*) Ratio
RF sputtered (4-5-Jul-05)	2.13	RPECVD on sapphire (4-5-Nov-04)	1.41
RF sputtered (6-7-Jul-05)	2.25	RPECVD on sapphire (24-25-Jan-05)	1.37
RPECVD on sapphire (18-May-04)	1.31	MBE GS-1322	1.23
RPECVD on glass (18-May-04)	1.09	MBE W431	1.11
RPECVD on sapphire (21-May-04)	1.48	Reactive evaporation (24-Jan-06)	2.53
RPECVD on glass (21-May-04)	1.37	Reactive evaporation (25-Jan-06)	3.30
RPECVD on sapphire (21-Jan-05)	1.44	Reactive evaporation (30-Jan-06)	2.83

Table 4.4: (In *3d*)/(N *1s*) ratios for InN samples

4.4. Secondary ion mass spectroscopy (SIMS)

4.4.1. Theory

Secondary ion mass spectroscopy (SIMS), also known as ion microprobe or ion microscope, is a powerful technique for determining the surface and near-surface composition in a wide range of solid materials [67]. This technique is element specific and is capable of detecting all elements including hydrogen and helium, and has extremely high sensitivity for detecting the elements of interest in the part-per-million (ppm) to part-per-billion range (ppb).

SIMS is a destructive surface analytical technique that gives good depth resolution, as well as high sensitivity to impurities. The impact of primary ion beam (oxygen O or cesium Cs), with energies ranging from a few 100 eV to 10s of keV, targeting the surface of the sample causes the surface layer of atoms of the sample to be stripped off (sputtered), largely as neutral atoms. However, a small fraction forms as positive or negative secondary ions that are collected for mass analysis. Continuous detection of these sputtered secondary ions allows SIMS to create a depth profile of the surface and underlying layers to a depth of 10 microns with a depth resolution of 2-5nm. The images below show how the primary ion-beam raster across the sample surface and leaving a crater in the sample with secondary ion being ejected off the surface.

SIMS analysis can be in two modes: static and dynamic. With the static mode, a complete mass spectrum can be recorded for surface analysis of the outer 5 Å or so, using a low sputtering rate (~ 1 Å/hr). This mode is restricted to shallow surface analysis because of the low sputter rate being used. On the other hand, dynamic mode makes use of higher sputter rate (~ 10 μm/hr) and finds application in depth profiling analysis.

The SIMS experiments were performed at the Australian Nuclear Science and Technology Organisation (ANSTO). The measurements were carried out using a Camica 5F dynamic SIMS system. The main steps of the SIMS analysis process can be summarized as follows [67]: the primary ions are produced by a caesium (1) or oxygen (2) source and are accelerated along the primary column (3-4) and focused onto the sample surface (5). The sputtered secondary ions pass through a secondary column (6-8), where they are collected and separated by charge (9). The secondary ions are then collected and focussed through the mass spectrometer (10-12). The analysed ions are then directed into detectors (13-14), and a signal is measured. The electron multiplier (17) amplifies the incoming signal for each element to be large enough to be measured. The SIMS system is explained in Figure 4.16.

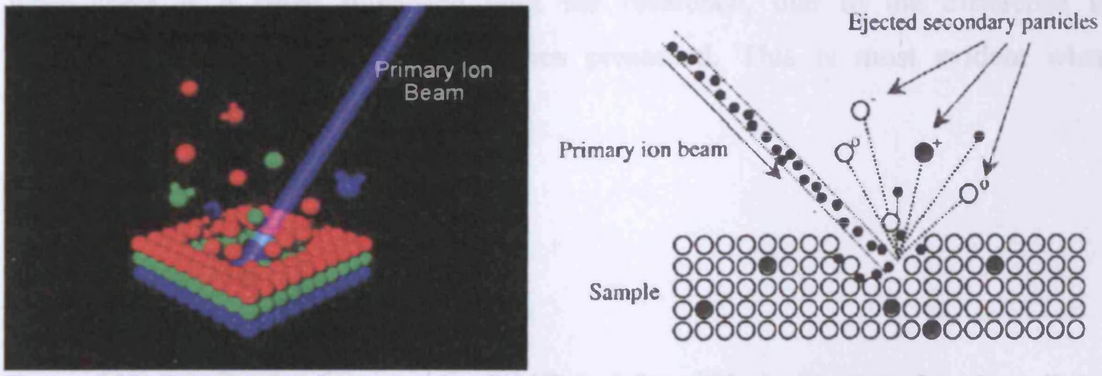

Figure 4.15: Primary ion beam bombarding the surface and ejecting secondary ion off the surface. From [67]

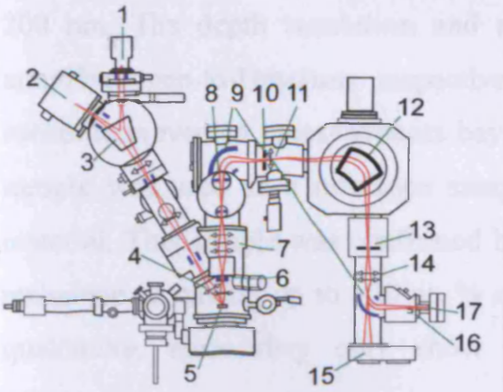

Figure 4.16: Camica 5F SIMS system. From [67]

1. Caesium Ion Source	10. Energy Slit
2. Duoplasmatron Ion Source	11. Spectrometer Lens
3. Primary Beam Mass Filter	12. Magnetic Sector
4. Immersion lens	13. Exit Slit
5. Specimen	14. Projector Lenses
6. Dynamic Transfer System	15. Channel Plate
7. Transfer Optical System	16. Faraday Cup
8. Entrance Slit	17. Electron Multiplier
9. Electrostatic Sector	

Semiconductor depth-profiling is a common application for SIMS analysis. For this work, the aim of this analysis is to examine the variation of composition with depth for indium nitride (InN) thin films grown by reactive evaporation. A SIMS depth profile is produced by sputtering the sample and monitoring the secondary ion signal of a given element as a function of time. Such an “ion signal versus time” plot contains the necessary information for the compositional elements, but the axes must be converted. The time axis is converted to a depth axis by measuring the depth of the crater at the end of the measurement. This should be done for each sample, since the sputter rate varies with spot focus and ion current.

SIMS is preferable as qualitative rather than quantitative depth profile technique, as the depth profile interpretation of the analysed sample has to be examined with reference of similar composition but known contents, which is not always obtainable. Moreover, the accuracy of quantitative interpretation can be seriously affected even when there is a small mismatch with the reference, due to the difference in concentration of yield enhancing species presented. This is most evident when examining percentage levels of a species.

4.4.2. Experiment

Using a Camica 5F dynamic SIMS system with a caesium ion sputter source an area of about 200 μm by 200 μm was raster scanned using and primary ion beam with a current of 10 nA. The measurements were carried out up to a depth of about 200 nm. The depth resolution and mass/elemental range are 1-2 nm and 1-500 amu/Hydrogen-to-Uranium, respectively. For all samples, charging effects at the substrate prevented measurements beyond that point. A polycrystalline RF sputtered sample was used as a reference sample to estimate the amount of oxygen in the material. This sample was confirmed by the elastic recoil detection analysis (ERDA) technique as having up to ~20 at. % oxygen. These results can only be regarded as qualitative, since they only show the percentage variation in the elemental composition.

4.4.3. Results and discussion

Depth profile measurements were performed on *n*-type InN grown on both sapphire and glass substrates by reactive evaporation. All the samples were grown at room temperature, but had a broad range of band gap from 0.7 eV to 2.0 eV. The purpose of the depth profile analysis was to estimate the amount of oxygen present in the material and study its influence on the band gap value. The methodology of Gao [68] was applied whereby Cs^+M (where M is the element mass being analyzed) ions are collected instead of M. Y. Gao stated that the matrix effect can be reduced considerably by employing Cs^+ ions and monitoring Cs^+M secondary ions. That is because almost all the sputtered particles in the SIMS analysis are electrically neutral and it can be assumed that in the recombination process of Cs^+M ions the sputtered neutral atoms of M with the high-density Cs^+ ions would dominate the process. Hence, high reolution analysis can be achieved. With a primary Caesium (Cs^+) ion beam, the signals of the monitored secondary ions were plotted as a function of the sputtering time. The secondary ions are normally comprised of the a $^{133}Cs^+$ ion and one neutral atom of interest, and in this work, those atoms were ^{1}H, ^{12}C, ^{14}O, ^{16}O, ^{27}Al, ^{28}Si, ^{113}In and ^{115}In. The Cs^+ secondary ion intensity was used as a reference during the measurements. The SIMS measurements for the InN samples are shown in figure 4.17.

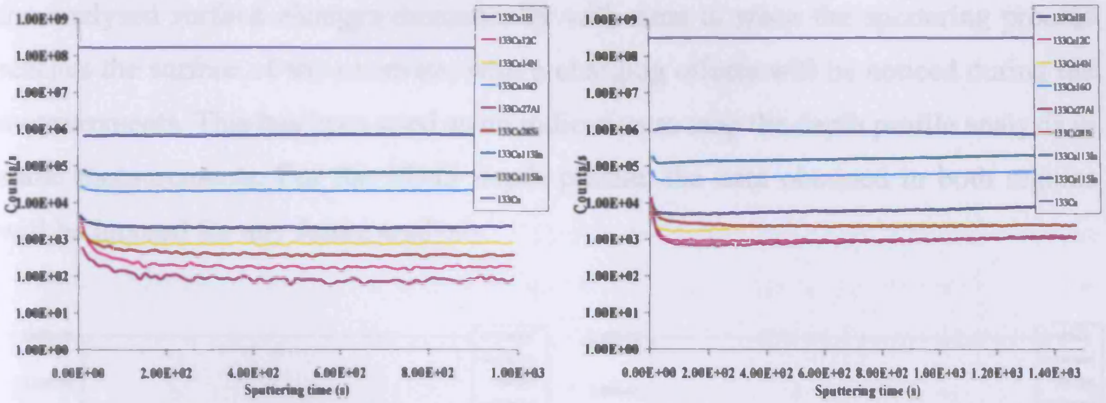

(a) $E_g = 0.70$ eV, $n = 1.33\times10^{19}$ cm^{-3}

(b) $E_g = 0.90$ eV, $n = 1.78\times10^{19}$ cm^{-3}

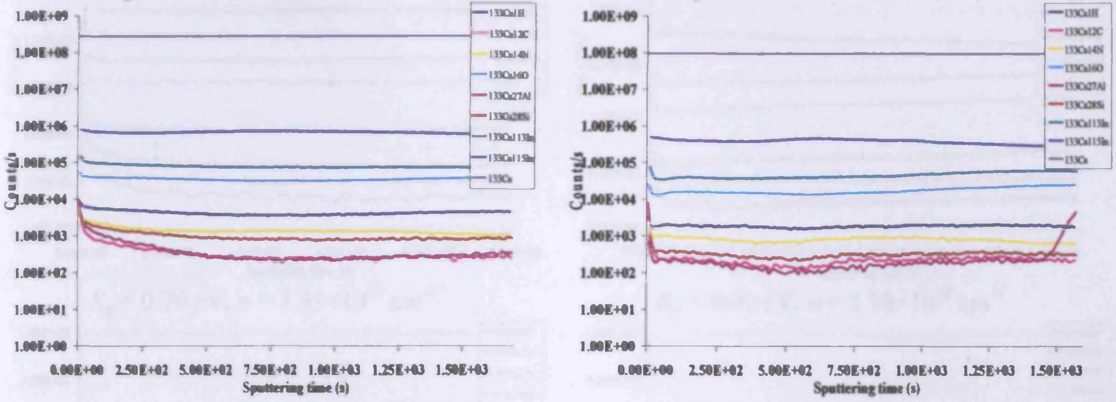

(c) $E_g = 1.50$ eV, $n = 5.98\times10^{18}$ cm^{-3}

(d) $E_g = 1.65$ eV, $n = 5.18\times10^{18}$ cm^{-3}

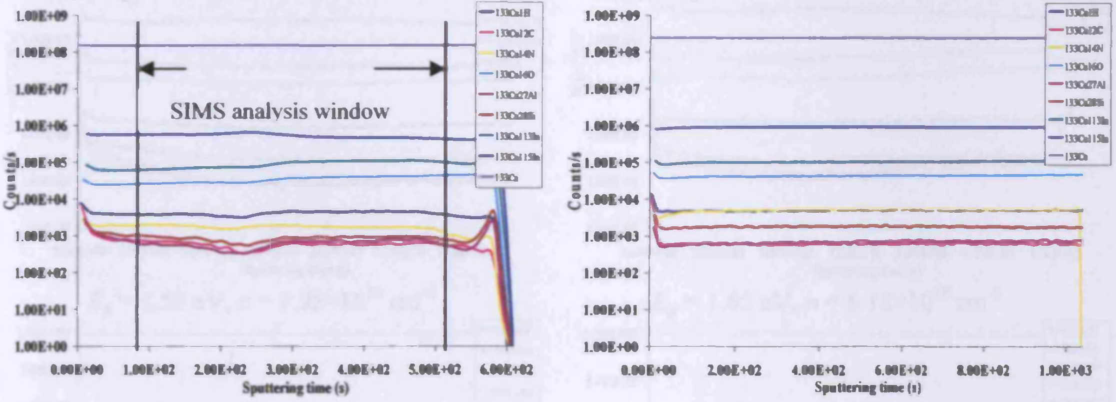

(e) $E_g = 1.9$ eV, $n = 1.24\times10^{19}$ cm^{-3}

(f) $E_g = 1.9$ eV, $n = \sim 10^{20}$ cm^{-3}

Figure 4.17: SIMS measurements for reactively evaporated InN

From Figure 4.17 (e) it can be seen that there are two regions where the depth profile analysis varied dramatically with time. The first region was observed just after the primary ion beam hits the sample. The variation can be attributed to the non-equilibrium state of the sputtering process, where the reference Cs$^+$ intensity would be still changing and yet stabilized. Another possible reason would be the surface contamination with an oxide layer and other impurities that would affect (at the start) the intensity of the secondary ions. The other region where the depth profile signal of the analysed surface changes dramatically with time is when the sputtering process reaches the surface of the substrate, where charging effects will be noticed during the measurements. This has been used as an indication to stop the depth profile analysis in some measurements. For the SIMS depth profile, the data obtained in both regions will be ignored for any future analysis.

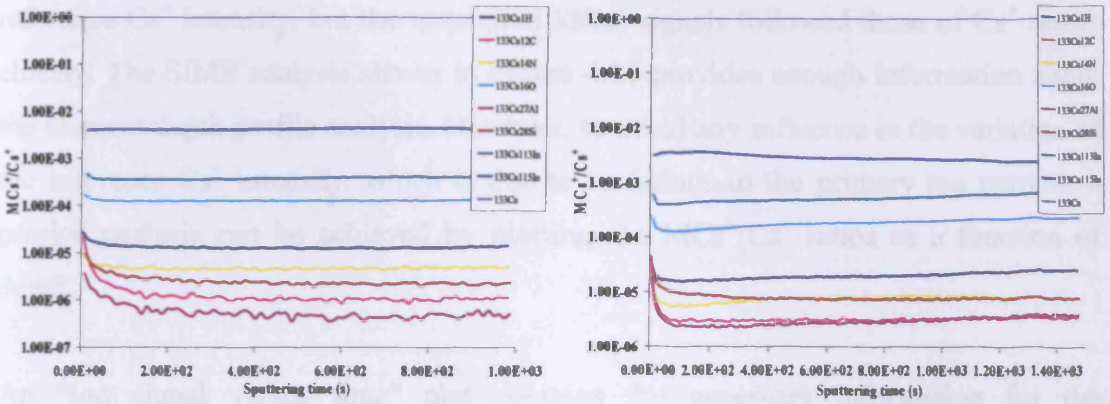

$E_g = 0.70$ eV, $n = 1.33\times10^{19}$ cm^{-3}

$E_g = 0.90$ eV, $n = 1.78\times10^{19}$ cm^{-3}

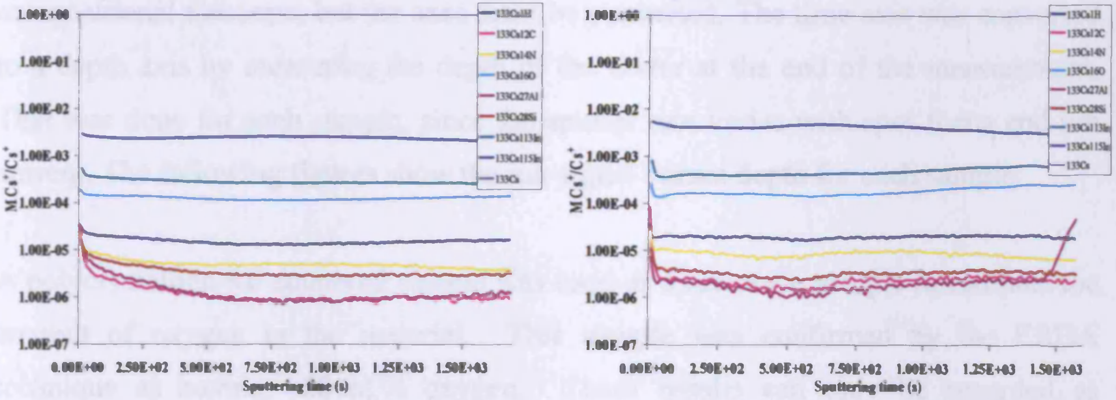

$E_g = 1.50$ eV, $n = 5.98\times10^{18}$ cm^{-3}

$E_g = 1.65$ eV, $n = 5.18\times10^{18}$ cm^{-3}

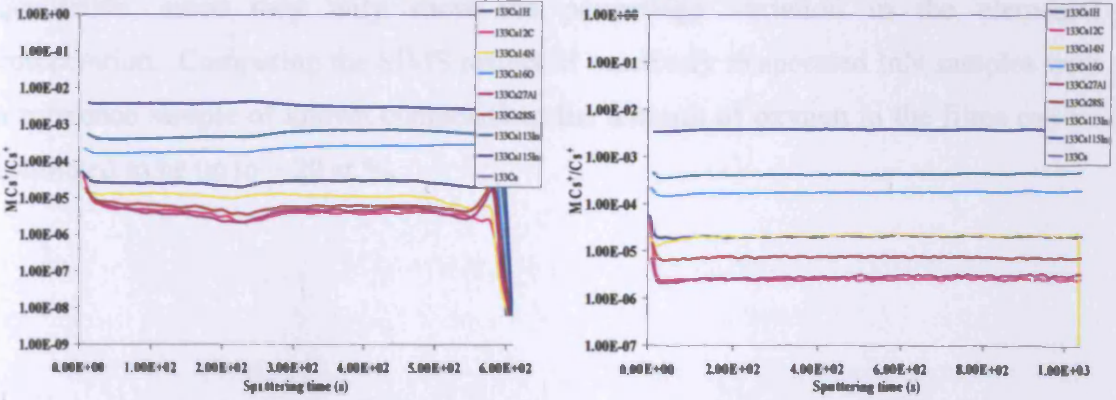

$E_g = 1.9$ eV, $n = 1.24\times10^{19}$ cm^{-3}

$E_g = 0.9$ eV, $n = \sim 10^{20}$ cm^{-3}

Figure 4.18: Plots of MCs$^+$/Cs$^+$ as a function of the sputtering time

It was found that the intensity of the reference Cs^+ secondary signal varied slightly with sputtering time and between samples. That could be caused by a variation of the primary ion current. In practice, due to the measurement system, the primary ion current amplitude varied slightly over time and that could not be avoided, despite using a "supposedly" constant current of 10 nA. However, the current variations were minimal. Signal intensities of the other monitored elements were influenced by the reference Cs^+ intensity, but the respective MCs^+ signals followed those of Cs^+ rather closely. The SIMS analysis shown in Figure 4.17 provides enough information about the element depth profile analysis. However, to avoid any influence in the variation of the reference Cs^+ intensity, which is due to variations in the primary ion current, a precise analysis can be achieved by plotting the MCs^+/Cs^+ ratios as a function of depth.

An "ion signal versus time" plot contains the necessary information for the compositional elements, but the axes must be converted. The time axis was converted to a depth axis by measuring the depth of the crater at the end of the measurement. That was done for each sample, since the sputter rate varies with spot focus and ion current. The following figures show the ion signal versus depth for each sample.

A polycrystalline RF sputtered sample was used as a reference sample to estimate the amount of oxygen in the material. This sample was confirmed by the ERDA technique as having ~20 at.% oxygen. These results can only be regarded as qualitative, since they only show the percentage variation in the elemental composition. Comparing the SIMS results of reactively evaporated InN samples with a reference sample of known composition, the amount of oxygen in the films can be estimated to be up to ~ 20 at.%.

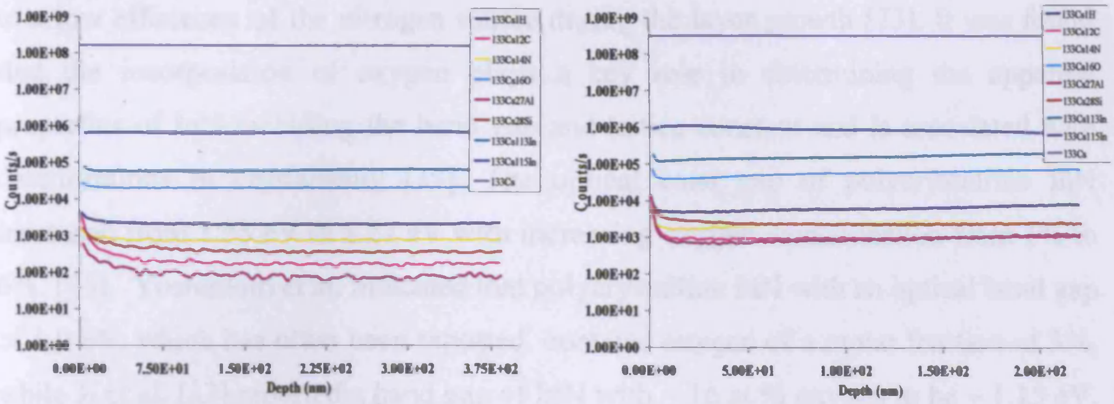

$E_g = 0.70$ eV, $n = 1.33\times10^{19}$ cm^{-3} $E_g = 0.90$ eV, $n = 1.78\times10^{19}$ cm^{-3}

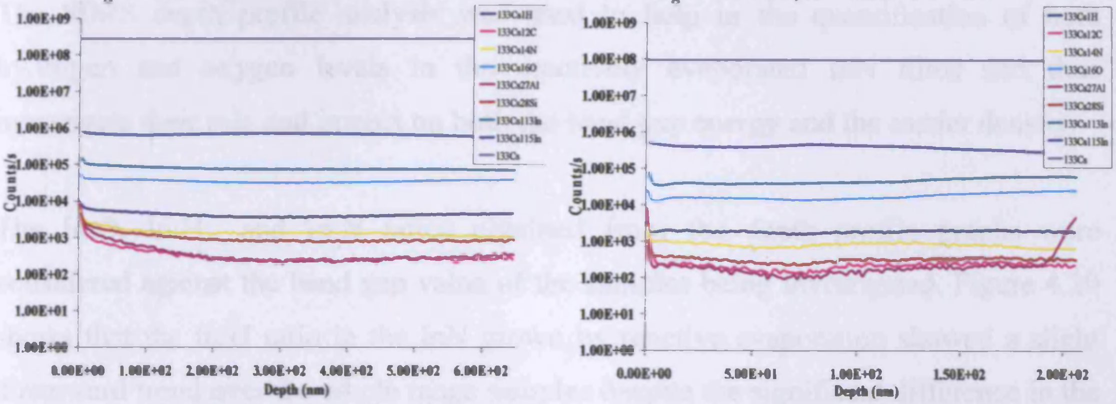

$E_g = 1.50$ eV, $n = 5.98\times10^{18}$ cm^{-3} $E_g = 1.65$ eV, $n = 5.18\times10^{18}$ cm^{-3}

Figure 4.19: Depth profile for reactively evaporated InN

Both hydrogen and oxygen were predicted to be shallow donors in InN [68-72]. Saito et al. [71] suspected that the high carrier density of InN films was due to impurities such as oxygen because of the very low growth temperature while Gallinat et al. [72], on the other hand, suggested that hydrogen was the dominant unintentional impurity donor in their film from their SIMS analysis. It was also concluded by Davis et al. [70] and Van der Walle [69] that hydrogen must be added to the list of potential dopants in InN.

Furthermore, several reports have suggested that the presence of oxygen may have a significant role in the different observations of the fundamental band gap of InN [12, 28, 35, 73, 74]. While Motlan et al. [12] interpreted the significant variations of the fundamental band gap with film thickness as related to the varying oxygen content in the films; Matsouka et al. [28] assumed that the presence of oxygen in the material may affect the apparent band gap of InN. One of reasons for findings of E_g higher than 0.9 eV could be the formation of oxynitrides or alloys of the InN-In$_2$O$_3$ type due to a low efficiency of the nitrogen source during the layer growth [73]. It was found that the incorporation of oxygen plays a key role in determining the apparent properties of InN including the band gap and lattice constant and is associated with deteriorations in crystallinity [35]. The optical band gap of polycrystalline InN increased from 1.55 eV to 2.27 eV with increasing oxygen contamination from 1% to 6%. [74]. Yoshimoto et al. indicated that polycrystalline InN with an optical band gap of 1.9 eV, which has often been reported, contains oxygen of a molar fraction of 3%, while Ji et al. [32] reported a band gap of InN with ~ 16 at.% oxygen to be ~ 1.15 eV. The SIMS depth profile analysis was used to help in the quantification of both hydrogen and oxygen levels in the reactively evaporated InN films and thus investigate their role and impact on both the band gap energy and the carrier density.

The In:O, In:H and In:N ratios obtained from the depth profile graphs were considered against the band gap value of the samples being investigated. Figure 4.20 shows that the In/H ratio in the InN grown by reactive evaporation showed a slight downward trend over the whole range samples despite the significant difference in the carrier concentration between samples. This observation contradicts the suggestions made on the role of hydrogen as a potential donor for InN. However it agrees well with the observations made by Wu et al. [75] and Ho et al. [76]. Wu et al., using SIMS analysis, concluded that there exist insufficient roles for O and H impurities as donor in InN, while Ho et al. indicated that the major source of unintentional donors is not impurity related. The observation made on oxygen by Wu et al. and Ho et al. agrees very well with the observation made on oxygen in this work. The inspection of the data obtained shows the ratio of indium to oxygen in different samples with different carrier concentrations is similar. This excludes oxygen as a donor for the high carrier concentration for the as-grown InN material. The oxygen level in the low band gap (0.7 eV) and high band gap (~ 2 eV) was found to be the same. The oxygen level in the reactively evaporated InN is estimated to be up to ~ 20 at.%. Butcher et al. [40, 41] noticed that an oxygen content of 37 at.% (44% In_2O_3) is required to increase the band gap from 0.7 to 2 eV. It can be seen there is insufficient oxygen in the InN grown by reactive evaporation to explain the difference in the band gap between 0.7 eV InN and ~ 2 eV InN. This important observation provides further evidence excluding InN – In_2O_3 alloying as the origin of the large optical band gap variations found in InN thin films.

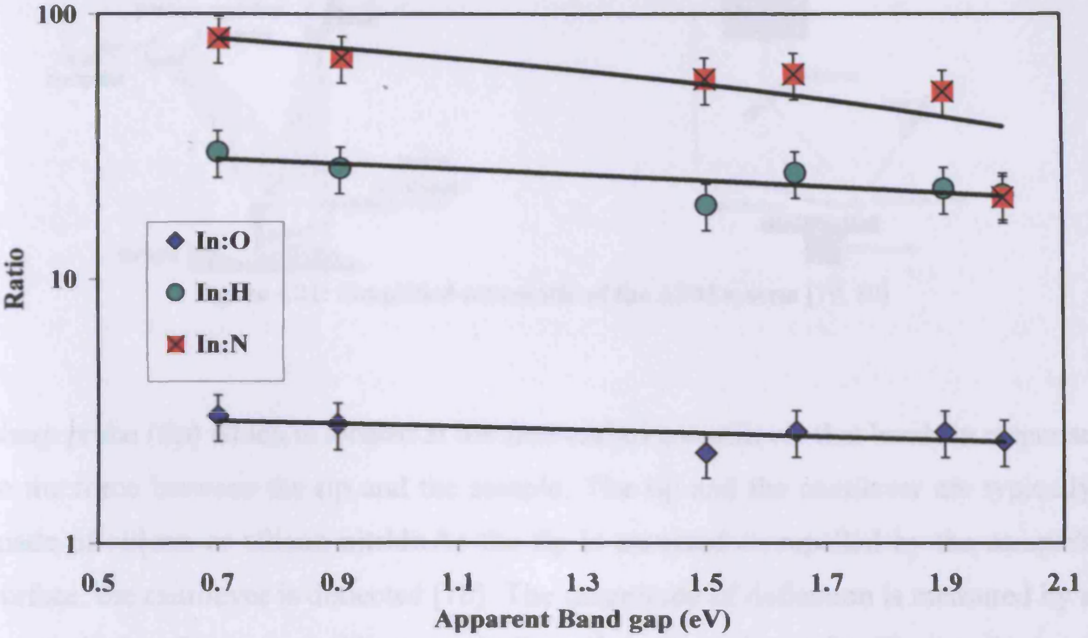

Figure 4.20: In:O, In:H and In:N ratios as a function of the band gap

The presence of large amounts of oxygen at the surface and grain boundaries of the reactively evaporated material, confirmed by SIMS, further discounts oxygen as a source of the surface accumulation effect of InN, since such accumulation was not observed for the reactively evaporated InN.

It can also be noted that the reactively evaporated indium nitride can be considered indium-rich material, due to the presence of excess indium on the surface and the bulk. This observation confirms the finding of the XPS analysis where it was considered that this indium-rich material is correlated with the absence with surface charge accumulation.

4.5. Atomic force microscopy (AFM)

4.5.1. Theory

Atomic force microscopy (AFM) is a powerful analysis technique for surface topographic studies and mapping surface features. AFM is based on the existence of a separation-dependency force between a surface and a tip [77]. An AFM utilizes a

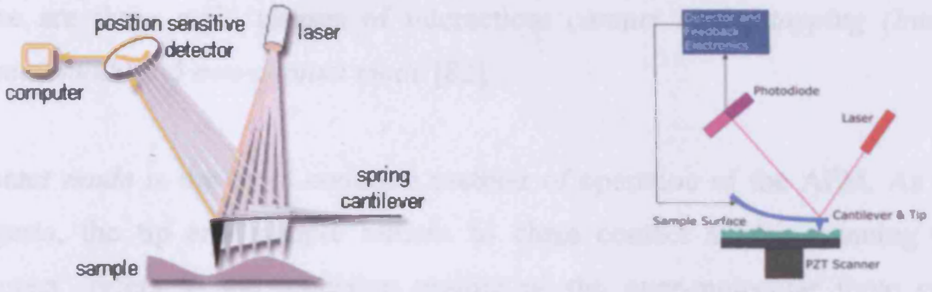

Figure 4.21: Simplified schematic of the AFM system [79, 80]

sharp probe (tip) which is located at the free-end of a cantilever that bends in response to the force between the tip and the sample. The tip and the cantilever are typically made of silicon or silicon nitride.As the tip is attracted or repelled by the sample's surface, the cantilever is deflected [78]. The magnitude of deflection is measured by a laser which reflects at an oblique angle from the end of the probe. Plotting the laser deflection against the tip position on the sample surface creates a "map" of the hills and valleys of the surface. This provides a high resolution image of the sample's surface. The technique is illustrated in Figure 4.21.

Two distance regimes are labelled on Figure 4.22: 1) the contact regime; and 2) the non-contact regime. In the contact regime, the cantilever is held less than a few Angstroms from the sample surface, and the interatomic force between the cantilever and the sample is repulsive. In the non-contact regime, the cantilever is held on the order of tens to hundreds of Angstroms from the sample surface, and the interatomic force between the cantilever and sample is attractive (largely a result of the long-range van der Waals interactions).

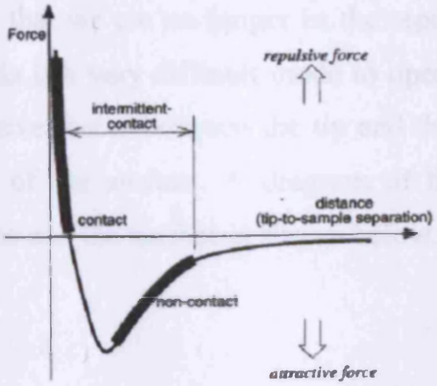

Figure 4.22: Contact regimes of AFM system [81]

There are three main classes of interaction: ***contact mode***, ***tapping (Intermittent-contact) mode*** and *non-contact mode* [82].

Contact mode is the most common method of operation of the AFM. As the name suggests, the tip and sample remain in close contact as the scanning proceeds. "Contact" refers to the repulsive regime of the inter-molecular force curve (see figure). As the instrument drags the tip over the surface, a detection device measures the cantilever's vertical deflection and provides an indication of the local sample height - in effect, measuring the 'repulsion' forces between tip and sample. The repulsive region of the curve lies above the x-axis. One of the drawbacks of remaining in contact with the sample is that there exist large lateral forces on the sample as the drip is "dragged" over the specimen.

Tapping (Intermittent-contact) mode is the next most common mode used in AFM. When operated in air or other gases, the cantilever is oscillated at its resonant frequency (often hundreds of kilohertz) and positioned above the surface so that it only taps the surface for a very small fraction of its oscillation period. This is still contact with the sample in the sense defined earlier, but the very short time over which this contact occurs means that lateral forces are dramatically reduced as the tip scans over the surface. When imaging poorly immobilised or soft samples, tapping mode may be a far better choice than contact mode for imaging.

Non-contact operation is another method which may be employed when imaging by AFM. In non-contact mode, the atomic force microscope's probe does not touch the surface of the sample. The cantilever must be oscillated above the surface of the sample at such a distance that we are no longer in the repulsive regime of the inter-molecular force curve. This is a very difficult mode to operate in ambient conditions with the AFM. The attractive forces between the tip and the surface are measured to draw a topographic map of the surface. A diagram of the force that could exist between the tip of the probe and the surface is shown below.

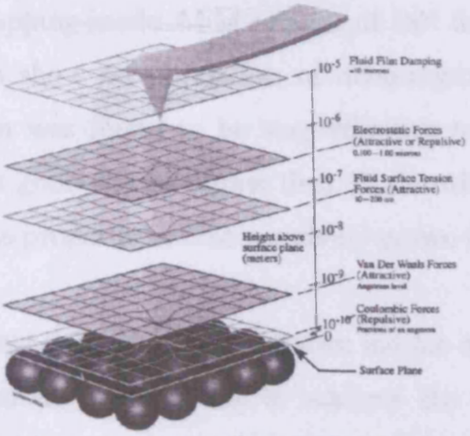

Figure 4.23: Forces between the tip of the probe and the surface. From [83]

4.5.2. Experiment

A Multimode SPM system made by Veeco was used for studying the roughness of the surface of the indium nitride grown by reactive evaporation. This Multimode system uses "Amplitude modulation" rather than "Frequency modulation" to regulate the tip-sample distance. The reactively evaporated InN grown at different substrate temperature ranged between 50 °C to 180 °C was studied. The apparent band gap was found to be 1.40-1.50 eV by absorption measurements.

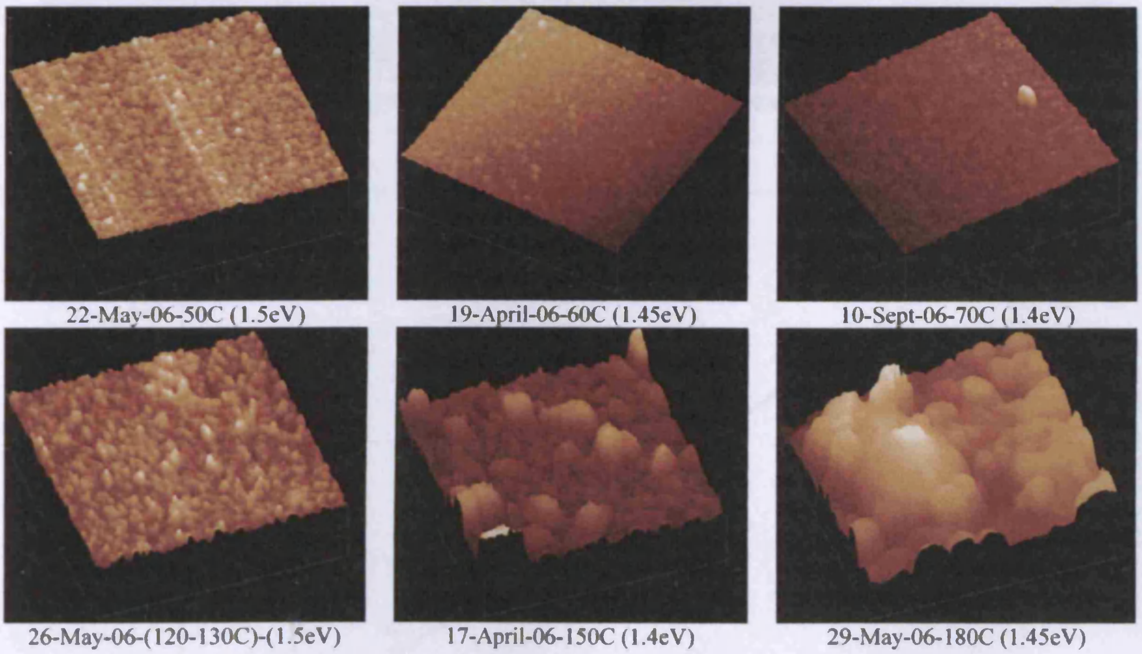
22-May-06-50C (1.5eV)

19-April-06-60C (1.45eV)

10-Sept-06-70C (1.4eV)

26-May-06-(120-130C)-(1.5eV)

17-April-06-150C (1.4eV)

29-May-06-180C (1.45eV)

Figure 4.24: AFM picture for InN sample grown by reactive evaporation

Figure 4.24 shows the tapping-mode AFM images of InN thin film grown on glass. The AFM morphologies show the formation of nano-crystalline particle structure. High temperature growth was found to be very effective to enhance grain growth. SEM pictures shows that grain size is higher than 30 nm which would eliminate the quantum size effect on the properties of the reactively grown films.

The root mean square (rms) roughness of the grown indium nitride was measured and plotted against the substrate temperature to address the effect of the substrate temperature on the surface morphology of reactive evaporated InN. A clear correlation was found where the root mean square roughness increases as the substrate temperature is increased from 50 °C to 180 °C. Figure 4.26 shows the plot of the rms roughness as a function of the substrate temperature.

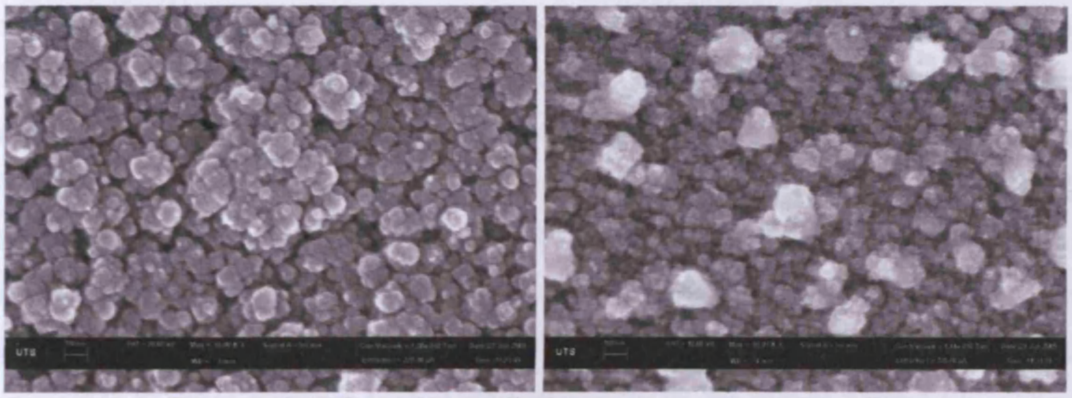

Figure 4.25: SEM picture for InN grown by reactive evaporation

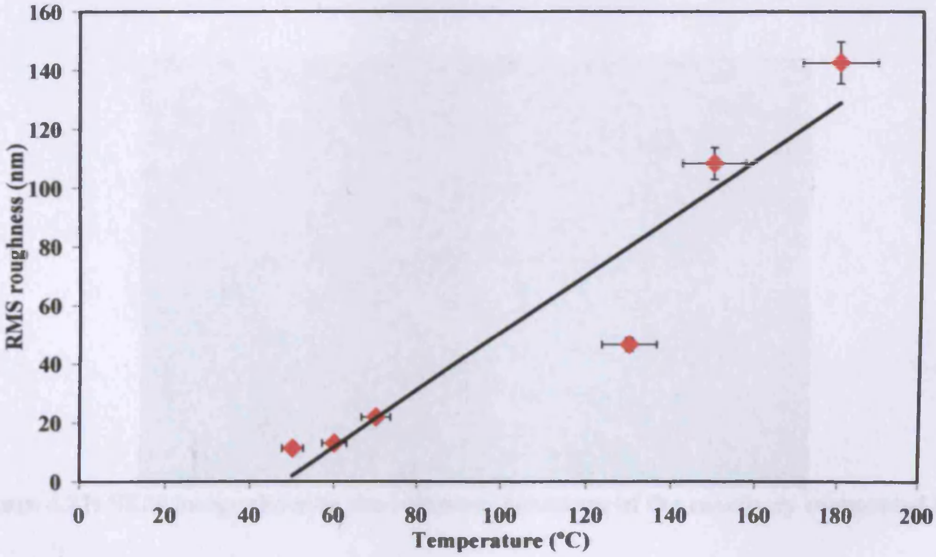

Figure 4.26: Plot of the rms roughness as a function of the substrate temperature

The rms roughness was found to increase from 11 nm for samples grown at substrate temperature of 50 °C to 143 nm for those grown at 180 °C. The lower surface roughness for the film grown at the lower substrate temperatures could be due to the small grain size. It may also be influenced by defects. The InN grown film showed a wurtzite polycrystalline structure with random orientation as confirmed by XRD discussed in section 4.2. The SEM image shown in figure 4.27 shows the columnar fibrous structure that InN grown by reactive evaporation would take. This would explain the high roughness level found in the sample analysed.

Tansley & Foley [84] also observed rough surface morphology for their RF sputtered polycrystalline InN, while Guo et al. [25] reported an increase in the rms roughness as the growth temperature increased. A similar observation was also made by Koblmüller et al. [59] and Ive et al. [85]. Lu et al. [21] assumed that the rough surface at higher temperature should arise due to the dissociations in the InN films. However, XRD analysis and Hall Effect measurements showed significant improvement on both electrical and structural quality of the reactive evaporated films. Furthermore, XRD confirmed the decrease in the FWHM of the InN (0002) diffraction peak, consequently improving the quality of the films. The appearance and increase in intensity of other diffraction peaks showing the polycrystalline structure, showing no preferred orientation, was also confirmed by XRD analysis. This emergence of other peaks at higher intensities may be the reason behind the increase in the surface roughness.

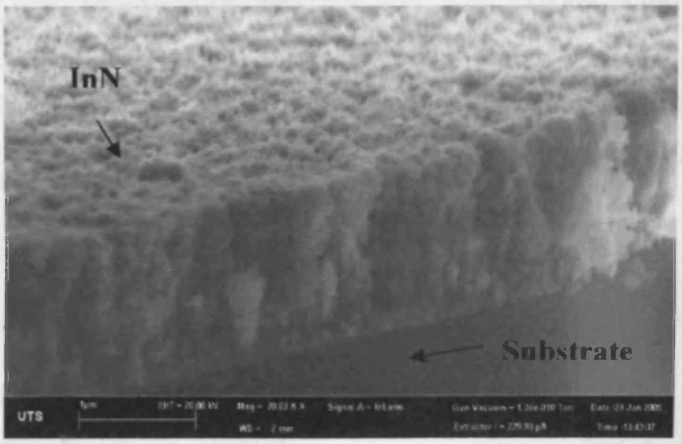

Figure 4.27: SEM image showing the columnar structure of the reactively evaporated InN

References

[1] http://www.mee-inc.com/sem.html

[2] D.B Holt, D.C. Joy, SEM Microcharacterization of Semiconductors, Academic Press Ltd, 1989, p5

[3] D.B Holt, D.C. Joy, SEM Microcharacterization of Semiconductors, Academic Press Ltd, 1989, p7

[4] D.K. Shroder, Semiconductor Material and Device Characterization, John Wiley & Sons, Inc., 1990, p513

[5] http://cmm.mrl.uiuc.edu/techniques/xray.htm

[6] H.P. Klug, L.E. Alexander, X-ray Diffraction Procedures for Polycrystalline and Amorphous Materials, Second Edition, Wiley-Interscince Publication 1974, p.120

[7] N.W. Achcroft, I. Mermin, Solid State Physics, International edition, Saunders College, 1976, p 96

[8] B.D. Cullity, Elements of X-ray Diffraction, Second Edition, Addison-Wesley Publishing Company, Inc., 1978, p 84

[9] Phillips X'pert Philips PW1710 diffractometer manual book

[10] W. Paskzkowicz, Powder Diffraction 14 (4) (1999) 258.

[11] W. Paskzkowicz, R. Černý and S. Krukowski, Powder Diffraction 18 (2) (2003) 114.

[12] Motlan, E.M. Goldys and T.L. Tansley, J. Cryst. Growth, 241 (2002), 165-170.

[13] S.J. Patil, D.S. Bodas, A.B. Mandale and S.A. Gangal, Thin Solid films 444 (2003), 52-57.

[14] N. Asai, Y. Inoue, H. Sugimura and O. Takai, Thin Solid Films 332 (1998), 267-271.

[15] J. Hovel and J. J. Cuomo, Appl. Phys. Lett. 20, 71 (1972).

[16] J. W. Trainor and K. Rose, J. Electron. Mater. 3, 821 (1974).

[17] B.R. Natarajan, A.H. Eltouky, J.E. Greene, Thin Soilid Films, 69, (1980), 201

[18] T. L. Tansley and C. P. Foley, Electron. Lett. 20, 1066 (1984).

[19] K.L. Westra, R.P.W. Lawson and M.J. Brett, J. Vac. Sci. Technol. A, 6, (1988), 1730.

[20] B.T. Sullivan, R.R. Parsons, K.L. Westra and M.J. Brett, J. Appl. Phys. 64 (8), (1988) 4144.

[21] H. Lu, W.J. Schaff, J. Hwang, H. Wu, W. Yeo, A. Pharkya and L.F. Eastman, Appl. Phys. Lett. Vol.77, No.16, (2000), 2548.

[22] J.-S. Hwang, C.-H. Lee, F.-H. Yang, K.-H. Chen, L.-G. Hwa, Y.-J. Yang, and L.-C. Chen, Mat. Chem. Phys. 72 (2001) 290-295.

[23] X. Wang, S-B. Che, Y. Ishitani and A. Yoshikawa, J. Appl. Phys. 99, 073512 (2006).

[24] Q. Guo, N. Shingai, M. Nishio, H. Ogawa, J. Cryst. Growth 189/190 (1998) 466-470.

[25] Q. Guo, K. Murata, M. Nishio and H. Ogawa, Appl. Surf. Sci. 169-170 (2001) 340-344.

[26] Q. Guo, M. Nishio, H. Ogawa and A. Yoshida, Jpn J. Appl. Phys. Vol.38 (1999) Pt.2, No. 5A, L490.

[27] K.M. Yu, Z. Liliental-Weber, W. Walukiewicz, W. Shan, J.W. Ager III, S.X. Li, R.E. Jones, E.E. Haller, H. Lu, and W.J. Schaff, Appl. Phys. Lett., 86, 071910, (2005).

[28] T. Matsouka, H. Okamoto and M. Nakao, Phys. Stat. Sol. (c) 0, No.7, 2806-2809 (2003).

[29] B.D. Cullity, Elements of X-ray Diffraction, Second Edition, Addison-Wesley Publishing Company, Inc., 1978, p 284

[30] P.P-T. Chen, K.S.A. Butcher, M. Wintrebert-Fouquet, R. Wuhrer, M. R. Phillips, K.E. Prince, H. Timmers, S.K. Shrestha and B.F. Usher, J. Cryst. Growth 288 (2006) 241-246.

[31] B.D. Cullity, Elements of X-ray Diffraction, Second Edition, Addison-Wesley Publishing Company, Inc., 1978, p 501

[32] X.H. Ji, S.P. Lau, H.Y. Yang, and Q.Y. Zhang, Thin Solid Films 515 (2007) 4619-4623.

[33] A. Yamamoto, T. Tanaka, A. G. Bhuiyan, K. Sugita, K. Kasashima, Y. Kimura, A. Hashimoto, and V. Yu. Davydov, 5th International Conference on Nitride Semiconductors (ICNS-5), Nara, Japan, May 25–30, 2003.

[34] S. Kumar, L. Mo, Motlan, and T.L. Tansley, Jpn. J. Appl. Phys. Vol.35, pt.1, No.4A, (1996), 2261-2265.

[35] E. Kurimoto, M. Hangyo, H. Harima, , M. Yoshimoto, T. Yamaguchi, T. Araki, Y. Nanishi, and K. Kisoda, Appl. Phys. Lett. Vol.84, No. 2, 212, (2004).

[36] Motlan, E.M. Goldys and T.L. Tansley, Thin Solid Films, 422 (2002), 28-32.

[37] M. Yoshimoto, Y. Yamamoto, W. Huang, H. Harima, J. Saraie, A. Chayahara, and Y. Horina, Appl. Phys. Lett., Vol. 83, No.17, 3480 (2003).

[38] M. Wintrebert-Fouquet, K.S.A. Butcher and Motlan, Phys. Stat. Sol. (c) 0, N0.7, 2785-2789 (2003).

[39] K.S.A. Butcher, M. Wintrebert-Fouquet, P.P-T Chen, T.L. Tansley, H. Dou, S.K. Shrestha, H. Timmers, M. Kuball, K.E. Prince and J.E. Bradby, J. Appl. Phys. Vol.95, No.11 (2004) 6124.

[40] K.S.A. Butcher, InN, a Historic review- from obscurity to controversy, in: Q. Guo (Ed), Advanced Material in Electronics, Research Signpost, 2004, p.1 , and references within.

[41] K.S.A. Butcher and T.L. Tansley, Superlattices Microstrcut. 38, 1, (2005) and reference within.

[42] K.S.A. Butcher, M. Wintrebert-Fouquet, P.P-T. Chen, K.E. Prince, H. Timmers, S.K. Shrestha, T.V. Shubina, S.V. Ivanov, R. Wuhrer, M.R. Phillips, and B. Monemar, Phys. Stat. Sol. (c) 2, No.7, 2263-2266 (2005).

[43] P. Specht, R. Armitage, J. Ho, E. Gunawan, Q. Yang, X. Xu, C. Kisielowski, E.R. Weber, J. Cryst. Growth 269 (2004) 111-118.

[44] K.S.A. Butcher, A.J. Fernandes, P.P-T. Chen, M. Wintrebert-Fouquet, H. Timmers, S.K. Shrestha, H. Hirshy, R.M. Perks, and B. F. Usher, J. Appl. Phys., 101, 123702, (2007).

[45] S. Yamaguchi, M. Kariya, S. Nitta, T. Takeuchi, C. Wetzel, H. Amano and I. Akasaki, J. Appl. Phys. Vol.85, No.11, (1999) 7682.

[46] I.J. Lee, J.W. Kim, T.-B. Hur, Y.-H. Hwang, and H.-K. Kim, Appl. Phys. Lett. Vol.81, No.3, (2002) 475.

[47] I.J. Lee, J.W. Kim, T.-B. Hur, Y.-H. Hwang, and H.-K. Kim, Appl. Phys. Lett. Vol.92, No.10, (2002) 5814.

[48] V. Cimalla, Ch. Förster, G. Kittler, I. Cimalla, R. Kosiba, G. Ecke, O. Ambacher, R. Goldhahn, S. Shokhovets, A. Georgakilas, H. Lu, and W. Schaff, Phys. Stat. Sol. (c) 0, No.7, 2818-2821 (2003).

[49] http://www.hkbu.edu.hk/~csar/xps.html

[50] D.K. Shroder, Semiconductor Material and Device Characterization, John Wiley & Sons, Inc., 1990, p554

[51] http://www.chem.qmul.ac.uk/surfaces/scc/scat5_3.htm

[52] Q. Guo, O.Kato, and A. Yoshida, J. Appl. Phys. 73, (11), 7969, (1993).

[53] X.D. Pu, J. Chen, W.Z. Shen, H. Ogawa and Q.X. Guo, J. Appl. Phys., 98, 033527 (2005).

[54] A. Wakahara and A. Yoshida, Appl. Phys. Lett. 54, 709 (1989).

[55] H. Shinoda and N. Matsukura, Diamond and related Materials 11 (2002), 896-900.

[56] J. A.Schreifels, J. E. Deffeyes, L. D. Neff and J. M. White, J. Electron Spectrosc. Relat. Phenom. 25, 191 (1982).

[57] T. L. Barr, Modern ESCA - The Principles and Practice of X-ray Photoelectron Spectroscopy (CRC Press, 1994).

[58] O. Takai, K. Ikuta and Y. Inoue, Thin Solid Films 318 (1998), 148-150.

[59] G. Koblmüller, C.S. Gallinat, S. Bernardis, J.S. Speck, G.D. Chern, E.D. Readinger, H. Shen and M. Wraback, Appl. Phys. Lett. 89, 071902 (2006).

[60] B.R. Ng, J. Cryst. Growth 269 (2004) 35-40.

[61] V.W. Chin, T.L. Tansley, and T. Osotchan J. Appl. Phys. 75 (11) (1994) 7365.

[62] H. Lu, William J. Schaff, Lester F. Eastman and C. E. Stutz, Appl. Phys. Lett. 82 (2003) 1736.

[63] I. Mahboob, T. D. Veal, C. F. McConville, H. Lu and W. J. Schaff, Phys. Rev. Lett. 92 (2004) 036804-1.

[64] I. Mahboob, T. D. Veal, L. F. J. Piper, C. F. McConville, Hai Lu, W. J. Schaff, J. Furthmuller and F. Bechstedt, Physical Review B, 69 (2004) 201307-1.

[65] V. Cimalla, G. Ecke, M. Niebelschütz, O. Ambacher, R. Goldhahn, H. Lu, and W.J. Schaff, Phys. Stat. Sol. C 2 (2005) 2254.

[66] V. Cimalla, M. Niebelschütz, G. Ecke, V. Lebedev, O. Ambacher, M. Himmerlich, S. Krischok, J. A. Schaefer, H. Lu, and W. J. Schaff, Phys. Stat. Sol. A 203 (2006) 59.

[67] http://www.ansto.gov.au/enviroment/capabilities_and_facilities

[68] Y. Gao, Surf. Interface Anal. **14**, 552 (1989).

[68] C. Stampfl, C.G. Van de Walle, D. Vogel, P. Kruger, and J. Pollmann, Phys. Rev. B 61, R7846 (2000).

[69] C.G. Van de Walle, Phys. Status Solidi B 235, 89 (2003).

[70] E.A. Davis, S.F.J. Cox, R.L. Lichti, C.G. Van de Walle, Appl. Phys. Lett.

Vol.82, No.4, 592, (2003).

[71] Y. Saito, N. Teraguchi, A. Suzuki, T. Araki and Y. Nanishi, Jpn. J. App. Phys. Vol.40 (2001), Pt.2, No.2A, L91-L93.

[72] C.S. Gallinat, G. Koblmüller, J.S. Brown, S. Bernardis, J.S. Speck, G.D. Chern, E.D. Readinger, H. Shen and M. Wraback, Appl. Phys. Lett 89, 032109 (2006).

[73] V.Yu. DAvydov, A.A. Klochikhin, R.P. Seisyan, V.V. Emtsev, S.V. Ivanov, F. Bechstedt, J. Furthmüller, H. Harima, A.V. Mudryi, J. Aderhold, O. Semchinova and J. Graul, Phys. Stat. Sol. (b) 229, No.3, R1-R3 (2002).

[74] J. Wu, W. Walukiewicz, S.X. Li, R. Armitage, J.C. Ho, E.R. Weber, E.E. Haller, H. Lu, W.J. Schaff, A. BArcz, and R. Jakiela, Appl. Phys. Lett. Vol.84, No.15, (2004) 2805.

[75] J.C. Ho, P. Specht, Q. Yang, X. Xu, D. Hao, and E.R. Weber, J. Appl. Phys. 98, 093712 (2005).

[76] K.S. Bridi, Scanning Probe Microscope, Applications in Science and Technology, CRC Press LLC, USA, 2003, p 17.

[77] http://www.tech-faq.com/atomic-force-microscope.shtml.

[78] http://www.che.utoledo.edunadarajahwebpageswhatsafm.html.

[79] http://en.wikipedia.org/wiki/Atomic_force_microscope

[80] R. Howland, L. Benatar, A Practical Guide to Scanning Probe Microscopy, First Edition, ThermoMicroscopes, 2000, p.6

[81] http://spm.phy.bris.ac.uk/techniques/AFM.

[82] http://www.ifm.liu.se/surfphys/laminate/common/Documents/AFMroberto.pdf .

[83] C.P. Foley, T.L. Tansley, Appl. Surf. Sci. 22/23 (1985) 663.

[84] T. Ive, O. Brandt, M. Ramsteiner, M. Giehler, H. Kostial, and K.H. Ploog, Appl. Phys. Lett. Vol.84, No.10, (2004) 1671.

Chapter 5

Optical and electrical properties of indium nitride

5.1. Optical Measurements

5.1.1. Theory

Optical measurement is considered a common method used for determining the band structure of a semiconductor. Photon-induced electronic transitions can occur between different bands, which lead to the determination of the energy band gap; also within a single band, the free-carrier absorption. The optical transmission spectrum of a semiconductor is affected by the band gap energy of the material. The cut-off point in the transmission spectrum is determined by the band gap of the material due to the absorption by the crystal; the absorption that occurs with electron transition from the valence band to the conduction band defines the energy band gap.

In this work, optical measurements were performed to determine the band gap and the refractive index of the reactively evaporated InN grown on c-plane sapphire and borosilicate glass substrates. Qualitative information about the carrier concentration and the thickness of the material can also be deduced from the information extracted from the transmission spectra.

5.1.1.1. Transmission

Consider a beam of monochromatic light, the transmission coefficient is defined by the ratio of the transmitted to the incident intensity and it can be expressed as [1]:

$$T = \frac{I_{sample}}{I_{incident}} \qquad \textit{(Equation 5.1)}$$

For a sample with a thickness x, an absorption coefficient α, and a reflectivity R, at normal incident, the transmission coefficient T can be expressed as [1]:

$$T = \frac{(1-R)^2 \exp(-\alpha x)}{1-R^2 \exp(-2\alpha x)} \qquad \text{(\textit{Equation 5.2})}$$

Combining equation (5.1) and (5.2), and neglecting the effect of reflection, the transmitted intensity through the sample as a function of the thickness is as follows:

$$I_{sample}(x) = I_{incident} \exp(-\alpha x) \qquad \text{(\textit{Equation 5.3})}$$

5.1.1.2. Absorption

Near the absorption edge the absorption coefficient can be expressed as [2]:

$$\alpha \approx (h\upsilon - E_g)^{\gamma} \qquad \text{(\textit{Equation 5.4})}$$

where $h\nu$ is the photon energy, E_g is the band gap of the material, and γ is a constant depending on the nature of the electronic transition responsible for the absorption. The constant γ equals to 1/2 or 3/2 for allowed direct transition and forbidden direct transitions, respectively. On the other hand, γ equals to 2 for indirect transitions.

With indium nitride (InN) having only direct allowed transitions, which means a direct band gap [3], the absorption coefficient (α) for direct allowed transition near the absorption edge can only follow the expression:

$$\alpha \approx (h\upsilon - E_g)^{1/2} \qquad \text{(\textit{Equation 5.5})}$$

Combining equation (5.3) and (5.5) yields the following relationship:

$$\left(\ln\left|\frac{I_{incident}}{I_{sample}}\right|\right)^2 x^{-2} \propto (h\upsilon - E_g) \qquad \textit{(Equation 5.6)}$$

where $\left(\ln\left|\frac{I_{incident}}{I_{sample}}\right|\right)$ represents the optical density (OD).

5.1.1.3. Refractive index

Knowledge of the refractive index (n), dispersion and its variation with temperature, *(dn/dT)* is of fundamental importance in the design of heterostructure lasers and waveguiding devices [4]. Interference effects in the transmission spectrum can be used to determine the refractive index of the material analysed. Constructive interference will occur if the following condition is satisfied [5]:

$$x = \frac{(2m+1)\lambda}{2n} \qquad \textit{(Equation 5.7)}$$

where m is an integer, x thickness of the film, λ is the wavelength, and n is the refractive index. The transmitted radiation will go through maxima whenever equation (5.7) is satisfied. So, the refractive index can be determined based on equation (5.7) for two different maxima at two different wavelengths which will lead to the following relationship [5]:

$$n = \frac{1}{\left(\frac{1}{\lambda_2} - \frac{1}{\lambda_1}\right)x} \qquad \textit{(Equation 5.8)}$$

5.1.2. Experiment

A Cary 5E UV-Vis-NIR and a Jasco V-570 UV-Vis-NIR both double beam spectrophotometers were used for the optical measurements. A simplified schematic diagram can be seen in figure 5.1. All the transmission measurements were performed at room temperature. The spectral range of the measurements was from 174 nm to 3300 nm, for the Cary 5E system, and 190 nm to 2500 nm for the Jasco V-570 system. The light sources used were a deuterium lamp used in the UV region and a quartz halogen lamp used in the visible/NIR region. A monochromator was used to deliver the selected wavelength to the sample. The detectors used were a photomultiplier tube for the UV-Vis region and a lead sulphide detector for the NIR region.

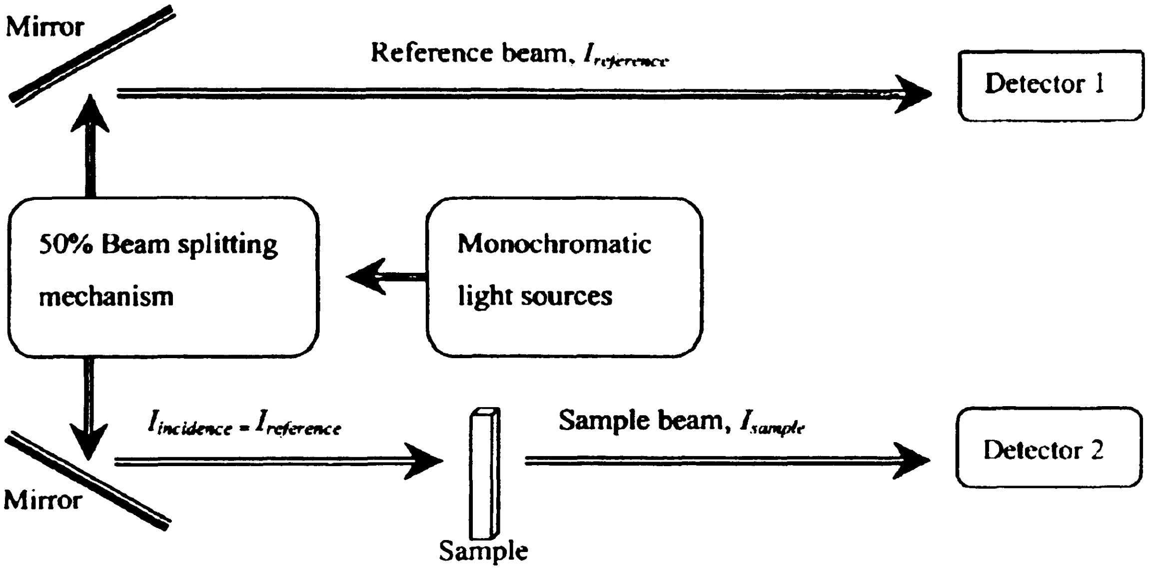

Figure 5.1: Simplified optical design of a double beam spectrophotometer.

In order to get accurate transmission spectra, baseline and zero corrections were performed before each sample was analysed. The zero correction was determined by blocking the path of the light to the sample and then measuring the background light. The baseline was determined by measuring the light transmission of a blank substrate as a function of wavelength. The relationship between the sample signal (*S*) and the corrected percentage transmission T_c is:

$$\%T_c = \left[\frac{(S)}{(Baseline)}\right] \times 100 \qquad (Equation\ 5.9)$$

Hence, the optical percentage transmission with the baseline correction will be:

$$\%T_c = \left[\frac{(I_{sample})}{I_{reference}(Baseline)}\right] \times 100 \qquad (Equation\ 5.10)$$

5.1.2.1. Band gap determination

A common approach was used to determine the band gap of the reactive evaporated InN. The absorption coefficient squared (α^2) was plotted against the photon energy to extract the band gap value. The band gap energy can be found by the x-intercept of the linear part on the α^2 profile (Figure 5.2). Another method was also used in this work; the optical density squared instead of the α^2 was plotted against the photon energy (equation (5.6) shows the relationship between the optical density squared (OD^2) and the α^2). From such a plot, the band gap value can be determined as well as a qualitative thickness analysis. Normally, what you would expect that a thicker sample would yield a steeper profile. Similarly, the x-intercept of the linear part of the OD^2 profile versus photon energy would give the band gap value of the InN thin film analysed.

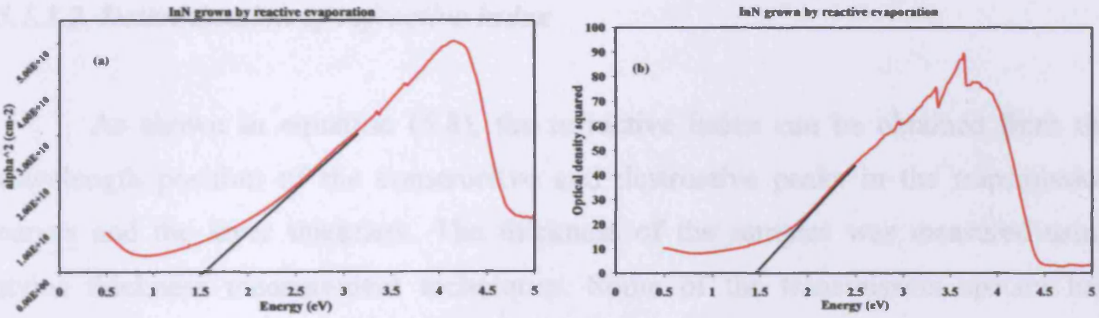

Figure 5.2: Absorption coefficient squared (α^2) and optical density squared against photon energy for reactively evaporated InN

5.1.3. Results and discussion

5.1.3.1. Transmission measurements

Figure 5.3 shows a series of transmission spectra for InN grown at different growth temperatures. One observation from the transmission spectra is the absence of free electron absorption at longer wavelengths (>2000 nm); this is indicative of a low carrier concentration material (less than or equal to $10^{19} cm^{-3}$). This is confirmed by Hall Effect measurements.

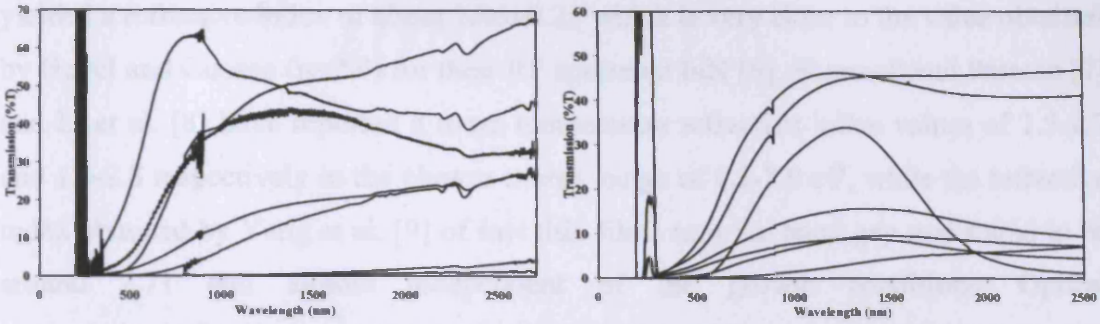

(a): InN grown at Macquarie University-Australia (b): InN grown at Cardiff University

Figure 5.3: Transmission spectra for reactively evaporated InN

The observation of different spectra in the transmission measurements means that these samples have many different properties such as: thickness, carrier concentration, band gap, and other structural properties. Investigation of some of these properties will be discussed in the following sections.

5.1.3.2. Determination of refractive index

As shown in equation (5.8), the refractive index can be obtained from the wavelength position of the constructive and destructive peaks in the transmission curves and the layer thickness. The thickness of the samples was measured using stylus thickness measurement techniques. Some of the transmission spectra had distinctive interference peaks that helped in the determination the refractive index of the reactively evaporated InN.

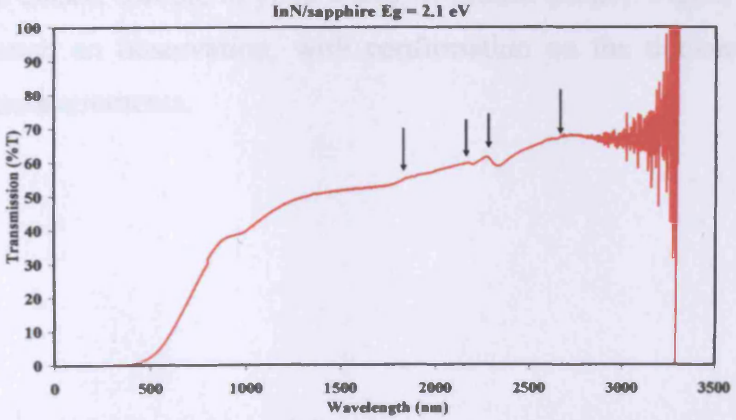

Figure 5.4: Transmission spectrum InN/sapphire with distinctive interference peaks

Applying equation (5.8) after extracting the wavelength positions of the constructive peaks from the transmission spectra obtained for InN (Figure 5.4), the calculations yielded a refractive index of about 2.86±0.25 which is very close to the value obtained by Hovel and Cuomo (n=2.9) for their RF sputtered InN [6]. Sharmell and Parman [7] and Li et al. [8] have reported a room temperature refractive index values of 2.5-2.7 and 1.6-2.8 respectively in the photon energy range of 1.5-3.0 eV, while the refractive index obtained by Yang et al. [9] of InN thin films near the band gap was found to be around 2.71 and almost independent of the growth conditions. Optical transmission/reflection measurements performed by Xu et al. showed that the InN layer had a refractive index of about 3.2-3.0 in the 2-3 μm wavelength region [10]. The slight difference in the refractive index compared to those reported could be due to the non-uniformity in the film.

5.1.3.3. Optical density

Equation (5.6) gives the relationship between the band gap of the material and what is called optical density (OD). The (OD^2) can be obtained from the transmission spectra and the band gap of the material can then be determined. The band gap energy can be found by the x-intercept of the linear part on an (OD^2) (slope) versus the photon energy. The value of the band gap can also be extracted from the absorption coefficient squared profile. However, the advantage of using the optical density square profile is that a qualitative comparison can be made on the thickness of the material which can be confirmed later using a Dektak thickness profiler. One would expect a thicker sample to yield a steeper profile (slope). Figure 5.5 gives clear indication of such an observation, with confirmation on the thickness comparison made by such measurements.

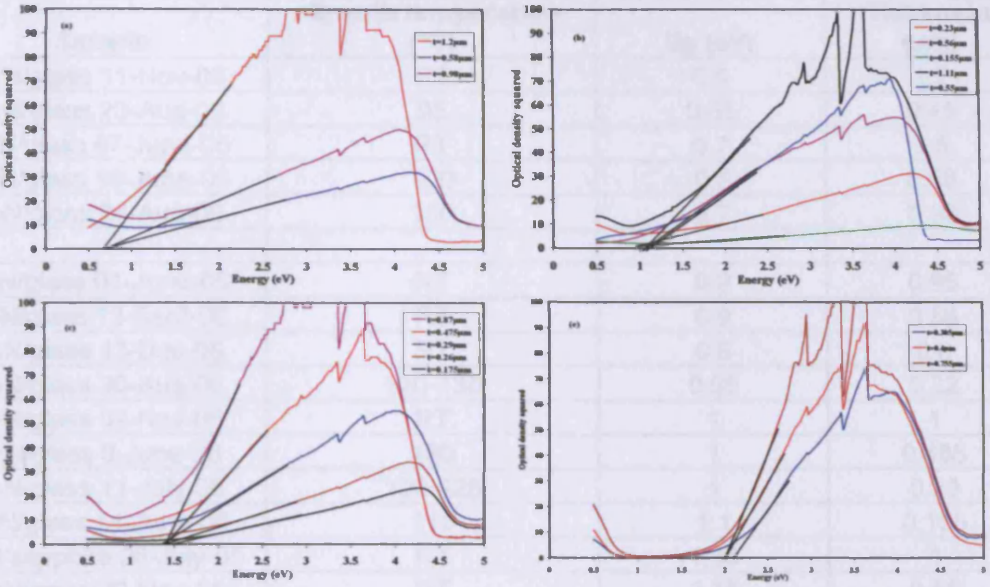

Figure 5.5: Optical density squared as a function of photon energy. (a) 0.6-0.7 eV, (b) 0.9-1.15 eV, (c) 1.4-1.5 eV and (d) 1.65-1.85 eV

5.1.3.4. Determination of Band gap

In this work, the band gap of InN was measured and an investigation of some of the reasons given behind the distinct value of the band gap has been carried out. Measurements of the optical absorption coefficient α (specifically α^2) were obtained as a function of photon energy. This is shown in figure 5.6 and indicates a spread in the measured band gap for different samples. The optical band gap was found to vary from sample to sample with values in the range 0.65eV to 2.15eV. Table 5.1 shows the band gap values along with the growth temperatures and film thicknesses.

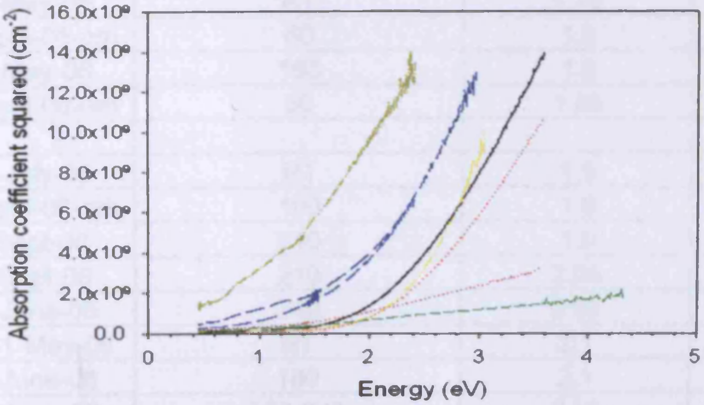

Figure 5.6: Absorption spectra for a range of different InN samples

Sample	Growth temperature (°C)	Eg (eV)	Thickness (um)
InN/glass 11-Nov-05	RT	0.6	1.2
InN/glass 23-Aug-06	95	0.65	0.45
InN/glass 07-June-05	RT	0.7	1.5
InN/glass 16-June-06	100	0.7	0.58
InN/glass 24-Aug-06	150	0.7	0.98
InN/glass 01-June-05	RT	0.9	0.95
InN/glass 13-Sept-06	RT	0.9	0.56
InN/glass 13-Dec-05	RT	0.9	0.5
InN/glass 30-Aug-06	120-130	0.95	0.32
InN/glass 09-Nov-05	RT	1	1
InN/glass 9-June-06	130	1	0.485
InN/glass 11-July-06	120-125	1	0.23
InN/glass 14-June-06	110	1.1	0.155
InN/sapphire 06-July-05	RT	1.15	1
InN/glass 22-Nov-05	RT	1.15	0.55
InN/glass 22-Aug-06	100	1.15	1.11
InN/glass 10-Sept-06	70	1.4	0.29
InN/glass 17-April-06	150	1.4	0.87
InN/glass 29-May-06-am	175-180	1.4	0.51
InN/glass 10-May-06	RT	1.45	0.56
InN/glass 19-April-06	60	1.45	0.475
InN/glass 29-May-06-pm	180	1.45	0.325
InN/sapphire 21-June-05	RT	1.5	0.82
InN/glass 22-May-06	50	1.5	0.175
InN/glass 26-May-06	120-130	1.5	0.26
InN/glass 25-Sept-06	90	1.6	0.99
InN/sapphire 07-July-05	RT	1.65	1.2
InN/glass 21-Nov-05	RT	1.65	0.8
InN/glass 24-April-06	90	1.65	0.19
InN/glass 31-May-06	150	1.7	0.45
InN/glass 27-Sept-06	170	1.7	0.85
InN/glass 14-Dec-05	RT	1.75	0.58
InN/glass 05-May-06	RT	1.75	0.53
InN/glass 25-April-06-pm	60	1.8	1.08
InN/glass 30-May-06	160	1.8	0.25
InN/glass 25-April-06-am	60	1.85	1.31
InN/glass 07-July-05	RT	1.9	0.36
InN/glass 19-April-06-am	100	1.9	1.43
InN/glass 8-Sept-06	210	1.9	0.36
InN/glass17-Sept-06	210	2.05	0.755
InN/glass 12-June-06	240	2.05	0.407
InN/sapphire 31-May-05	RT	2.1	0.6
InN/glass 26-June-06	180	2.1	0.535
InN/glass 11-June-06	230-240	2.15	0.305

Table 5.1: Band gap values for InN grown by reactive evaporation

As mentioned before, there has been much speculation on the main reason behind the observation of huge variations in the band gap value. In this section, some of these theories will be discussed. The observation of different band gap values for InN grown by the same growth technique and characterized under the same conditions will help give a clear understanding of some of the properties of the material in a hope to solve the mystery of InN.

5.1.3.5. Mie resonance effect

The variation in band gap for reactively evaporated InN (as shown in figure 5.6) was found to have a dependence on the distance between the evaporation source and the substrate. Lower or higher band gaps were obtained when the substrate was respectively positioned closer to, or further from the evaporation source. This is presumed to be dependent on the amount of indium (In) that is incorporated in the growth. From the XRD data, the density of In-clusters was qualitatively determined by the calculation of the ratio of the intensity of InN(002) diffraction to In(101) or In(110) diffraction peaks. It was observed that the absorption edge decreased with the amount of indium clustering in the film. This is clearly seen in figure 5.7. Such an observation can be explained in terms of what is known as Mie resonance. This phenomenon (Mie resonance) arises from the interaction of an incident electromagnetic wave with multipolar excitations of electrons in metallic clusters [13]. It was also found that InN grown by reactive evaporation at temperatures higher than 150 °C showed an absorption edge higher than 1.5 eV and no presence of In-segregates was detected in the XRD measurements. Shubina et al. investigated the effect of Mie resonance on the band gap of InN [13]. They observed a decrease in the absorption edge with presence of In-clusters in the film. An absorption edge of 1.4 eV was suggested for film without such clusters. Furthermore, Ho et al. observed a red-shift in the PL peak energy with increasing excess indium [14]. All these observations would confirm the role of Mie resonance effect on the determination of the "true" value of the InN band gap. However, this Mie effect cann not be singled out to be the only reason to describe the wide range obtained for the band gap.

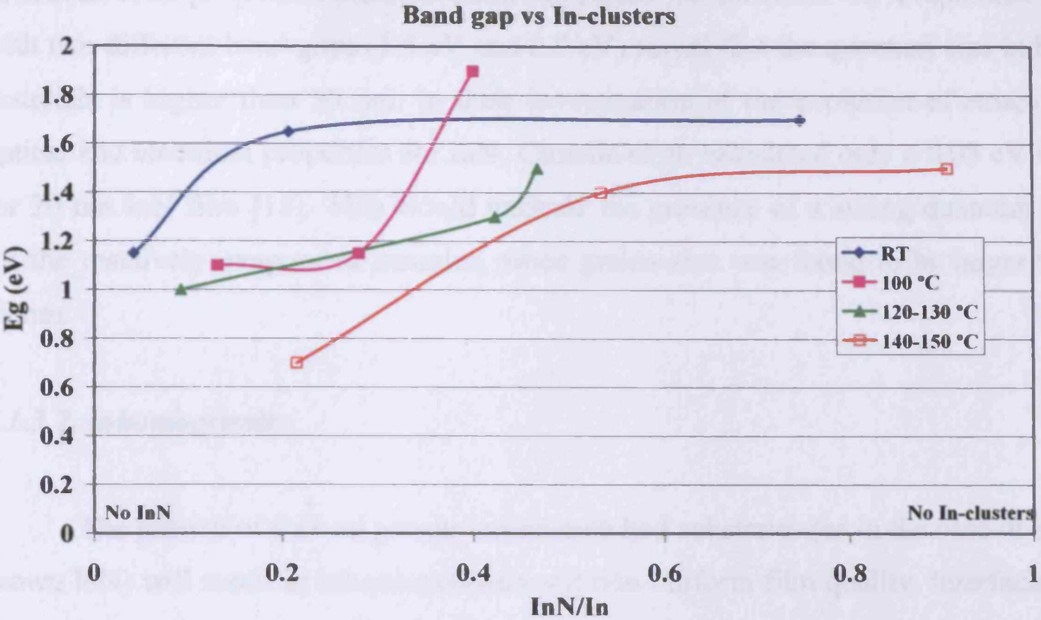

Figure 5.7: Apparent band gap as a function of In-quantity in the InN material

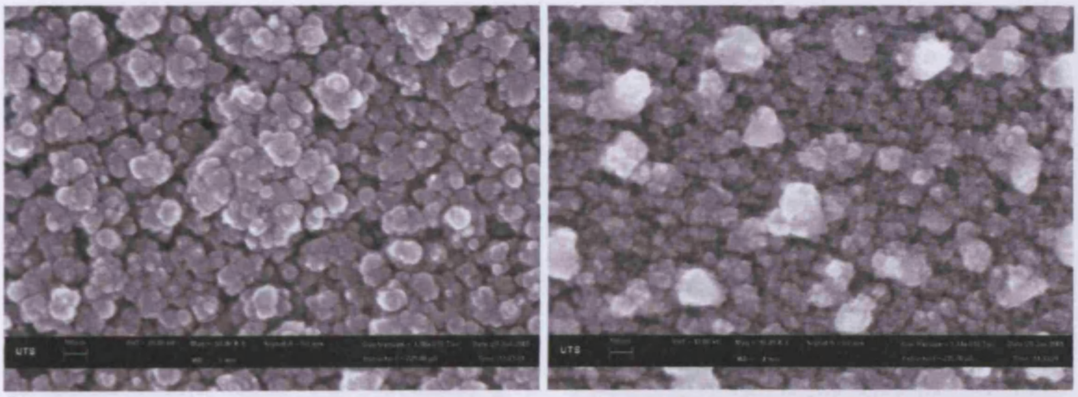

(a) InN/sapphire 21-June-05 E_g=1.5 eV (b) InN/glass 01-june-05 E_g=0.9 eV

Figure 5.8: SEM picture for InN grown by reactive evaporation

5.1.3.6.. Quantum size effect

Since most, but not all, of the polycrystalline InN showed high band gap, quantum size effect was considered as one of the reason for this observation. Davydov et al. suggested that a reason for the observation of E_g higher than 0.9 eV could be the spontaneous formation of needle-like nano-crystals during heteroepitaxial growth of InN, which is accompanied by a blue shift of the absorption edge due to quantum-size effects [15]. However, there have been reports on polycrystalline InN showing lower band gap. Anderson et al. observed strong PL for polycrystalline InN at ~0.8 eV [16]. Similarly, PL at ~ 0.85 eV was observed from polycrystalline RPE-CVD grown InN by Kuball et al. [17]. SEM pictures, shown in figure 5.8, for reactively evaporated InN with two different band gaps (1.5 eV and 0.9 eV) reveal that the quantum size in both materials is higher than 50 nm. In their investigation of the evolution of structural, optical and electrical properties for InN, Cimalla et al. calculated only a 0.03 eV shift for 20 nm InN film [18]. This would exclude the presence of a strong quantum size for the reactively evaporated samples, since grains size was found to be larger than 50 nm.

5.1.3.7. Inhomogeneity

The growth of InN on poorly lattice-matched substrates (as in the case of most grown InN) will result in inhomogeneous and non-uniform film quality. Interfacial or nucleation layers form a region near substrate which is poly-crystalline; as the film thickens, the material begins to coalesce. These features can be seen in figure 5.9 below that shows a cross section of InN grown by RPE CVD and reactive evaporation.

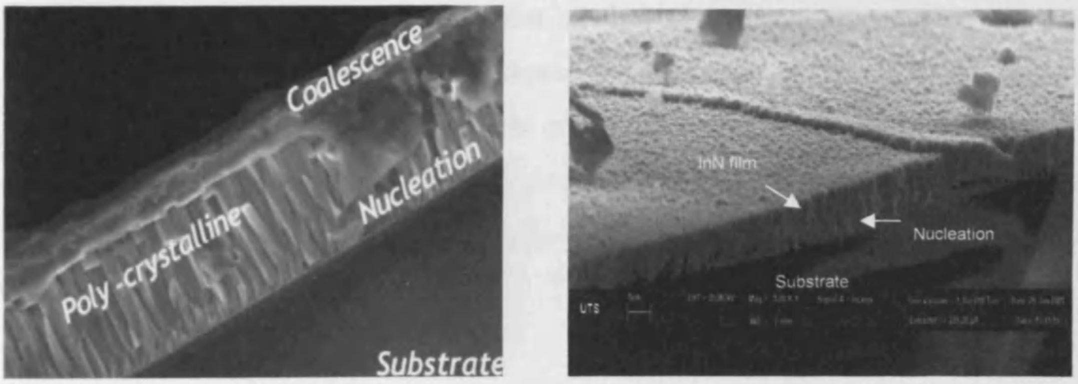

(a) InN/sapphire grown by RPE-CVD (b) InN/sapphire grown by reactive evaporation

Figure 5.9: SEM picture for InN grown by RPE-CVD and reactive evaporation

Swartz et al. also pointed out the non-uniformity and inhomogeneity of InN film with depth [19]. They believed that the InN layers are inhomogeneous with thickness in the growth direction. Alexandrov et al. suggested that sample inhomogeneity offers a possible explanation of the presence of a large difference in the reported values for InN [20]. They found that the low energy features arise as growth artefacts due to the formation of alloys at the interface of InN with sapphire substrates or with AlN or GaN buffer layers. It was concluded that the presence of interfacial layers may play an important role in determining the absorption and photoluminescence properties of InN. A simplified model for inhomogeneous material growth can be illustrated as shown in figure 5.10. Standard absorption measurements ‘see’ a convoluted apparent band gap, with defect density decreasing away from the substrate. The influence of the Moss-Burstein shift described by the variation in Ef due to the reduction in defect carriers as thickness increases; assuming the band gap energy E_g is constant.

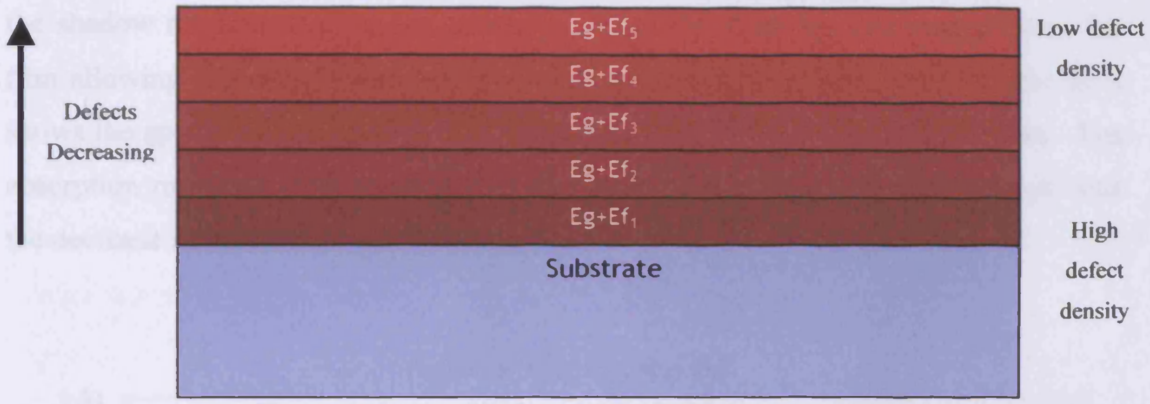

Figure 5.10: Simplified model for InN inhomogeneity

This experiment will illustrate the presence of inhomogeneity and its effect from both the electrical and optical properties point of view. A measurement system that allows highly localised optical absorption measurements was set up. InN samples were placed on a moveable x-y-z micrometer stage, in between a white light source and a small diameter (<50mm) glass fibre. This fibre was coupled to a spectrometer where the optical absorption of the material could be measured. The system used in this experiment is shown in figure 5.11.

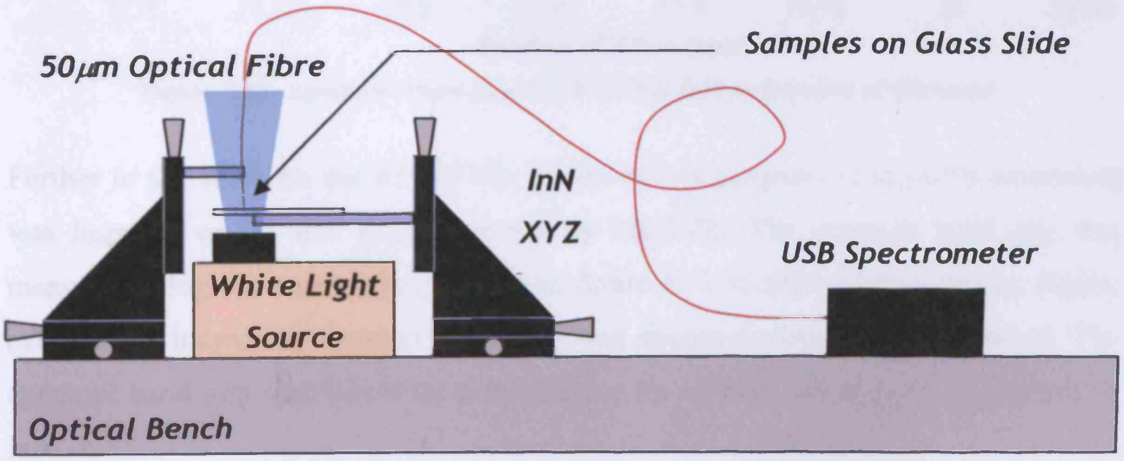

Figure 5.11: Absorption measurement system

The experiment was conducted on InN grown by three different groups:

1- RPE-CVD InN grown at Macquarie University, Australia [21].
2- MOVPE InN grown at Montpellier University, France [22]
3- Reactively evaporated InN grown at Cardiff University (this work).

The RPE-CVD material showed a graded material thickness over a distance of around a millimetre near the edge of the sample. This difference in thickness was a result of the shadow masking during the growth process. The fibre tip was scanned over the film allowing the measurement of the band gap at different thicknesses. Figure 5.12 shows the apparent band gap ($E_g + E_f$) as a function of the position of the fibre. The absorption measurements showed that the apparent band gap of InN increased with the decrease in the thickness of the sample.

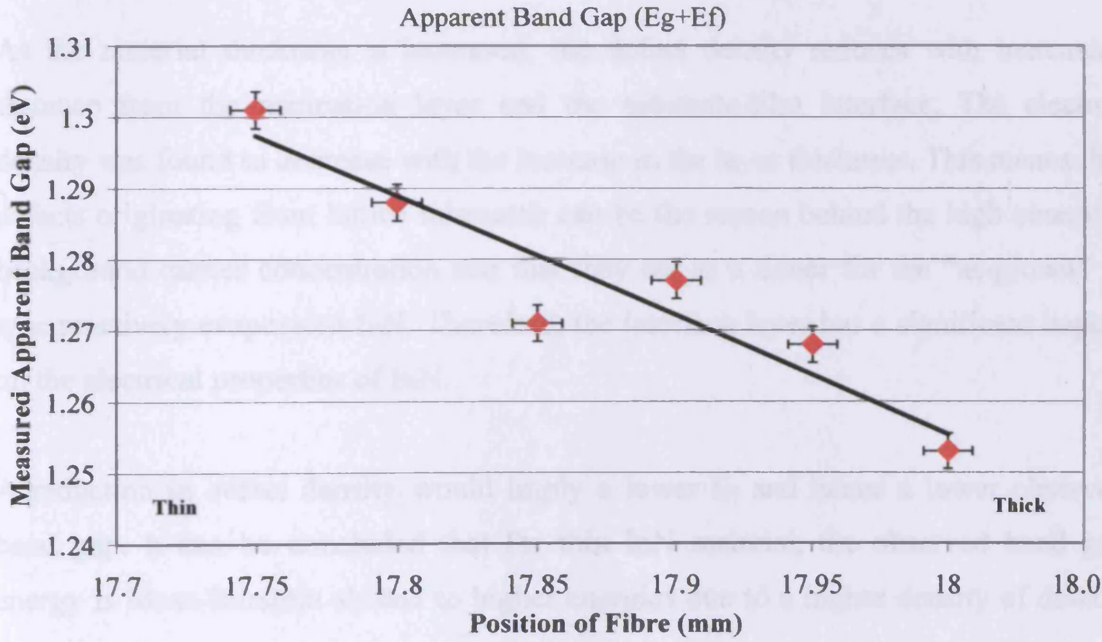

Figure 5.12: Apparent band gap of RPE-CVD InN as function of thickness

Further to the work on the RPE-CVD grown InN, a progressive dry etch processing was imposed on an InN sample grown by MOVPE. The apparent band gap was measured using the same system shown in figure 5.11 at different thicknesses. Again, evidence of increasing apparent band gap was shown as samples were thinned. The apparent band gap was found to be increasing by ~0.3eV per dry etch of ~80nm of InN.

A similar increase in the apparent band gap with the thickness of the film was also observed for reactively evaporated InN. From the optical measurements carried out on a UV-VIS-NIR spectrophotometer the band gap of InN was extracted from the plot of absorption coefficient squared as a function of the photon energy for different samples of InN grown by reactive evaporation. An increase in the band gap value was observed as the thickness of the samples decreased. This observation on different ranges of band gap values is represented in figure 5.13.

The similar observations made on InN grown by three different growth techniques can only be explained to be due to the inhomogeneity and non-uniformity of the grown InN. A high density of defects and the formation of an interface layer between the poorly lattice-matched substrate and the film could affect significantly on the film quality along the film thickness.

As the material thickness is increased, the defect density reduces with increasing distance from the nucleation layer and the substrate-film interface. The electron density was found to decrease with the increase in the layer thickness. This means that defects originating from lattice mismatch can be the reason behind the high observed background carrier concentration and that they act as a donor for the "as-grown" n-type reactively evaporated InN. Therefore, the interface layer has a significant impact on the electrical properties of InN.

A reduction in defect density would imply a lower E_f and hence a lower observed band gap. It can be concluded that for thin InN material, the observed band gap energy is Moss-Burstein shifted to higher energies due to a higher density of defect-related carriers.

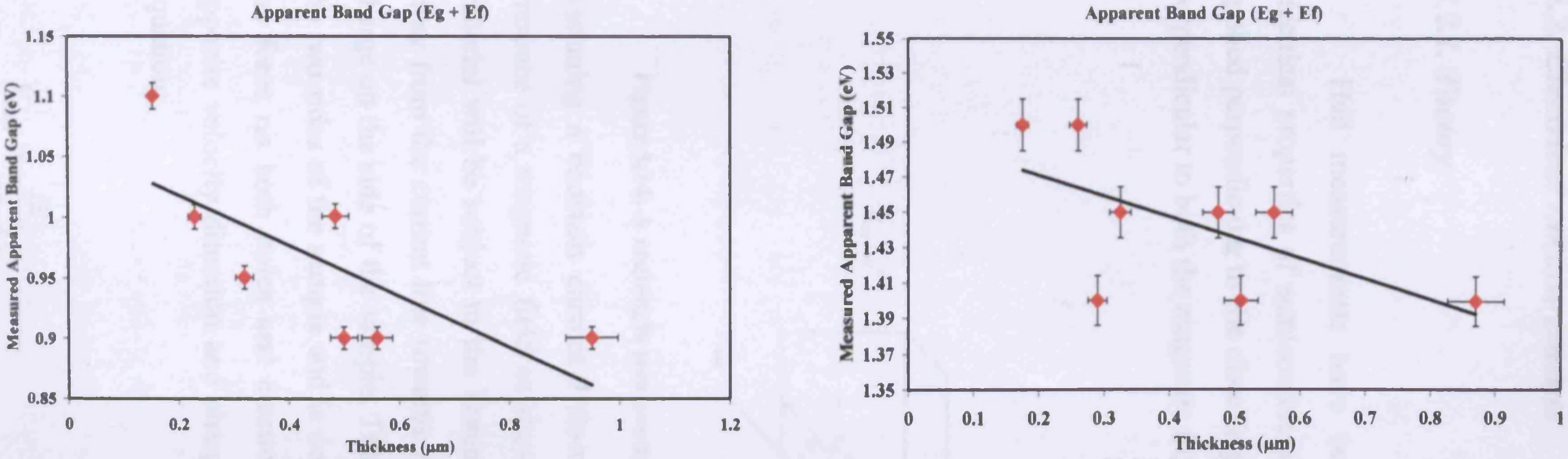

(a) 0.9-1.15 eV

(b) 1.4-1.5 eV

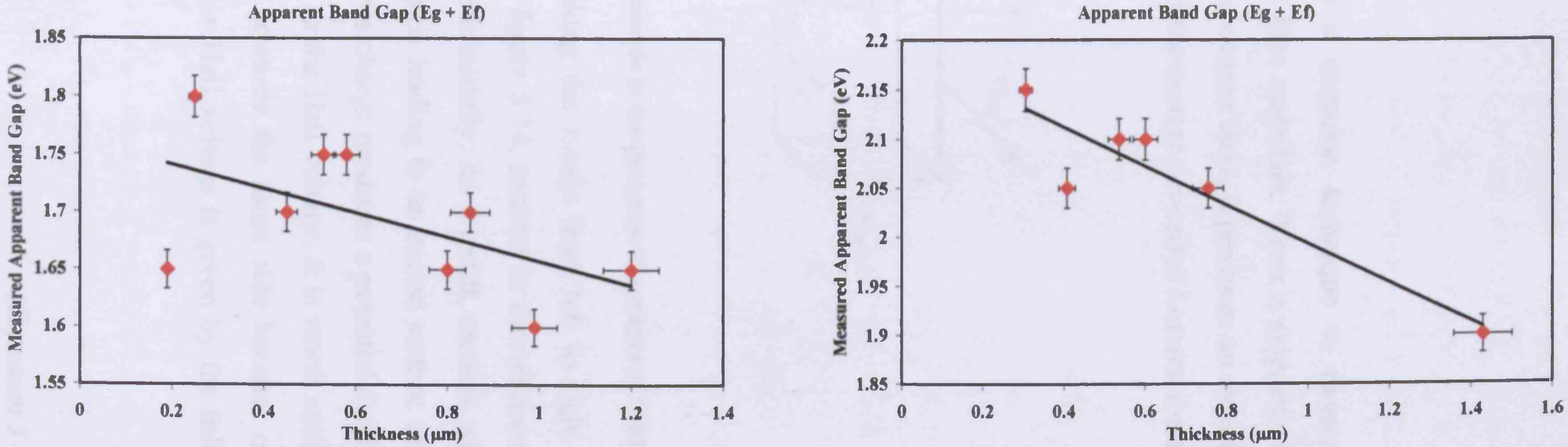

(c) 1.6-1.8 eV

(d) 1.9-2.15 eV

Figure 5.13: Apparent band gap of reactively evaporated InN as function of thickness

5.2. Electrical measurements

5.2.1. Theory

Hall measurements have become a common technique to measure the electrical properties of semiconductor thin film materials. When a magnetic field is applied perpendicular to the direction of the current flow, it produces an electric field perpendicular to both the magnetic field and the current (so-called Lorentz force).

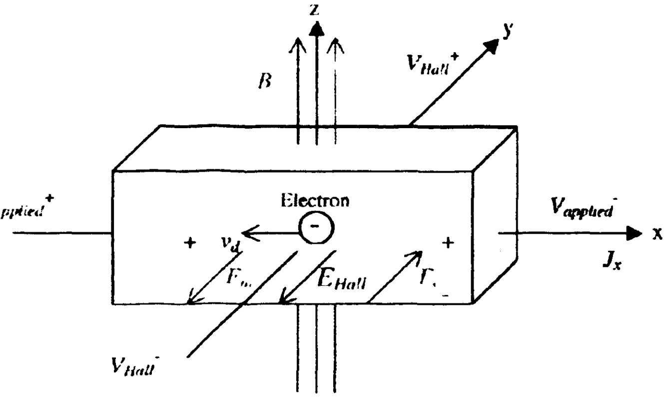

Figure 5.14: A rectangle semiconductor sample in the presence of a magnetic field

Assuming a constant current *I* flowing along the x-axis from left to right in the presence of a magnetic field as shown in figure 5.14, carriers in the semiconductor material will be subject to the Lorentz force initially. As a result, carriers will drift away from the current line towards the y-axis leading to an excess surface electrical charge on the side of the sample. This excess charge produces a potential drop across the two sides of the sample and is defined as the Hall voltage. It is worth noting that the force on both holes and electrons is towards the same side because of their opposite velocity direction and charge. This Hall voltage is given by the following equation:

$$V_{Hall} = \frac{IB}{qn_c d} \qquad \textit{(Equation 5.11)}$$

where I is the current, B the magnetic field, d sample thickness, q charge (1.6×10^{-19} C) and n_c the carrier density. The carrier density can be calculated from the measured Hall voltage, and the sign of the Hall voltage determines the nature of the carrier charges. The Hall voltage is negative for *n*-type semiconductors, and positive for *p*-type materials.

The Hall mobility, for a known resistivity ρ, is defined as:

$$\mu_H = \frac{1}{qn_c\rho} = \frac{d.|V_{Hall}|}{IB\rho} \qquad \textit{(Equation 5.12)}$$

In this work, the electrical properties of InN thin films were measured by a Hall Effect system based on the Van der Pauw method [23]. Van der Pauw showed how the specific resistivity and the Hall Effect of a flat sample of arbitrary shape can be measured without knowing the current pattern if the following conditions are met:

- The contacts are at the circumference of the sample.
- The contacts are sufficiently small.
- The sample is homogenous in thickness.
- The surface of the sample is singly connected, i.e. the sample does not have isolated holes.

For simplicity, consider a flat square of conducting material with four successive metallic contacts *a*, *b*, *c*, and *d* on each corner as shown in figure 5.15. The notation $R_{bd,ac}$ defined by Van der Pauw represents the resistance related to the potential difference between contacts *a* and *c* per unit current through the contacts *b* and *d*. The Hall mobility can be determined by measuring the change in resistance $R_{bd,ac}$ when a magnetic field is applied normal to the sample. The resistivity and the Hall mobility of the material are defined by Van der Pauw as follows:

$$\rho = \frac{\pi d}{\ln 2}\frac{(R_{ab,cd} + R_{bc,da})}{2}F \qquad \text{(Equation 5.13)}$$

where F is a function of the ratio $\frac{R_{ab,cd}}{R_{bc,da}}$

$$\mu = \frac{d}{B}\frac{\Delta R_{bd,ac}}{\rho} \qquad \text{(Equation 5.14)}$$

with d is the thickness of the sample, B is the magnetic field, and $\Delta R_{bd,ac}$ the change of the resistance $R_{bd,ac}$ due to the magnetic field.

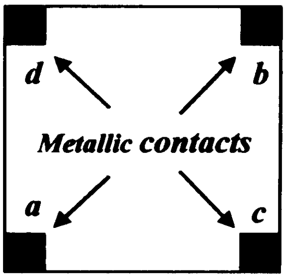

Figure 5.15: A square shaped sample with metallic contacts in the corners for the Van der Pauw method Hall effect measurements

5.2.2. Experiment

The samples used in the Hall measurements for this work were 5mm × 5mm in size to assure uniform thickness over the area examnined. Indium contacts were used as ohmic contacts for the InN films. Prior to the deposition of the contacts, the samples were cleaned with acetone for 5 minutes and then rinsed in DI water (18 MΩ-cm). The samples were then placed in the evaporator where the In contacts were deposited on the surface through a mask. After contact deposition, samples had the same structure as that shown in figure 5.15.

Each contact was checked using a semiconductor spectrum analyser by performing I-V characterization for each sample before each measurement. The sample surface under examination was subjected to high currents initially to break down the oxide layer between the In and the InN prior to performing the Hall measurement. The system used for the Hall measurement on InN samples for this work is shown in the Figure 5.16.

This system was used for resistivity, mobility and carrier concentration measurements. As shown, the system consists of a magnet with a magnet power supply that can supply a field up to 1 Tesla, a Keithley Programmable 220 Current Source to provide a steady current the sample, a Keithley 196 Auto-Ranging Digital Multimeter to measure the voltage across the contacts of the sample, a sample holder and a computer. The measurement process was automated using a LabVIEW program that controlled all parts of the system. As in any non-ideal system, errors occur due to equipment accuracy, material non-uniformity, and contact noise. To reduce such errors, for each sample, many measurements were carried out (5-10 times) and the final result was an average of all measurements. The Hall measurements were carried out in both Macquarie University – Sydney, and Cardiff University. To make sure that both systems were working correct, some measured in Sydney were again measured using the system at Cardiff University. To further confirm theses results, some samples were sent to Dr. Dave Look at Wright State University – USA for testing. The results obtained by the three systems were in good agreement.

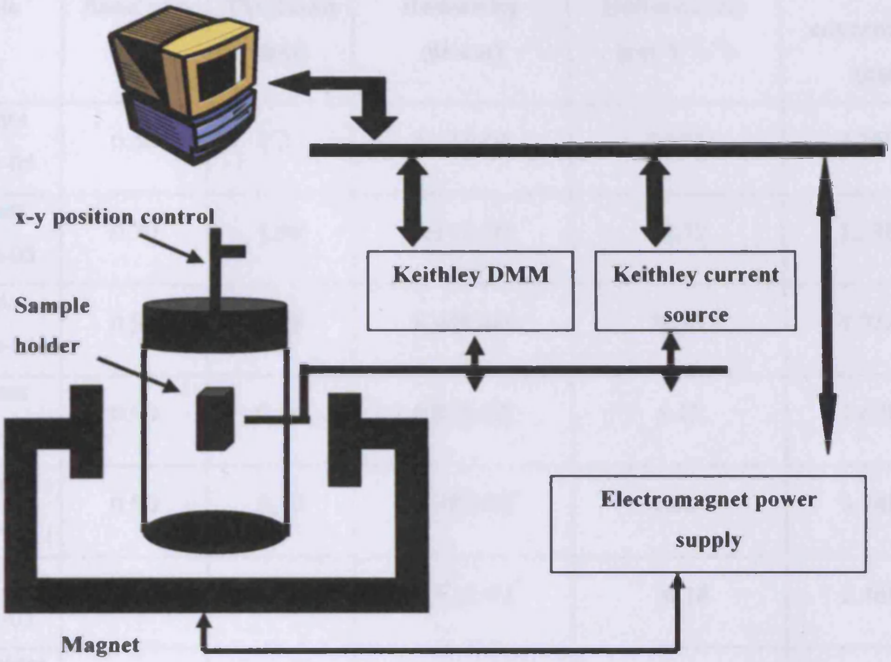

Figure 5.16: Hall effect system

5.2.3. Results and Discussion

From transmission measurements, the absence of free electron absorption at long wavelength (> 2000 nm) suggests that the reactively evaporated grown InN possesses relatively low carrier concentration ($\leq 10^{19}$ cm^{-3}). The carrier concentration was confirmed by the Hall Effect measurements performed at both Cardiff University and Macquarie University. Table 5.2 shows the obtained results for InN grown by reactive evaporation at room temperature.

The resistivity of the investigated samples (see table 5.2) was found to be higher than 10^{-2} Ω-cm. Comparing the resistivity of the indium nitride grown by reactive evaporation and the resistivity of indium nitride grown by RF sputtering and remote plasma enhanced chemical vapour deposition (RPE-CVD) at Macquarie University, and some MBE grown samples from Cornell University, it can be noticed that the reactively grown InN had higher resistivity (more than 2 orders of magnitude) than any of the other samples (see table 5.2 and 5.3 for comparison).

Sample	Band gap (eV)	Thickness (μm)	Resistivity (Ω-cm)	Hall mobility ($cm^2V^{-1}s^{-1}$)	carrier concentration (cm^{-3})
InN/glass 11-Nov-05	0.60	1.20	4.11E-02	54.95	2.76E+18
InN/glass 07-June-05	0.70	1.50	8.31E-02	58.72	1.33E+19
InN/glass 01-June-05	0.90	0.95	8.44E-02	26.41	1.78E+19
InN/glass 13-Sept-06	0.90	0.56	6.83E-02	5.45	1.67E+19
InN/glass 13-Dec-05	0.90	0.50	2.28E-02	40.64	6.74E+18
InN/glass 09-Nov-05	1.00	1.00	1.57E-02	16.16	2.46E+19
InN/sapphire 06-July-05	1.15	1.00	4.90E-01	1.73	7.36E+18
InN/glass 22-Nov-05	1.15	0.55	5.76E-03	25.18	4.31E+19
InN/glass 10-May-06	1.45	0.56	9.40E-02	9.51	6.99E+18
InN/sapphire 21-June-05	1.50	0.82	1.35E-01	7.75	5.98E+18
InN/glass 21-Nov-05	1.65	0.80	2.95E+00	0.41	5.18E+18
InN/glass 05-May-06	1.75	0.53	5.14E-02	14.75	8.23E+18
InN/glass 14-Dec-05	1.75	0.58	3.33E-01	1.98	9.45E+18
InN/sapphire 31-May-05	2.10	0.60	7.88E+00	19.15	1.59E+17

Table 5.2: Hall effect results for InN grown at room temperature

Sample	**Resistivity** (Ω·cm)	**Carrier Concentration** (cm^{-3})
MBE GS1353	0.0024	$3.4x10^{18}$
MBE GS1337	0.0014	$5.0x10^{18}$
MBE GS1310	0.0027	$2.0x10^{18}$
MBE GS1322	0.0017	$3.5x10^{18}$
MBE GS1311	0.0027	$2.1x10^{18}$
RF sputtered 3/Aug/06	0.0084	$8.4x10^{19}$
RF sputtered 6/Jul/05	0.0017	$9.6x10^{19}$
RF sputtered 4-5/Jul/05	0.0023	$3.4 x10^{19}$
RF sputtered 23/Jun/05	0.0073	$8.5x10^{20}$
RPECVD 15-16/May/04	0.00067	$1.1x10^{20}$
RPECVD 24-25/Sep/03	0.0028	$6.5x10^{19}$

Table 5.3: Hall effect results for InN grown by other methods

The data given in Table 5.3 are for samples used in the study of the nature of nitrogen related point defects in common forms of InN (the publication is attached in Appendix A). Using a similar growth technique with RF nitrogen plasma source instead of dc plasma as has been used for the growth of InN in this work, Sato and Sato reported a resistivity as high as 2.5 Ω-cm [24]. They observed an increase in resistivity from (5.6×10^{-4} to 2.5 Ω-cm) with a reduction in growth rate. However, the material quality deteriorated with the decrease of the growth rate which was confirmed by a significant decrease in the Hall mobility. Most of the reported resistivity values elsewhere were of lower values than the values obtained for InN grown at room temperature in this work. Hovel and Cuomo reported RF sputtered InN with resistivity of $(3\text{-}5)\times10^{-3}$ Ω-cm [6]. They attributed that high conductivity to a high density of native defects. Natarajan et al. [25] reported values within the range 10^{-2}-10^{-4} Ω-cm while Motlan et al. obtained a resistivity in the range 1.6×10^{-3}- 4×10^{-3} Ω-cm [26]. They associated their low resistivity with shallow impurities. Sharmell and Parman reported electrically conductive RF sputtered InN with a conductivity of approximately 4.3×10^{3} $(\Omega\text{-cm})^{-1}$ [7]. The resistivity was 3.4×10^{-4} Ω-cm for InN grown by ALE [27]. Similarly, Hall measurements showed all HVPE grown InN samples to be heavily conducting of $\sim10^{-4}$ Ω-cm [28], while Feiler et al. obtained *p*-type InN with resistivity of ($3\text{-}5\times10^{-4}$ Ω-cm) for InN grown by PLD [29].

Theoretically, the predicted values for the high value mobility of InN is far from the wide range of values obtained experimentally (refer to chapter two). For InN grown by reactive evaporation at room temperature, the measured Hall mobility showed very low mobilities compared to the reported value for InN grown by MBE and MOCVD. Table 5.2 shows a maximum Hall mobility of less than 60 $cm^2V^{-1}s^{-1}$. These low value mobilities can be attributed to the poor crystalline structure of the material [34]. All the films grown were polycrystalline of hexagonal structure but with no preferred orientation. The poor crystalline quality can be due to the low growth temperature used in producing the InN films. Inhomogeneous impurity distributions can be considered another reason for such low mobilities [26]. Excess In incorporation cannot be ruled out as additional reason for the low mobility and high carrier concentration material [14].

The mobility values in Table 5.2 can be considered comparable and close to some of the older literature where InN was mainly grown by sputtering and reactive evaporation, with the exception of the work reported by Tansley and Foley [35], where they achieved the highest Hall mobility for InN of 2700 $cm^2V^{-1}s^{-1}$. Trainer and Rose produced *n*-type InN with Hall mobility of 20 $cm^2V^{-1}s^{-1}$ using reactive evaporation [36]. A mobility of 20-50 $cm^2V^{-1}s^{-1}$ was reported for InN grown using reactive cathodic sputtering by Puchevrier and Menoret [37]. The maximum Hall mobility of the InN thin film on the ZnO/α-Al_2O_3 substrate (60 $cm^2V^{-1}s^{-1}$) was two times higher than that of the InN film grown on bare α-Al_2O_3 substrates (30 $cm^2V^{-1}s^{-1}$) at the same growth temperature according to the high-grade crystallinity [38]. In an attempt to reproduce the material grown by Tansley and Foley, that achieved the highest mobility and lowest carrier concentration ever reported for InN, Motlan, Goldys and Tansley using the same sputtering system used to produce the material reported in 1986, reported a Hall mobility that lies in the range (2 – 306) $cm^2V^{-1}s^{-1}$ [26] Another attempt was taken also using the same system by Butcher et al. [39]; they produced low carrier concentration material of less than 10^{17} cm^{-3}, but only with a maximum mobility of 25 $cm^2V^{-1}s^{-1}$.

The presence of indium segregates would give a good explanation of the relatively low mobility and high carrier concentration of the reactively evaporated InN films. In their investigation of the influence of excess indium incorporation on the electrical properties of MBE-grown InN, Ho et al. noticed that the carrier concentration increased while the mobility decreased as the concentration of excess indium was increased [14]. They suggested that the presence of excess indium provided free carrier to the crystals and formed defects, which acted as electron scattering centres. Ho et al. also suggested that the excess indium segregated partly as a form of indium-clusters in the bulk crystal but might also partly segregate on the surface of the epilayers. The presence of indium was observed when the films were analysed by secondary electron microscope (SEM) for surface analyses and X-ray diffraction (XRD) for structure analysis. SEM clearly revealed the presence of indium dots on the surface as seen in figure 5.17. For confirmation, XRD analysis was performed, and one of the pure indium metal diffraction peaks, In(101) or In(110) and sometimes both diffraction peaks were observed both the crystalline quality and the electrical properties of the grown material. More about the XRD analysis and its explanation are discussed in details in the previous chapter.

As-grown InN is always *n*-type with a very high background carrier concentration [40]. There have been several reports on the carrier concentration of InN, and much speculation about the origin of this high background carrier concentration. Most of the sputtered InN resulted in high carrier concentration and low mobilities, of course, with the exception of the work of Tansley and Foley [35]. Using RF sputtering growth technique, Tansley and Foley reported the lowest carrier concentration for InN despite the polycrystalline nature of the material. They achieved a value as low as 5.3×10^{16} cm^{-3} at room temperature which decreased to 3×10^{16} cm^{-3} at 150 K for the same sample. In the early attempts at producing InN, the carrier concentration of InN mostly ranged between 10^{19} and 10^{21} cm^{-3}. Hovel and Cuomo reported *n*-type polycrystalline InN with carrier concentration of $(5\text{-}8)\times10^{18}$ cm^{-3} [6]. The high carrier concentration was attributed to a high density of native defects. Trainer and Rose produced n-type InN films using reactive evaporation [36]. The films had a carrier concentration of 10^{20} cm^{-3}. Using reactive cathodic sputtering, Puchevrier and Menoret produced InN with relatively low carrier concentration of $(3\text{-}10)\times10^{18}$ cm^{-3} [37]. Westra, Lawson and Brett obtained 7×10^{19} cm^{-3} and 2×10^{20} cm^{-3} carrier

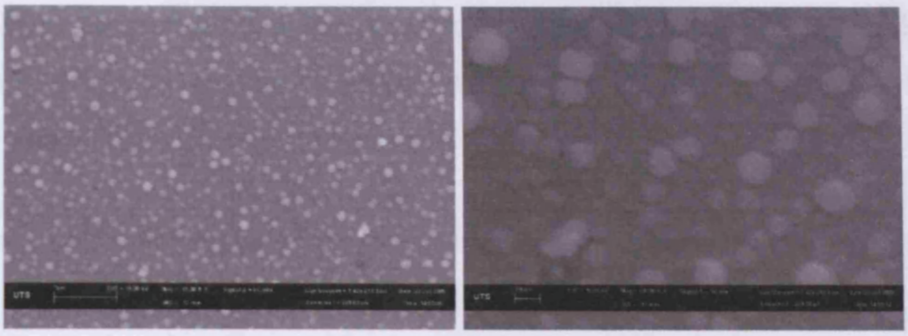

Figure 5.17: SEM pictures showing the presence of In-clusters on the surface of InN

concentration [41], while Sullivan et al. obtained InN with carrier concentration ranging from 3×10^{20} cm^{-3} to 6×10^{20} cm^{-3} [3]. Consistently high concentration levels have been reported for sputtered material, despite efforts to improve the quality of the grown material [38, 42-45]. In the early 1990s and with the use of MOVPE and MBE growth techniques, these reports also showed high carrier densities in the order of 10^{20} cm^{-3} [46-50]. However, with the development of the growth techniques and with precise control on the growth conditions significant improvement in the electrical properties was achieved.

From optical transmission measurements shown in the previous section, it was predicted that InN films grown by reactive evaporation possessed relatively low carrier concentration (less than 10^{19} cm^{-3}) due to the lack of free electron absorption. The Hall measurements confirm the low carrier density inferred by the optical transmission measurements. The carrier concentration ranged from 1.59×10^{17} to 4.31×10^{19} cm^{-3} for different ranges of band gap values. It is worth noting here that the lowest carrier density obtained was actually attributed to the highest band gap value obtained (2.1 eV). This observation would stand against the claims that the Moss-Burstein effect is the main reason for the observation of the high band gap InN films. More discussion on this issue will be revealed in the following section. The values obtained for reactively evaporated InN shows the consistency in growing relatively low carrier concentration material, which is still up-to-date one of the main challenges that faces the InN film growth.

Another significant observation is that the carrier concentrations of the reactively evaporated InN are orders of magnitudes less than those of RF sputtered InN, despite the similarity in the crystalline structure (polycrystalline) and the oxygen level present in the material which was confirmed by the secondary ion mass spectroscopy analysis (SIMS). The SIMS analysis is presented in the previous chapter in detail.

5.2.3.1. Effect of substrate temperature on the electrical properties

As mentioned earlier in this chapter, the low Hall mobility measured for InN grown by reactive evaporation may be explained by the poor crystalline structure affecting the electrical properties of the material. Higashiwaki et al. confirmed that the quality of InN film was strongly dependent on the growth temperature and significantly affected the mobility of the material grown [51]. A strong correlation between the structural quality and the measured carrier mobilities was also observed by Wang et al. [52]. There were several reports showing a correlation between the electrical properties and the crystalline structure of InN. Gou et al. observed an improvement in the electrical properties of RF sputtered InN with an increase of the growth temperature [44]. They attributed this improvement to improvements in the crystalline structure. The Hall mobility increased smoothly from 18 $cm^2V^{-1}s^{-1}$ for films deposited at a substrate temperature of 100 °C to 115 $cm^2V^{-1}s^{-1}$ at 500 °C while Lu et al. achieved a Hall mobility of 542 $cm^2V^{-1}s^{-1}$ with an electron concentration of 3×10^{18} cm^{-3} on a film grown at similar temperatures but using the MBE growth technique [53]. Lu et al. suggested that the improvement in the electrical properties of InN with increasing substrate temperature is associated with better crystalline quality at higher growth temperature. Saito et al. observed better electron mobility for a film with better surface morphology [54]. Yamamoto et al. reported improvement in the electrical properties with the increase in the growth temperature [55]. They concluded that improvement of morphology is needed to attain high electron mobility in InN films; they found that samples with a relatively smooth surface have a higher mobility (700-730 $cm^2V^{-1}s^{-1}$). The improvement of crystal quality resulted in commensurate improvement in electrical properties, with an electron mobility of 800 $cm^2V^{-1}s^{-1}$ and an electron concentration of 9×10^{18} cm^{-3} [22].

In an attempt to obtain better electrical properties, presumably by improving the crystalline structure of the grown material, InN films were grown by reactive evaporation at different growth temperature ranging from room temperature up to

240 °C. The limitation on the temperature was defined by the resistive heater used in the growth system. The obtained films were characterised by XRD, AFM, and Hall Effect. XRD results showed significant improvement in the crystallinity of the films affected by the increase of the substrate temperature. The full width half maximum (FWHM) of the InN (002) diffraction peak was found to decrease with the increase of the substrate temperature, and more diffraction peaks corresponding to InN were observed. AFM measurements also showed dependence on the substrate temperature. AFM and XRD analysis are discussed in details in the previous chapter. However, the Hall Effect results for these samples will be the subject of discussion in this part of the chapter.

The band gap of the reactive evaporated grown InN covers a wide range from 0.65 to 2.15 eV. This variation in E_g, despite similar growth conditions is discussed in detail in section 5.1.3. The Hall Effect measurements found a correlation between the structural quality and the electrical properties of the InN films grown by reactive evaporation. It is evident that the quality of InN films is strongly dependent on the substrate temperature. With substrate temperature ranging from room temperature up to 240 °C, a correlation between the Hall mobility of the reactively evaporated InN and the substrate temperature is therefore apparent. Generally, the Hall mobility was found to increase with an increase of the substrate temperature. This increase in the Hall mobility was found to be a result of the improvement in the crystalline structure of the reactively evaporated InN. Obtaining better structural quality InN was confirmed by XRD analysis with the observation of the decrease in (FWHM) of the (002) InN diffraction peak (see Figure 4.6 and Figure 4.7). Figure 5.18 shows the plot of the FWHM of the (002) InN diffraction peak and the Hall mobility versus the substrate temperature for different ranges of band gap values.

A significant effect of the temperature on the material quality can be clearly seen from the graphs when the substrate temperature was increased from room temperature to 240 °C. A general observation is that the FWHM tends to decrease while the mobility increased with the increase in the substrate temperature with some exception for some samples and this will discussed below.

Samples with similar or close band gap values were combined to make the discussion easier. Figure 5.18 (a) is associated with InN films having band gap values of 0.9-1.15 eV. In this figure, the FWHM was clearly decreasing with the increase in the substrate temperature. Furthermore, the Hall mobility was increasing as expected with the improvement in the crystalline structure until it reached a maximum value as high as 1100 $cm^2V^{-1}s^{-1}$ corresponding to carrier concentration of 3.74×10^{19} cm^{-3} when a substrate temperature 110 °C was used. However, the mobility showed a decrease in its value despite the improvement in the FHWM when the substrate temperature was increased to 125 °C. XRD measurements showed excess of indium in the sample grown at 125 °C compared to the one grown at substrate temperature of 110 °C which lead to the decrease in the Hall mobility despite the decrease in the FWHM as also observed in the XRD analysis. This sample (grown at 125 °C) showed a Hall mobility of 890 $cm^2V^{-1}s^{-1}$ and carrier density of ~ 1.90×10^{19} cm^{-3}. Stress analysis showed that both samples (grown at 110 °C and 125 °C) were under a combination of both biaxial stresses (resulting from the lattice mismatch between the film and substrate) and hydrostatic stresses (results from homogenous incorporation of point defects). However, the sample grown at substrate temperature of 125 °C showed less stresses than the one grown at 110 °C, which explains the decrease in the carrier concentration. When the substrate temperature was increased to 130 °C, the strain decreased which led to a further decrease in the carrier concentration to reach 1.44×10^{19} cm^{-3} with an increase in the Hall mobility (1065 $cm^2V^{-1}s^{-1}$) with the further improvement in the crystalline structure.

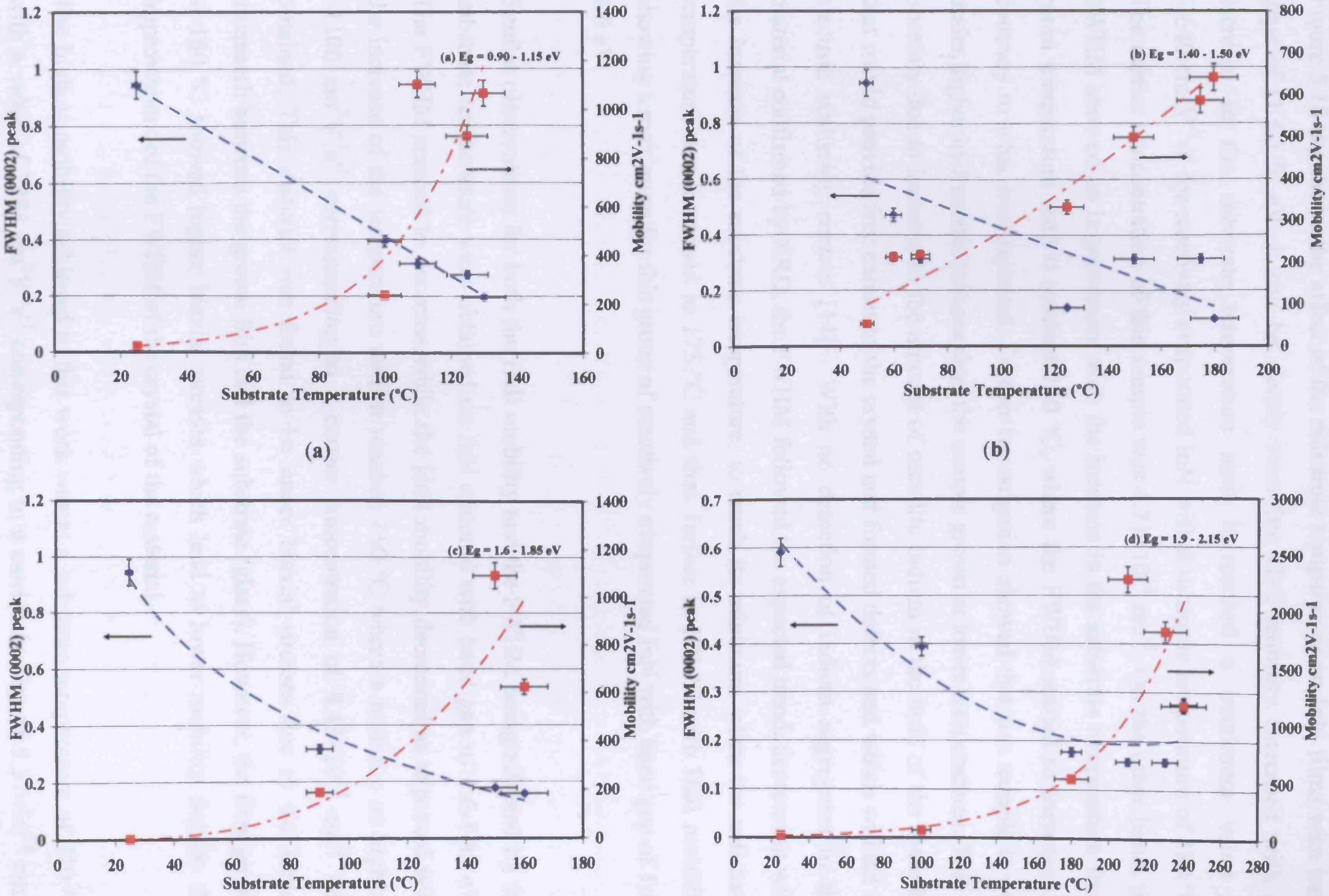

(a) (b)

(c) (d)

Figure 5.18: FWHM (002) InN peak and the Hall Mobility versus substrate temperature

Figure 5.18 (b) shows the effect of the substrate temperature on InN films with band gaps of (1.4-1.5) eV. It can be clearly seen that Hall mobility increased with an increase in the substrate temperature until it reached a maximum value of ~ 640 $cm^2V^{-1}s^{-1}$ for reactively evaporated InN with a substrate temperature of 180 °C. The carrier concentration of this sample was 4.71×10^{18} cm^{-3}. On the other hand, the FWHM showed an improvement with the increase in the substrate temperature from room temperature until it reached 150 °C, where the FWHM started to increase, in contrary to what was expected. Further investigation showed that this sample it was under higher hydrostatic stresses than the sample grown at lower temperatures. This is possibly due to increase in the amount of metallic indium in the bulk of the material that would provide free carrier to the crystal and formed defects and which will act as electron scattering centres [14]. With no detection of indium segregates in the material confirmed by XRD, the FWHM followed the expected trend, decreasing with the increase of the substrate temperature, to reach its minimum when the substrate temperature was increased to 175 °C and then further to 180 °C with Hall mobility showing a maximum for this group of reactively evaporated InN with band gap of 1.4-1.5 eV.

Similar observations for both the Hall mobility and the FWHM being affected by the substrate temperature were obtained on InN material with band gap of 1.6-1.85 eV. The FWHM seemed to decrease while the Hall mobility decreased as expected with the increase of the temperature until it reached 150 °C where a mobility as high as ~1100 $cm^2V^{-1}s^{-1}$ corresponding to a carrier concentration of 8.43×10^{18} cm^{-3} was obtained. This material was found to be under biaxial stresses due to the lattice mismatch between the grown film and the substrate (glass). However, the film grown at 160 °C showed higher biaxial stresses which lead to lower mobility despite the improvement of the FWHM of the crystal of the material.

The highest mobility achieved in this work was at a substrate temperature of 210 °C with a value of 2284 $cm^2V^{-1}s^{-1}$ corresponding to a carrier density of 5.37×10^{18} cm^{-3}. Figure 5.18 (d) shows that the Hall mobility reached this maximum value when the sample was grown at 210 °C but then dropped when the substrate temperature was increased to 230 °C, and dropped even further when the temperature was 240 °C. XRD analysis found a decrease in the FWHM of the diffraction peaks corresponding to the reflection from InN crystal planes. This means that the crystalline structure of the InN film improved when the substrate temperature increased from 210 °C to 230 °C. However, the measurements of the lattice constants (a & c) showed that the film changed from being under linear stresses (possibly caused by the incorporation of point defects on the basal plane) for the film grown at a substrate temperature of 210 °C, and this would explain the relatively high background carrier density (5.37×10^{18} cm^{-3}), to being under both linear and biaxial (resulting from the lattice mismatch between the film and substrate) stresses for film grown at substrate temperature of 230 °C. When the substrate was increased to 240 °C, the InN film quality started to deteriorate. XRD results showed an increase in the FWHM and the presence of excess indium segregates was observed with the detection of the In(101) diffraction peak. This would explain the drop in the Hall mobility and the increase in the carrier density of the material.

Contrary to the Hall mobility, which showed a strong correlation to the substrate temperature, the carrier concentration of the InN films grown by reactive evaporation at different temperatures, did not show any systematic dependence or clear correlation with the substrate temperature. Guo et al. similarly found that the carrier concentration was almost independent of the substrate temperature with a value in the order of 10^{20} cm^{-3} for their RF sputtered InN [44]. The carrier concentration in this work was found to be in the range of (10^{17}-10^{19} cm^{-3}) despite achieving Hall mobility as high as 2284 cm^{2}V^{-1}s^{-1}. The reactively evaporated InN films were found to be heavily compensated. Chin, Tansley and Osotchan reported a compensation level as high as 60% for their RF sputtered InN despite the high produced Hall mobility of 2700 cm^{2}V^{-1}s^{-1} [30]. Furthermore, Fareed et al. predicted room temperature mobility for InN as high as 5000 cm^{2}V^{-1}s^{-1} [32]. Experimentally, they only managed to achieve a mobility of 850 cm^{2}V^{-1}s^{-1} for samples with electron carrier concentration of $\sim 4\times10^{18}$ cm^{-3} indicating a high level of compensation in their material. The high level of compensation would suggest that the reactively evaporated InN films are defect dominated. This would explain why the carrier concentration measured seemed to be completely independent of the substrate temperature on the contrary of what was observed for the Hall mobility. This will also explain the relatively high carrier concentration (10^{17} – 10^{19} cm^{-3}) of the InN grown by reactive evaporation at different temperature ranges.

Significant improvement in the electrical properties of reactively evaporated InN has been achieved in this work. The Hall mobility showed a large increase from ~ 60 $cm^2V^{-1}s^{-1}$ or less for samples grown at room temperature to a value as high as 2284 $cm^2V^{-1}s^{-1}$.for material grown at elevated temperatures. For samples with band gap value of 0.6-0.7 eV, the mobility increased from 60 $cm^2V^{-1}s^{-1}$ with carrier concentration of 1.33×10^{19} cm^{-3} to 1390 $cm^2V^{-1}s^{-1}$ with carrier concentration of 1.64×10^{19} cm^{-3}, while a mobility of 1100 $cm^2V^{-1}s^{-1}$ and carrier concentration of 3.75×10^{19} cm^{-3} was measured for material with band gap of 0.9-1.15 eV compared to a value of 40 $cm^2V^{-1}s^{-1}$ measured for sample grown at room temperature. with a mobility as low as 20 $cm^2V^{-1}s^{-1}$ for InN grown on sapphire at room temperature, the improvement in the crystalline structure with the increase in the substrate temperature yielded great increase in the mobility to a value as high as 2284 $cm^2V^{-1}s^{-1}$ corresponding to carrier concentration of ~ 5×10^{18} cm^{-3} for reactively evaporated InN with band gap of 2.05 eV. This is the highest mobility achieved using the reactive evaporation growth technique and is all the more impressive given that the InN was polycrystalline. Furthermore, this growth technique showed consistency in growing good quality InN with high mobilities and relatively low carrier concentrations. With improved control on the growth parameters and system, reactive evaporation holds great potential to produce InN films with better crystalline quality and electrical properties. Similar polycrystalline material were reported by Tansley & Foley who achieved the best experimental electrical properties for RF sputtered InN (2700 $cm^2V^{-1}s^{-1}$, 5.3×10^{16} cm^{-3}) [35], however, there have been severe difficulties in reproducing the same quality material by the same method or even different growth techniques. Many growth techniques have been employed for the growth of good quality InN material but the high predicted values for mobility never been achieved experimentally. Recently, with the development in the growth technique and precise control of the growth parameters, significant improvement in the quality of InN has been reported. The growth of InN on sapphire by HVPE resulted in films with carrier concentration of 3×10^{19} cm^{-3} and Hall mobility of 890 $cm^2V^{-1}s^{-1}$ [56]. Meanwhile, free electron concentrations ranging from 5.3×10^{18} to 2×10^{19} cm^{-3}, and mobilities ranging from 630-1110 $cm^2V^{-1}s^{-1}$ have been measured, which represent the highest mobilities reported for MOVPE grown InN [57].

On the other hand, MBE growth showed better electrical properties more than any other growth technique. Inushima et al. reported InN grown on sapphire by MBE with carrier concentration 5×10^{19} cm^{-3} and Hall mobility as high as 1700 cm^{2}V^{-1}s^{-1} [12]. Saito et al. obtained electron mobility of 830 cm^{2}V^{-1}s^{-1} and a corresponding carrier density of 1×10^{19} cm^{-3} at room temperature [58]. The Hall mobility of the grown InN was 1500 cm^{2}V^{-1}s^{-1} and the residual electron concentration was 2×10^{18} cm^{-3} [51, 59]. InN layers grown by MBE with thickness between 200 nm to 7.5 μm were unintentional doped with carrier concentrations ranging from 3.5×10^{17} to 5.5×10^{18} cm^{-3} and Hall mobilities ranging from several hundreds up to 2050 cm^{2}V^{-1}s^{-1} [60], while the Hall concentration of electron, for InN epilayers with oxygen concentration 0.1%, ranged from 9×10^{18} to 1.2×10^{19} cm^{-3} in the best samples, and their mobility was found to be as high as ~ 1900 cm^{2}V^{-1}s^{-1} as reported by Davydov et al.[61, 62]. Further to these reports, Xu et al. reported the highest mobility achieved for MBE grown InN with a mobility reaching a maximum of 2370 cm^{2}V^{-1}s^{-1} and corresponding bulk carrier concentration of 2.8×10^{17} cm^{-3} [10]. With relatively low carrier concentration, high mobility and high resistivity InN film (reactively evaporated), and for polycrystalline material with large available surface area at the grain boundaries, surface charge accumulation was not observed for this material, otherwise, high carrier concentrations would be present. This would give a good explanation why such a polycrystalline material would have electron carrier density and mobility in the same range as the MBE and MOVPE grown material.

5.3. Correlation between electrical and optical properties of InN (Moss - Burstein Effect)

As mentioned in chapter two, two proposed models have been introduced to explain the extent of the Moss-Burstein effect in InN [35, 63]. Both models can be described in figure 5.19.

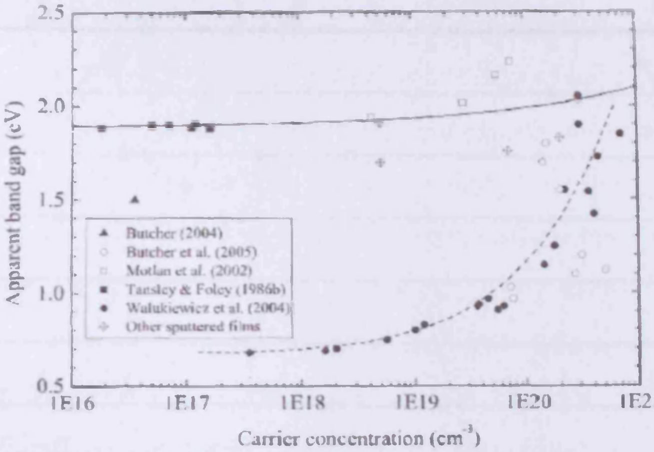

Figure 5.19: Burstein-Moss shift the absorption edge with increasing carrier concentration combining both models. From [64]

A new means for determining the maximum extent of the Moss-Burstein effect has been demonstrated for high carrier concentration InN using temperature dependent absorption measurements since tailing states at the bottom of the conduction band have a different energy dependence than the free electrons present in the conduction band itself. The maximum extent of Moss-Burstein effect at a carrier concentration of 5×10^{20} cm^{-3} was found to be 0.72 eV which means that a sample with band edge absorption at 1.88 eV had a band gap greater of 1.16 eV, which is significantly larger than the proposed value for low carrier concentration MBE grown InN (0.7 eV). Full details about this work can be found in the paper with title: "Stoichiometry effects and the Moss-Burstein effect for InN" attached in Appendix A.

Figure 5.20 shows the band gap as a function of the carrier density for different range of band gaps for reactively evaporated InN. It can be clearly seen that with increasing carrier concentration there is an increase in the apparent band gap of InN.

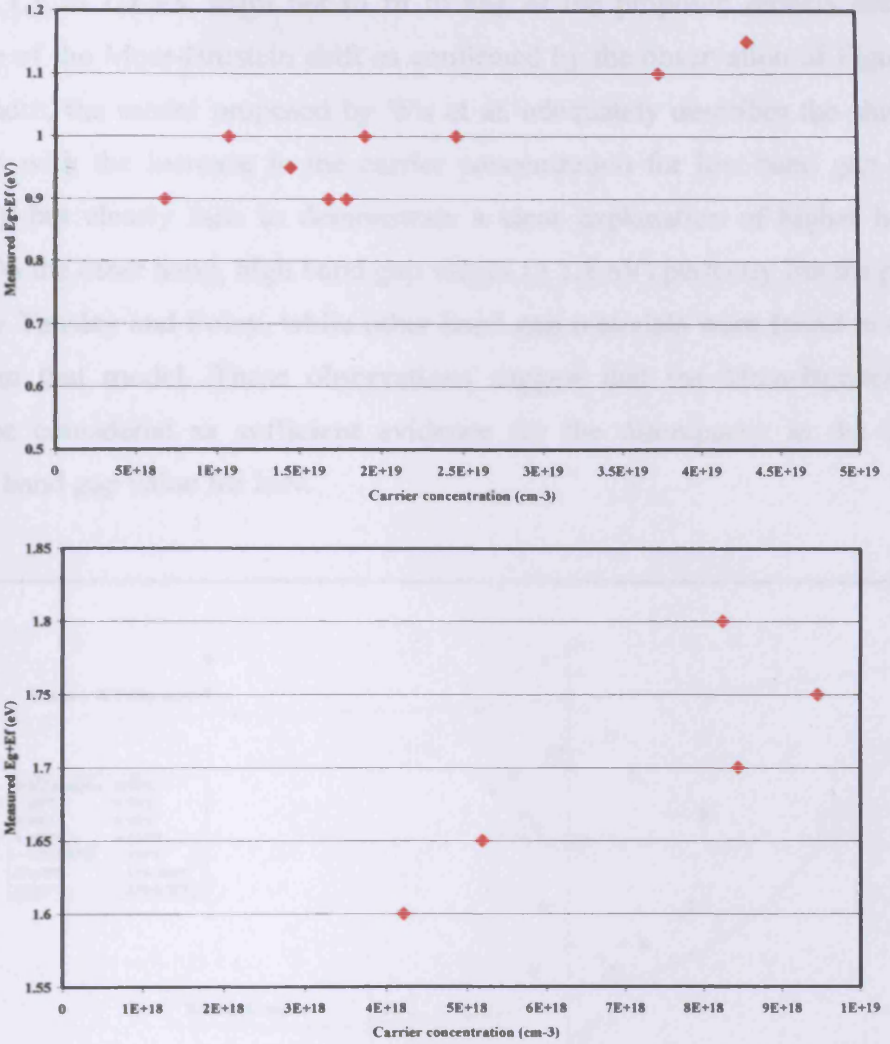

Figure 5.20: Apparent band gap as a function of the carrier concentration

The increase in the carrier density was found to be due to the inhomogeneity and non-uniformity of the material and the presence of native defects in the crystalline structure of the films. So, it can be concluded that InN grown by reactive evaporation is affected with by the Moss-Burstein effect. However, the question always remains, what is the extent of this shift? To help answer this question, the apparent band gap was plotted over the whole range of measured band gaps (reactively evaporated) as a function of the carrier density (Figure 5.21). Also in the plot, both models proposed by Tansley and Foley [35] and Wu et al. [63] describing the extent of the Moss-Burstein effect on the observation of the absorption edge of InN are debated. The InN samples were grown at different substrate temperatures and showed band gap values that spread over a range between 0.6 to 2.15 eV. InN samples with apparent band gap between 1.1 to 1.7 eV seem not to fit to any of the proposed models despite the existence of the Moss-Burstein shift as confirmed by the observation of Figure 5.20. Furthermore, the model proposed by Wu et al. adequately describes the shift in the band gap with the increase in the carrier concentration for low band gap material (< 1 eV), but clearly fails to demonstrate a clear explanation of higher band gap values. On the other hand, high band gap values (> 1.8 eV) perfectly fits the proposed model by Tansley and Foley, while other band gap materials were found to decrease with from that model. These observations suggest that the Moss-Burstein effect cannot be considered as sufficient evidence for the discrepancy in the observed different band gap value for InN.

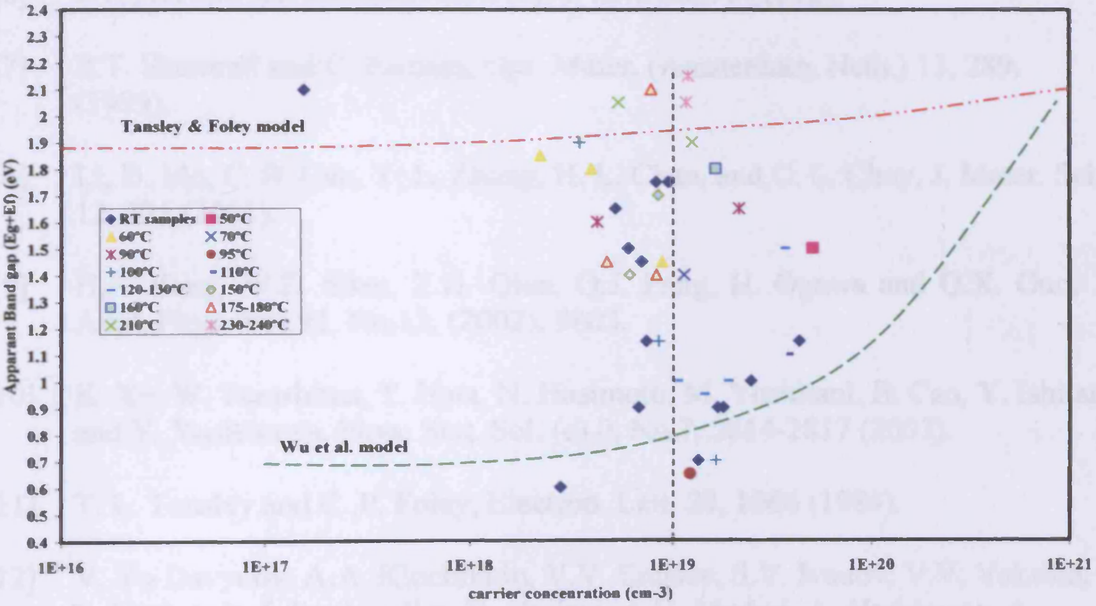

Figure 5.21: Apparent band gap as a function of the carrier concentration

References

[1] J.I. Pankove, Optical Processes in Semiconductors, Solid State Physical Electronics Series, Prentice Hall, Inc., New Jersey 1971, p 93.

[2] S.M. Sze, Physics of Semiconductor Devices, 2nd edition, John Wiley and Sons, Inc., 1981, p 40-41.

[3] B.T. Sullivan, R.R. Parsons, K.L. Westra and M.J. Brett, J. Appl. Phys. 64 (8), (1988) 4144.

[4] H.P. Zhou, W.Z. Shen, H. Ogawa and Q.X. Guo, J. Appl. Phys. Vol. 96, No.6, (2004), 3199.

[5] J.I. Pankove, Optical Processes in Semiconductors, Solid State Physical Electronics Series, Prentice Hall, Inc., New Jersey 1971, p 94-95.

[6] J. Hovel and J. J. Cuomo, Appl. Phys. Lett. 20, 71 (1972).

[7] R.T. Shamrell and C. Parman, Opt. Mater. (Amsterdam, Neth.) 13, 289, (1999).

[8] Li, D. Mo, C. B. Cao, Y. L. Zhang, H. L. Chan, and C. L. Choy, J. Mater. Sci. 12, 725 (2001).

[9] H.F. Yang, W.Z. Shen, Z.G. Qian, Q.J. Pang, H. Ogawa and Q.X. Guo, J. Appl. Phys. Vol.91, No.12, (2002), 9803.

[10] K. Xu, W. Terashima, T. Hata, N. Hasimoto, M. Yoshitani, B. Cao, Y. Ishitani and Y. Yoshikawa, Phys. Stat. Sol. (c) 0, No.7, 2814-2817 (2003).

[11] T. L. Tansley and C. P. Foley, Electron. Lett. 20, 1066 (1984).

[12] V. Yu Davydov, A.A. Klochikhin, V.V. Emtsev, S.V. Ivanov, V.V. Vekshin, F. Bechstedt, J. Furthmuller, H. Harima, A.V. Mudryi, A. Hashimoto, A. Yamamoto, A.J. Aderhold, J. Graul, E.E. Haller, Phys. Status Solidi b 230 (2002) R4.

[13] T.V. Shubina, S.V. Ivanov, V.N. Jmerik, D.D. Solnyshkov, V.A. Vekshin, P.S. Kop'ev, A. Vasson, J. Leymarie, A. Kavokin, H. Amano, K. Shimono, A. Kasic, and B. Monemar, Phys. Rev. Lett. Vol.92, No.11, (2004) 117407.

[14] J.C. Ho, P. Specht, Q. Yang, X. Xu, D. Hao, and E.R. Weber, J. Appl. Phys. 98, 093712 (2005).

[15] V.Yu. DAvydov, A.A. Klochikhin, R.P. Seisyan, V.V. Emtsev, S.V. Ivanov, F. Bechstedt, J. Furthmüller, H. Harima, A.V. Mudryi, J. Aderhold, O. Semchinova and J. Graul, Phys. Stat. Sol. (b) 229, No.3, R1-R3 (2002).

[16] P.A. Anderson, T.E. Lee, C.E. Kendrick, W. Diehl, R.J. Kinsey, V.J. Kennedy, A. Markwitz, R.J. Reeves, S.M. Durbin, Proc. SPIE 5277 (2004) 90.

[17] M. Kuball, J.W. Pomeroy, M. Wintrebert-Fouquet, K.S.A. Butcher, Hai Lu, W.J. Schaff, J. Cryst. Growth 269 (2004) 59.

[18] V. Cimalla, Ch. Förster, G. Kittler, I. Cimalla, R. Kosiba, G. Ecke, O. Ambacher, R. Goldhahn, S. Shokhovets, A. Georgakilas, H. Lu, and W. Schaff, Phys. Stat. Sol. (c) 0, No.7, 2818-2821 (2003).

[19] C.H. Swartz, R.P. Tompkins, N.C. Giles, T.H. Myers, H. Lu, W.J. Schaff, and L.E. Eastman, J. Cryst. Growth 269 (2004) 29-34.

[20] D. Alexandrov, K.S.A. Butcher, M. Wintrebert-Fouquet, J. Cryst. Growth 269 (2004) 77.

[21] M. Wintrebert-Fouquet, K.S.A. Butcher, P.P.-T. Chen, J. Cryst. Growth 269 (2004) 134.

[22] B. Maleyre, O. Briot and S. Ruffenach, J. Cryst. Growth 269 (2004) 15-21.

[23] L.J. Van der Pauw, *Philips Research Reports* 13: 1–9 (1958).

[24] Y. Sato and S. Sato, J. Cryst. Growth 146 (1995), 262-265.

[25] B.R. Natarajan, A.H. Eltouky, J.E. Greene, Thin Soilid Films, 69, (1980), 201

[26] Motlan, E.M. Goldys and T.L. Tansley, J. Cryst. Growth, 241 (2002), 165-170.

[27] T. Inushima, T. Shiraishi and V.Yu. Davydov, Solid State Comm. 110 (1999), 491-495.

[28] D.Y. Song, V. Kuratkov, M. Basavaraj, D. Rosenbladt, S.A. Nikishin, M. Holtz, A.L. Syrkin, A.S. Usikov, V.A. Ivantsov and V.A. Dmitriev, J. Appl. Phys. 99, 116103 (2006).

[29] D. Feiler, R. Stanley Williams, A. Alec Talin, H. Yoon and M.S. Goorsky, J. Cryst. Growth 171 (1997), 12-20.

[30] V.W. Chin, T.L. Tansley, and T. Osotchan J. Appl. Phys. 75 (11) (1994) 7365.

[31] B.R. Ng, J. Cryst. Growth 269 (2004) 35-40.

[32] R.S.Q. Fareed, R. Jain, R. Gaska, M.S. Shur, J. Wu, W. Walukiewicz and M. Asif Khan, Appl. Phys. Lett. Vol.84, No.11, (2004), 1892.

[33] C.H. Swatrz, R.P. Tompkins, N.C. Giles, T.H. Myers, H. Lu, W.J. Schaff, and L.E. Eastman, J. Cryst. Growth 269 (2004) 29-34.

[34] A. Ohtomo, H. Kimura, K. Saito, T. Makino, Y. Segawa, H. Koinuma and M. Kawasaki, J. Cryst. Growth 214-215, 284-8, (2000).

[35] T. L. Tansley and C. P. Foley, Electron. Lett. 20, 1066 (1984).

[36] J. W. Trainor and K. Rose, J. Electron. Mater. 3, 821 (1974).

[37] N. Puychevrier and M. Menoret, Thin Solid Films vol.36, 141 (1976) p.141.

[38] K. Ikuta, Y. Inoue, O. Takai, Thin Solid Films 334 (1998) 49-53.

[39] K.S.A. Butcher, M. Wintrebert-Fouquet, Motlan, S.K. Shrestha, H. Timmers, K.E. Prince, T.L. Tansley, Mater. Res. Soc. Symp. Proc. 743 (2003) 707.

[40] A.G. Bhuiyan, A.Hashimoto and A. Yamamoto, J. Appl. Phys. 94 (2003), 2779 and references within.

[41] K.L. Westra, R.P.W. Lawson and M.J. Brett, J. Vac. Sci. Technol. A, 6, (1988), 1730.

[42] K. Kubota, Y. Kobayashi, and K. Fujimoto, J. Appl. Phys. Vol.66 (1989) 2984-7.

[43] W.A. Bryden, S.A. Ecelberger and T.J. Kistenmacher, Appl. Phys. Lett. 64 (21), (1994) 1844.

[44] Q. Guo, N. Shingai, M. Nishio, H. Ogawa, J. Cryst. Growth 189/190 (1998) 466-470.

[45] N. Saito and Y. Igasaki, Appl. Surf. Sci. 169-170 (2001) 349-352.

[46] A. Wakahara and A. Yoshida, Appl. Phys. Lett. 54, 709 (1989).

[47] T. Matsuoka, H. Tanaka, T. Sasaki, and A. Katsui, *Proceedings of the Sixteenth International Symposium on GaAs and Related Compounds, Karuizawa, Japan*, September 25–29, 1989 (Institute of Physics, Bristol, 1990), p. 141.

[48] C.R. Abernathy, S.J. Pearton, F. Ren, P.W. Wisk, J. Vac. Sci. Technol. B. V11, (1993), 179-182.

[49] S. Strite, D. Chandrasekhar, D. J. Smith, J. Sariel, H. Chen, N. Teraguchi,and H. Morkoc, J. Cryst. Growth 127, 204 (1993)

[50] V.V. Mamutin, V.A. Veshin, V.Yu. Davydov, V.V. Rantikov, T.V. Shubina, S.V. Ivanov, P.S. Kopev, M. Karlsteen, U. Söderwall and M. Willander, Phys. Stat. Sol. (a) 176, 247 (1999).

[51] M. Higashiwaki and T. Matsui, Phys. Stat. Sol. (c) 0, No.1, 360-363 (2002).

[52] X. Wang, S-B. Che, Y. Ishitani and A. Yoshikawa, J. Appl. Phys. 99, 073512 (2006).

[53] H. Lu, W.J. Schaff, J. Hwang, H. Wu, W. Yeo, A. Pharkya and L.F. Eastman, Appl. Phys. Lett. Vol.77, No.16, (2000), 2548.

[54] Y. Saito, N. Teraguchi, A. Suzuki, T. Araki and Y. Nanishi, Jpn. J. App. Phys. Vol.40 (2001), Pt.2, No.2A, L91-L93.

[55] A. Yamamoto, T. Tanaka, K. Koide and A. Hashimoto, Phys. Stat. Sol. (b) 194, No.2, 510-514 (2002).

[56] Y. Kumagai, J. Kikuchi, Y. Nishizawa, H. Murakami, and A. Koukitu, J. Cryst. Growth 300 (2007) 57-61.

[57] S.P. Fu, T.J. Lin, W.S. Su, C.Y. Shieh, Y.F. Chen, C.A. Chang, N.C. Chen and P.H. Chang, J. Appl. Phys. 99, 126102 (2006).

[58] Y. Saito, T. Yamaguchi, H. Kanazawa, K. KAno, T. Araki, Y. Nanishi, N. Teraguchi and A. Suzaki, J. Cryst. Growth 237-239 (2002) 1017-1021.

[59] M. Higashiwaki and T. Matsui, Jpn. J. Appl. Phys. Vol.41 (2002), Pt.2, No.5B, L540-542.

[60] J. Wu, W. Walukeiwicz, K.M. Yu, J.W. Ager III, E.E. Haller, H. Lu, W.J. Schaff, Y. Saito and Y. Nanishi, Appl. Phys. Lett. Vol.80, No.21, (2002) 3867.

[61] V.Yu. Davydov, A.A. Klochikhin, V.V. Emtsev, S.V. Ivanov, V.V. Vekshin, F. Bechstedt, J. Furthmüller, H. Harima, A. Hashimoto, A. Yamamoto, A.V. Mudryi, J. Aderhold, J. Graul, and E.E. Haller, Phys. Stat. Sol. (b) 230, No.2, R4-R6 (2002).

[62] V.Yu. Davydov, A.A. Klochikhin, V.V. Emtsev, D.A. Kurdyukov, S.V. Ivanov, V.V. Vekshin, F. Bechstedt, J. Furthmüller, H. Harima, A. Hashimoto, A. Yamamoto, A.V. Mudryi, J. Aderhold, J. Graul, and E.E. Haller, Phys. Stat. Sol. (b) 234, No.3, 787-795 (2002).

[63] J. Wu, W. Walukiewicz, S.X. Li, R. Armitage, J.C. Ho, E.R. Weber, E.E. Haller, H. Lu, W.J. Schaff, A. BArcz, and R. Jakiela, Appl. Phys. Lett. Vol.84, No.15, (2004) 2805.

[64] S.K. Shrestha, Characterisation of indium nitride films with swift ions and radioisotope probes, University of New South Wales, 2005 (PhD thesis).

Chapter 6

Summary and Conclusion

This thesis discusses many aspects of InN growth and characterisation. A wide range of growth techniques were described in chapter 2 and the various limitations associated with each. One common characteristic of the systems described is that of their relative complexity and cost; generally expensive systems yielding material with a wide range of properties. The main thrust of this investigation was to explore a simple and cheap method of growing InN thin films that allowed flexible control of key growth parameters including temperature, stoichiometry. To this end, indium nitride (InN) has been grown on both c-plane sapphire and borosilicate glass substrates by reactive evaporation. The reactive evaporation growth technique proved to be simple, cost-effective and offered the advantage of low growth temperature. A reduction of the growth temperature was compensated by the adding of energy to the nitrogen gas surrounding the substrate through the generation of dc active plasma making deposition possible without reaching the very high temperatures necessary in other growth techniques. The growth rate was found to be 5-10 μm/hr. the growth temperature ranged from room temperature to 240 °C and was found to be a critical growth parameter and had significant impact on both the electrical and structural properties of the grown material.

The films grown at room temperature were of polycrystalline nature with hexagonal structure but with no preferred orientation. A strong correlation was observed between the crystalline structure and the substrate temperature. With the increase of the substrate temperature a significant improvement in the crystalline structure was observed. The films were still of polycrystalline nature but with more preferred orientation along the vertical c-axis.

The lattice parameter values obtained for indium nitride grown by reactive evaporation ranged between 3.5025 Å to 3.6121 Å for the *a*-lattice and from 5.7122 Å to 5.8054 Å for the *c*-lattice. The divergence in the values of the lattice parameters from the most recently accepted values was attributed to the nitrogen content in the films and consequently the non-stoichiometry of the material, but not to the presence of oxygen in the material. In addition, it was observed that the lattice parameters were affected by the substrate temperature and more relaxed films were grown at higher temperatures. It was also found that the defect density was reduced with increasing distance from the nucleation layer and the substrate-film interface which resulted in reduced carrier concentration and consequently better electrical properties.

In a surface chemical composition analysis of the reactively evaporated InN revealed that the binding energies at ~396.10 eV and ~ 443.80 eV attributed to (N *1s*) and (In *3d5*) peak components, respectively, were associated with the formation InN. Further study on the nature of nitrogen related point defects distinguished two distinct forms of point defects; one of these appears to be an interstitial form of nitrogen, common in some forms of polycrystalline InN (grown by RF sputtering and reactive evaporation). The other was a mixture of the nitrogen on metal anti-site defect and a lower density of indium vacancies and interstitial nitrogen found in epitaxial films grown by MBE and CVD techniques. XPS analysis also showed the In-rich nature of the reactively evaporated InN. This was also confirmed by SIMS analysis. The presence of excess indium lead to the growth of higher defect density material and consequently affected the carrier concentration of the material. Hydrogen cannot be completely excluded completely as a donor.

The electrical properties of InN grown by reactive evaporation were investigated. A Hall mobility as high as ~ 2285 $cm^2V^{-1}s^{-1}$ was obtained with the elevation of the substrate temperature to 210 °C. Contrary to the Hall mobility, which showed a strong correlation to the substrate temperature, the carrier concentration did not show any systematic dependence or clear correlation with the substrate temperature. Carrier concentration ranged between 1.59×10^{17} cm^{-3} to 4.31×10^{19} cm^{-3} which are considered relatively low compared to other reported values on InN.

The role of oxygen and its effect on the film properties was investigated. SIMS analysis estimated the presence of oxygen to be up to ~ 20 at.%. Despite the high presence of oxygen in the material, no detection of In_2O_3 was observed by the XRD analysis, however, its presence could be suspected from the observation of the voids observed by the SEM imaging acting as sites for oxygen adsorption. The oxygen alloying possibility can be excluded and InN-In_2O_3 alloying cannot be considered as the origin of the large optical band gap variations found in InN thin films. The presence of large amounts of oxygen at the surface and grain boundaries of reactively evaporated material, confirmed by SIMS, further discounts oxygen as a source of the surface electron accumulation effect in InN, since such accumulation was not observed for reactively evaporated InN. Consequently, this rules out the surface charge accumulation as a candidate for the high background carrier concentration for as-grown n-type InN.

The apparent band gap obtained from the absorption edge was found to vary from 0.65 eV to 2.15 eV depending on the amount of indium incorporated during the growth. This shows a significant role of Mie resonance effect on the determination of the true value of the band gap; however, it cannot be singled out as the only reason to describe the wide range obtained for the band gap. Also the quantum size effect can ruled out as a reason behind the variations in the band gap. The grain size were found to be higher than 30 nm when InN was grown at room temperature and exceeded 250 nm with the increase of the substrate to above 150 °C.A reduction in defect density would imply a lower observed band gap. It can be concluded that for thin InN material, the observed band gap energy is Moss-Burstein shifted to higher energies due to a higher density of defect-related carriers which shows the significant role of the inhomogeneity, non-uniformity and the stoichiometry of the material in the determination of the band gap. However, the extent of the Moss-Burstein shift cannot be as sufficient evidence for the discrepancy in the observed apparent band gap value for InN.

It can be suggested that the different defect structure observed for polycrystalline (RF sputtered and reactively evaporated) material and single-crystal (mainly grown by MBE and CVD) may be related to the different optical absorption edge and electrical properties seen for that material. It is clear that stoichiometry and homogeneity of InN is a critical issue and solving this problem can help in determining the true band gap value of the material which lies in the range between 1.1-1.5 eV

The reactive evaporation growth technique showed consistency in growing good quality InN with high mobilities and relatively low carrier concentrations. With precise control on the growth parameters and system, reactive evaporation holds great potential to produce InN films with better crystalline quality and electrical properties.

It is apparent that considerable work is still needed to determine all the properties of InN and resolve the controversy and mystery surrounding this material. More efforts should be spent to improve the grown film quality and obtain film with low background carrier concentration and lower defect density. The highest mobilities obtained for InN are still lower than the predicted. It is also essential for device realisation to achieve p-type doping InN, which is still not possible because of the high background donors. This would make improvements in the electrical properties a great challenge to overcome. Optical properties are still under discussion; in particular, the band gap argument needs to be settled which adds another challenge in the understanding of the InN characteristics. Furthermore, finding a suitable substrate with good lattice and thermal match would reduce the crystalline defects and that is very essential for high performance devices.

Appendix A

Publications

JOURNAL OF APPLIED PHYSICS **101**, 123702 (2007)

The nature of nitrogen related point defects in common forms of InN

K. S. A. Butcher,[a] A. J. Fernandes, P. P.-T. Chen, and M. Wintrebert-Fouquet
Physics Department, Macquarie University, Sydney, New South Wales 2109, Australia

H. Timmers and S. K. Shrestha
School of Physical, Environmental, and Mathematical Sciences, University of New South Wales at the Australian Defence Force Academy, Canberra ACT 2600, Australia

H. Hirshy and R. M. Perks
Cardiff School of Engineering, Cardiff University, The Parade, Cardiff CF24 3AA, United Kingdom

Brian F. Usher
Department of Electronic Engineering, La Trobe University, Bundoora VIC 3086, Australia

(Received 11 September 2006; accepted 30 March 2007; published online 18 June 2007)

The role of point defects related to the presence of excess nitrogen is elucidated for InN thin films grown by different techniques. Elastic recoil detection analysis has shown the presence of excess nitrogen in state-of-the-art InN films. Using x-ray photoelectron spectroscopy and x-ray diffraction it is shown that two distinct forms of point defects can be distinguished; one of these appears to be an interstitial form of nitrogen, common in some forms of polycrystalline InN. The other is associated with a combined biaxial and hydrostatic strain observed for molecular beam epitaxy (MBE) and chemical vapor deposition (CVD) grown films, and may be a mixture of the nitrogen-on-metal antisite defect and lower densities of indium vacancies and interstitial nitrogen. The high density of defects present in all the InN samples examined suggests that stoichiometry related point defects dominate the electrical and optical properties of the material. The difference in the type of point defect observed for polycrystalline (rf sputtered) and epitaxial (MBE and CVD) InN supports existing evidence that the Moss-Burstein effect is not an adequate description of the apparent band-gap difference between InN samples grown by different techniques. © *2007 American Institute of Physics.* [DOI: 10.1063/1.2736654]

I. INTRODUCTION

The volatility of nitrogen led to an early expectation that all InN films would be metal rich; however, several techniques have now shown that many state-of-the-art InN films tend to contain excess nitrogen. Using elastic recoil detection analysis (ERDA) up to 33% excess nitrogen has been reported for some forms of InN.[1–3] Energy dispersive x-ray (EDX) analysis has confirmed such results.[4] In addition UV-Raman measurements have indicated a "near-surface" molecular species present when high excess nitrogen is observed.[2] In this paper we present further data, collected using high resolution x-ray photoelectron spectroscopy (XPS), which unambiguously confirms the presence of nitrogen related defects in InN films grown by a number of techniques. We also compare x-ray diffraction (XRD) and XPS data with ERDA results to provide some insight into the possible origin of point defects that might be related to nitrogen rich InN stoichiometry.

Improvements in the crystallinity and electronic properties of molecular beam expitaxy (MBE) grown InN over the last five years have resulted in a marked increase in interest in this material.[5,6] However, despite this improvement in material quality, compared to other semiconducting materials, InN is still limited to extremely high carrier concentrations, in excess of 1×10^{17} cm^{-3}, while the maximum electron mobility of 2100 cm^2/V s so far achieved for MBE grown material[7] is only about half the value of the theoretical maximum.[8,9] The defect structure of InN is therefore a particularly important topic. At present the material physics of InN is only partially understood. Some original assumptions have had to be revised. For instance, the assertion that the electron carrier concentration dependence of the optical absorption edge for epitaxial material was due entirely to a Moss-Burstein effect has been shown to be incorrect. It has been demonstrated that this phenomenon accounts for less than 60% of the apparent change in the band gap represented by the curve in Fig. 1.[10] Bulk oxygen and other impurity species, with the possible exception of hydrogen, appear to be at concentrations too low to account for the carrier concentrations observed.[11–13] As shown in this paper, the deviations from 1:1 nitrogen to indium stoichiometry represent the inclusion of native defects at far higher densities than the combined foreign impurity content. Native defects are therefore a distinct possibility as a source of the high background carrier concentration of InN, and even in the presence of hydrogen considerable film nonstoichiometry would result if the hydrogen was not interstitial. At the highest carrier concentrations observed for InN, percentage amounts of carriers would have to be present to act as donors. Stoichiometry variations can account for such high levels. Native defects present at these high concentrations will have an impact on both the optical absorption properties and on the crystal lat-

---

[a] Author to whom correspondence should be addressed. Tel.: 61 (0)29850 8916; Fax: 61 (0)29850 8115; electronic mail: sbutcher@ics.mq.edu.au

0021-8979/2007/101(12)/123702/11/$23.00

© 2007 American Institute of Physics

Downloaded 21 Jun 2007 to 131.251.0.11. Redistribution subject to AIP license or copyright, see http://jap.aip.org/jap/copyright.jsp

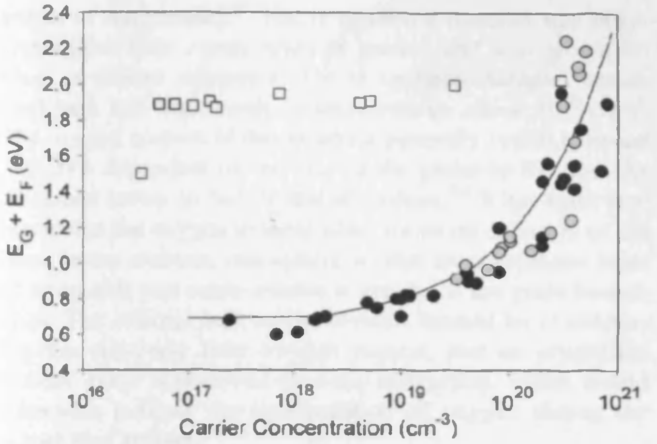

FIG. 1. Band-gap energy plus Fermi-level energy (from absorption square plots) vs carrier concentration for a selection of MBE (black circles), RPE-CVD (gray circles), and rf sputtered (white squares) data taken from Ref. 6.

tice constants. Large changes in the regular lattice arrangement will also affect the value of the band gap itself. Hence, the Moss-Burstein effect cannot be the only phenomenon that influences the optical absorption edge of InN.

Nonetheless, it is interesting that a substantial number of epitaxial InN samples have been reported to follow the same carrier concentration versus absorption edge trend represented by the curve in Fig. 1 (though with some notable exceptions[6,10]), and although the Moss-Burstein effect does not completely explain this trend, it would appear that a common defect structure might be present for such samples. Figure 1 displays the optical absorption edge (from absorption square measurements) versus carrier concentration data for a selection of samples taken from Ref. 6. For this paper we have studied epitaxial films at the higher absorption-edge part of the epitaxial material trend, given by the curve in Fig. 1. As shown elsewhere,[6,10] and as indicated in Fig. 1, other forms of InN do not follow the trend shown in the figure and are in clear violation of the proposed Moss-Burstein solution of apparent band-gap variation. These films appear to have consistently high apparent band gaps as measured by optical absorption. We have also studied the defect structure of some of these materials.

Assumptions regarding the propensity of InN to be nitrogen deficient are also challenged here. It has long been assumed that nitrogen vacancies were the dominant native defect for InN.[5,6] Ho *et al.*[14] have recently reported carrier concentrations of 4×10^{21} cm^{-3} for MBE InN purposely grown using indium rich conditions—supporting the case for nitrogen vacancies as a possible donor species for InN. However, high carrier concentrations have also been observed for extremely nitrogen rich InN,[2,12,15] suggesting that for film growth under certain conditions other native defects may be important. In the following sections we establish the veracity of the measurements for the nitrogen rich material and then attempt to determine the possible native defect structure of such material.

II. FILM PROPERTIES

As outlined above, the samples studied for this paper represent two broad groups of InN materials: epitaxial samples, which appear to approximately follow the upper and middle sections of the defect line represented in the plot of absorption edge versus carrier concentration given in Fig. 1, and rf sputtered polycrystalline samples that do not follow this trend, but are also represented in Fig. 1. The defect line shown in the figure was previously thought to represent a severe Moss-Burstein effect for epitaxial InN samples, whereby a ~0.65 eV band gap was modified to a higher absorption edge by the presence of a high electron carrier concentration in the conduction band. It has since been shown that the Moss-Burstein effect can only account for a maximum of 60% of the change in absorption edge: for a material with a 5×10^{20} cm^{-3} electron carrier concentration. The maximum extent of conduction band filling with free electrons can be delineated using temperature dependent absorption measurements since tailing states at the bottom of the conduction band have a different energy dependence than the free electrons present in the conduction band itself. On this basis it was shown that the maximum extent of the Moss-Burstein effect at this carrier concentration was 0.72 eV and that the resulting band gap for a sample with absorption edge at 1.88 eV had to be at or above 1.16 eV.[10] This value is quite different to the ~0.65 eV band gap claimed for a lower carrier concentration epitaxial material. Despite this difference and the failure of the Moss-Burstein effect to explain all of the observed variations in absorption edge, it appears that samples that approximately follow the defect line of Fig. 1 may be dominated by a common set of defects.

In contrast, the nonepitaxial polycrystalline material studied here appears to have some very different optical properties compared to the epitaxial material, as is shown in Fig. 1, and is often referred to as the "high band-gap material."

InN thin films produced by four different techniques were examined during this work. MBE materials were supplied by Cornell University and the Ioffe Institute. The Ioffe MBE material was grown epitaxially directly on sapphire substrates. The Cornell material was grown epitaxially on a thick 200 nm AlN template as described elsewhere,[16] and this material has been shown to have oxygen levels sometimes as low as 3×10^{16} cm^{-3}, while other bulk impurity levels, with the possible exception of hydrogen, have also been shown to be at too low a concentration level to explain the bulk carrier concentration.[11] A number of native defects have been suggested as possible donors in InN;[6,17] therefore, in the presence of the relatively large values of nonstoichiometry the influence of native defects needs to be seriously considered.

Remote plasma enhanced chemical vapor deposition (RPE-CVD), rf sputtered and reactively evaporated InN thin films grown at Macquarie University were also examined. The RPE-CVD material was grown epitaxially on sapphire and was also grown on glass substrates. This method of growth is described in a number of related publications.[12,15,18] The bulk oxygen content of the RPE-CVD samples has been measured by secondary ion mass spectroscopy (SIMS) and found to generally be much less than the film carrier concentrations (sometimes by up to two

Downloaded 21 Jun 2007 to 131.251.0.11. Redistribution subject to AIP license or copyright, see http://jap.aip.org/jap/copyright.jsp

orders of magnitude).[12] The rf sputtered material was polycrystalline, with *c*-axis oriented grains, and was grown on glass or silicon substrates. The rf sputtered samples examined here had high carrier concentrations above 10^{20} cm^{-3}. The oxygen content of this material generally varied between 3%–20% dependent on the size of the grains in the film. As discussed below in Sec. V and elsewhere,[5,6] it has been proposed that the oxygen in these films forms on exposure of the films to the ambient atmosphere so that an amorphous layer of hydroxide and oxide species is present at the grain boundaries. The internal bulk of the crystals formed by rf sputtering has relatively little oxygen present, and no crystalline indium oxide is observed by x-ray diffraction, which would otherwise indicate the incorporation of oxygen during the actual film growth.

Like the rf sputtered material, the thin films grown by reactive evaporation were polycrystalline and were grown on glass or sapphire substrates. The reactively evaporated material has a similar oxygen content as the rf sputtered InN, but is different in that the carrier concentrations are reproducibly low in comparison to the rf sputtered material, with values typically in the range of 2×10^{17}–5×10^{19} cm^{-3}. Absorption measurements in the visible to near infrared range confirm the low carrier concentrations of this material since the strong free electron absorption visible for InN samples with higher carrier concentrations is generally absent, as shown in Fig. 2. The variable apparent band gap observed in the absorption measurements of the figure does not appear to show any significant carrier concentration dependence. Preliminary results, discussed elsewhere (as are details of the film growth for the reactively evaporated samples),[10] indicate that the variation is, however, related to material stoichiometry.

Though for this study, as described in the following sections, a number of measurement techniques were applied to most of the samples, for the reactively evaporated samples only XPS measurements were carried out, and these measurements were only performed for comparison with the XPS data of the higher carrier concentration rf sputtered material.

III. ELASTIC RECOIL DETECTION ANALYSIS RESULTS

In this section we present a selection of our ERDA measurements on InN samples for comparison with the XRD results. Large variations from ideal 1:1 stoichiometry, when present, can be easily observed for many materials using a number of techniques. However, typical methods for determining metal-nitride ratios for nitride compounds, although in some cases having a good precision, lack the accuracy required to help understand structural and electronic properties. Rutherford backscattering spectroscopy (RBS), under best experimental conditions, is 3%–5% accurate for determining elemental concentrations.[19,20] Furthermore, the nitrogen signal in RBS is typically obscured by the signal from the substrate elements so that even poorer accuracy is achieved. Energy and wavelength dispersive spectroscopies, which require calibration standards, have a stoichiometric accuracy of approximately 3%–5%. Secondary ion mass spectroscopy, also requiring standards, can only be regarded as a semiquantitative technique, especially when analyzing percentage amounts of a material since matrix effects can be particularly strong.[20] X-ray photoelectron spectroscopy and Auger electron spectroscopy are both only 10% accurate even when using standards.[20] In contrast, ERDA, which has recently been developed for the analysis of InN films,[3,21] can determine the N/In ratio of a film with an accuracy of better than 2% since, in contrast to RBS, the technique intrinsically separates the nitrogen signal from the signal from other elements. In our measurements[21] a 200 MeV Au ion projectile beam was incident on the InN samples, and recoil ions were detected at a recoil angle of 45° using a position sensitive ionization detector. The detector is capable of determining both the recoil ion energy and the energy loss of the ions as they transit sections of the detector. Using heavy Au projectile ions ensures that all elements within the InN films are separated kinematically for film thicknesses up to approximately 1 μm. Some nitrogen loss occurs during the measurement. However, this has been demonstrated to follow the bulk molecular depletion model, and can be corrected.[21] Using a sulfur projectile beam as an alternative to Au, nitrogen loss can be avoided, and such analysis on several InN films has confirmed the results with the Au projectiles.[22]

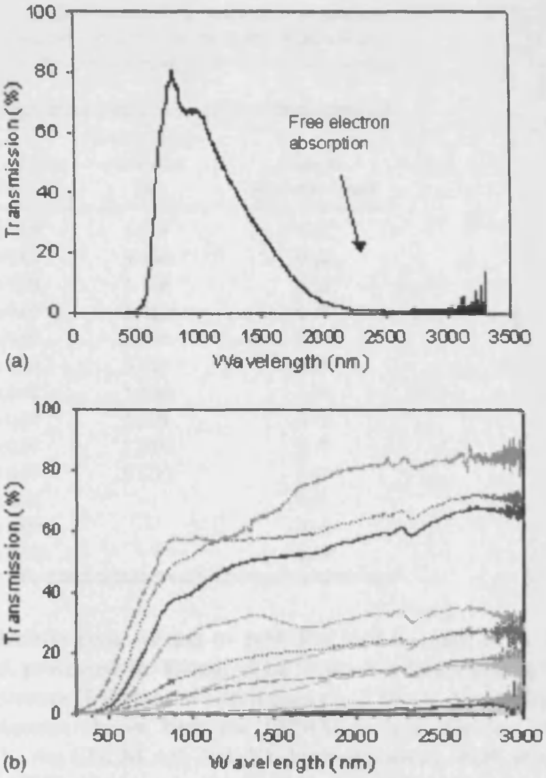

FIG. 2. (a) Absorption data for a rf sputtered InN sample with carrier concentration over 10^{20} cm^{-3}. The strong infrared absorption is free electron absorption, which results from having a large density of electrons present in the conduction band. (b) Absorption data for a number of InN samples grown by reactive evaporation. These samples show no evidence of free electron absorption in the region measured.

Our ERDA measurements have shown that many state-of-the-art InN films have a nitrogen excess. Significantly, thin (<1 μm), moderately *n*-type InN films grown by MBE

Downloaded 21 Jun 2007 to 131.251.0.11. Redistribution subject to AIP license or copyright, see http://jap.aip.org/jap/copyright.jsp

TABLE I. N/In ratios measured by ERD for various rf sputtered, RPE-CVD, and MBE grown InN samples. In this case the Cornell MBE samples were grown on AlN buffer layers 200 nm thick; the Ioffe MBE samples were grown directly on sapphire with no intentional buffer layer. Also shown in the table is the *c* axis lattice parameter carrier concentrations and thicknesses of the samples.

InN Sample ID	Carrier concentration (cm^{-3})	N/In	*c* axis lattice parameter (Å)	Sample thickness (μm)
rf InN (20/Mar/03)	4.7×10^{20}	1.21 ± 0.03	5.744	0.51
RPE-CVD (17/May/04)	3.1×10^{20}	1.34 ± 0.01	5.734	0.44
RPE-CVD (3/Oct/03)	4.0×10^{20}	1.26 ± 0.05	5.738	0.22
RPE-CVD (15/Sep/03)	2.5×10^{20}	1.15 ± 0.05	5.714	0.18
RPE-CVD (31/Jul/03)	3.1×10^{20}	1.10 ± 0.03	5.708	0.18
RPE-CVD (19/May/04)	1.0×10^{20}	1.01 ± 0.01	5.707	0.59
RPE-CVD (22/May/03)	8.0×10^{19}	1.05 ± 0.02	5.698	0.76
RPE-CVD (26/May/04)	8.0×10^{19}	1.03 ± 0.01	5.698	0.72
MBE Ioffe InN W275	2.5×10^{19}	1.04 ± 0.02	5.7005	0.70
MBE Ioffe InN W431	⋯	1.07 ± 0.03	5.7213	0.33
MBE Cornell InN GS-1322	3.5×10^{18}	1.02 ± 0.02	⋯	0.55
MBE Cornell InN GS-1337	5.0×10^{18}	1.04 ± 0.03	⋯	0.60
MBE Cornell InN GS-1353	3.4×10^{18}	1.06 ± 0.03	⋯	0.50

tend to have a few at. % excess nitrogen present,[3,21] with examples shown in Table I. Also shown in the table are the N/In ratios for a rf sputtered sample, a material which we have previously shown to typically have very high N/In ratios,[1–3] and for InN samples grown by RPE-CVD. For the RPE-CVD material it has been shown that film growth at lower temperatures (<400 °C) results in the incorporation of increasing amounts of excess nitrogen and that those epitaxial samples with greater excess nitrogen have a higher carrier concentration.[12]

Theoretical calculations by Stampfl *et al.*[17] show that the formation energies for excess nitrogen species in InN are very high. However, those calculations assume a condition of thermodynamic equilibrium during growth, and growth techniques, such as sputtering, RPE-CVD, and some types of MBE, utilize plasma sources that operate well away from conditions of thermodynamic equilibrium. The lowest potential energy for the excited reactive species created by a nitrogen plasma is greater than 6 eV. Hence, more than enough excess energy is available to establish defects with high formation energies. Defects involving excess nitrogen are therefore possible in InN when using plasma sources for film growth. Nitrogenation of substrates prior to growth is another example of a nonequilibrium treatment in MBE systems that may have some similarity to the conditions described here.

IV. HIGH RESOLUTION X-RAY PHOTOELECTRON SPECTROSCOPY RESULTS

XPS is a mature, established technique for determining the chemical composition of surfaces. Several well regarded texts describe the technique, for example, Briggs and Seah[23] and Barr.[24] The latest generation of XPS systems have seen considerable improvement compared to the systems from just a few years back—the energy resolution of elemental spectra is less than half of what it was five years ago. Past XPS studies of InN have therefore shown a broad N 1*s* photoelectron peak related to InN. For instance, the N 1*s* InN peak presented by Kumar *et al.*[25] shows a full width at half maximum (FWHM) of approximately 3.75 eV. For the measurements shown here the FWHM is typically less than 1 eV. An ESCALAB 220i-XL high-sensitivity, high resolution XPS system manufactured by VG Scientific was used for the measurements. A set of typical N 1*s* core level surface spectra is shown in Fig. 3 for representative InN films grown by MBE, RPE-CVD, rf sputtering, and reactive evaporation. All the surface spectra shown were calibrated to the C 1*s* binding energy for adventitious carbon, known to be present at 284.8 eV.[26,27]

The N 1*s* core level photoelectron peaks are of interest here since any peaks not related to InN bonding indicate a nitrogen rich defect structure. A number of N 1*s* peaks are visible in the spectra shown in Fig. 3. Oxygen is present at the surface of all the samples studied but is most commonly bound as indium hydroxide or indium oxide and is not of interest here. Peak identifications and positions of the N 1*s* photoelectron peaks are provided in Table II. The peaks were deconvoluted using the standard VG provided vendor software. In the past the peaks observed near ~403.7 eV have been attributed to a number of N–O species and/or to molecular nitrogen (see the discussion in Ref. 26). Molecular nitrogen is a possibility here (though we do not discount the presence of some proportion of N–O surface bound species) as we have previously identified a surface contribution of this species using UV Raman.[2] The peak at ~399.5 eV may be attributed to N–H species, as observed during the NH_3 dosing of metals.[28] N–H species may be expected as a hydrolysis product of InN following exposure to the water in air, via the reaction

$$\mathrm{InN} + 3\mathrm{H_2O} \rightarrow \mathrm{NH_3} + \mathrm{In(OH)_3}. \qquad (1)$$

Partial hydrolysis of InN would, of course, result in the presence of chemisorbed NH and NH_2 species. We have previously identified the presence of the other reaction product in Eq. (1), i.e., $In(OH)_3$, at the surface of InN, though this spe-

Downloaded 21 Jun 2007 to 131.251.0.11. Redistribution subject to AIP license or copyright, see http://jap.aip.org/jap/copyright.jsp

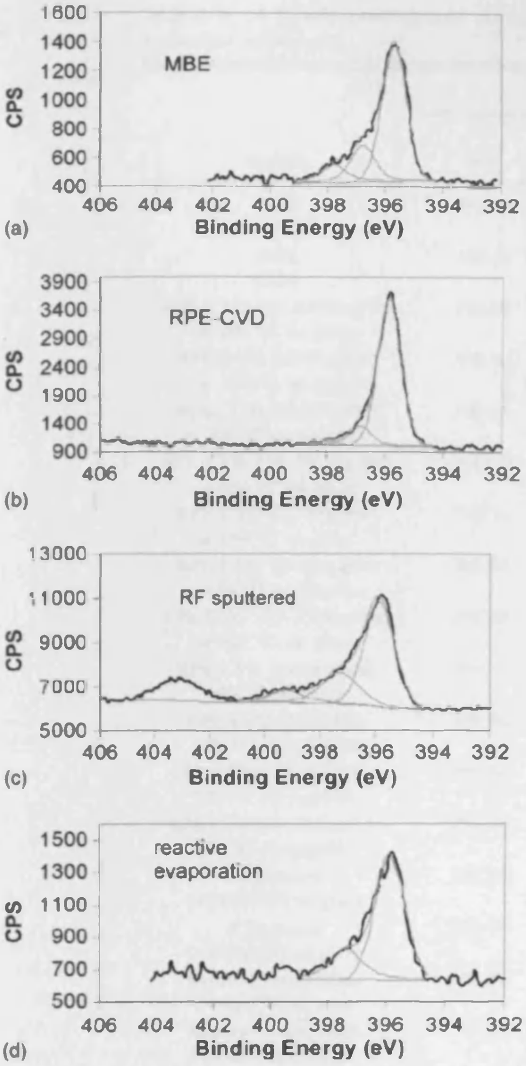

FIG. 3. The figure shows the N 1*s* spectra obtained by XPS at the surface of indium nitride. The samples were grown by different methods. (a) MBE sample GS-1332; (b) grown by RPE-CVD on *c*-plane sapphire at 450 °C, 21 May 2004; (c) grown by rf sputtering on glass, 4–5 July 2005; and (d) grown by reactive evaporation on glass, 25 January 2006. The data for (a) was measured at a different time over a slightly different energy range; however, no other nitrogen related peaks were observed in a wide energy scan.

cies is visibly converted to the oxide under the Al *Kα* radiation often used for XPS studies.[29] In the case of one of the RPE-CVD samples the peak at ~399.5 eV may also have been due to C–N bonding. This is discussed in further detail below.

The peak at approximately 397.8 eV is similar in position to the 398.2 eV peak observed by Schreifels *et al.*[28] on dysprosium dosed with molecular nitrogen; those authors attributed the peak to chemisorbed atomic nitrogen, which apparently exists as an intermediary step in the chemical formation of a dysprosium nitride. If the species observed here at 397.8 eV represents a form of atomic nitrogen in InN, then its presence would explain some of the excess nitrogen observed by ERDA in the InN samples. This particular peak was not observed for RPE-CVD samples that were examined relatively soon after film growth, nor was the peak always easily observed after argon ion etching of those samples with only a small excess of nitrogen measured by ERDA. The peak was observed for all rf sputtered samples and for samples grown by reactive evaporation, regardless of their age prior to analysis. It was also present for one of the MBE samples examined, though that sample was examined some months after film growth.

The peak at ~396.0 eV has previously been attributed to InN, albeit with lower resolution measurements, and these results are consistent with that observation.[25] The smaller peak at ~396.9 eV, observed only for the RPE-CVD and MBE samples, has not been observed previously because of the lower energy resolution of the XPS systems used prior to this. Of course, XPS peaks need not result from chemical shifts. A number of potential nonchemical origins were examined here. The possibility that the peak could be a shake-up peak related to the main InN N 1*s* peak is excluded since with argon ion etching of the RPE-CVD samples this peak was observed to grow substantially in relation to the main InN N 1*s* peak. As shown in Fig. 4, the ~396.9 eV contribution was also observed to be larger for those RPE-CVD samples for which ERDA showed a greater amount of excess nitrogen (i.e., for samples grown at lower temperatures), suggesting that the peak has a distinct chemical origin. The figure compares three samples with varying levels of excess nitrogen present. It is also unlikely that a shake-up peak would be present for the RPE-CVD and MBE samples, and not for the reactively evaporated or rf sputtered samples.

It may be suspected that Fermi level variations at the sample surface due to electron accumulation at the InN surface may have caused a shift of the 396.0 eV peak to 396.9 eV. However, it can also be shown that the peak at ~396.9 eV is not related to surface variations in the Fermi level of the material. Figure 5 shows a N 1*s* spectrum for a sample that was etched with argon ions and then heated to remove physisorbed species. The contribution at ~396.9 eV is clearly seen. The figure also shows the In 3*d* peak for the same sample, for which there is no evidence of a similar shift in energy from the main In 3*d* InN related peak. Variations in the Fermi level with sample depth should cause the same energy shift for all the core level spectra. This is clearly not observed here.

For the polycrystalline rf sputtered and reactively evaporated samples, there also appears to be no reliance of the N 1*s* spectra on Fermi level effects since, as explained in Sec. II, the reactive evaporation samples have a relatively low carrier concentration compared to the rf sputtered material; yet, as shown in Table II, there is no discernible change in the N 1*s* peak positions related to the difference in carrier concentration of the two materials. The reactively evaporated polycrystalline material also spans the carrier concentrations of the RPE-CVD and MBE samples, which suggests that the presence of the ~396.9 eV peak in the epitaxial material, and not in the polycrystalline materials, is again unrelated to variations in the Fermi level of the materials studied.

Egelhoff, Jr.[30] has reviewed the mechanisms that lead to changes in binding energy for XPS core level peaks. It is

Downloaded 21 Jun 2007 to 131.251.0.11. Redistribution subject to AIP license or copyright, see http://jap.aip.org/jap/copyright.jsp

TABLE II. N 1*s* core photoelectron surface positions for MBE, RPE-CVD, RF sputtered, and reactively evaporated InN samples.

	Core level assignment (eV)				
Sample	InN	Defect	Atomic N	N–H or C–N	N–O or molecular N
MBE GS-1322	395.59	396.69	⋯	⋯	⋯
MBE W431	395.71	396.72	397.92	⋯	⋯
RPE-CVD (25–26/May/04) at 200 °C on glass	395.99	397.08	397.99	399.49	⋯
RPE-CVD (18/May/04) at 300 °C on glass	395.90	396.98	398.09	⋯	⋯
RPE-CVD (18/May/04) at 300 °C on sapphire	395.87	396.89	397.86	⋯	⋯
RPE-CVD (19–20/May/04) at 400 °C on glass	395. 65	396.74	397.74	⋯	⋯
RPE-CVD (21/May/04) at 450 °C on glass	395.74	396.84	397.92	⋯	⋯
RPE-CVD (21/May/04) at 450 °C on sapphire	395.87	396.86	397.92	⋯	⋯
RPE-CVD (22–23/May/04) at 500 °C on glass	395.61	396.74	⋯	⋯	⋯
RPE-CVD (27/May/04) 550 °C on glass	395.71	396.97	⋯	⋯	⋯
RPE-CVD (5/Jan/05) 510 °C on sapphire	395.81	396.77	⋯	⋯	⋯
RPE-CVD (21/Jan/05) 530 °C on sapphire	395.88	396.94	⋯	⋯	⋯
RPE-CVD(24–25/Jan/05) 560 °C on sapphire	395.80	396.84	⋯	⋯	⋯
rf Sputtered (4–5/Jul/05) on glass	395.85	⋯	397.23	399.12	403.05
rf Sputtered (6–7/Jul/05) on glass	396.17	⋯	397.71	399.61	403.88
Reactive evaporation (24/Jan/06) on glass	396.07	⋯	397.50	399.04	⋯
Reactive evaporation (25/Jan/06) on glass	395.88	⋯	397.38	⋯	⋯
Reactive evaporation (30/Jan/06) on glass	396.11	⋯	397.48	399.29	⋯

apparent that even if the peak at 396.9 eV for the RPE-CVD and MBE materials is not due to a chemical shift, the binding energy shift represented by this peak is most likely the result of variations in the electronic structure of the N 1*s* core level electrons related to the main InN N 1*s* peak. In either case it appears that the peak at ~396.9 eV represents a defect species present only in the epitaxial RPE-CVD and MBE grown InN samples. The presence of this defect may be related to the difference in the optical properties observed for the epitaxial and polycrystalline materials studied.

In the case of the first RPE-CVD sample shown in Table II, the low 200 °C growth temperature for that sample does not allow for the efficient dissociation of the metal organic used as the indium source during the film growth. Consequently, some hydrocarbon is incorporated in the InN film when using CVD techniques at such low temperatures. This is shown in Ref. 12 where the carbon content of a sister sample was shown to be as high as 10 at. % in the bulk—though this is still much less than the excess nitrogen that was shown to be present in that same sister sample. If C–N bonds are formed during the growth of such a film, then this may contribute to the N 1*s* XPS peak at 399.49 eV, shown in Fig. 4(a), as suggested by the work of Kumar *et al.*[31] In that same reference, a smaller C–N contribution at 398.1 eV is also identified, and, therefore, there is also the possibility of a small C–N contribution in that binding energy region for the 200 °C RPE-CVD sample examined here. For the rf sputtered and reactively evaporated samples the absence of a carbon source during the actual growth process excludes the presence of a C–N based contribution to the ~399.5 eV peaks seen for those samples.

V. X-RAY DIFFRACTION ANALYSIS

In this section we compare XRD data with the ERDA results to provide further insight into nitrogen rich InN stoichiometry. The use of x-ray diffraction for defect analysis is well established and is based on observations of the

Downloaded 21 Jun 2007 to 131.251.0.11. Redistribution subject to AIP license or copyright, see http://jap.aip.org/jap/copyright.jsp

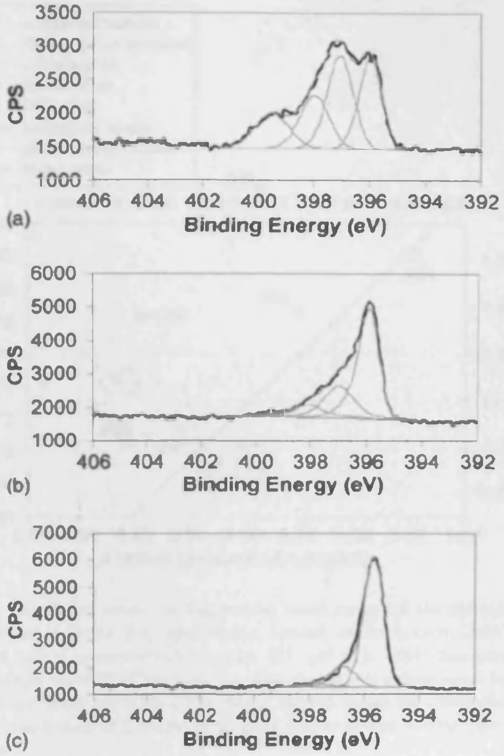

FIG. 4. The figure shows the N 1*s* spectra obtained by XPS at the surface of indium nitride. The samples were grown by RPE-CVD at (a) 200 °C, (b) 300 °C, and (c) 400 °C. The samples grown at higher temperature have less excess nitrogen and lower carrier concentration (Ref. 13).

changes in the lattice constants and unit cell size.[32] It is noteworthy that changes in the physical dimension of a film, which may relate to the accumulation of defects at grain boundaries or at other extended defect sites do not generally have a strong influence on the lattice constants measured by XRD.[32] The accumulation of indium clusters at grain boundaries, for instance, would have little influence on the data presented here. In essence only defects present in the crystal bulk are observed by this technique. It is quite possible that indium, nitrogen, or even oxygen accumulations may be present at grain boundaries and at other extended defect sites for the material examined. However, this analysis would not identify the presence of those defects. Therefore, unlike many other analysis techniques that cannot distinguish between materials in the crystal bulk and materials at grain boundaries, this study provides specific analyses of the defects present in the crystal bulk.

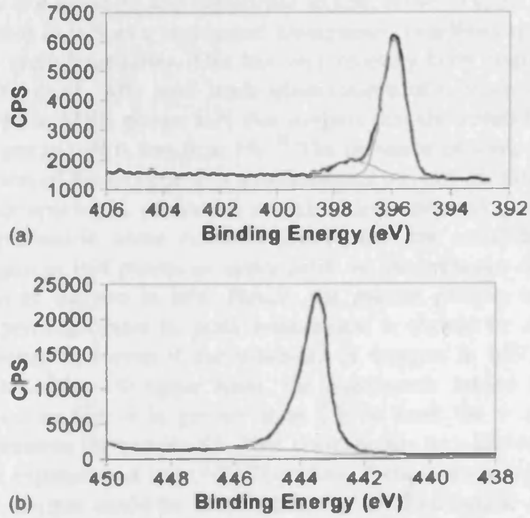

FIG. 5. The figure shows (a) the N 1*s* spectrum and (b) the In 3*d*5 spectrum obtained by XPS for indium nitride which had been argon ion etched and heated. The sample was grown on 24–25 January 2005 at 560 °C on sapphire by RPE-CVD.

Used in conjunction with other analysis techniques, XRD based defect analysis can be very effective for nitride films, and there is a long history of its use for such applications. For instance, in 1979, while changing the growth parameters for GaN to achieve variations in film stoichiometry, Lagerstedt and Monemar[33] observed a decrease in the lattice constants for a Ga rich material, which they associated with the presence of nitrogen vacancies. They observed a reduction in the lattice parameters following the relationship $\Delta a/a=\Delta c/c=-V_N/N_{GaN}$, where V_N is the nitrogen vacancy density and N_{GaN} is the number of GaN molecules. With an increase in growth rate Lagerstedt and Monemar also observed an increase in the *a* and *c* lattice parameters, which they attributed to an increase in interstitial species. Overall, up to a 1% variation in the lattice parameters was observed for undoped GaN.

Kisielowski *et al.*[34] were able to use Raman and photoluminescence spectroscopies in conjunction with XRD to demonstrate the coexistence of hydrostatic and biaxial strain in GaN. The biaxial strain resulted from a lattice mismatch, while the hydrostatic strain was shown to result from point defects. Using high resolution XRD, Harutyunyan *et al.*[35] built on the earlier work of Kisielowski *et al.*[34] analyzing the effect of buffer layer stoichiometry on the strain in GaN films. Residual hydrostatic strain in the epilayers was attributed to the presence of point defects.

For the case of InN, the XRD stress analysis of Specht *et al.*[13] is particularly useful. In that paper the strain effects of pure hydrostatic, biaxial (basal plane), and uniaxial (linear) stress applied along the *c* axis have been calculated. The lattice parameters calculated by Specht *et al.* for pure instances of the three types of stress are shown in Fig. 6.

It is worth reiterating at this point that the MBE and RPE-CVD samples examined here are from the upper and middle sections of the defect line given in the absorption edge versus carrier concentration plot of Fig. 1. That is, they are of medium to high carrier concentration and have been shown to be nitrogen rich.[12] Samples of lower carrier concentration at the lower end of the defect line, with ~0.65 eV absorption edge, tend to be much thicker than the samples examined here and may exhibit different defect structures and therefore different XRD lattice constants. Certainly in contrast to the material we have examined, there has been some ~0.65 eV material with reported *c* lattice constant values that are lower than the accepted value,[4,36] indicating the presence of a different type of defect than those examined here, possibly related to indium rich stoichiometry.

Downloaded 21 Jun 2007 to 131.251.0.11. Redistribution subject to AIP license or copyright, see http://jap.aip.org/jap/copyright.jsp

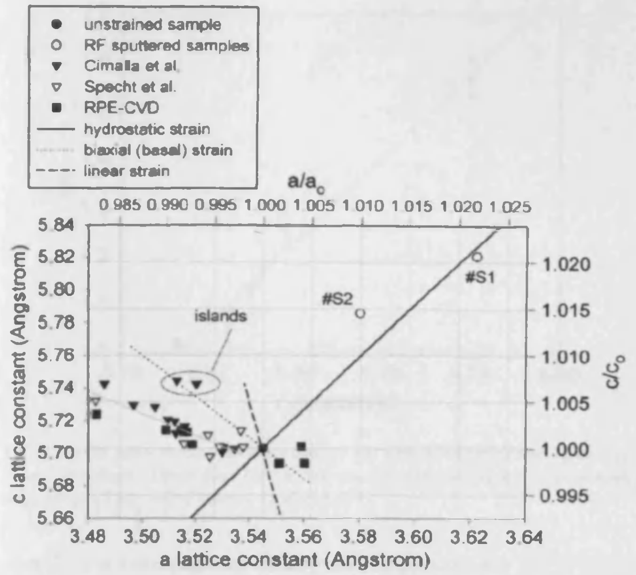

FIG. 6. The figure shows the theoretical strain cases for the three different types of stress shown (i.e., hydrostatic, biaxial, and uniaxial). Data for two nitrogen rich rf sputtered InN samples (S1 and S2), MBE data reported in the literature and RPE-CVD data, are also shown. An approximate line of fit through the MBE and RPE-CVD data is shown to aid the comparison. The island growth data of Cimalla *et al.* (Ref. 40) is shown for interest.

rf sputtered InN samples can have quite large amounts of excess nitrogen present.[1–3] An example of this is shown in Table I. As reported elsewhere,[1–3,10,12] the table also shows that there is an increase in the c-axis lattice constant associated with high levels of excess nitrogen content. These rather large changes in lattice constant indicate that the incorporation of excess nitrogen is accompanied by considerable strain. Some recent reports (for example, Davydov *et al.*[37]) have suggested that this change in lattice constant is the result of InN:In$_2$O$_3$ alloying. However, as outlined by Butcher[5] and by Butcher and Tansley,[6] this form of alloy does not occur to any significant extent, most oxygen being present in InN as a segregated amorphous contribution at the InN grain boundaries. This has very recently been confirmed by Xu *et al.*, who have made observations of oxygen segregation in MBE grown InN that suggest that the solubility of oxygen in InN is less than 1%.[38] The presence of some small portion of the oxygen as a substitutional oxygen on nitrogen donor species is, of course, not excluded, and may possibly be present in some cases. However, the low solubility of oxygen in InN places an upper limit on the presence of this form of oxygen in InN. Hence, the greater portion of the oxygen segregates to grain boundaries. It should be noted, however, that even if the solubility of oxygen in InN were close to the 1% upper limit, the hydrostatic lattice strain shown in Fig. 6 is greater than 2% in both the c and a parameters for sample S1. This corresponds to a lattice volume expansion of over 6%. Therefore, there is no possibility that oxygen could be responsible for the hydrostatic strain shown in the rf sputtered samples, despite the relatively high oxygen content of the rf sputtered films.

The extent and type of stress resulting from excess nitrogen incorporation can be determined by a comparison with the unstressed lattice constants. Here, we use the values of $a=3.545$ Å and $c=5.703$ Å used by Specht *et al.*[13] Both lattice constants are required for a proper evaluation. Goldhahn *et al.*[36] have provided values for two nitrogen rich rf sputtered samples from our laboratory. These samples had $c=5.821$ and 5.786 Å and $a=3.622$ and 3.58 Å for InN grown on glass (S1) and Si (S2), respectively. These values are plotted in Fig. 6. For the case of pure hydrostatic strain, the c and a axes change in proportion to each other, as shown by the straight solid line in the figure. Sample S1 on amorphous glass shows pure hydrostatic stress within the range of experimental error. Sample S2 on Si shows a slight deviation from a pure hydrostatic situation, which may relate to the lattice mismatch between the substrate and the film. However, it appears to still have a very large component of hydrostatic stress apparent. In analogy to GaN, an increase in hydrostatic stress for InN can be related to the homogeneous incorporation of point defects. Hydrostatic strain in InN may result from N_{In} and In_N substitutional point defects, V_N and V_{In} vacancies and from N_i and In_i interstitial native point defects. Given the large covalent radius of In compared to N, the point defects In_N, N_i, and In_i are expected to result in lattice expansion, whereas the other point defects should lead to lattice compression. Since excess nitrogen has been identified in these films by ERDA measurements, it would appear that the XRD data are commensurate with an increase in some form of interstitial nitrogen or an interstitial complex involving nitrogen. The XPS results in the previous section have shown the presence of a peak at approximately 397.8 eV, which may be attributed to an atomic nitrogen species in rf sputtered InN. Therefore, we attribute the positive hydrostatic strain in rf sputtered materials to the presence of a large density of what tentatively appears to be atomic nitrogen interstitials in the lattice.

The N/In ratios shown in Table I for RPE-CVD samples demonstrates that other methods of growth can also access conditions that result in large amounts of excess nitrogen. We have investigated the a and c lattice parameters of such epitaxial films using a high resolution Philips Xpertz x-ray diffraction system and have found that they do not indicate the hydrostatic expansion of the nonepitaxial polycrystalline rf sputtered samples. This is shown in Fig. 6, but is shown elsewhere to also be true for much larger values of film strain that result from exceptionally high values of excess nitrogen in epitaxial InN films.[12] A comparison of Figs. 1 and 6 in Ref. 12 show the strong correlation between the N/In ratio and the strain in the RPE-CVD based material. This correlation is also shown in our Fig. 7, where the RPE-CVD data of Fig. 6 and other RPE-CVD data are replotted showing the N/In ratio for that data versus the c axis lattice parameter. The combined foreign impurity concentrations (hydrogen, oxygen, and carbon) of the samples in Ref. 12 are far too low to account for any notable change in the strain of the samples compared to the much larger amounts of excess nitrogen present. It should be noted that other InN data, which were shown not to follow the carrier concentration versus absorption edge trend represented by the curve in Fig. 1 (Ref. 39)—some of which is represented in Table I—do not follow the trend of Fig. 7. For the readers' interest, Fig. 8 shows the

Downloaded 21 Jun 2007 to 131.251.0.11. Redistribution subject to AIP license or copyright, see http://jap.aip.org/jap/copyright.jsp

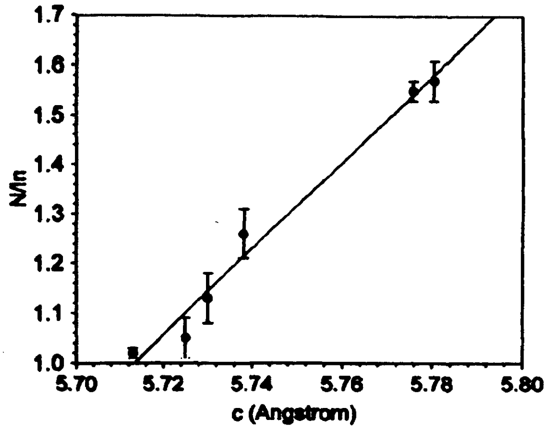

FIG. 7. N/In ratio vs the *c* axis parameter for RPE-CVD data shown in Fig. 6 and elsewhere. These data follow the carrier concentration vs absorption edge trend of the curve shown in Fig. 1.

correlation between the absorption edge and the N/In ratio for RPE-CVD that follows the absorption edge versus carrier concentration trend represented by the curve in Fig. 1.

VI. DISCUSSION

As shown in Table I and elsewhere,[3,21] between 2% and 7% excess nitrogen has been observed for the thin (<1 μm) MBE samples examined here. Similar and higher values have been observed for RPE-CVD grown materials dependent on the growth temperature.[12] For both MBE (Refs. 7 and 40) and RPE-CVD (Ref. 18) materials the carrier concentration has been observed to decrease as the film thickness is increased, indicating a source of donors near the interface. XRD indicates the origin of a second form of excess nitrogen related to this effect. Figure 6 shows data from Cimalla *et al.*[40] and Specht *et al.*[13] for MBE grown InN and also some of our data for RPE-CVD samples. The data of Cimalla *et al.* is for a series of Cornell MBE samples of increasing thickness, the thinnest samples showing the greatest strain, and samples of 1 μm thickness showing the least strain on the graph. Cimalla *et al.* attributed the strain in their samples to a biaxial stress caused by the lattice mismatch between the InN and the GaN and AlN buffer layers used. It is evident in the figure, however, that the strain of their samples was not purely biaxial (except perhaps for their reported island growth case, as shown in Fig. 6). Even taking into account the possibility of the unstrained lattice values being closer to those given by other authors,[41,42] it is apparent that the data of Cimalla *et al.*,[40] and Specht *et al.*,[13] and also the RPE-CVD data shown in the figure, all have a reduced lattice volume compared to the case of pure biaxial strain. Vector analysis therefore indicates that a component of either hydrostatic strain or linear strain is present. Hydrostatic strain is the expected result in the case where simple native point defects are incorporated, and given the nonstoichiometry of the material, it is the more likely of the two possibilities. Both of these cases, however, are likely to involve the incorporation of defects, with a higher density of defects being present with higher strain values, i.e., near the substrate interface. Interestingly, the greatest strain observed for the RPE-CVD samples occurred for those samples grown at the lower growth temperatures investigated, i.e., those samples with higher excess nitrogen content[12] indicating that other growth conditions can be important. It should be noted that in Fig. 6 the more heavily strained RPE-CVD samples, and also the more heavily strained MBE samples studied by Cimalla *et al.*,[40] were those with the highest carrier concentrations. The introduction of point defects into these heavily strained samples undoubtedly occurs as a means of stress reduction that becomes energetically more favorable as the stress in the film increases. The case for these epitaxial InN samples therefore appears to be analogous to observations of combined hydrostatic and biaxial stress in GaN, where biaxial stress due to lattice mismatch has been shown to be accompanied by hydrostatic stress due to point defects, which themselves result from stoichiometry variations.[34,35]

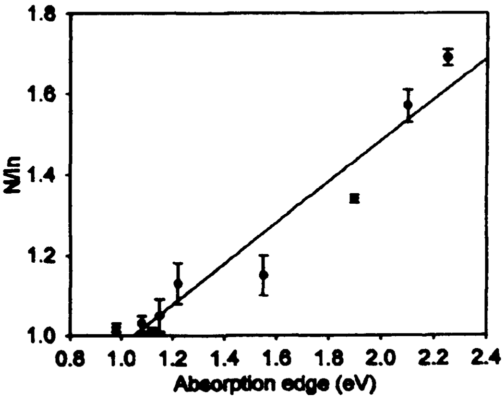

FIG. 8. N/In ratio vs absorption edge data for RPE-CVD data that follow the carrier concentration vs absorption edge trend of the curve shown in Fig. 1.

It is evident in Fig. 6 that a significant reduction of the *c* lattice parameter occurs for the MBE and RPE-CVD samples compared to the pure biaxial strain case. There are only three of the six simple native defects that could result in this reduction: nitrogen vacancies, indium vacancies, and nitrogen-on-indium antisite defects (since the nitrogen ion is smaller than the indium ion). Laakso *et al.*[43] carried out positron annihilation experiments on MBE grown samples from the same source as that used by Cimalla *et al.* and were not able to observe any nitrogen vacancies. Although this does not exclude their presence, the overall nitrogen rich stoichiometry of these thin films (<1 μm) would suggest that significant concentrations of nitrogen vacancies are not present. However, indium vacancies were observed by Laakso *et al.*, and their density was found to be considerably higher near the substrate interface. An exact value of the In vacancy concentration at the interface could not be determined by Laakso, though a lower limit of 5×10^{18} cm^{-3} for the thinnest sample examined (120 nm) was determined. This value may be as much as an order of magnitude too low to explain the change in the *c* lattice constant shown in Fig. 6 for samples of Cimalla *et al.* of ~100 nm thickness. For samples of that thickness a 0.3%–0.5% difference in the lattice constant is shown, compared to pure biaxial strain (dependent on the exact value of the zero strain lattice constants) and should

Downloaded 21 Jun 2007 to 131.251.0.11. Redistribution subject to AIP license or copyright, see http://jap.aip.org/jap/copyright.jsp

equate to a vacancy concentration estimated at least 5×10^{19} cm^{-3}. Another problem is that In vacancies are believed to be shallow acceptors in InN rather than donors,[17,44] so that the presence of In vacancies does not explain the strong n-type conductivity of the material, though it may explain the presence of the high levels of compensating acceptors, as have been observed by Look *et al.*[11] for Cornell n-type MBE materials.

The excess nitrogen observed by ERDA (again for MBE samples from the same source as that examined by Cimalla *et al.*, i.e., Cornell samples) is also not fully explained by the relatively low density of indium vacancies present. The XPS surface results of Table II indicate that at least two forms of nitrogen defect can be present in the epitaxial RPE-CVD and MBE samples. One of these is a relatively low concentration of atomic nitrogen, also observed for the polycrystalline rf sputtered and reactively evaporated materials, that is most likely an interstitial species and possibly a significant donor species for this material, though its presence does not explain the reduction in lattice constants for the MBE and RPE-CVD samples compared to the pure biaxial stress case. The origin of the second, higher density species observed by XPS at a binding energy of ~396.9 eV is less certain. Given the presence of the interstitial species and the presence of indium vacancies, it seems a strong possibility that a mobile interstitial nitrogen atom may be available to fill an indium vacancy. Room temperature mobility of excess nitrogen has been observed in rf sputtered samples.[2] A high level of nitrogen-on-indium sites would explain both the low c lattice constant observed for the samples of Fig. 6 (compared to the case of pure biaxial strain) and the presence of excess nitrogen in thin MBE samples. The theoretical results of Stampfl *et al.*[17] and of Jenkins and Dow[44] indicate that the nitrogen on the indium antisite defect will act as a deep level trap for both electrons and holes in InN. Hence, if this defect is present, it will be optically active but will not supply donor species. The increased n-type carrier concentration observed for thin, more heavily strained MBE samples and for thin, nitrogen rich (also more heavily strained) RPE-CVD samples may be explained by the presence of the interstitial nitrogen species, present in lower concentrations than the ~396.9 eV defect, but as shown in Fig. 4 the ~397.8 eV defect (attributed to interstitial nitrogen) is observed to be present at higher concentrations for those samples with higher carrier concentrations. The donor capability of interstitial nitrogen has not been investigated theoretically for InN. However, its presence in large quantities in some rf sputtered material may explain the high n-type carrier concentrations observed for those samples.

One interesting point to note is that the XPS results above confirm the presence of a nitrogen related surface defect for both MBE and RPE-CVD grown InN (the ~396.9 eV defect). Furthermore, this defect does not appear to be present for the rf sputtered or reactively evaporated nonepitaxial polycrystalline materials. Given that the film surface and the substrate-film interface both represent discontinuities of the film, some defects may be common at both interfaces, though further research may be necessary to confirm this. We suggest, however, that the nitrogen-on-indium antisite defect may be incorporated in the strained region near the substrate interface for InN on GaN or AlN buffer layers, and for InN on sapphire. A higher density of this defect present for thin epitaxial samples and for those grown at lower temperatures, in combination with associated indium vacancies and nitrogen interstitials, as described above, may be responsible for some portion of the upper part of the carrier concentration dependent absorption edge data observed for epitaxial InN materials and represented by the curve in Fig. 1. In contrast, the presence of large amounts of interstitial atomic nitrogen (without indium vacancies or nitrogen on indium antisite defects) in the polycrystalline materials may dominate their optical absorption properties through different mechanisms (albeit yet to be properly understood) and result in the higher apparent band gap observed for those materials over a wide range of carrier concentrations.

VII. CONCLUSIONS

We have shown, through a combination of ERDA, XPS, and XRD results, that at least two distinct nitrogen related defects are observed in indium nitride materials. What appears to be an interstitial form of atomic nitrogen is present in many forms of InN but appears to have a relatively high concentration density in rf sputtered polycrystalline nonepitaxial InN. Another native defect was shown to be prevalent in epitaxial InN grown by MBE or RPE-CVD in strained regions such as that near the interface between the substrate and film, where a combination of a biaxial and what is probably a hydrostatic strain is evident. On the basis of XRD and XPS data we suggest that the source of this defect may be a combination of indium vacancies and a higher density of nitrogen-on-indium antisite defects, though more complex defect structures certainly cannot be ruled out as possible explanations at this stage. The effects of these defects in epitaxial materials were most prominent for thinner films and for films with greater overall excess nitrogen present. This is shown by XRD data, which indicate a stronger deviation from unstrained values for such films. Higher carrier concentrations are also present in such circumstances, though this may be related to the interstitial nitrogen also present at higher concentration. XPS also reveals an increased contribution to a N 1s photoelectron peak at ~369.9 eV, which may be related to the presence of nitrogen on indium antisite defects in epitaxial materials. We further suggest that the carrier concentration related dependence observed for the optical absorption edge data of MBE and other epitaxial materials is strongly related to the presence of the defects present in this materials. The different defect structures observed for polycrystalline materials, may be related to the different optical absorption edge and electrical properties seen for that material.

ACKNOWLEDGMENTS

The authors would like to acknowledge the support of an Australian Research Council Discovery grant and of a Macquarie University Research Development grant. They would

Downloaded 21 Jun 2007 to 131.251.0.11. Redistribution subject to AIP license or copyright, see http://jap.aip.org/jap/copyright.jsp

also like to thank Dr. W. Schaff of Cornell and Dr. S. Ivanov of the Ioffe Institute for the supply of samples.

[1] K. S. A. Butcher, M. Wintrebert-Fouquet, Motlan, S. K. Shrestha, H. Timmers, K. E. Prince, and T. L. Tansley, Mater. Res. Soc. Symp. Proc. **743**, 707 (2003).

[2] K. S. A. Butcher *et al.*, J. Appl. Phys. **95**, 6124 (2004).

[3] H. Timmers, S. K. Shrestha, and A. P. Byrne, J. Cryst. Growth **269**, 50 (2004).

[4] T. V. Shubina *et al.*, Phys. Status Solidi A **202**, 377 (2005).

[5] K. S. A. Butcher, in *InN, an Historic Review: From Obscurity to Controversy*, Advanced Material in Electronics, edited by Q. Guo (Research Signpost, Kerala, India, 2004), p. 1.

[6] K. S. A. Butcher and T. L. Tansley, Superlattices Microstruct. **38**, 1 (2005).

[7] H. Lu, W. J. Schaff, L. F. Eastman, J. Wu, W. Walukiewicz, D. C. Look, and R. J. Molnar, Mater. Res. Soc. Symp. Proc. **743**, 317 (2003).

[8] B. R. Nag, J. Cryst. Growth **269**, 35 (2004).

[9] V. M. L. Chin, T. L. Tansley, and T. Osotchan, J. Appl. Phys. **75**, 7365 (1994).

[10] K. S. A. Butcher, H. Hirshy, R. M. Perks, M. Wintrebert-Fouquet, and P. P.-T. Chen, Phys. Status Solidi A **203**, 66 (2006).

[11] D. C. Look, H. Lu, W. J. Schaff, J. Jasinski, and Z. Liliental-Weber, Appl. Phys. Lett. **80**, 258 (2002).

[12] P. P.-T. Chen *et al.*, J. Cryst. Growth **288**, 241 (2006).

[13] P. Specht, R. Armitage, J. Ho, E. Gunawan, Q. Yang, X. Xu, C. Kisielowski, and E. R. Weber, J. Cryst. Growth **269**, 111 (2004).

[14] J. C. Ho, P. Specht, Q. Yang, X. Xu, D. Hao, and E. R. Weber, J. Appl. Phys. **98**, 093712 (2005).

[15] K. S. A. Butcher *et al.*, Phys. Status Solidi C **2**, 2263 (2005).

[16] H. Lu, W. J. Schaff, J. Hwang, H. Wu, W. Yeo, A. Pharkya, and L. F. Eastman, Appl. Phys. Lett. **77**, 2548 (2000).

[17] C. Stampfl, C. G. Van De Walle, D. Voggel, P. Krugger, and J. Pollman, Phys. Rev. B **61**, R7846 (2000).

[18] M. Wintrebert-Fouquet, K. S. A. Butcher, and P. P.-T. Chen, J. Cryst. Growth **269**, 134 (2004).

[19] W. A. Grant, in *Rutherford Back-Scattering Spectroscopy*, Methods of Surface Analysis: Techniques and Applications, edited by J. M. Walls (Cambridge University Press, Cambridge, 1989), p. 299.

[20] J. M. Walls, in *Methods of Surface Analysis*, Methods of Surface Analysis: Techniques and Applications, edited by J. M. Walls (Cambridge University Press, Cambridge, 1989) p. 1.

[21] S. K. Shrestha, K. S. A. Butcher, M. Wintrebert-Fouquet, and H. Timmers, Nucl. Instrum. Methods Phys. Res. B **219–220**, 686 (2004).

[22] S. K. Shrestha and H. Timmers, Nucl. Instrum. Methods Phys. Res. B (in press), available online.

[23] *Auger and X-Ray Photoelectron Spectroscopy*, Practical Surface Analysis Vol. 1, 2nd ed., edited by D. Briggs and M. P. Seah (Wiley, Chicester, 1990).

[24] T. L. Barr, *Modern ESCA: The Principles and Practice of X-ray Photoelectron Spectroscopy* (CRC, Boca Raton, FL, 1994).

[25] S. Kumar, L. Mo, Motlan, and T. L. Tansley, Jpn. J. Appl. Phys., Part 1 **35**, 2261 (1996).

[26] J. F. Moulder, W. F. Stickle, P. E. Sobol, and K. D. Bomben, in *Handbook of X-Ray Photoelectron Spectroscopy*, edited by J. Chastain, p. 22. (Perkin-Elmer, Physical Electronics Division, Eden Prairie, 1992), p. 22.

[27] M. K. Bahl, R. O. Woodall, R. L. Watson, and K. J. Irgolic, J. Chem. Phys. **64**, 1210 (1976).

[28] J. A. Schreifels, J. E. Deffeyes, L. D. Neff, and J. M. White, J. Electron Spectrosc. Relat. Phenom. **25**, 191 (1982).

[29] M. Wintrebert-Fouquet, K. S. A. Butcher, and Motlan, Phys. Status Solidi C **0**, 2785 (2003).

[30] W. F. Egelhoff, Jr., Surf. Sci. Rep. **6**, 253 (1987).

[31] S. Kumar, K. S. A. Butcher, and T. L. Tansley, J. Vac. Sci. Technol. A **14**, 2687 (1996).

[32] B. Henderson, *Defects in Crystalline Solids* (Arnold, London, 1972), pp. 36–37, 136–138.

[33] O. Lagerstedt and B. Monemar, Phys. Rev. B **19**, 3064 (1979).

[34] C. Kisielowski *et al.*, Phys. Rev. B **54**, 17745 (1996).

[35] V. S. Harutyunyan, A. P. Aivazyan, E. R. Weber, Y. Kim, Y. Park, and S. G. Subramanya, J. Phys. D **34**, A35 (2001).

[36] R. Goldhahn *et al.*, Mater. Res. Soc. Symp. Proc. **743**, 361 (2003).

[37] V. Yu. Davydov *et al.*, Phys. Status Solidi B **234**, 787 (2002).

[38] X. Xu, P. Specht, R. Armitage, J. C. Ho, E. R. Weber, and C. Kisielowski, Appl. Phys. Lett. **87**, 092102 (2005).

[39] K. S. A. Butcher *et al.*, Phys. Status Solidi C **2**, 2263 (2005).

[40] V. Cimalla *et al.*, Phys. Status Solidi C **0**, 2818 (2003).

[41] W. Paszkowicz, R. Cerny, and S. Krukowski, Powder Diffr. **18**, 114 (2003).

[42] V. Yu. Davydov *et al.*, Phys. Status Solidi B **229**, R1 (2002).

[43] A. Laakso *et al.*, J. Cryst. Growth **269**, 41 (2004).

[44] D. W. Jenkins and J. D. Dow, Phys. Rev. B **39**, 3317 (1989).

Downloaded 21 Jun 2007 to 131.251.0.11. Redistribution subject to AIP license or copyright, see http://jap.aip.org/jap/copyright.jsp

phys. stat. sol. (a) **203**, No. 1, 66–74 (2006) / **DOI** 10.1002/pssa.200563504

Stoichiometry effects and the Moss–Burstein effect for InN

K. S. A. Butcher[*, 1], **H. Hirshy**[2], **R. M. Perks**[2], **M. Wintrebert-Fouquet**[1], and **P. P-T. Chen**[1]

[1] Physics Department, Macquarie University, Sydney, 2109 NSW, Australia
[2] Cardiff School of Engineering, Cardiff University, The Parade, Cardiff, CF24 3AA, UK

Received 18 August 2005, revised 12 October 2005, accepted 14 October 2005
Published online 4 January 2006

PACS 61.10.Nz, 68.55.Ln, 73.61.Ey, 78.20.Ci, 78.40.Fy

We examine the Moss–Burstein effect for InN and demonstrate an independent method for determing its magnitude for high carrier concentration material. Consequently it is shown that the extent of the Moss–Burstein effect is less than 0.72 eV for a high carrier concentration sample with a 1.88 eV absorption edge. Early results are also provided for high band-gap low carrier concentration InN films that can be grown reprodcibly, vindicating the work of early groups in the field. The role of stoichiometry is examined in relation to point defects that appear to be common to many forms of InN.

© 2006 WILEY-VCH Verlag GmbH & Co. KGaA, Weinheim

1 Introduction

In this paper we examine variations of the properties of InN that appear to be related to In : N stoichiometry. To this end the Moss–Burstein effect for InN is investigated and it is shown that the effect's maximum extent can be measured and that it is not as great as previously assumed. Consequently it is shown that MBE and other samples grown with high carrier concentration have a band-gap greater than 0.7 eV. It is also shown that InN grown by other techniques may have other band-gaps. Much of this change appears to be attributable to changes in stoichiometry rather than oxygen inclusion, quantum effects or the Moss–Burstein effect. Finally we report that low carrier concentration polycrystalline material can now be reproducibly grown with varying band-gap.

2 Problems with Moss–Burstein effect

A number of recent papers have assumed that for InN all the past variation in apparent band-gap measured by absorption methods may be explained by the influence of the Moss–Burstein effect, after taking into account band renormalisation [1–4]. Walukiewicz et al. [3] have attributed an increase in the absorption edge energy from 0.7 eV, to ~2.3 eV at a carrier concentration of 10^{21} cm^{-3}, to the Moss–Burstein effect. As illustrated in Fig. 1, the Moss–Burstein effect occurs in materials with high carrier concentration: for the effect to operate the carrier concentration must be above the conduction band density of states, i.e. the Fermi level (E_F) must be in the conduction band. When this occurs the valence band (VB) to conduction band (CB) transition energy of electrons, following optical absorption, is increased since the Pauli exclusion principle requires that electrons must transit to unfilled states above or near the Fermi level. The Moss–Burstein effect therefore causes an increase in the apparent band-gap of a material when measured by optical absorption. Figure 2 demonstrates some of the variation in apparent band-gap as measured by the absorption technique. From this figure it is evident that the assumption that the Moss–Burstein effect is the sole explanation for the variation in band-gap for InN based materials igno-

---

[*] Corresponding author: e-mail: sbutcher@physics.mq.edu.au

© 2006 WILEY-VCH Verlag GmbH & Co. KGaA, Weinheim

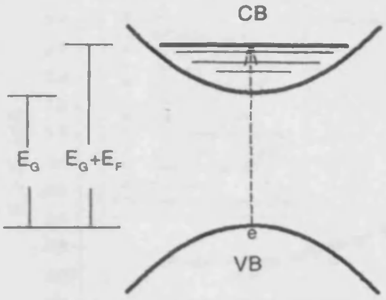

Fig. 1 Band diagram demonstrating the Moss–Burstein effect, E_G = band-gap energy, $E_G + E_F$ = band-gap plus Fermi energy.

res a large part of the literature on InN. There have been many reports of low carrier concentration high band-gap material. In fact there is such a wide variation in data for InN that at least five separate apparent Moss–Burstein trends have been reported over the years [3, 7, 8, 13, 18], and interestingly these trends appear to be related to the different methods of film growth used.

Somewhat incredibly, in their argument to support of the influence of the Moss–Burstein effect for InN, Yu et al. [4] have wrongly asserted that "Early optical absorption studies on InN films deposited by sputtering or e-beam evaporation with relatively high carrier concentrations ($>10^{19}$/cm^3) and low mobilities (<100 cm^2/V s) were used to derive a fundamental band gap of 1.9–2.1 eV."

This statement is certainly untrue, the early 1.89 eV band-gap of InN was bolstered by the work of Tansley and Foley [8], who were able to grow RF sputtered InN with a maximum room temperature electron mobility of 2700 cm^2/V s for a carrier concentration of 5.3×10^{16} cm^{-3} [19]. There have also been a number of other examples of low carrier concentration and/or high mobility material grown by RF or DC sputtering with high band-gaps ≥1.7 eV [9–11, 13, 20], and at least one report of epitaxial MBE material with a mobility of 600 cm^2/V s and room temperature band-gap of 2.1 eV [21]. The inability to reproduce such results in recent times has perhaps influenced the sensibilities of some researchers, however in a later section of this paper we are able to report results for InN that can reproducibly be grown with low carrier concentration and high to low band-gap. The higher band-gap examples of this material is shown to be in obvious contradiction to the Moss–Burstein effect proposed for MBE grown InN.

We suggested in an earlier publication that the large change in the absorption edge as a function of carrier concentration for MBE grown material was unlikely to be due to the Moss–Burstein effect alone [16].

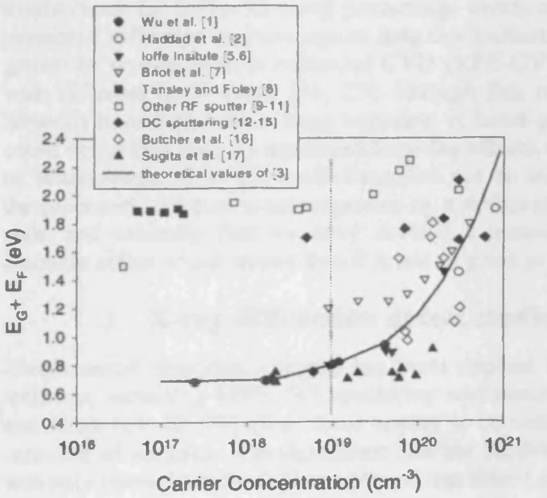

Fig. 2 $E_G + E_F$ values, found from absorption square data, versus carrier concentration. The solid line is the theoretical Moss–Burstein effect suggested by Walukiewicz et al. [3].

© 2006 WILEY-VCH Verlag GmbH & Co. KGaA, Weinheim

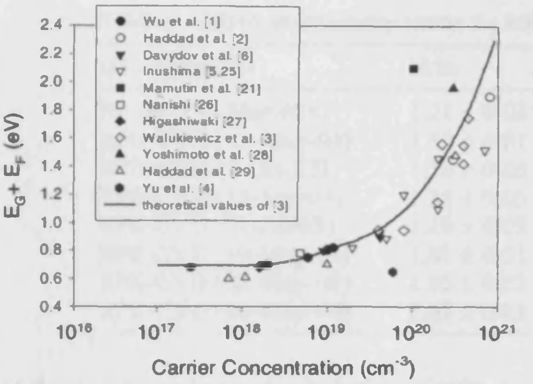

Fig. 3 Apparent band-gap versus carrier concentration for MBE grown material.

Figure 3 shows a collection of apparent band-gap information for MBE grown InN; the solid line again indicates the theoretical Moss–Burstein effect calculated by Walukiewicz et al. [3]. It is useful to point out for comparison the data point at 0.65 eV with carrier concentration 6×10^{19} cm^{-3}, which is for a polycrystalline sample recently reported by the Cornell group [4], and the data point at 2.1 eV with carrier concentration of 10^{20} cm^{-3} for epitaxial (single crystal) InN with electron mobility of 600 cm^2/V s reported by the Ioffe group in 2000 [21]. Though these two samples had similar carrier concentrations there was a difference of 1.45 eV in their apparent band-gaps, and most interestingly it was the epitaxial material that had the higher apparent band-gap – disspelling the myth that polycrystallinity is in some undefined way responsible for the observation of higher band-gap material, and bringing into question the extent of the Moss–Burstein effect compared to other effects that might influence the apparent band-gap of InN samples.

The belief in a strong Moss–Burstein effect for InN is soley based on observations of a change in apparent band-gap with carrier concentration, a trend which appears to be evident for much, though notably not all, of the data of Fig. 3. However other effects may have a carrier concentration dependence. The high carrier concentration of 10^{21} cm^{-3}, which is the approximate upper limit of unintentional doping in InN, equates to an impurity concentration of 3%. If this doping is due to native defects then it must result from sample nonstoichiometry and/or nonhomogeneity. Past elastic recoil detection analysis (ERDA) measurements of MBE grown material [11, 22, 23] indicates that excess nitrogen is a likely cause of such nonstiochiometry. It is well known that the inclusion of small amounts of nitrogen can result in large band-gap shifts for the dilute nitrides of GaAsN and GaInAsN (e.g. [24]). A similar effect might result for InN with small percentage levels of excess nitrogen present. In our previous papers we presented reflection and absorption data that indicated a different effective electron mass for InN samples grown by remote plasma enhanced CVD (RPE-CVD) with the same or similar carrier concentration but with different In:N ratios [16, 25]. Though this work indicated that an alloy system might well exist between In and N, with a large variation in band-gap indicated, the extent of the Moss–Burstein effect could not at that time be separated from the effects of such alloying. The proposed Moss–Burstein effect of Walukiewicz et al. [3] could therefore not be tested. However, we are now able to show, firstly that the proposed variation is accompanied by a defect structure seen for MBE and other closely related materials, and secondly that we have devised a means of measuring the maximum extent of the Moss–Burstein effect which shows that it is not as great as previously reported.

3 X-ray diffraction defect studies of InN

Elastic recoil detection analysis has been applied to a wide range of InN samples grown by different methods, including MBE, RF sputtering and remote plasma enhanced CVD (RPE-CVD). As reported elsewhere [11, 22, 23] all of these appear to be somewhat nitrogen rich. Table 1 demonstrates this for a selection of samples. It is significant that the ERDA results provided in Table 1, and in other references, was only carried out for InN samples of less than 1 micrometre thickness (a limitation of the technique).

© 2006 WILEY-VCH Verlag GmbH & Co. KGaA, Weinheim

Table 1 ERDA stoichiometry results for InN grown by various methods.

InN sample ID	N/In	InN sample ID	N/In
RF InN (20-Mar-03)	1.21 ± 0.03	MBE Ioffe InN W275	1.04 ± 0.02
RPE-CVD (17-May-04)	1.34 ± 0.01	MBE Ioffe InN W431	1.07 ± 0.03
RPE-CVD (3-Oct-03)	1.26 ± 0.05	MBE Cornell InN GS-1322	1.02 ± 0.02
RPE-CVD (15-Sep-03)	1.15 ± 0.05	MBE Cornell InN GS-1337	1.04 ± 0.03
RPE-CVD (31-Jul-03)	1.10 ± 0.03	MBE Cornell InN GS-1353	1.06 ± 0.03
RPE-CVD (19-May-04)	1.01 ± 0.01		
RPE-CVD (22-May-03)	1.05 ± 0.02		
RPE-CVD (26-May-04)	1.03 ± 0.01		

Unfortunately, as is discussed elsewhere [25], there appear to be no experimental techniques capable of measuring stoichiometry to an accuracy greater than ERDA, we must therefore rely on indirect methods of determining the stoichiometry and the nature of defects for InN, especially when the divergence from 1:1 stoichiometry is less than 2%. Specht et al. [31] have outlined the usefulness of X-ray diffraction in this case, and have calculated the change in the lattice parameters of hexagonal InN for pure cases of hydrostatic strain, biaxial (basal plane) strain and uniaxial (linear) strain. Figure 4 shows these cases of pure strain and also some X-ray diffraction data for RPECVD, MBE and RF sputtered samples.

Hydrostatic strain seems to be associated with the excess nitrogen present in RF sputtered samples. As shown in Table 1, very high levels of excess nitrogen have been found in some RF sputtered samples. Samples #S1 and #S2 in Fig. 4 were our RF sputtered samples measured by Goldhahn [32], the strong hydrostatic strain shown by these samples is commensurate with the presence of interstitial nitrogen the existence of which is postulated elsewhere [34]. Stampfl et al. [35] have pointed out that atomic interstitial nitrogen is unlikely to exist due to its high formation energy, the strong reactivity of atomic nitrogen also seems to preclude this possibility, however molecular nitrogen is known to incorporate in the dilute group III nitrides [36] and is a likely candidate here. Raman results showing the presence of molecular nitrogen near the surface of these samples would seem to confirm this possibility [34].

Samples grown by MBE and RPE-CVD show quite different results compared to RF sputtered samples, so far we have not detected the presence of interstitial nitrogen through X-ray diffraction measurements. Figure 4 shows data for MBE grown samples from two reports in the literature, and for some of

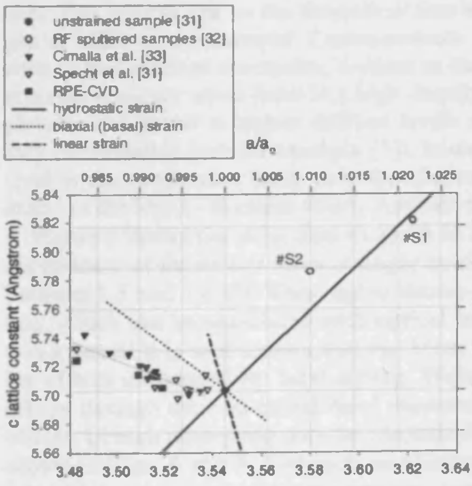

Fig. 4 Lattice constants found by X-ray diffraction for various InN samples.

© 2006 WILEY-VCH Verlag GmbH & Co. KGaA, Weinheim

our RPE-CVD samples (the growth of which is described elsewhere [37]). Interestingly these samples all appear to show the same trend. It is perhaps not surprising that data for RPE-CVD samples should seem similar to that for MBE samples, since the two growth techniques are somewhat similar, with RPE-CVD basically being a higher pressure form of MBE that uses a metalorganic as the metal source. The data of Cimalla et al. [33] is for samples grown by the Cornell group and shows greater divergence from the unstrained condition for thinner samples. In contrast the RPE-CVD data shows greater divergence for samples grown at lower temperature, which are also those samples that have a greater amount of excess nitrogen present. Although Cimalla et al. interpreted the strain in their films as being biaxial strain due to the lattice mismatch between the AlN and GaN buffer layers used and the InN epitaxial layers, it is evident from Fig. 4, that although some component of biaxial strain was present for those samples, the strain present was not pure biaxial strain, but a combination of biaxial and some other strain, either linear or hydrostatic. The presence of either of these alternate forms of strain is indicative of the inclusion of point defects in the InN lattice, and given that excess nitrogen has been identified by ERDA in thin (less than 1 micrometer) samples, and recalling that Cimalla et al. observed greater strain for thinner samples, it would seem that a stoichiometry related defect is apparent. Elsewhere we have speculated that nitrogen on indium anti-site defects and a lesser concentration of indium vacancies are probably indicated [38]. Interestingly the particular RPE-CVD samples shown in Fig. 4 also sit along the theoretical Moss–Burstein line of Walukiewicz et al. [3] shown in Figs. 2 and 3 (other RPE-CVD samples have been produced that sit above or below this line [16]) though with the samples with greater strain having higher carrier concentration and higher apparent band-gap [38]. The data of Specht et al. [31] also sits along the high carrier concentration part of the plot of Walukiewicz et al. though any correlation between strain and band-gap has not been reported in that article. It does appear however that highly strained samples, with excess nitrogen present are evident in the high carrier concentration limit of the theoretical plot of Walukiewicz et al., we therefore suspected that some component of the change in apparent band-gap might not be due to the Moss–Burstein effect but due to real changes in the band-gap related to the presence of excess nitrogen and the accompanying strain at the film-substrate interface.

4 The Urbach limit for the measurement of the Moss–Burstein effect

From the previous section it is evident that an independent measurement of the extent of the Moss–Burstein effect is required to help identify other carrier concentration dependent influences on the magnitude of the apparent band-gap. Figure 5 shows some temperature dependent absorption data for an RPE-CVD sample with a room temperature carrier concentration of 5×10^{20} cm^{-3}. The film has a room temperature $E_G + E_F$ value of 1.88 eV, as is clearly shown in the plot by the extrapolations of the absorption square data to the x-axis. This sample sits on the theoretical line of Walukiewicz et al. [3], and has similarly low levels of oxygen as MBE grown material. Commensurate with the high carrier concentration of this sample is the presence of free electron absorption, evident as the low energy absorption peak visible in the plot. Free electron absorption occurs when there is a high density of electrons in the conduction band. These electrons absorb photons and transit to higher unfilled levels above the Fermi level. The extent of free electron absorption may be modelled (see for example [2]), however such modelling cannot indicate the energy of the Fermi-level in the conduction band, only the electron density. Therefore it does not provide an indication of the extent of the Moss–Burstein effect. Another method is required to determine this information.

Figure 6 shows the same data as given in Fig. 5 but plotted as a logarithmic function. The temperature dependence of the data is more strongly evident in this plot, especially in the sub-band absorption region, between 1.5 and 1.8 eV. This region shows characteristics that are typical of an Urbach type of absorption, which can be associated with optical transitions involving band-tailing. For high carrier concentration material it is well known that the Moss–Burstein effect occurs in competition with the band lowering effects introduced by band tailing. Walukiewicz et al. [3] and Haddad et al. [2] accounted for such effects through their so-called band renormalization. Tansley and Foley [8] also took into account such effects. Urbach absorption may be identified through temperature dependent measurements such as those shown in Figs. 5 and 6. For such measurements the absorption (or absorption square) data is linear on a log plot over a range of temperatures, however a characteristic of Urbach absorption is that the plots

© 2006 WILEY-VCH Verlag GmbH & Co. KGaA, Weinheim

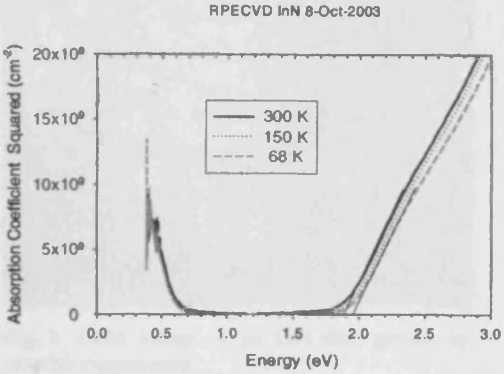

Fig. 5 (online colour at: www.pss-a.com) Absorption square plots measured at various temperatures for an RP-CVD grown InN sample.

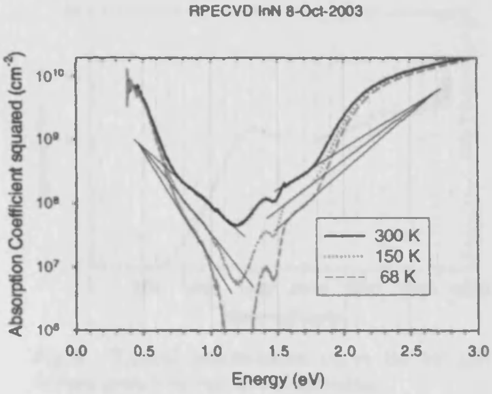

Fig. 6 (online colour at: www.pss-a.com) A log plot of the absorption data for the same sample as shown in Fig. 5.

measured at different temperatures extrapolate back to a single point sometimes referred to as the converging energy [39]. The data shown in Fig. 6, between 1.5 and 1.8 eV, is therefore a classic example of Urbach absorption due to the presence of band-tailing. The interesting thing about this plot is that a second Urbach region is evident between approximately 0.72 and 1.15 eV. This region is also caused by band-tailing, but is not due to band-tail to band transitions, as is the case for the higher energy Urbach region, but is due to transitions from band-tails extending from below the conduction band. These states are contributing to electron transitions to empty states above or near the Fermi level. This provides us with a useful probe of the maximum extent of the Moss–Burstein effect for this sample. The onset of the low energy Urbach region for the room temperature data occurs at approximately 0.72 eV. It can not be said with certainty that the onset of the Urbach region does not ocurr at lower energy since the actual onset may be buried in the free electron absorption peak, however the 0.72 eV visible onset value is a direct measure of the absolute maximum extent of the Moss–Burstein effect for this sample since the minimum energy at which this Urbach absorption can occur relates to electrons, in the tail states just below the conduction band minimum, transiting near to, or just above, the Fermi level. At room temperature with a value of $E_G + E_F$ equal to 1.88 eV, we can confidently say that the E_G for this sample is greater than or equal to 1.16 eV a value well above the 0.7 eV claimed for lower carrier concentration MBE material but apparently in excellent agreement, though perhaps only coincidentally, with the band-gap value reported by Maleyre et al. [7].

From this examination it is obvious that stoichiometry issues need to be given much greater consideration for InN than has previously been the case. It may well be that the higher carrier concentration InN actually has a different band-gap than some lower carrier concentration material, though this possibility clearly requires further investigation. It is however now evident that the theoretical calculations of $E_G + E_F$ for high carrier concentration material, given as E in the papers by Haddad et al. [2] and Walukiewicz et al. [3], were based on incorrect values of E_G in those papers and cannot be conjured as data supporting a 0.7 eV band-gap.

In the following section we show that large variations of band-gap are apparent even for samples with no free electron absorption.

5 Low carrier concentration InN by reactive evaporation

As mentioned above, the high band-gap low carrier concentration material of such workers as Tansley and Foley [8] has been questioned in recent years because of an inability to grow such films reproducibly. We had in fact obtained two lower carrier concentration, high band-gap InN samples by RF sputter-

© 2006 WILEY-VCH Verlag GmbH & Co. KGaA, Weinheim

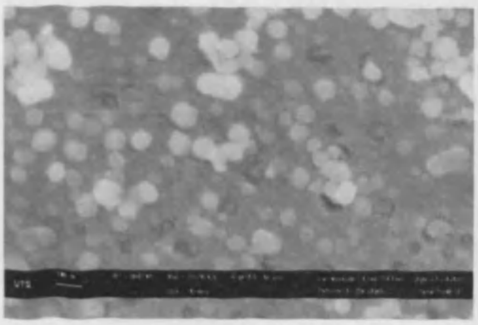

Fig. 7 SEM image of an InN film grown by reactive evaporation.

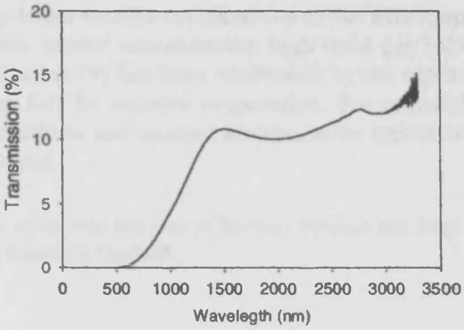

Fig. 8 Typical transmission curve for an InN sample grown by reactive evaporation.

ing in 2002 (briefly reported in [11]) but were unable to reproduce those results. To test an aspect of growth that may have been apparent during earlier work, we decided to attempt growth by reactive evaporation. The technique will be described more fully at a later date, basically it involves evaporating indium metal through a nitrogen plasma. Growth rates of approximately 5 μm/hour can be achieved, though not surprisingly X-ray diffraction indicates some free indium in all the films grown. The films are polycrystalline with misoriented grain structures. The crystallinity is typically much poorer than for RF sputtered material, though grains of up to 200 nm may be apparent (see Fig. 7) the strong *c*-axis orientation of sputtered material is not present. It is worth commenting however that this grain size is too large for quantum size effects to be present. Cimalla et al. [33] have calculated that a grain size of 20 nm would only result in a 0.03 eV shift in the absorption edge for InN.

SIMS results indicate that the films have oxygen levels of 10–20%, which is commensurate with a large available surface area between InN grains (see [25]). Despite this relatively high oxygen concentration, and the poor sample crystallinity a range of apparent band-gaps from 2.1 to below 0.7 eV can be accessed simply by varying the metal source-substrate distance. Figure 8 shows the transmission data for a typical sample, the most important feature of this spectrum is the total lack of any free carrier absorption at high wavelengths (low energies), only interference fringes are evident. This is indicative of samples with a relatively low carrier concentration, for InN, of probably less than 10^{19} cm^{-3}. In fact this appears to be a fairly typical result for this material, with almost all of the samples grown showing no evidence of free electron absorption. Preliminary Hall measurements have so far only been carried out for a few samples, but carrier concentrations range from 4×10^{17} to 2×10^{18} cm^{-3}, provided high currents are used to breakdown the oxide barrier at the sample surface. Electron mobilities are low to moderate (~ max. 170 cm^2/V sec), however from this data it is evident that the early reports of low carrier concentration polycrystalline material made by several pioneering InN research groups is vindicated. The physical cause of the low carrier concentrations observed is not yet understood, though it may relate to the indium inclusions present in the material. The variation of band-gap for this material is also not understood, though it appears to relate to sample stoichiometry. However, samples can be reproduced with relative ease for future study. It is further hoped that improved crystallinity will result in higher carrier mobilities for this material.

4 Conclusions

A new technique for determining the maximum extent of the Moss–Burstein effect has been demonstrated for high carrier concentration InN, and it is shown that a sample with band-edge absorption at 1.88 eV had a band-gap of greater than 1.16 eV. A value significantly larger than the 0.7 eV claimed for lower carrier concentration MBE grown InN. It is shown that the stoichiometry and defect structure of

© 2006 WILEY-VCH Verlag GmbH & Co. KGaA, Weinheim

InN samples is significant and it is suggested that these may make notable contributions to the band-gap variations observed for this material. The early reports of low carrier concentration, high band-gap InN by such workers as Tansley and Foley [8] and Hovel and Cuomo [9] has been vindicated by the reproducible growth of low carrier concentration, high band-gap InN by reactive evaporation. For material grown by this technique it is also shown that quantum size effects and oxygen incorporation appear to have little influence on the large variation of band-gaps observed.

Acknowledgements We wish to acknowledge the support of the Australian Institute of Nuclear Science and Engineering for SIMS measurements, and the support of the Australian Research Council.

References

[1] J. Wu, W. Walukiewicz, W. Shan, K. M. Yu, J. W. Ager III, E. E. Haller, Hai Lu, and W. J. Schaff, Phys. Rev. B **66**, 201403 (2002).
[2] D. B. Haddad, J. S. Takur, V. M. Naik, G. W. Auner, R. Naik, and L. E. Wenger, Mater. Res. Soc. Symp. Proc. **743**, 701 (2003).
[3] W. Walukiewicz, S. X. Lai, J. Wu, K. M. Yu, J. W. Ager III, E. E. Haller, Hai Lu, and W. J. Schaff, J. Cryst. Growth **269**, 119 (2004).
[4] K. M. Yu, Z. Liliental-Weber, W. Walukiewicz, W. Shan, J. W. Ager III, S. X. Li, R. E. Jones, E. E. Haller, H. Lu, and W. J. Schaff, Appl. Phys. Lett. **86**, 071910 (2005); carrier concentration of polycrystalline sample GS-1489 of Fig. 3 of Yu et al. provided by private communication with W. J. Schaff.
[5] T. Inushima, V. V. Mamutin, V. A. Vekshin, S. V. Ivanov, T. Sakon, M. Motokawa, and S. Ohoya, J. Cryst. Growth, **227–228**, 481 (2001).
[6] V. Yu Davydov, A. A. Klochikhin, V. V. Emtsev, S. V. Ivanov, V. V. Vekshin, F. Bechstedt, J. Furthmuller, H. Harima, A. V. Mudryi, A. Hashimoto, A. Yamamoto, A. J. Aderhold, J. Graul, and E. E. Haller, phys. stat. sol. (b) **230**, R4 (2002).
[7] B. Maleyre, O. Briot, S. Ruffenach, and B. Gil, phys. stat. sol. (c) **2**, 1379 (2005).
[8] T. L. Tansley and C. P. Foley, J. Appl. Phys. **59**, 3241 (1986).
[9] H. J. Hovel and J. J. Cuomo, Appl. Phys. Lett. **20**, 71 (1972).
[10] Motlan, E. M. Goldys, and T. L. Tansley, J. Cryst. Growth **241**, 165 (2002).
[11] K. S. A. Butcher, M. Wintrebert-Fouquet, P. P.-T. Chen, T. L. Tansley, and S. Srikeaw, Mater. Res. Soc. Symp. Proc. **693**, 341 (2002).
[12] V. A. Tyagai, A. M. Evstigneev, A. N. Krasiko, A. F. Andreeva, and V. Ya. Malakhov, Sov. Phys.-Semicond. **11**, 1257 (1977).
[13] B. R. Natarajan, A. H. Eltoukhy, J. E. Greene, and T. L. Barr, Thin Solid Films **69**, 201 (1980).
[14] K. L. Westra, R. P. W. Lawson, and M. J. Brett, J. Vac. Sci. Technol. A **6**, 1730 (1988).
[15] B. T. Sullivan, R. R. Parsons, K. L. Westra, and M. J. Brett, J. Appl. Phys. **64**, 144 (1988).
[16] K. S. A. Butcher, M. Wintrebert-Fouquet, P. P.-T. Chen, K. E. Prince, H. Timmers, S. K. Shrestha, T. V. Shubina, S. V. Ivanov, R. Wuhrer, M. R. Phillips, and B. Monemar, phys. stat. sol. (c) **2**, 2263 (2005).
[17] K. Sugita, H. Takatsuka, A. Hashimoto, and A. Yamamoto, phys. stat. sol. (b) **240**, 421 (2003).
[18] V. Yu Davydov, A. A. Klochikhin, V. V. Emtsev, S. V. Ivanov, V. V. Vekshin, F. Bechstedt, J. Furthmuller, H. Harima, A. V. Mudryi, A. Hashimoto, A. Yamamoto, A. J. Aderhold, J. Graul, and E. E. Haller, phys. stat. sol. (b) **230**, R4 (2002).
[19] T. L. Tansley and C. P. Foley, Electron. Lett. **20**, 1066 (1984).
[20] N. Puychevier and M. Menoret, Thin Solid Films **36**, 141 (1976).
[21] V. V. Mamutin, T. V. Shubina, V. A. Vekshin, V. V. Ratnikov, A. A. Toropov, S. V. Ivanov, M. Karlsteen, U. Sodervall, and M. Willander, Appl. Surf. Sci. **166**, 87 (2000).
[22] H. Timmers, S. K. Shrestha, and A. P. Byrne, J. Cryst. Growth **269**, 50 (2004).
[23] S. K. Shrestha, H. Timmers, K. S. A. Butcher, M. Wintrebert-Fouquet, and P. P.-T. Chen, Nucl. Instrum. Methods Phys. Res. B **234**, 291 (2005).
[24] W. Shan, W. Walukiewicz, J. W. Ager III, E. E. Haller, J. F. Geisz, D. J. Friedman, J. M. Olson, and S. R. Kurtz, Phys. Rev. Lett. **82**, 1221 (1999).
[25] K. S. A. Butcher and T. L. Tansley, Superlattices Microstruct. **38**, 1 (2005).
[26] T. Inushima, T. Sakon, and M. Motokawa, J. Cryst. Growth **269**, 173 (2004).

© 2006 WILEY-VCH Verlag GmbH & Co. KGaA, Weinheim

[27] Y. Nanishi, Y. Saito, and T. Yamaguchi, Jpn. J. Appl. Phys. **42**, 2549 (2003).

[28] M. Higashiwaki and T. Matsui, J. Cryst. Growth **251**, 494 (2003).

[29] M. Yoshimoto, H. Yamamoto, W. Huang, H. Harima, J. Saraie, A. Chayahara, and Y. Horino, Appl. Phys. Lett. **83**, 3480 (2003).

[30] D. B. Haddad, H. Dai, R. Naik, C. Morgan, V. M. Naik, J. S. Thakur, G. W. Auner, L. E. Wenger, H. Lu, and W. J. Schaff, Mater. Res. Soc. Symp. Proc. **798**, Y12.7.1 (2004).

[31] P. Specht, R. Armitage, J. Ho, E. Gunawan, Q. Yang, X. Xu, C. Kisielowski, E. R. Weber, J. Cryst. Growth **269**, 111 (2004); private communication with P. Specht indicates that the MBE films produced for this paper agree with the Moss–Burstein trend of Ref. [4].

[32] R. Goldhahn, S. Shokhovets, V. Cimalla, L. Spiess, G. Ecke, O. Ambacher, J. Furthmuller, F. Bechstedt, H. Lu, and W. J. Schaff, Mater. Res. Soc. Symp. Proc. **743**, 361 (2003).

[33] V. Cimalla, Ch. Förster, G. Kittler, I. Cimalla, R. Kosiba, G. Ecke, O. Ambacher, R. Goldhahn, S. Shokhovets, A. Georgakilas, H. Lu, and W. Schaff, phys. stat. sol. (c) **0**, 2818 (2003).

[34] K. S. A. Butcher, M. Wintrebert-Fouquet, P. P.-T. Chen, T. L. Tansley, H. Dou, S. K. Shrestha, H. Timmers, M. Kuball, K. E. Prince, and J. E. Bradby, J. Appl. Phys. **95**, 6124 (2004).

[35] C. Stampfl, C. G. Van De Walle, D. Voggel, P. Krugger, and J. Pollman, Phys. Rev. B **61**, R7846 (2000).

[36] W. Li, M. Pessa, T. Ahlgren, and J. Decker, Appl. Phys. Lett. **79**, 1094 (2001).

[37] M. Wintrebert-Fouquet, K. S. A. Butcher, and P. P.-T. Chen, J. Cryst. Growth **269**, 134 (2004).

[38] K. S. A. Butcher, P. P.-T. Chen, M. Wintrebert-Fouquet, H. Timmers, and S. K. Shrestha, Nitrogen Related Point Defects in InN, submitted.

[39] S. M. Wasim, C. Rincon, G. Marin, P. Bocaranda, E. Hernandez, I. Bonalde, and E. Medina, Phys. Rev. B **64**, 195191 (2001).

© 2006 WILEY-VCH Verlag GmbH & Co. KGaA, Weinheim

Realisation of a Novel GaN/ InN Heterostructure FET Device

D. Alexandrov[#1], R. Perks[#2], S. Butcher[#3], H. Hirshy[#2], J. Kettle[#2] and M. Wintrebert-Fouquet[#3]

[#1] Department of Electrical Engineering, Lakehead University, 955 Oliver Road, Thunder Bay, Ontario, P7B 5E1, Canada
[#2] Cardiff School of Engineering, Queens Buildings, The Parade, Cardiff, CF24 3AA, UK
[#3] Physics Department, Macquarie University, Sydney, 2109, NSW, Australia.

Abstract

In this paper we describe the theoretical background, material growth and fabrication process for a novel GaN/InN heterostructure field effect transistor. As proposed by Alexandrov [1], this study into the influence of exitons over the transport phenomena in Wurtzite $In_xGa_{1-x}N$ describes the formation of a conductive channel at the GaN/InN interface. The conductivity of such channel is dependent on the destruction of exitons in their interaction with the GaN – $In_{0.5}Ga_{0.5}N$ interface. Predicted output I-V characteristics of the device are shown in figure 1.

The GaN/InN heterostructure was grown using a remote plasma enhanced CVD process. A 50nm low resistivity InN layer was grown onto a sapphire substrate with a further 50nm of high resistivity GaN. A cross sectional diagram of the proposed device is given in figure 2.

We are currently investigating a two stage lithography process for the fabrication of these devices. Large scale features (typically <100μm) are to be defined through standard photolithography; for example, contact pads, mesa isolation. The small scale structures, namely the Source-Gate-Drain are defined using a Raith 50 electron beam lithography system. An example of test structures of different gate length is shown in figure 3. These features were written into PMMA resist. Following development, a 50nm layer of gold was deposited onto the PMMA; the resultant gold features were defined following lift off. Mesa isolation is defined through dry etching. An Oxford Instruments inductively coupled plasma etching system using BCl_3/Cl_2 chemistry has been used to investigate the etching characteristics of this layer structure. Simple indium metal ohmic contacts are proposed for the Source and Drain. We are currently investigating the possibility of utilising FOx® flowable oxides from Dow Corning in the Gate isolation layer. This material is cured through electron beam exposure.

References

[1] Alexandrov D, *"Exitons of the structure in wurtzite $In_xGa_{1-x}N$ and their properties"*, J. Cryst. Growth, 246, 325-340, (2002)

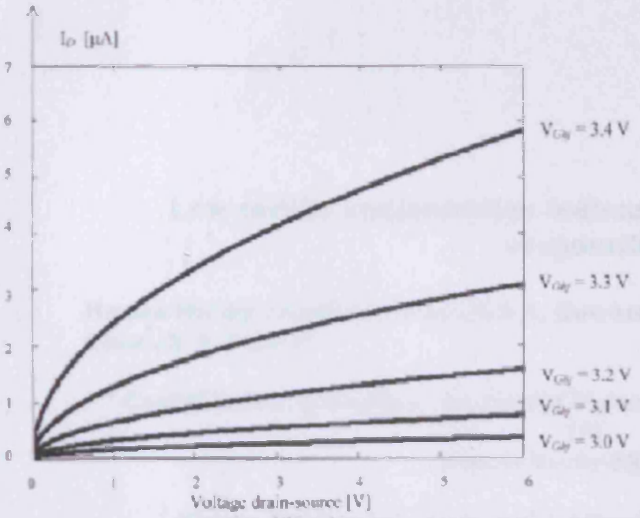

Figure 1: Output current – voltage characteristics of n-channel FET.

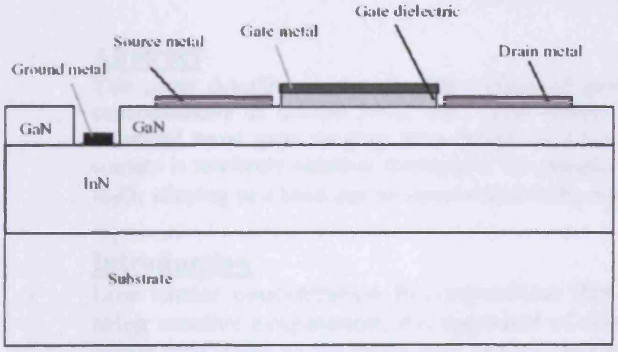

Figure 2: Cross section of the proposed device.

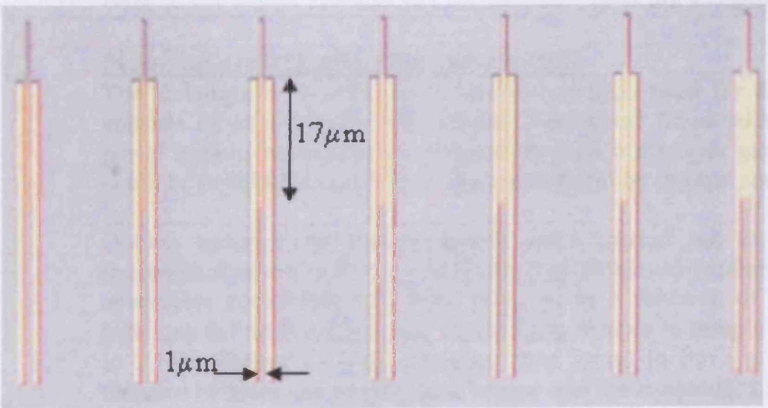

Figure 3: Source-Gate-Drain features defined by electron beam lithography following a gold lift off process.

Low carrier concentration indium nitride grown by reactive evaporation

Hassan Hirshy[1], Richard Perks[1], K.S.A. Butcher[2], M. Wintrebert-Fouquet[2], P. P-T Chen[2], K.E. Prince[3]

[1] *Cardiff School of Engineering, Cardiff University, The Parade, Cardiff, CF24 3AA, UK.*
E-mail:HirshyH@cf.ac.uk

[2] *Physics Department, Macquarie University, Sydney, NSW 2109, Australia.*

[3] *Australian Nuclear Science and Technology Organisation, Private Mail Bag 1, Menai, NSW 2234, Australia.*

Abstract

This paper describes a reproducible method of growing thin film Indium Nitride with low carrier concentrations of around $3\times10^{17}cm^{-3}$. This simple growth method yields thin film material with measured band gaps ranging from 0.7eV to 2.1eV. Compositional studies show that the oxygen content is relatively constant throughout the samples; this brings into question the influence of InN–In_2O_3 alloying as a band gap moderator and shifts emphasis towards material stoichiometry.

Introduction

Low carrier concentration Polycrystalline thin films of Indium nitride have been grown using reactive evaporation. An appraisal of this material in terms of its important material parameters, such as the band-gap, lattice constants and effective electron mass is described by Butcher and Tansley [1]. Reports suggesting a band gap of 0.65eV for this material [2] seem to contradict much of the earlier work claiming a higher band gap of around 2eV [3].

Material growth and characterization

The technique of reactive evaporation has been used for the growth of InN. The system consists of an Edwards 308 thermal evaporator fitted with DC plasma electrodes. High purity indium metal was evaporated through a nitrogen gas plasma. The substrate holder could be positioned at different distances from the indium source.

Optical transmission measurements were carried out at room temperature using the spectrophotometer with a spectral range of 200nm to 3300nm. Measurements of the optical absorption coefficient (a^2) were obtained as a function of photon energy. The measured band gap for different samples varied from sample to sample with values in the range 0.7eV to 2.1eV (Figure 1). This variation was found to have a functional dependence on the distance between the evaporation source and the substrate. Lower or higher band gaps were obtained when the substrate was respectively positioned closer to, or further from the evaporation source. This is presumed to be dependent on the amount of In that is incorporated in the growth.

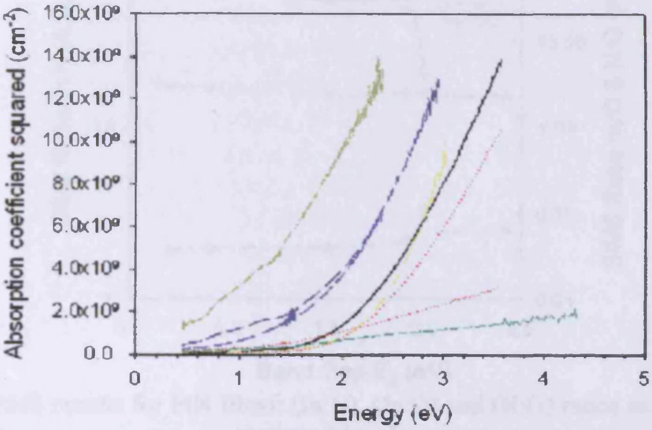

Figure 1: Absorption spectra for a range of different InN samples.

The resistivity was found to be in the range 1.0 to 1.3 ? -cm. Furthermore, the Hall measurements confirm the low carrier density inferred by the optical transmission measurements. The carrier concentration of high band gap (1.9eV) InN on sapphire was found to be as low as 3×10^{17}cm^{-3} with a mobility ranging between 25–50 cm^{2}V^{-1}s^{-1}. For low band gap (0.7eV) InN, the mobility ranged between 30–125cm^{2}V^{-1}s^{-1} but with carrier concentration of 2–7×10^{18}cm^{-3}. The low mobility can be attributed to the poor crystalline structure of the films [4].

The XRD spectra showed that the films are polycrystalline and not c-axis oriented. Both lattice parameters could therefore be easily extracted. The lattice constants were found to be a=3.513Å and c=5.7909Å. The presence of the Indium (101) peak in the XRD spectra, characteristic of metallic In, suggests some degree of In agglomeration in the film. This is in fact confirmed by the presence of In droplets, details of which may be found in Butcher et al [5].

A reference sample of polycrystalline RF sputtered InN with a known oxygen composition (obtained via ERDA) was used to compare the SIMS data for these samples (Figure 2). The amount of oxygen in the films was estimated to be up to ~ 20 atomic percent. The important point here is the ratio of indium to oxygen in the low band gap InN (0.7eV) and the high band gap (~2eV) are similar. This provides evidence that InN – In_2O_3 alloying is not the origin of the large optical band gap variations found in InN thin films; rather, it is more likely related to the In:N ratio and material stoichiometry [5].

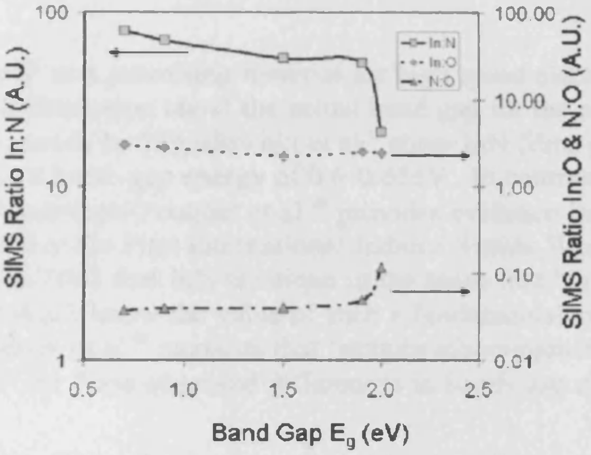

Figure 2: SIMS results for InN films: (In:N), (In:O) and (N:O) ratios as a function of measured band gap.

Conclusions

Low carrier concentration (3×10^{17}cm-3 to 7×10^{18}cm^{-3}) InN thin films have been grown reproducibly using reactive evaporation in the presence of a dc nitrogen plasma at room temperature. Other growth techniques such as RF sputtering generally yield carrier concentrations greater than 1×10^{19}cm^{-3}. Band gaps have been measured for different samples grown by this method ranging from 0.7eV to 2.1eV; these values were derived from the optical absorption data and were found to be related to the amount of In incorporated during the growth. This technique yielded polycrystalline with hexagonal structure. Compositional studies (SIMS) indicate that the oxygen content is relatively constant through the entire set of samples; this brings into question the influence of InN – In_2O_3 alloying as the source of band gap variability.

References:

[1] K. S. A. Butcher and T. L. Tansley, Superlattices and Microstructures, 38, 1 (2005).

[2] M. Higashiwaki, T. Matsui, J. Cryst. Growth, 269, 162, (2004).

[3] T. L. Tansley and C. P. Foley, J. Appl. Phys., 59, 3241, (1986).

[4] A. Ohtomo, H. Kimura, K. Saito, T. Makino, Y. Segawa, H. Koinuma and M. Kawasaki, J. Cryst. Growth 214-215, 284-8, (2000).

[5] K.S.A. Butcher, H. Hirshy, R.M. Perks, M. Wintrebert-Fouquet and P. P-T. Chen, Phys. Stat. Sol. (a) 203, 1, 66-74, (2006).

Variations in the observed band gap of Indium Nitride.

Richard Perks and Hassan Hirshy
Cardiff School of Engineering, Cardiff University, The Parade, Cardiff, CF24 3AA, UK

Introduction

The emergence of InN[i] as a promising material for high speed electronic devices has brought with it much discussion about the actual band gap for the material. For example, estimations made by Higashiwaki et al [ii] show InN films grown by plasma assisted MBE to have a band-gap energy of 0.6-0.65eV. In contrast, recent RPE CVD material grown by Wintrebert-Fouquet et al [iii] provides evidence for a band gap closer to 1.8eV. It was noted at the First International Indium Nitride Workshop in Fremantle Australia in 2003 that InN is unique in the sense that "in the dawn of the 21st century, we still don't know the value of such a fundamental material property". The work of Alexandrov et al [iv] suggests that 'sample inhomogeneity offers a strong possible explanation' for these observed differences in band- gap energy.

The Band Gap Challenge

Most Indium Nitride material grown currently is not homogeneous, poor lattice matched substrates result in variable quality growth. Interfacial or nucleation layers form a region near substrate which is poly-crystalline; as the film thickens, the material begins to coalesce. These features can be seen in figure 1 below. This is a cross section of InN grown by RPE CVD (courtesy of S. Butcher, Macquarie University, Australia).

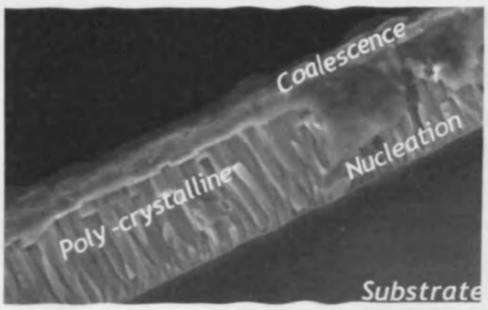

Figure 1 : SEM of RPE CVD InN

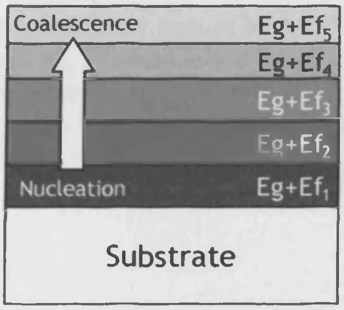

Figure 2 : Simplified inhomogeneity

Figure 2 illustrates a simplified model of inhomogeneous material growth. Standard absorption measurements 'see' a convoluted apparent band gap, with defect density decreasing away from the substrate. The influence of the Moss-Burstein shift described by the Fermi Energies $Ef_1>Ef_2>$...etc; assuming the band gap energy Eg is constant.

Experimental Observations

Inr our experiments, we devised a system that would allow highly localised optical absorption measurements to be made. InN samples were placed on a moveable x-y-z micrometer stage, in between a white light source and a small diameter (<50μm) glass fibre. This fibre was coupled to a spectrometer where the optical absorption of the material could be measured.

The first experiments focussed on the RPE CVD material. Near the edge of the material, shadow masking during the growth process provided a graded material thickness over a distance of around a millimetre.

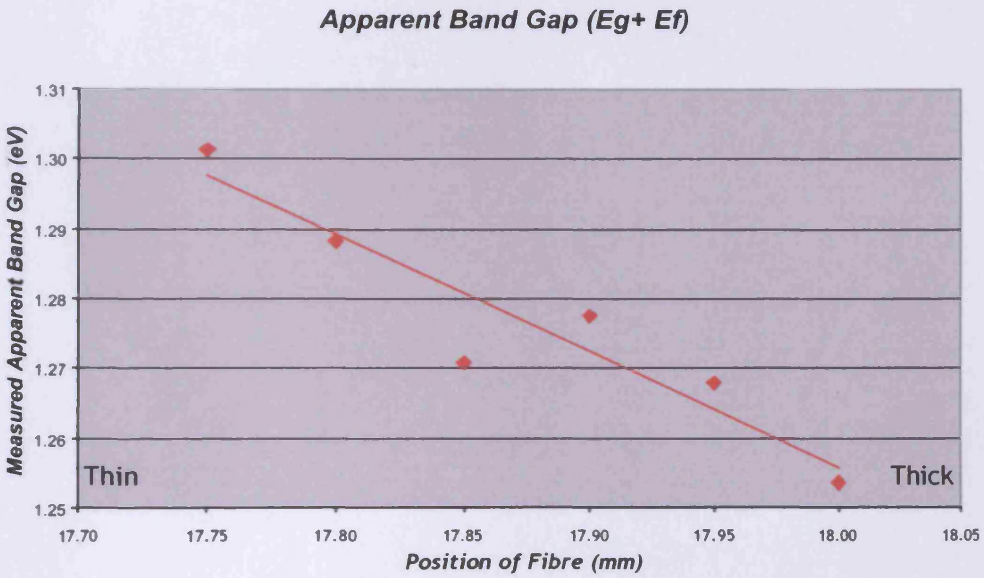

Figure 3 : Variation in measured band gap for changing InN thickness.

Further to this, we progressively dry etched a sample of InN grown by MOVPE (courtesy of O. Briot at the University of Montpellier, France) and subsequently measured the optical absorption at different thicknesses. Again, we found evidence of increasing apparent band gap as samples are thinned. The apparent band gap increasing by ~0.3eV per dry etch of ~80nm of InN.

Conclusions

From these initial experiments, we conclude that for thin InN material, the observed band gap energy is Moss-Burstein shifted to higher energies due to a higher density of defect-related carriers. As the material thickness is increased, the defect density reduces as the material begins to coalesce. A reduction in defect density would imply a lower Ef and hence a lower observed band gap. Our observations agree with this assumption.

---

[i] "Indium Nitride Emerges", Butcher et al, AIP Congress, Sydney (2002)

[ii] Higashiwaki M. et al, J.Cryst.Growth 269 (2004) 162-166

[iii] Wintrebert-Fouquet W. et al, J. Cryst. Growth 260 (2004) 134-138

[iv] Alexandrov A. et al, J. Cryst. Growth 269 (2004) 77-86

CARDIFF UNIVERSITY ★ PRIFYSGOL CAERDYDD